NOVEL MODES OF COMMUNICATION BETWEEN NEURONAL ACTIVITY AND MICROGLIAL PROCESS DYNAMICS

by

Lasse Dissing-Olesen

M.Sc., University of Southern Denmark, 2009

A THESIS SUBMITTED IN PARTIAL FULFILLMENT OF

THE REQUIREMENTS FOR THE DEGREE OF

DOCTOR OF PHILOSOPHY

in

THE FACULTY OF GRADUATE AND POSTDOCTORAL STUDIES

(Neuroscience)

THE UNIVERSITY OF BRITISH COLUMBIA

(Vancouver)

April 2015

Abstract

Microglia are morphologically dynamic cells that survey neuronal dendrites and rapidly respond to ATP. However, the role of ATP in mediating neuron-microglia communication remains to be determined. We therefore investigated the question whether high neuronal activity would evoke ATP release and thereby trigger a change in microglial process dynamics. To address this we used acute hippocampal brain slices and two-photon laser scanning microscopy and we developed a novel method for fixation and immunolabeling of microglia processes.

We discovered that multiple brief applications of NMDA triggered a transient outgrowth of microglia processes similar to application of ATP. The outgrowth was reversible and repeatable, indicating that it was not due to excitotoxic damage. ATP release, secondary to NMDAR activation, was the key mediator as blocking purinergic receptors abolished outgrowth. Hemichannel opening is a well-defined mechanism for ATP release, but outgrowth still occurred in the absence of the hemichannel protein pannexin 1 and in the presence of the hemichannel blocker carbenoxolone. Utilizing whole cell patch clamping we demonstrated that activation of dendritic NMDAR on single neurons was sufficient to trigger microglia process outgrowth. These results suggest that dendritic neuronal NMDAR activation triggers ATP release via a hemichannel-independent mechanism.

It is well established that high neuronal activity leads to a reduction in extracellular Ca^{2+} which causes opening of astrocytic Cx43 hemichannels and subsequent ATP release. We therefore investigated whether hemichannel opening could trigger a change in microglial process dynamics. Indeed, removal of extracellular Ca^{2+} triggered a microglial response, which we refer

to as microglial process focalization because it was distinctively different from the NMDA-evoked process outgrowth. This focalization was also mediated by ATP as it was blocked by selective blockade of microglial purinergic receptors and we observed a strong inverse relationship between the concentration of extracellular Ca^{2+} and microglial responses. Carbenoxolone, which did not block NMDA-evoked process outgrowth, resulted in a dose-dependent block of microglial process focalization which is consistent with the mechanism of ATP release being opening of Cx43 hemichannels.

Taken together, our data provide novel insight into how high neuronal activity triggers release of ATP as a mechanism for enhancing neuron-microglia communication.

Preface

The majority of the work presented in this dissertation has been peer-reviewed and accepted by internationally recognized scientific journals.

The work presented in chapter 2 has been published as:

Dissing-Olesen L., LeDue J.M., Rungta R.L., Hefendehl J.K., Choi H.B., MacVicar B.A. (2014). Activation of neuronal NMDA receptors triggers transient ATP-mediated microglial process outgrowth. **The Journal of Neuroscience** 34: 10511-10527.

All the experiments published in this paper were conceived and designed by myself with the exception of the Matlab script (J.M.L) and the *in vivo* experiments (J.K.H). I conducted all of the data collection, analysis, and manuscript preparation. Dr. MacVicar provided assistance and advice on experimental design and helped with editing the manuscript.

The method presented in chapter 4 has been published as:

Dissing-Olesen L. and MacVicar B.A. (2015). Fixation and Immunolabeling of Brain Slices: SNAPSHOT Method. **Current Protocols in Neuroscience** 71: 1.23.1 – 1.23.12.

I came up with the initial idea and successfully developed this simple, but innovative, method to address unique biological questions. The method was crucial for enabling the discoveries presented in chapter 2 and 3 and it has allowed me to contribute significantly to my colleague's research (Mills et al., 2014, Zhang et al., 2014a).

Certificate of approval:

The animal studies presented in this thesis were performed with ethics approval from the University of British Columbia Animal Care Committee (certificate # A11-0116 and A11-0031).

Table of Contents

List of Figures

List of Abbreviations

ACSF - artificial cerebrospinal fluid

ADP – adenosine diphosphate

AMP - adenosine monophosphate

AMPA - α-Amino-3-hydroxy-5-methyl-4-isoxazolepropionic acid

APV - (2 R)-amino-5-phosphonovaleric acid; (2 R)-amino-5-phosphonopentanoate

ATP - adenosine triphosphate

BAPTA - 1,2-bis(o-aminophenoxy)ethane-N,N,N',N'-tetraacetic acid

BBB - blood-brain barrier

CA - cornu ammonis

CALHM - calcium homeostasis modulator

cAMP - cyclic-adenosine monophosphate

CBX - carbenoxolone

CD - cluster of differentiation

CNS - central nervous system

CNQX - 6-cyano-7-nitroquinoxaline-2,3-dione

CR - compliment receptor

Cx - connexin

CX3C - chemokine C-X3-C motif

dLGN - dorsal lateral geniculate nucleus

DMSO - dimethyl sulfoxide

EM - electron microscopy

EGTA - ethylene glycol tetraacetic acid

EPSC - excitatory postsynaptic current

EPSP - excitatory postsynaptic potential

FFA - flufenamic acid

FPKM - fragments per kilobase of transcript sequence per million mapped fragments

GABA - gamma-aminobutyric acid

GAPDH - glyceraldehyde 3-phosphate dehydrogenase

GFP - green fluorescent protein

GFAP - glial fibrillary acidic protein

HEPES - 4-(2-hydroxyethyl)-1-piperazineethanesulfonic acid

HT - hydroxytryptamine

Iba - ionized calcium-binding adapter molecule

IHC - immunohistochemistry

IP_3 - inositol 1,4,5-trisphosphate

KO - knock out

L-NAME - L-NG-Nitroarginine Methyl Ester

LPS - lipopolysaccharide

MCSF - macrophage colony stimulating factor

mRNA - messenger ribonucleic acid

NMDA - N-Methyl-D-aspartic acid

nNOS - neuronal nitric oxide synthase

NO - nitric oxide

Panx - pannexin

PBS - phosphate buffered saline

PFA - paraformaldehyde

PI - propidium iodide

PI3K - phosphoinositide-3-kinase

PLC - phospholipase C

PPADS - pyridoxalphosphate-6-azophenyl-2',4'-disulfonic acid

PSD - postsynaptic density protein

PTIO - carboxy-2-phenyl-4,4,5,5-tetramethyl-imidazoline-1-oxyl-3-oxide

P8 - postnatally day 8

RB2 - reactive blue 2

RT - room temperature

siRNA - small interfering RNA

SR - sulforhodamine

TNF - tumor necrosis factor

TTX - tetrodotoxin

UDP - uridine diphosphate

UTP - uridine triphosphate

VNUT - vesicular nucleotide transporter

Acknowledgements

First and foremost, I would like to thank my Ph.D. supervisor, Dr. Brian A. MacVicar, who has been an encouraging mentor throughout the years. His enthusiasm and drive for big ideas and high impact science have been truly inspiring. I am extremely grateful for all the scientific opportunities that he has given me and for the great times that we have spent together outside the lab.

Secondly, I would like to thank the members of my research advisory committee, Drs. Lynn Raymond, Wolfram Tetzlaff, Yu Tian Wang, and Fabio Rossi as well as Drs. Ann Marie Craig, Shernaz Bamji, and Kurt Haas for their interest in my research and for all their insightful feedback and advice.

Thirdly, I would like to express my gratitude to the Heart and Stroke Foundation of Canada for granting me a Doctoral Research Award and a North Award.

A very special thank you goes to all the members of the MacVicar lab, past and present, who each and every one has helped provide a friendly atmosphere in the lab and confirmed how much it means to me to be working as a team. I would furthermore like to thank my other friends and colleagues at UBC, past and present, especially: Drs (and Drs to be) Matthew Parsons, Tiffany Timbers, Andrew Giles, Simon Chen, Tabrez Siddiqui, Janaina Brusco, Kasper Podgorski, Steve Connor, Fergil Mills, Stefano Brigidi, Wilder Scott, Elena Groppa, Bahareh Ajami, Dayne Beccano-Kelly, Barak Caracheo, Donovan Ashby, Evan Ardiel, Emil Gustavsson, Abdullah

Gharaibeh, and Majd Mustafa. I value every single scientific discussion we have had and I am looking forward to many more in the future.

Thankful thoughts also go to my early scientific mentors and friends, especially Drs. Bente Finsen and her lab, Trevor Owens, Inigo Azcoita, Ishar Dalmau, Morten Løbner, and Morten Thaysen-Andersen.

Above all I want to thank my parents and my grandparents, for showing me the true value of hard work. Their daily passion for their work is my greatest inspiration and without their love and support I simply would not be at this stage in my life.

To my girls, Kelly & Ella, you are my greatest motivation to succeed and the best thing that has ever happened to me. I love you with all of my heart.

Chapter 1: Introduction

Microglia are a population of resident immune effector cells that occupy all regions of the central nervous system (CNS). They are derived from specific progenitors in the yolk sac and form a self-renewable population in the CNS that is not replaced by peripheral myeloid cells (Ajami et al., 2007; Mildner et al., 2009; Ginhoux et al., 2010; Ajami et al., 2011; Kierdorf et al., 2013; Swinnen et al., 2013). Any type of disease or injury in the CNS inevitably triggers microglial responses, and therefore, the role of microglia in CNS pathologies has been extensively studied (Kreutzberg, 1996; Streit, 2002; Kettenmann et al., 2011). However, much less is known about how microglia respond to high levels of neuronal activity and to acute and transient disturbances in CNS homeostasis.

Microglial are dynamic cells that constantly survey their surroundings (Nimmerjahn et al., 2005). In the absence of pathological stimuli, microglia present a ramified morphology with several long processes extending from a relatively small soma. Most of these processes have multiple branches and filopodia-like protrusions that are often observed in close proximity with synaptic elements (Wake et al., 2009; Tremblay et al., 2010). While the soma is stationary the processes are highly motile and persistently extend and retract thereby contributing to the notion of an ongoing surveillance of surrounding synapses (Davalos et al., 2005; Nimmerjahn et al., 2005). Microglia remain in their resting surveillance state during non-pathological conditions partly through direct neuron-microglial interaction by ligand-receptor binding like cluster of differentiation (CD)200-CD200r, CD22-CD45, CD47-CD172a, and chemokine C-X3-C motif (CX3C)L1-CX3CR1 (Biber et al., 2007; Hanisch and Kettenmann, 2007) and the extracellular presence of inhibitory molecules such as transforming growth factor-β1 and interleukin-10 (Butovsky et al., 2014). In contrast, pathological insults cause microglia to transition into

activated immune effectors within hours to days due to a disruption of the 'calming' signals and activation of microglial receptors such as cytokine and chemokine receptors, TLRs (*Toll-like receptors*), PAMPs/DAMPs (*pathogen –damage/danger associated molecular patterns*) and RAGE (*Receptor for advanced glycan endproducts*) (Pocock and Kettenmann, 2007; Kettenmann et al., 2011).

High levels of neuronal activity may enhance neuron-microglia communication without altering the inhibitory signals or evoking pathological stimuli leading to a rapid (secs to mins) and transient alteration of ramified surveying microglia that may play a crucial role in sensing and assessing the fate of specific synapses. Several interesting investigations of neuron-microglial interaction and communication have been performed in the developing brain, in organotypic brain slices, in the juvenile and adult CNS, and during inflammation which combined with the reports on microglial process dynamics have motivated and inspired the worked presented in this dissertation.

1.1 Neuron-microglia interaction and communication

1.1.1 During development

Pioneering research has established that microglial cells play an important role in eliminating synapses during development and that microglia-neuron interaction is essential for establishing neuronal circuits. Precise neuronal connectivity is achieved by initial overrepresentation of neuronal connections followed by refinement through synapse elimination referred to as synaptic pruning. Insufficient removal of synapses during development causes imbalances in excitation and inhibition in the nervous system which can have a global and long-lasting impact on brain wiring with substantial implications for neurological disorders associated

with aberrant connectivity, including epilepsy (Besseling et al., 2013), schizophrenia (Stephan et al., 2009; van den Heuvel and Kahn, 2011) and depression (Williams et al., 2014).

Molecules of the classic complement cascade, C1q and C3, are localized in the developing retinogeniculate system (Stevens et al., 2007) and have been demonstrated to guide microglial mediated elimination of synapses. Microglial-mediated complement-dependent elimination of inactive synapses is crucial for eye-specific segregation, and the compliment receptor (CR)3 and C3 deficiency results in impairments in segregation (a larger area of dLGN (dorsolateral geniculate nucleus) is occupied by input from the ipsilateral eye). That microglia preferentially engulfed inactive synapses was elegantly demonstrated by injection of different colored fluorescent tracers into the eyes which allow the synaptic inputs from each eye to be distinguished in the dorsal lateral geniculate nucleus (dLGN). Inputs from eyes injected with tetrodotoxin (TTX) were preferentially engulfed by microglia compared to inputs from eyes injected with forskolin (Schafer et al., 2012). Additionally, it was demonstrated that C1q expression is regulated by astrocytic transforming growth factor-β and that mice deficient for the transforming growth factor-β receptor in retinal neurons have reduced C1q expression and consequently less eye-specific segregation due to impaired microglial mediated synapse elimination (Bialas and Stevens, 2013). An alternative approach to investigate the importance of microglia during development is to examine the impact of reduced number of microglia. Mice deficient for CX3CR1 (the second CX3CR1 exon was replaced by the EGFP gene) had reduced microglia numbers during development (postnatally 8 (P8)-P28) which correlated with an increased number of dendritic spines (PSD95 puncta / μm^3) presumably due to lack of microglia-mediated synaptic pruning. Stimulated emission depletion '*STED*' microscopy was used to demonstrate that microglia did indeed engulf synaptic material in stratum radiatum of the cornu

ammonis (CA)1 in P15 mice and immune electron microscopy (EM) for PSD95 and green fluorescent protein (GFP) (expressed by microglia) confirmed the engulfment.

During development synaptogenesis result in an increase in synaptic multiplicity (i.e. individual synaptic boutons making excitatory connections with multiple dendritic spines) which can be observed as an increase in the amplitude of excitatory postsynaptic potential (EPSP). Synaptic multiplicity was diminished in CX3CR1 deficient mice supposedly because pruning is part of the synaptic plasticity required for synaptic multiplicity to occur. This was further validated by reconstruction of serial sectioning electron microscopy and functionally by showing a significant reduction in the duration and latency of drug-evoked seizures in the CX3CR1 deficient mice (Paolicelli et al., 2011). Interestingly, these mice continued to display decreased functional brain connectivity in adulthood and show behaviors related to social-interaction deficits (Zhan et al., 2014). However, without further validation, it is too early to say whether these dramatic deficits in synaptic circuit and behavior in CX3CR1 deficient mice compared to wild type mice can be ascribed to a reduction in microglia function. A major caveat with this model is that CX3CR1 deficiency not only affects microglial cells but also immune cells in the periphery (a subset of natural killer cells and certain T cell populations) (Imai et al., 1997) which are likely to also impact the CNS (Dantzer et al., 2008)

Direct evidence of microglial-neuron interaction was accomplished by real-time imaging of microglia in zebrafish larvae. It was hereby demonstrated that the motility of microglial processes would slow down upon contacts with neurons and bulbous tips would enlarge. Interestingly, the interaction was mediated by neuronal activity as uncaging of glutamate induced a polarization of microglial processes that extended towards the area where glutamate had been uncaged. Microglial process polarization was not observed in the presence of TTX and 1,2-bis(o-

aminophenoxy)ethane-N,N,N',N'-tetraacetic acid (BAPTA) indicating that microglia respond to a neuronal signal triggered by the uncaging of glutamate. Overexpression of the human inward rectifier K channel 2.1 reduced excitability in neurons and also reduced microglial process polarization. Astonishingly, calcium imaging of visually evoked responses in tectal neurons revealed that microglia contacted activated neurons and that the neuronal activity (amplitude of calcium responses) declined upon contact. In contrast translocation or diversion of microglial processes increased the spontaneous neuronal activity (Li et al., 2012).

1.1.2 Organotypic brain slices

An alternative way of investigating the functional interaction between microglia and neurons has been via depletion and replenishment of microglia. In agreement with the silencing effect of neuronal activity reported in zebrafish larva, microglia were also found to have protective functions against neuronal excitotoxicity in murine organotypic hippocampal slices. The CA1 pyramidal neurons are extremely vulnerable to prolonged treatment with N-Methyl-D-aspartic acid (NMDA, 10 µM for 4 hours) compared to neurons in dentate gyrus and CA3. This was validated by quantification of propidium iodide uptake of $NeuN^+$ neurons. Depletion of microglia by treatment with liposome-encapsulated clodronate or treatment of slices from CD11b-HSVTK (*herpes simplex virus thymidine kinase)* mice with ganciclovir (Heppner et al., 2005; Grathwohl et al., 2009; Varvel et al., 2012) increased the neuronal vulnerability to excitotoxicity. Astonishingly, replenishment of microglia-depleted slices with primary microglia, which acquired a ramified morphology, significantly reduced neuronal vulnerability (12 days after replenishment) (Vinet et al., 2012). Along the same lines, depleting microglia with clodronate has also been shown to increase spontaneous and miniature excitatory postsynaptic

currents (EPSC) in murine organotypic hippocampal slice. Replenishment of microglia (using cellular debris as a negative control treatment) showed a complete rescue of the EPSC eight days after replenishment. In cultures the EPSC were higher in neurons cultured without microglia than when neurons were cocultured together with microglia. This correlated with a higher spines numbers and PSD95^{+} puncta in neurons cultured without microglia. Microglia also showed engulfment of synaptic material (Ji et al., 2013).

1.1.3 In the juvenile and adult CNS

Microglia interactions with synapse are not restricted to development and have also been observed in both the juvenile and the adult CNS. Notably, microglia processes actively contribute to experience-dependent modification and elimination of synapses in the healthy brain. Microglial interaction with synapses was evaluated by *in vivo* two-photon imaging (using a thin skull preparation on CX3CR1-enhanced (E)GFP x Thy1-(*yellow*)YFP mice anesthetized with fentanyl / midazolam / metatomadin), serial section electron microscopy and three-dimensional reconstructions of pre-embedding immunoperoxidase labeling of Iba1^{+} microglia during normal and altered sensory experience in the visual cortex of juvenile mice (P28–P39). During normal visual experience 94% of microglial processes were found to be in direct contact with a synapse. As observed in the zebrafish larva, microglia processes would pause upon contact with a synapse. Duration of contacts varied between 5 and 50 min and evoked both increased growth and elimination for small spines. This could potentially indicate that microglia are capable of monitoring the functional status of synapses and regulating structural changes and elimination either through direct contact or indirect signaling that requires close microglia–synapse proximity. Alternatively, microglial processes preferentially localize to small dynamic

dendritic spines. Manipulating the visual experiences through light deprivation and reexposure altered microglial process dynamics. Dark adaptation decreased process motility but increased extracellular space around microglial processes while light exposure reversed these behaviors (Tremblay et al., 2010). Similar observations were also reported in the adult mouse (6-10 weeks) where *in vivo* two-photon imaging (using a thin skull preparation on ionized calcium-binding adapter molecule **(**Iba)1-EGFP x Thy1-GFP mice anesthetized with ketamine / xylazine) was used to demonstrate that motile microglial processes would briefly pause for 4-5 min upon contact with presynaptic boutons or dendritic spines. This is in agreement with the initial *in vivo* observations that found that the duration of microglia-synapse contact is 3-4 min (using thinned skull preparation on 1.5-15 months old CX3CR1 mice anesthetized with ketamine / xylazine, urethane or isoflurane)(Nimmerjahn et al., 2005). The microglia-synapse interactions were further supported by pre-embedding immuno-EM (using the avidine-biotinylated enzyme complex ABC method to label Iba1) which convincingly showed direct microglia-synapse contacts. Interestingly, lowering neuronal activity (by lowering body temperature to 32°C or injecting TTX into the eyes) resulted in decreased contact frequency in the visual cortex. Following cerebral ischemia (30 min after middle cerebral artery occlusion), contacts between microglial processes and synaptic boutons lasted > 60 min (Wake et al., 2009). It is worth highlighting that all the studies referred to above used a thin skull preparation for in vivo imaging as it has been reported that dendritic spine dynamics through an open-skull glass window, but not a thinned-skull window, is associated with high spine turnover and substantial morphological changes (activation) of microglia during the first month after surgery (Xu et al., 2007). A more recent study performed in 7 weeks old rats has however questioned microglia-synapse interaction under physiological conditions as these interactions are rare. Using post-

embedding immunogold labeling of Iba1 and actin they showed by electron microscopy that only about 3.5 % of the synapses are in direct contact with microglia in the frontal cortex (Sogn et al., 2013). However there are limits to this study. First of all post-embedding immunolabeling was used which reduces the number of accessible epitopes compared to pre-embedding immunolabeling as used in the other studies. Secondly, they also used immunogold labeling and thereby relied on the presence of individual gold particles for cell identification in contrast to immunoperoxidase labeling used in the other studies, which provided a more widespread precipitate for cell labeling. However, the most important point is that this study report the proportion of synapses that were contacted by microglial processes (3.5 %) while the other studies report the proportion of microglial processes that are contacting synapses (94%). Since, there are many more synapses than microglial processes these observation support the idea that motile microglial processes survey surrounding synapses by briefly visit one synapse after another and possibly around 3.5 % of synapses at any given time. This therefore leads to the intriguing questions whether microglial process surveillance is driven by synaptic activity and whether microglia are responding to synaptic signals and cues. We speculated that microglia processes in the adult brain might get recruited to specific synapses similar to what is observed in the developing visual system. However, while inactive synapses are more likely to be eliminated during development we suggest that microglia might have a preference for highly active synapses in the adult CNS.

Several studies have shown that microglia process dynamics can be altered by increasing neuronal activity via several different manipulations. Stimulation of α-Amino-3-hydroxy-5-methyl-4-isoxazolepropionic acid (AMPA) and kainate receptors in the retina to depolarize neurons or increasing neuronal activity by blocking gamma-aminobutyric acid (GABA)

inhibition via application of bicuculline triggered microglial process extension (Fontainhas et al., 2011). Bicuculline application has also been shown to increase microglia process motility *in vivo* (Nimmerjahn et al., 2005). However, increasing neuronal activity by stimulation of Schaffer collaterals in acute hippocampal brain slices did not affect microglia process motility (Wu and Zhuo, 2008). Lowering of neuronal activity in the retina, either by blockage of AMPA, kainite, or NMDA receptors or by application of GABA (to stimulate inhibition) resulted in retraction of microglial processes (Fontainhas et al., 2011). TTX on the other hand had no effect on microglial process motility in vivo (Nimmerjahn et al., 2005).

1.1.4 During inflammation

Distal and peripheral nerve injury triggers a morphological change in microglia specifically in the region of the CNS corresponding to the innervation site of the lesioned nerves (Blinzinger and Kreutzberg, 1968; Matthews et al., 1976; Kreutzberg, 1996; Banati, 2002). This process takes days but results in proliferation of microglia and removal of synapses, referred to as 'synaptic stripping' (Blinzinger and Kreutzberg, 1968; Kreutzberg, 1996). A similar phenomenon was also observed days after the inductions of localized inflammation (Trapp et al., 2007).

Microglia can also affect synaptic transmission within minutes during inflammation and depending on the inflammatory stimuli microglia can either contribute to synaptic potentiation or depression (Pascual et al., 2012; Zhang et al., 2014a). Treatment of acute hippocampal brain slices with lipopolysaccharide (LPS, 500 ng / ml) has been reported to trigger synaptic potentiation by evoking adenosine triphosphate (ATP) release from microglia. ATP was found to trigger the release of astrocytic glutamate which increased excitatory postsynaptic currents

through a metabotropic glutamate receptor 5-dependent mechanism. The potentiation was blocked by the anti-inflammatory drug minocycline and abolished in slices from microglia deficient mice (PU-$1^{-/-}$) and LPS receptor (TLR4) deficient mice. The '*PU-1'* experiments were performed in organotypic brain slices because PU-$1^{-/-}$ offspring die at birth.

Potentiation was also blocked by inhibitors of the purinergic receptor P2Y1 and application of a P2Y1 agonist (MRS2365) mimicked the LPS-induced effects. LPS-induced increases in EPSCs were prevented by application of the toxin, fluoroacetate (which is commonly used to inhibit metabolism in astrocytes (Fonnum et al., 1997; Andersson et al., 2007; Henneberger et al., 2010)). Importantly stimulation of P2Y1 also induced potentiation in PU-$1^{-/-}$ mice. LPS triggered ATP release in microglia cultures, which was enhanced more than 4-fold when microglia were co-cultured with astrocytes. Finally, P2Y1 stimulation and LPS-induced potentiation are mGluR5 dependent (Pascual et al., 2012). Alternatively, application of LPS (15 mg / ml) in combination with oxygen deprivation, based on the rational that hypoxia often occurs together with neuroinflammation, was observed to trigger synaptic depression both in juvenile rats and adult mice. Surprisingly, the effect of LPS was mediated via stimulation of the CR3 (also known as CD11/CD18) receptor and not the classic LPS receptor, TLR4. Synaptic depression also occurred in $TLR4^{-/-}$ mice while it was abolished in $CR3^{-/-}$ mice (Zhang et al., 2014a). In summary, the synergistic effect of CR3 stimulation with LPS and hypoxia promoted NADPH (*nicotinamide adenine dinucleotide phosphate*) oxidase-mediated production of reactive oxygen species that in turn induced PP2A regulated endocytosis of AMPA receptors and consequently synaptic depression (Zhang et al., 2014a). Taken together these studies demonstrate that microglia are capable of functionally altering synaptic transmission. Interestingly, CR3 stimulation with the blood protein, fibrinogen has also previously been shown to evoke

microglial release of reactive oxygen species (Davalos et al., 2012). Thus, it can be speculated that a small hemorrhagic stroke or BBB disruption during multiple sclerosis (as proposed by the authors) causes synaptic depression due to microglial release of reactive oxygen species. Whether this is associated with a neuroprotective function to eliminate excessive synaptic excitotoxicity or whether these are examples of microglia-neuron interactions that have gone awry and contribute to pathology will have to be determined.

1.2 Microglia process dynamics

The motility of the processes has been estimated to be approximately 1.5 μm /min *in vivo* which allow each microglia to survey its entire surrounding extracellular space in one and a half hour. This is however a rough estimate based on a maximum-intensity projection of microglial processes in the cortex which reveal that 15% of the total surrounding tissue volume was surveyed by microglial processes within an hour (Nimmerjahn et al., 2005) and previous reports stating that the extracellular space take up approximately 20-25% of the total volume in adult rodents (Sykova, 2004). The extracellular space in the newborn rats is 36-41% in cortical layer 0.46% in white matter but become reduced to 19-23% in cortical layers and 20% in white matter (Lehmenkuhler et al., 1993). Interestingly, it has more recently been observed using the real-time iontophoretic tetramethylammonium method that the extracellular volume changes during awake and sleep circles and that the extracellular space of cortex in sleeping mice was 25% and 23% for ketamine/xylazine anesthetized mice while the extracellular volume was only 15% in awake mice (Xie et al., 2013). Hence it would be interesting to see whether the rate of microglial process surveillance remains the same during these changes in extracellular volume.

1.2.1 Laser-induced process extension

The same pioneering study that changed the concept of microglia from dormant tissue macrophages to highly dynamic surveillants of the brain parenchyma also reported for the first time that microglia respond rapidly to local disruption of the blood brain barrier in the mouse cortex. Laser-induced lesions were achieved by application of high laser power to a local area of vessels. Astonishingly, the surrounding microglia responded by extending their processes towards the lesion and within minutes all the processes would focalize or converge around the lesioned area. The microglial somas would round up but did not migrate and no morphological changes were observed in astrocytes visualized by sulforhodamine (SR)101 loading within the first four hours post lesion. Spontaneous engulfment and evacuation of tissue components did occur in the unlesioned brain but multiple lesion-evoked spherical-shaped inclusions were reported indicating a lesion-induced increase in phagocytotic activity (Nimmerjahn et al., 2005). Several studies have since then observed a similar microglial response to laser-induced lesion in different species and preparations. In acute brain slices it was demonstrated that focalization of microglial processes around the lesion served a functional role in restraining the damaged area and supposedly engulfing it as described above. A lesion-evoked shift in microglia morphology was characterized by retraction of filapodia-like protrusions and polarization of processes i.e. processes at the side of the cell soma in close proximity to the lesion extend while processes at the opposite side of the soma retract. Process outgrowth was determined to be chloride dependent as it was inhibited by pharmacological interventions against Cl^- channels (tamoxifen and DIDS *(4,4'-Diisothiocyano-2,2'-stilbenedisulfonic acid)*) and by removal of extracellular Cl^- (Hines et al., 2009).

Laser-induced lesions *in vivo* in the barrel cortex or in the fondus of the eye also showed initial microglial process focalization around the lesion within the first hour followed by migration of microglial cell bodies towards the lesion within the next 24 h (Kim and Dustin, 2006; Eter et al., 2008). Lesion-induced movement of microglial cell bodies has also been shown ex vivo in the retina in both young and old mice (Lee et al., 2008; Liang et al., 2009; Damani et al., 2011). Likewise, astrocyte migration towards the lesion after 48 hours has also been reported (Kim and Dustin, 2006) but these findings have been challenged by more recent data demonstrating that astrocytes do not migrate towards a lesion. Subpopulations of astrocytes did however direct their processes toward the lesion, and a distinct subset located at juxtavascular sites proliferated (Bardehle et al., 2013). The microglia would stay at the lesion site for weeks presumably clearing the area for debris and promoting repair, and the lesion itself would be less apparent already within days. The microglia at the lesion site disaggregated faster in younger mice and **t**here was a direct correlation between lesion area and the recovery time (Eter et al., 2008; Damani et al., 2011).

Blood leukocytes responded to laser-induced lesions in the brain parenchyma but remain in the perivascular space. In contrast, they surrounded a laser-induced lesion of the meninges within 30 min (demonstrated in LysM-EGFP mice) (Kim and Dustin, 2006). Taken together, this highlights microglia as the first and possibly sole responders to small local damages to the brain parenchyma. Thus, an intriguing question is how the complex spatial information about local tissue damage is detected and interpreted by microglia. In the periphery the information is delivered in the form of diffusible molecules. For example, highly motile leukocytes in zebrafish larva migrate to the site of damage in response to a wave of reactive oxygen species extending as far as 200 μm from the wound margin (Niethammer et al., 2009). In the mouse, swarming of

neutrophils to laser-induced lesions in the ear dermis is mediated by lipid leukotriene B4 (Yokomizo et al., 1997; Lammermann et al., 2013).

In the brain, ATP is the key trigger of rapid microglial responses. Microglial processes extension triggered by laser-induced lesions or mechanical injury by a glass pipette in mouse cortex were blocked by purinergic receptor antagonists, exogenously applied ectonucleotidases (apyrase, which hydrolyzes ATP to adenosine monophosphate (AMP)), and even by application of ATP itself as well as adenosine diphosphate (ADP) (the rationale for this will be discussed later). Microglial processes also extended towards the tip of electrodes containing ATP or ADP (Davalos et al., 2005).

These data have since been supported by the demonstrations that local and bath application of ATP onto acute hippocampal brain slices and retinal explants, respectively, both trigger microglial process outgrowth (Wu et al., 2007; Fontainhas et al., 2011). Importantly, it was demonstrated that the effect of ATP on microglia process dynamics *in vivo* is via the activation of the purinergic receptor, P2Y12, as no outgrowth was observed within the first 40 min after a laser-induced lesion or insertion of an ATP containing electrode in P2Y12 receptor deficient mice (Haynes et al., 2006). These findings were further validated in zebrafish larvae where microglial process outgrowth towards a laser-induced lesion was blocked by P2Y12 morpholino knock down and the selective P2Y12 receptor antagonist MRS2395. Inhibition of reactive oxygen species which blocked the response to damage in the periphery (Niethammer et al., 2009) had no effect on microglial process outgrowth (Sieger et al., 2012). Notably, we conducted a series of pilot experiments to investigate whether lipid leukotriene B4 would have a similar chemotaxic effect on microglia as it has on neutrophils in the periphery. However, both bath

application and local application of lipid leukotriene B4 failed to induce a morphological change of microglia (data not shown).

1.2.2 Purinergic receptors in the CNS

ATP is considered the principal purinergic signaling molecule in the CNS and ATP and its derivatives activate different purinergic signaling systems which are particularly abundant in glia (Fields and Burnstock, 2006; Verkhratsky et al., 2009). However, release of purines (e.g. ATP, ADP, and adenosine) as well as pyrimidines (e.g. uridine triphosphate (UTP) and uridine diphosphate (UDP)) accompanies cell damage and death and acts as a universal "danger" signal. Consequently, the purinergic signaling system is found in virtually every cell type throughout the body (Dubyak and el-Moatassim, 1993; Burnstock, 2006) and in the majority of all living cells across species (Burnstock and Knight, 2004). There are three families of purinergic receptors; metabotropic P1 adenosine receptors, ionotropic P2X ATP receptors and metabotropic P2Y purine and pyrimidine receptors (Burnstock, 2007). P1 receptors are seven-transmembrane spanning G protein-coupled receptors and include A1, A2A, A2B, and A3. Both A1 and A3 are Gi protein coupled (inhibit cAMP production) while A2A and A2B are Gq protein coupled (linked to inositol triphosphate (IP3)-mediated release of intracellular Ca^{2+}) (Fredholm et al., 2007; Muller and Jacobson, 2011). P2X receptors include P2X1-7 which are all ligand-gated nonselective cation (Na^{+} / K^{+} / Ca^{2+}) channels assembled from homo or heterotrimers (Khakh, 2001; Roberts et al., 2006). Similar to P1 receptors, P2Y receptors are seven-transmembrane spanning protein-coupled receptors. P2Y receptors can be divided into two groups; P2Y1,2,4,6,11 which are Gq protein coupled and P2Y12,13,14 which are Gi proteins (Burnstock, 2007). In addition, P2Y receptors are differentially and preferentially activated by

various nucleotides: P2Y1,11-13 are sensitive to ATP/ADP, P2Y4,6 are activated by UTP / UDP, P2Y2 is activated by ATP/UTP, and P2Y14 receptors are sensitive to pyrimidines sugars (e.g. UDP-glucose and UDP-galactose) (Lazarowski, 2010).

Based on transcriptome analyses there seems to be a strong consensus that resting surveilling rodent microglia express A1,3, P2X4,7, and P2Y6,12,13 and potentially P2X1 and P2Y2. RNA-sequencing was utilized to generate a high-resolution transcriptome of purified microglia, astrocytes, neurons, oligodendrocytes, oligodendrocyte precursors, and endothelial cells from P7 mouse cortex. Expression levels were reported as fragments per kilobase of transcript sequence per million mapped fragments (FPKM). A FPKM cut-off at 1 was chosen for simplicity but obviously with the risk of neglecting genes of high important despite their low expression. Microglia express: Adora1,3 (A1 and A3 genes), P2rx1,4,7, and P2yr2,6,12,13. In comparison astrocytes express: Adora1,2a,2b, P2rx4,6,7 and P2ry1, neurons express Adora1, P2rx4,5 and P2ry1, oligodendrocytes (including precursors) express: Adora1, P2rx4,7 and P2ry1,2,12, and endothelial cells express: Adora2a, P2rx4,5 and P2Y14. Microglial P2ry6,12,13 were the only purinergic receptors expressed in the CNS with FPKM > 100 (Zhang et al., 2014b). In support of these data, RNA-sequencing of microglia isolated from 5 and 24 months old mice showed that adult microglia also express P2rx4,7 and P2ry6,12,13 and that out of the 21,025 transcripts measured, P2ry6,12,13 were among the top 50 of transcripts with the highest enrichment in microglia compared to transcripts from the whole brain. P2ry12 showed the highest enrichment in microglia of all transcripts (Hickman et al., 2013; Butovsky et al., 2014). These results confirm previous reports of mRNA expression in cultured mouse and rat microglia (using polymerase chain reaction) that also showed that microglia express: A1,3, P2rx4,7, and P2ry2,6,12,13 (Light et al., 2006; Visentin et al., 2006; Koizumi et al., 2007). Very low levels of

P2Y1 have also been reported (Visentin et al., 2006) but that might potentially arise from contamination with astrocytes.

Taken together, the mRNA expression pattern in microglia across different preparations (i.e flow cytometry-sorted microglia, primary postnatal cultured microglia, embryonic stem cell derived microglia) seems surprisingly to be very consistent (Beutner et al., 2013; Hickman et al., 2013) and these findings have been validated by *in situ* hybridization indicating that it truly reflects the messenger ribonucleic acid (mRNA) expression of resting surveilling microglia *in vivo*. The next step is obviously to investigate the protein expression and compare it to these transcriptome analyses. Thus far two-dimensional difference gel electrophoresis and mass spectrometry analyses for microglia showed that mRNA and protein levels exhibited similar trends in expression (Hickman et al., 2013).

Peripheral nerve injury evoked microglial expression of P2Y14 (Kobayashi et al., 2012) while P2Y14 which is constitutively expressed by the mouse microglia cell line 'N9' was downregulated by LPS treatment (Bianco et al., 2005). It remains unclear whether microglia can express P2Y11 (Barragan-Iglesias et al., 2014). Microglia expressed significantly higher levels of P2rx7 than macrophages and macrophages did not express P2ry12, 13 (Butovsky et al., 2014). In contrast, macrophages expressed significantly higher levels of P2rx4. Interestingly, P2rx4 increased with age (from 5 to 24 months) while P2ry7 and P2ry12,13 all decreased (Hickman et al., 2013), thereby indicating that microglia undertake a more macrophage-like phenotype with age. This is also supported by morphological changes as it has been observed that the soma of microglia enlarged and their processes retracted with aging (Hefendehl et al., 2014).

1.2.3 The P2Y12 receptor

Fortunately, P2Y12 receptor expression has been investigated quite extensively (Foster et al., 2001; Hollopeter et al., 2001; Zhang et al., 2001; Haynes et al., 2006; Butovsky et al., 2014). P2Y12 receptors are almost exclusively expressed in the brain, in platelet-producing megakaryocytes in the bone marrow, in circulating platelets and at very low levels (only mRNA) in macrophages. Northern blot of mRNA from different human tissue samples (i.e. brain, colon, heart, kidney, liver, lung, lymphocytes, placenta, skeletal muscle, small intestine, spleen, thymus, testis) showed that P2Y12 is exclusively expressed in the brain (platelets and megakaryocytes was not included in this analysis) (Hollopeter et al., 2001). Northern blot of mRNA from a similar array of tissue samples from adult rats confirmed this expression (Sasaki et al., 2003). In the brain, P2Y12 mRNA and protein are selectively expressed in microglia based on in situ hybridization and immunohistochemistry (IHC) (Sasaki et al., 2003; Haynes et al., 2006; Kobayashi et al., 2008; Hickman et al., 2013). The P2Y12 protein was reported to be evenly distributed on microglia throughout the adult mouse brain and spinal cord (both white and gray matter) and it co-labeled 100% with EGFP expressing microglia (CX3CR1-EGFP transgenic mice) and $CD11b^+$ microglia (Haynes et al., 2006). P2Y12 mRNA expression occurred as early as P0 (it was not detected at E13 or at E16) and increased over the next 6 weeks (Sasaki et al., 2003). Interestingly, infiltrating monocytes did not express P2Y12 (Butovsky et al., 2014).

P2Y12 is a G_i-protein coupled receptor. Binding of either ATP or ADP triggers conformation changes of the receptor and results in the dissociation of its α- and βγ-subunits. The α-subunit inhibits the activity of adenylate cyclase mediated production of cyclic-adenosine monophosphate (cAMP) which, in turn, results in a block of cAMP dependent pathways. The βγ-subunit can induce activation of various phosphoinositide-3-kinase (PI3K) isoforms. PI3K is a

key regulator of multiple signaling transduction pathways including cell survival, proliferation, growth, metabolism, and motility. All PI3K isoforms are inhibited by wortmannin and LY294002. The action of PI3K in mediating morphological changes and motility has been ascribed to its activation of AKT (protein kinase B) (Enomoto et al., 2005) which regulates actin organization and cell motility (Morales-Ruiz et al., 2000; Higuchi et al., 2001). PI3K also activates the small Rho *(guanosine triphosphate)* GTPase molecule Rac (Han et al., 1998; Fleming et al., 2000) which then in turn triggers actin polarization (Peyrollier et al., 2000; Wang et al., 2002; Heo and Meyer, 2003; Inoue and Meyer, 2008). Interestingly, some studies also suggest that Rac triggers a positive feedback loop that further activates PI3K (Servant et al., 2000; Weiner et al., 2002; Yang et al., 2012) and that this feedback loop also involves actin polarization (Srinivasan et al., 2003).

A minor attribute of the βγ-subunit is the activation of the phospholipase C (PLC) (Zhu and Birnbaumer, 1996) pathway although this pathway is predominantly activated by the α-subunit of Gq-protein coupled receptor. PLC cleaves phospholipid phosphatidylinositol 4,5-bisphosphate into inositol 1,4,5-trisphosphate (IP_3) and diacyl glycerol. IP_3 triggers release of Ca^{2+} from endoplasmic reticulum and mitochondria via activation of IP_3 receptors.

The main reason for investigating the P2Y12 receptor has previously been as a therapeutic target due to its role in platelet aggregation. Platelets or thrombocytes plays a crucial role along with coagulation factors to blood coagulation by stop bleeding at thereby facilitate wound repair at the site of endothelium disruption (Laki, 1972). Activated platelets (by collagen exposed following endothelium damage) secrete ATP (from their δ granules) leading to an autocrine activation of P2Y12(Gi) and P2Y1(Gq) and their respective signaling pathways (decrease in cAMP, stimulation of actin polymerization, and an increase in intracellular Ca^{2+}). Stimulation of

both P2Y1 and P2Y12 are required for full platelet aggregation (Jin and Kunapuli, 1998; Resendiz et al., 2003) and both collagen- and thrombin-induced platelet aggregation is strongly impaired in platelets from P2Y1 deficient mice (Leon et al., 2001), platelets from patients with bleeding disorders linked to defects in P2Y12 receptors, and when P2Y12 receptors were blocked (by ARL 66096) (Cattaneo and Gachet, 1999).

Clinically, P2Y12 has received a lot of attention as it has been successfully targeted with pharmacological interventions and it have been shown in multiple clinical trials and studies to reduce the incidence of myocardial infarction (heart attack) and stroke in patients at high risk (e.g. patients with coronary artery disease and cerebrovascular disease) (Quinn and Fitzgerald, 1999; Yusuf et al., 2001; Diener et al., 2004). Hence, two groups of drugs have been developed, one group requiring oxidation by hepatic enzymes for pharmacological activity (e.g. Clopidogrel (Bristol-Myers Squibb/Sanofi) and Prasugrel (Effient/Efient)), and the second group that does not need hepatic activation (e.g. Ticagrelor (AstraZeneca), Cangrelor (the Medicines Company) and Elinogrel (Portola Pharmaceuticals/Novartis)).

Notably, none of the clinical trials and studies has investigated how the treatment affects microglia. It is uncertain whether these drugs cross the BBB so they might not have a chronic effect on microglial process dynamics. However, as discussed above, microglia responded rapidly to vessel disruptions in a P2Y12-dependent manner. Thus, one could speculate that treatment with P2Y12 receptor inhibitors might impact the functional role of microglia responses to a hemorrhage. It has been estimated that anti-thrombotic therapies increase the risk of intracerebral hemorrhage by 12% (7,000 of the 60,000 annually occurring intracerebral hemorrhages in the US alone) (Hart et al., 2005). Several studies and clinical trials have indicated that treatment with clopidogrel in combination with a traditional anticoagulant such as

aspirin (an inhibitor of cyclooxygenase enzymes) and warfarin (inhibitor of vitamin K) increases the risk of intracerebral hemorrhage and plausibly the mortality (Yusuf et al., 2001; Diener et al., 2004; Fintel, 2007; Hassan et al., 2007; Cordina et al., 2009). Hence, it remains unknown whether the combination of anti-thrombotic therapies or blockage of microglial P2Y12 receptors is the main contributor to the enhanced risk of intracerebral hemorrhage. It is possible that blockage of microglial P2Y12 receptors causes a stronger clinical manifestation of spontaneously occurring hemorrhages and therefore appear to enhance the risk. Taken together this illustrates the need for improving the understanding of P2Y12-dependent microglial process dynamics.

1.2.4 ATP-induced chemotaxis in cultured microglia

Cultured microglia do not display the ramified morphology reported *in vivo* and in acute organotypic brain slices. However, some microglia culture preparations express P2Y12, and demonstrate an F-actin-dependent morphological change referred to as membrane ruffling upon stimulation by ATP and ADP. Application of a gradient of ATP also triggers P2Y12-mediated microglial migration that can be quantified using Boyden and Dunn chemotaxis chambers (Honda et al., 2001; Farber et al., 2008). Both ATP and ADP-induced membrane ruffling and migration were blocked by the P2Y12 selective blocker AR-C69931MX (but not by the P2Y12 insensitive inhibitor pyridoxalphosphate-6-azophenyl-2',4'-disulfonic acid (PPADS)) while macrophage colony stimulating factor (MCSF)-induced membrane ruffling was unaffected by AR-C69931MX. Both ATP-induced membrane ruffling and migration were also abolished in microglia from P2Y12 receptor deficient mice while MCSF still triggered membrane ruffling (Haynes et al., 2006). Blocking PI3K (inhibited by wortmannin), PLC (inhibited by U73122),

elevation of intracellular Ca^{2+} (by chelating intracellular Ca^{2+} with BAPTA), and AKT inhibited the activation of Rac, which is essential for microglial migration (Honda et al., 2001; Nasu-Tada et al., 2005; Irino et al., 2008). Interestingly, F-actin, Rac and the commonly used microglial marker Iba1 co-localize during MCSF-induced membrane ruffling and zymosan-induced phagocytosis. MCSF-induced activation of Rac was also mediated through activation of PI3K and PLC. Importantly, Iba1 enhances Rac activation as expression of mutant Iba1 (substitution on the calcium binding domain) suppressed membrane ruffling and phagocytosis (Ohsawa et al., 2000; Imai and Kohsaka, 2002). Introduction of a Rac-FRET *(fluorescence resonance energy transfer)* sensor in microglia in zebrafish larva demonstrated that Rac accumulates at the bulbous tips at the leading edge of extending processes. In contrast, impairment of endogenous Rac activity (by expression of a human Ras (Kardash et al., 2010)) resulted in a loss of oriented movement of microglial processes and a failure to facilitate the formation of bulbous tips (Li et al., 2012) indicating that Rac is required for both migration of cultured microglia and microglial process extension in vivo. The requirement for PLC and presumably IP_3 triggered release of Ca^{2+} could potentially be ascribed to the action of the βγ-subunit downstream of P2Y12 receptor activation. However, it seems more likely that PLC activation is due to co-activation of a Gq-protein coupled receptor. Co-activation of both Gi and Gq signaling pathways are necessary for full ADP-induced platelet aggregation (Jin and Kunapuli, 1998). The Gq-protein coupled P2Y6 receptor is highly expressed on microglia and would be a likely candidate.

1.2.5 ATP induced microglial process outgrowth

Culturing of microglia on 3D collagen gels allowed for investigation of process dynamics as microglial processes extended towards an ATP gradient in this model system. A ceiling effect of

ATP-induced process extension was observed at 50 µM ATP in this model (500 µM resulted in a similar response in terms of process extension). In agreement with the data on membrane ruffling and migration, ATP and ADP-induced process extension was also blocked by AR-C69931MX (and not PPADS) and was moreover shown to be dependent on PI3K (blocked by LY29004 and wortmannin) and PLC (blocked by U73122) (Ohsawa et al., 2010). Importantly, ATP-induced microglial process outgrowth in acute brain slices was also impaired when PI3K was blocked (by wortmannin) (Wu et al., 2007). Other studies using cultured microglial in 3D matrix gels also reported that ATP triggered microglial process and furthermore demonstrated that ATP-induced process outgrowth did not occur when the P2Y12 receptors were downregulated. Under these circumstances, ATP was found to be repulsive (Orr et al., 2009). P2Y12 downregulation has previously been correlated with microglial activation and when ramified microglia are transitioning into an ameboid morphology (Haynes et al., 2006). In the studies referred to above, microglial activation and consequently P2Y12 downregulation was induced by stimulation (for 24 h) with LPS (TLR-4 agonist), lipoteichoic acid (TLR-2 agonist), CpG oligodeoxynucleotides (TLR9 agonist), Tumor necrosis factor (TNF) and β-amyloid. Interestingly, downregulation of P2Y12 was accompanied with an upregulation of the Gs-coupled adenosine receptor A2A and thereby a potential shift in the cellular response to ATP and its derivates from Gi-mediated signaling to G_s-mediated signaling. Consequently, microglial processes retracted when ATP was applied indicating that cAMP evokes process retractions while inhibition of cAMP promotes or is required for process outgrowth. Increasing cAMP levels by application of forskolin triggered process retraction and significantly reduced ramification in untreated (P2Y12 expressing) and LPS treated microglia. This was observed both in rodent and in human microglia (Orr et al., 2009). The same laboratory later published that norephinephrine also caused retraction of

microglial processes presumably through stimulation of the G_s-coupled receptor β_2 (Gyoneva and Traynelis, 2013). Notably, ATP and ADP induced membrane ruffling and migration of cultured microglia (in Dunn chemotaxis chamber) was also blocked by increasing cAMP levels (by forskolin and dibutyryl cAMP) (Nasu-Tada et al., 2005).

Another measure of the effect of ATP on microglial purinergic receptors is by Ca^{2+} imaging. *In vivo* imaging of intracellular Ca^{2+} in microglia following introduction of the fluorescent Ca^{2+} indicator *(Oregon-Green-BAPTA)* OGB-1 by single cell electroporation revealed a pronounced Ca^{2+} signal in the microglia soma and in the processes as an immediate response to local ATP application and nearby neuronal damage (Eichhoff et al., 2011; Varvel et al., 2012; Brawek et al., 2014). A similar observation was recently made in acute brain slices from transgenic mice expressing GCaMP5 (a genetically encoded Ca^{2+} indicator based on the fusion of GFP and calmodulin) together with tdTomato (Gee et al., 2014). The Ca^{+} responses were transient (~30 sec) even during prolonged application of ATP (5 min). Stimulation of both P2Y and P2X receptors with selective agonists triggered Ca^{2+} signals while stimulation of the fractalkine receptor (CX3CR1) and metabotrophic glutamate receptors (with transACPD) did not. Depletion of intracellular Ca^{2+} stores (with thapsigargin) blocked P2Y-induced Ca^{2+} signals but not P2X-induced Ca^{2+} signals as expected. Surprisingly, no damage-induced Ca^{2+} signals in microglia were observed when neuronal damage was performed in the presence of ATP (after the ATP-induced Ca^{2+} signals had recovered). Importantly, neuronal damage did not induce a Ca^{2+} signal during thapsigargin treatment either (Eichhoff et al., 2011) supporting the idea that microglia respond to damage (laser-induced lesion) via selective activation of P2Y receptors. Whether, microglial Ca^{2+} responses are required for process motility has not yet been revealed.

Finally, local application of ATP induced a large inward current in retinal microglia (no outward current) (Fontainhas et al., 2011) and an inward current followed by an outward current carried by K^+ in CA1 microglia (Wu et al., 2007; Wu and Zhuo, 2008). In contrast, local application of glutamate, AMPA, or GABA did not trigger an electrical response in either retinal or CA1 microglia. Trains of high frequency stimulations of schaffer collateral also failed to evoke a current in CA1 microglia. Blockage of P2Y receptors (by reactive blue (RB)2) or K^+ channels (by Cs^+ in the patching pipette or by bath application of Quinine) abolished both the outward current and microglial process extension while application of P2X receptor antagonists did not have any effect. Application of a non-hydrolysable P2Y12 agonist (2-MeSADP) also triggered an outward current similar to application of ATP and ADP but only a reduced extension of microglial processes (Wu et al., 2007). Taken together, this indicate that the ATP-evoked outward current is mediated by activation of P2Y receptors, possibly P2Y12 but it also raising the question whether hydrolysis of ATP by endogenous ectonucleotidases are required for microglial process outgrowth.

1.2.6 Ectonucleotidases

The lifetime and the concentration of extracellular ATP and its derivates (ADP, AMP, and adenosine) are determined by the activity of membrane-anchored ectonucleotidases (Zimmermann, 1992; Robson et al., 2006). The brain expresses all known members of the ectonucleotidase families which simplified include; ectonucleoside triphosphate diphosphohydrolase (CD39) that hydrolyzes ATP/ADP to AMP and ecto-5'-nucleotidases (CD73) that hydrolyze AMP to adenosine. Additional families include purine nucleoside phosphorylase 'PNPase', nucleotide pyrophosphatase/phosphodiesterase 'NPP', and alkaline

phosphatases (Zimmermann, 2006). The halflife of ATP in the brain has been estimated to be as short as approximately 200 msec (Dunwiddie et al., 1997) and a similar rapid conversion of ATP has been reported in lung tissue (Ryan and Smith, 1971). Importantly, the activity of ectonucleotidases is dependent on the concentration of extracellular divalent cations (e.g. Ca^{2+} and Mg^{2+}). In the absence of a divalent cation, hydrolysis of radioactive ATP by B lymphocytes could hardly be detected, while addition of either 1.5 mM extracellular Ca^{2+} or Mg^{2+} stimulated a robust hydrolytic activity (Wang and Guidotti, 1996). Ramified microglia express high levels of CD39 while CD73 is only expressed upon activation (e.g. following facial nerve lesion and focal cerebral ischemia) (Kreutzberg et al., 1978; Schoen et al., 1992; Braun et al., 1997; Dalmau et al., 1998; Braun et al., 2000; Zhang et al., 2014b). Expression of CD39 allows microglia to generate a purinergic gradient with the highest concentration of ATP at the side of the cell that is facing the source of ATP release. One could therefore predict a spatial asymmetry in receptor activation that subsequently would be translated into a cellular polarity that rearranges the cells cytoskeleton. Astonishing, human neutrophils could detect as little as a 1% difference of an artificial gradient across their surface (Zigmond, 1977). Mechanistically, it has been demonstrated that AKT is spatially restricted to the area of highest G-protein coupled receptor activation. GFP-tagged AKT was used to visualize the spatial location of phosphorylated AKT in chemotaxing cells and it was demonstrated that as cells moved up a gradient of chemoattractant the GFP-tagged AKT translocated to the plasma membrane selectively to the side of the cell that faced the highest concentration of ligand (Meili et al., 1999). This suggests that activation of G protein-coupled receptors and all of the downstream responses triggered by chemoattractants are sharply localized at the leading edge of chemotaxing cells (Parent and Devreotes, 1999) and potentially at the leading edge of microglial processes extending towards the source of ATP

release. This will be investigated in chapter 1**.** As observed in migrating microglia, inhibition of PI3K (with LY 294002) blocked translocation of AKT in neutrophils and blockage of Rho GTPase activation (with clostridium difficile toxin A) abolished actin polymerization and morphological changes (Servant et al., 2000; Lin et al., 2012). This strongly supports the observation that Rac accumulates at the leading edge of microglial process extending toward the source of ATP in the zebrafish larvae (Li et al., 2012). Furthermore, CD39-deficient monocytes didn't migrate in an *in vivo* model of angiogenesis (Goepfert et al., 2001) and ATP-induced migration of cultured microglia from CD39 deficient mice was significantly impaired (Complement 5-induced migration was not altered in CD39 deficient microglia compared to wild type) (Farber et al., 2008).

1.2.7 Purinergic gradients for microglial chemotaxis

Intriguingly, a few studies have demonstrated that ectonucleotidases might regulate microglial migration and process extension towards a source of ATP in a more complex manner besides generating a concentration gradient of ATP across the cell. Ectonucleotidases do not only influence the lifetime and concentration of ATP, by hydrolysis of ATP to adenosine, they also generate the physiological ligand for P1 receptors resulting in a plausible co-activation of both P1 and P2 receptors. This might potentially allow the cell to amplify the external ATP signal and thereby improve its orientation and migration in chemotactic gradient fields. In retinal astrocytes, ATP sensitivity is increased by co-stimulation with adenosine (Newman, 2003) and ATP-mediated migration of human neutrophils requires co-stimulation of A3 and P2Y2 (Chen et al., 2006). In strong support of this concept, ATP did not trigger migration of microglia from CD39 deficient mice (which are incapable of hydrolyzing ATP) but migration could be restored by co-

application of ATP and adenosine (adenosine application without ATP did not induce migration). Application of ATP together with a soluble CD39 ectonucleotidase (apyrase) also triggered migration (Farber et al., 2008). Both A1 and A3 (Gi protein coupled receptors) were important for microglial migration as migration of microglia from A1 deficient mice was impaired (Farber et al., 2008) and both A1 and A3 antagonists (but not A2A) reduced ADP-induced migration (Ohsawa et al., 2012). The absence of CD39 was also found to reduce microglia / macrophage migration (accumulation) using *in vivo* models of focal brain ischemia, entorhinal cortex lesion, and facial nerve lesion (Farber et al., 2008).

Taken together these data indicate that co-activation of P1 (A1,3) and P2 (P2Y12) receptors are necessary for microglial migration and that ectonucleotidases are required for the generation of adenosine for P1 receptor stimulation. The same conditions appear to apply for microglial process outgrowth as application of the nonhydrolysable P2Y12 receptor agonist (2-MeSADP) only triggered a reduced extension of microglial processes, compared to application of ATP and ADP, while application of ADP together with either adenosine or a P1 receptor agonist enhanced 2-MeSADP-induced extension (quantified using a 3D collagen gel). Breakdown of adenosine by adenosine deaminase or application of P1 receptor antagonists (CGS-15943) also reduced ADP-evoked process extension. It was further demonstrated that the action of adenosine on process outgrowth was mediated through activation of the A3 receptor selectively as only A3 agonists in combination with 2-MeSADP would restore outgrowth and, on the other hand, only selective A3 receptor antagonists blocked ADP-evoked process extension (blockage of A1, A2A, A2B had no effect) (Ohsawa et al., 2012).

Importantly, the formation of adenosine from ATP requires the activity of at least two families of ectonucleotidases CD39 (for hydrolyzing ATP to AMP) and CD73 (for hydrolyzing

AMP to adenosine), while ramified resting surveiling microglia express high levels of CD39 they do not express CD73. It can be speculated that isolated and cultured microglia, as utilized in the studies referred to above, express CD73 (even though none of the studies mentioned above investigated it) but it would be intriguing to investigate whether ramified CD73 negative microglia *in vivo* or in acute brain slices also require co-stimulation of P1 receptors (like A3) and P2Y12 for process outgrowth. If that is the case, it opens up for a very fascinating scenario where microglia might plausibly be depending on other cell types for regulating their process dynamics. CD73 is expressed in different areas of the brain predominantly by oligodendrocyte precursors and oligodendrocytes (Kreutzberg et al., 1978; Fastbom et al., 1987; Zhang et al., 2014b) suggesting that they might play an unforeseen role in microglia process dynamics. Interestingly, CD73 expression in certain areas of the brain have been brought into question by immunolabeling studies that report that CD73 is not expressed in areas such as dentate gyrus and CA1 (Zimmermann et al., 1993). In that case adenosine would have to be generated extracellularly from ATP by an enzyme other than CD73 or generated intracellularly and released. It has previously been reported that neurons and astrocytes are capable of releasing adenosine (Wall and Dale, 2007) and the level of extracellular adenosine in hippocampal slices following electrical stimulation was not affected by inhibition of CD73 (with alpha, beta-methylene ADP) (Lloyd et al., 1993). Trapping intracellular adenosine (with L-homocysteine thiolactone) decreased both the basal and the evoked levels of extracellular adenosine by 85% while energy depletion, which enhances intracellular adenosine levels, resulted in a 16 fold increase in extracellular adenosine levels following stimulation (Lloyd et al., 1993). This implys that microglial process dynamics might be altered during the circadian rhythm where the concentration of extracellular adenosine can fluctuate up to eight fold (Radulovacki et al., 1984;

Huston et al., 1996; Strecker et al., 2000). However, recordings of field EPSP in the CA1 demonstrates that ATP gets hydrolyzed to adenosine (Lee et al., 1981; Cunha et al., 1994; Cunha et al., 1998)

Taken together the observations discussed above highlight that ATP-evoked microglia migration and process outgrowth requires the formation of a purinergic gradient generated by each individual microglia. This offers an explanation on how isolated microglia can extend their processes in a collagen gel without the presence of other cells or chemotaxins. It also offers a plausible explanation on how application of endogenous ATP and ADP can serve as potent inhibitors of direct process extension towards a laser-induced lesion (Davalos et al., 2005) as it can be assumed that application of ATP and ADP simply disrupt the gradient and divert the directed extension towards a lesion due to the formation of stronger gradients.

1.2.8 Alternatives to ATP-induced process outgrowth and migration

In addition to ATP-induced microglial process outgrowth serotonin, nitric oxide (NO), and fibrinogen have been reported to potentially exert a chemotaxic function for microglial processes. Serotonin has been reported to enhance lesion evoked microglial process extension in acute brain slices and ATP-induced migration in culture (Krabbe et al., 2012). Microglial serotonin receptor expression is not well established at P7 as microglia do not express mRNA for any of the 14 members of the serotonin receptors family analyzed (5-hydroxytryptamine (5-HT)) (Zhang et al., 2014b). However, mRNA for the G_i-protein coupled 5-HT5A receptor and the Gs-protein coupled 5-HT7 receptor have been identified in adult microglia (Krabbe et al., 2012). Interestingly, serotonin application exerted a similar effect on microglia migration in CD39 deficient mice as application of adenosine (Farber et al., 2008). Adenosine is known to promote

microglia migration by activation of Gi-coupled A1,3 receptors, thus it is tempting to speculate that serotonin might be activating the Gi-protein coupled 5-HT5A receptor in synergy with P2Y12 receptor activation to promote microglia migration.

Accumulation of microglia at the site of nerve crush injury in leeches was abolished by blocking ATP receptors but also by inhibition of NO synthesis (by L-NG-Nitroarginine Methyl Ester (L-NAME)) and by scavenging NO (with carboxy-2-phenyl-4,4,5,5-tetramethyl-imidazoline-1-oxyl-3-oxide (PTIO) and methylene blue) (Duan et al., 2003; Ngu et al., 2007; Duan et al., 2009). Investigations of the effect of NO on microglia process dynamics *in vivo* in the murine spinal cord have contributed conflicting findings. Microglial processes were attracted by an electrode containing an NO donor but bath application of the donor caused process retraction and the chemotaxis was also blocked by hydrolysis of ATP (with apyrase) (Dibaj et al., 2010). Thus further investigations are required to draw conclusions on the effect of NO on microglial process dynamics.

Microglia *in vivo* extended their processes towards an electrode containing fibrinogen (physiological concentration of fibrinogen in plasma) but not albumin and ACSF. Injection of wild type plasma (to mimic a hemorrhage) evoked accumulation of microglia at the injection site within three days while fibrinogen free plasma and plasma containing mutant fibrinogen that lacks the CR3 (CD11b/CD18) binding motif did not (Davalos et al., 2012). It would be very interesting to investigate whether fibrinogen can also trigger microglial process extension in P2Y12 deficient mice which would indicate that fibrinogen would be sufficient for recruitment of microglial processes to the site of hemorrhage even if P2Y12 receptors are blocked by anti-thrombotic treatment (as discussed earlier).

There a several other candidates for inducing chemotaxis for microglial migration however, ATP and its derivates a key factors within the CNS that alter microglial process dynamics and the mechanism of ATP release will therefore be the focus of the next section.

1.3 Mechanisms of ATP release

ATP does not cross the plasma membrane of viable cells and it might even seem counterintuitive that a cell would ever release their crucial energy source to signal to its surroundings as part of physiological regulated mechanism. Nonetheless, ATP release has been reported by a couple of different mechanisms especially via hemichannel opening. Hence, the following section will focus on the evidence for ATP release through hemichannels and how their opening is evoked followed by a few examples of alternative mechanism for ATP release such as lesion-evoked, vesicular, and other non hemichannel pore-forming proteins

1.3.1 Hemichannels

Two non-related families of proteins, connexin (Cx) and pannexin (Panx) have the property of forming hemichannels. The mammalian family of Panx consists of three genes (Panx1,2,3) while the Cx family includes more than 20 different genes. Open hemichannels serve as an aqueous conduit for relatively large intracellular molecules (molecular weight < 1 kDa) such as ATP (507.18 Da) and glutamate (147.13 Da) to enter the extracellular space. The average cytoplasmic concentration of ATP has been reported to range between 5 - 10 mM (Di Virgilio et al., 1998) thus opening of hemichannel is an extremely potent mechanism for release of ATP. A common approach for studying hemichannel opening is therefore the flux of hydrophilic fluorescent DNA binding dye molecules (<1 kDa) either by investigating dye uptake (influx)

following bath application of a dye or by examining dye loss (efflux) following loading of the cells of interest. All hemichannels are hexamers, with the exception of Panx2 that might also form octamers (Ambrosi et al., 2010). Each monomer is a four transmembrane spanning protein with cytoplasmic N- and C- terminals and one cytoplasmic loop and two extracellular loops (Milks et al., 1988; Yeager and Gilula, 1992; Unger et al., 1999; Wang and Dahl, 2010). Importantly, Cxs also form gap junctions with each other by connecting with a Cx hemichannel from an adjacent cell and thereby forming a direct link between the two adjacent cells. In contrast, there are no *in vivo* evidences that Panx forms gap junctions (Sosinsky et al., 2011). Although, Panx1 gap junctions have been reported in expression systems (i.e. *Xenopus* oocytes, C6 glioma cells, epithelial cells) (Bruzzone et al., 2003) (Lai et al., 2007) (Vanden Abeele et al., 2006) some of these data have since been questioned (Boassa et al., 2007). Unlike Cx, Panx1,3 are glycosylated (Penuela et al., 2007; Scemes et al., 2007) and hydrophilic glycans might presumably prevent Panx hemichannels from connecting with opposing hemichannels. Panx2 also contains a predicted glycosylation site, but whether the protein is glycosylated has not been established (Boassa et al., 2007; Boassa et al.,2008; Penuela et al., 2007; Penuela et al., 2009; Penuela, Gehi & Laird, 2012). Whether Panx2 forms a functional channel was also questioned until recently (Bruzzone et al., 2003) but it has now been revealed that Panx2 can form functional hemichannels in expression systems (i.e proteoliposome assay and *Xenopus* oocytes) (Ambrosi et al., 2010). Panx2 contributed to dye efflux in cultured neurons as depletion of both Panx1 and Panx2 was necessary for preventing dye efflux (Bargiotas et al., 2011)

Panx1,2 but not Panx3 are expressed in the CNS (Baranova et al., 2004) (Vogt et al., 2005). Panx1 protein expression has been reported throughout the brain particularly in CA1 pyramidal neurons where both the apical dendrites in the stratum radiatum as well as the somas were found

to be immunoreactive. Immunoelectron microscopy was applied to further conclude that Panx1 is prominent at the postsynaptic sites. The density of goldparticles was more than five times higher at the postsynaptic terminals than at the presynaptic terminals and Panx1 immunoreactivity co-localized with PSD-95 in hippocampal neurons both *in vitro* and *in vivo* (Zoidl et al., 2007). However, the selectivity of the antibody used to immunolabel Panx1 in this study (chicken anti-Px1, no. 4515) has more recently been brought in question because immunoreactivity with this, and many other commonly used Panx1 antibodies, was observed in Panx1 deficient mice (Bargiotas et al., 2011; Bargiotas et al., 2012). Only, the 'CT-395'antibody against mouse panx1 (raised in rabbit) did not show any immunoreactivity in Panx1 deficient mice (Penuela et al., 2007). However, immunolabeling with an antibody whose specificity has not been questioned also demonstrated Panx1 expression throughout the brain and reported that the Panx1 was expressed in the vast majority of pyramidal neurons but only in a small subset of interneurons. Interestingly, purkinje cells and pyramidal neurons were the only cells that displayed surface expression of Panx1 (Zappala et al., 2006).

Transcriptome analysis of P7 mouse brains indicated that neurons express Panx1,2 and Cx36; astrocytes express Cx26,43,45; oligodendrocytes (including precursors) express Panx1,2 and Cx26,30,32,47; and endothelial cells express Panx1 and Cx37,40,43,45. In contrast microglia have very low expression of Panx1,2 and do not express Cxs. Notably, astrocytic Cx43 (gene name; Gja1) > 500 FPKM and oligodendrocyte Cx32,47 (gene names; Gjb1 and Gjc2) was around 200 FPKM (Zhang et al., 2014b).

The conductance of a fully open single Cx hemichannel has been reported to be 220 pS, which is approximately twice that of a gap junction (Contreras et al., 2003; Saez et al., 2005). In contrast the unitary conductance of Panx1 hemichannels has been determined to be 550 pS (Bao

et al., 2004a). Panx hemichannels can also be distinguished pharmacologically from Cx hemichannels. Probenecid blocks Panx but not Cx and flufenamic acid (FFA) blocks Cx but not Panx (Lohman and Isakson, 2014). Carbenoxolone (CBX) is the most commonly used blocker of hemichannel opening and it blocks both Panx and Cx. Synthetic blocking peptides (also referred to as mimetic peptides) have been demonstrated extremely useful for targeting specific hemichannels. The short peptide ^{10}panx was found to be a potent inhibitor of Panx1 hemichannel opening. ^{10}panx shares the same 10 amino acids as one of Panx1's extracellular loops (Pelegrin and Surprenant, 2006). Blocking peptides with the same sequence as segments of the extracellular loop of Cx43 has also been shown to block the flux through this channel (Desplantez et al., 2012). Gap26 and Gap27 share the same amino acid sequences as found on the two extracellular loops and have been shown to block both Cx43 gap junctional communication and Cx43 hemichannel opening (Warner et al., 1995; Evans and Boitano, 2001; Wang et al., 2012). Gap19 on the other hand shares the same amino acid sequence as part of the intracellular loop and selectively inhibits Cx43 hemichannel opening without affecting Cx43 gap junctions. The interaction between the C-terminal of Cx43 and its intracellular loop plays a functional role for Cx43 hemichannel opening (Ponsaerts et al., 2010) and it has been demonstrated that GAP19 blocks Cx43 hemichannel opening by binding to its C-terminal (Boengler et al., 2013; Wang et al., 2013). Biotin-Gap19 was shown to bind to purified Cx43 C-terminal tails using a streptavidin-coated sensor chip and pre-incubation with a peptide corresponding to the active sequence of the C-terminal blocked the inhibitory effect of Gap19 (Wang et al., 2013). Gap19 prevented the opening of Cx43 hemichannels when Cx43 was expressed in C6 cells with an IC_{50} of approximately 50 μM. 250 μM of GAP19 blocked ~97% of ATP release through Cx43 hemichannels while 400 μM of Gap19 did not affect gap junction

(measured as junctional conductance in Cx43 expressing cell pairs). 250 μM of Gap19 significantly improved adult mouse cardiomyocyte viability following ischemia/reperfusion both *in vitro* and *in vivo* compared to mutated Gap19 (Gap19 reduced swelling of cardiomyocytes *in vitro* and infarct area *in vivo*). GAP19 was administered intravenous as 25 mg/kg which were estimated to correspond to ~250 μM (Wang et al., 2013).

1.3.2 ATP release through opening of pannexin hemichannels

Multiple lines of evidence support the role of Panx1 in ATP release in a vast variety of cells. The most convincing proof that ATP is released through opening of Panx1 hemichannels is the work by Dr. Ravichandran's laboratory. The lab demonstrated that apoptotic Jurkat cells (induce by anti-Fas or UV exposure) released ATP and UTP through caspase-mediated opening of Panx1 to attract immune cells. Inhibition of caspase activity (with zVAD-fmk) and hydrolysis of ATP (by apyrase) did not block apoptosis but prevented migration of immune cells towards apoptotic cells (Elliott et al., 2009). CBX, probenecid, small interfering (si)RNA against Panx1, and a novel Panx1 inhibitor, trovafloxacin, all inhibited the release of ATP and UTP without affecting apoptosis (Chekeni et al., 2010; Poon et al., 2014). Like ATP, UTP is an important purinergic receptor agonist for microglia. *In vivo* microdialysis has revealed that UTP is released following KA-induced damage and that UTP stimulation of microglial P2Y6 receptors promoted phagocytosis (Koizumi et al., 2007). Jurkat cells with stable overexpression of Panx1 showed Panx1 siRNA-sensitive increase of ATP and UTP release. Apoptosis was accompanied by a CBX-sensitive current that was significantly enhanced (from 500 to 2000 pA) in cells overexpressing Panx1. Profound increases in caspase activity and Panx siRNA-sensitive dye uptake was also observed in apoptotic cells. A thorough screen revealed that Panx1 was

efficiently cleaved by caspase 3 as two hours after induction of apoptosis both procaspases and uncleaved Panx1 were undetectable (by western blotting). CBX did not block cleavage of Panx1 but inhibition of caspases (with zVAD) did. Panx1 has two cleavage sites one in the intracellular loop and one at the C-terminal and only cleavage of the C-terminal site evoked the CBX-sensitive current and ATP release. Mutating the C-terminal cleavage site did not block apoptosis but abolished the CBX-sensitive current and ATP release (Chekeni et al., 2010). To further validate the cleavage-mediated activation of Panx1 a human Panx1 variant was generated in which the C-terminal caspase cleavage site was substituted with a tobacco etch virus protease site. This Panx1 variant was expressed in different expression systems and cleavage of this novel site (by application of tobacco etch virus proteases inside the patch electrode) evoked a CBX-sensitive current (Sandilos et al., 2012).

Panx1 is ubiquitously expressed and has been identified in brain, heart, skeletal muscle, skin, testis, ovary, placenta, thymus, prostate, lung, liver, small intestine, pancreas, spleen, colon, blood endothelium and erythrocytes (Baranova et al., 2004; Penuela et al., 2013). Thus, since the first demonstration of Panx-1 mediated ATP release, following depolarization of Panx1 expressing oocytes (Bao et al., 2004a), Panx1-mediated ATP release has been demonstrated from various different cell types including T cells, taste buds, skeletal muscles, airway epithelial cells, erythrocytes, smooth muscle cells, pituitary cells, and endothelial cells. Stimulation of T cells with anti-CD3 antibody triggered CBX-sensitive release of ATP and application of ^{10}panx was found to retain a higher level of intracellular ATP (Schenk et al., 2008). Using transfected CHO cells as biosensors it was shown that gustatory stimulation caused CBX-sensitive release of ATP in mouse taste buds (Huang et al., 2007; Huang et al., 2009). Electrical stimulation (45 Hz, 400 1-ms pulses) of rat skeletal myotubes triggered ^{10}panx-sensitive ATP release which peaked after

3 min but stayed elevated for 30 min (Buvinic et al., 2009). Hypotonic-evoked ATP release from rat pituitary cells, airway epithelial cell, and isolated tracheas were blocked by CBX, probenecid, and siRNA against Panx1 (but not FFA) (Li et al., 2011b; Li et al., 2011a). ATP release was enhanced by overexpression of Panx1 and did not occur in tissue from (Ransford et al., 2009; Seminario-Vidal et al., 2011). Probenecid and ^{10}panx, as well as mefloquine (another well characterized Panx1 blocker (Iglesias et al., 2009)) also blocked ATP-mediated constriction of resistance arteries. Electroporation with siRNA against Panx1 also decreased the constriction while electroporation of Panx1-green fluorescent protein enhanced constriction (Billaud et al., 2011). Exposure of human erythrocytes to different oxygen levels demonstrated an inverse relationship between oxygen levels and ATP release which was also significantly reduced by CBX, probenecid, and ^{10}panx (Sridharan et al., 2010), Finally, thrombin-evoked ATP release from human umbilical vein endothelial cells was blocked by CBX and shRNA against Panx1 (Godecke et al., 2012).

Activation of NMDAR is one of the most well-established triggers of Panx1 hemichannels opening in the CNS. Hence NMDAR will be introduced first followed by a discussion about NMDA-evoked opening of neuronal hemichannels.

1.3.3 NMDA receptors

NMDAR are ionotropic glutamate receptors (permeable to Na^+, K^+, and Ca^{2+}) that are present at excitatory synapses where they play an important role in mediating synaptic transmission, plasticity and excitotoxicity. They are regulated by unique features such as the requirement for co-activation by extracellular glycine and a voltage-sensitive block by extracellular Mg^{2+}. Several distinct NMDAR subtypes have been identified, GluN1, GluN2A-D,

and GluN3A,B (Dingledine et al., 1999; Cull-Candy et al., 2001; Collingridge et al., 2009; Traynelis et al., 2010) which interact with various intracellular signaling molecules associated with the postsynaptic density. Functional NMDAR are tetra-heteromers (possibly pentamers) that are composed of two obligatory GluN1 subunits (containing the glycine-binding domain) in combination with at least one GluN2 subunit (containing the glutamate-binding domain). GluN3 is not required in functional NMDAR but can co-assemble with GluN1, N2 complexes (Das et al., 1998; Perez-Otano et al., 2001). At resting membrane potentials, NMDAR containing GluN2A or GluN2B subunits are blocked by extracellular Mg^{2+} (Villarroel et al., 1995; Premkumar and Auerbach, 1996; Wollmuth et al., 1998) and depolarization e.g. by activation of AMPA receptors to relieve the voltage-dependent Mg^{2+} block, is therefore required to allow the flux of ions through the NMDAR. NMDAR containing NR2C,D are less sensitive to extracellular Mg^{2+} (Monyer et al., 1992; Ishii et al., 1993; Schwartz et al., 2012). With the exception of the cerebellum GluN2A,B are the predominant GluN2 subunits in the majority of the brain especially in the hippocampus. GluN2B expression is higher than GluN2A in the neonatal brain but over the course of development GluN2A expression increases while GluN2B expression decline (Monyer et al., 1994; Paoletti, 2011). GluN2A and GluN2B containing NMDAR can functionally be distinguished by selective non-competititive inhibitors e.g. Ifenprodil (Williams, 1993; Tovar and Westbrook, 1999), CP 101,606 (Brimecombe et al., 1998) and Ro 25-6981(Fischer et al., 1997) display a higher selectivity for GluN2B containing NMDAR.

Interestingly, glial cells have also been reported to express NMDAR. Transcriptome analysis (P7 mice) indicated that microglia might have very low expression of Grin1,2a (gene names for GluN1,2A), astrocytes express Grin1,2c,3a, and oligodendrocytes (including precursors) express

Grin1,2a,3a (Zhang et al., 2014b). This is further supported by several studies that show NMDAR subtype expression on both astrocytes (Schipke et al., 2001; Krebs et al., 2003; Lalo et al., 2006; Lee et al., 2010) and oligodendrocytes (Karadottir et al., 2005; Salter and Fern, 2005; Micu et al., 2006; Cao and Yao, 2013). Evidence of the presence of functional NMDAR in cultured microglia also exists (Liang et al., 2010; Murugan et al., 2011). Cultured microglia have been reported to express mRNA for GluN1, N2A-D, and N3A and treatment for 12-24 hours with 300 µM of NMDA (in Mg^{2+}-free solution with D-serine) resulted in the production of several proinflammatory cytokines (e.g. IL-1β, interferon γ, and TNFα), and reactive oxygen species which was reduced when NMDA was applied together with MK801. The supernatant from NMDA treated microglia (300 µM for 1h) triggered excitotoxicity and death when applied to neuronal cultures. Surprisingly, less than 12% of microglia showed Ca^{2+} responses to NMDA (300 µM NMDA for more than 2 min, cell were loaded with FURA 2-AM) (Kaindl et al., 2012). Both mRNA and protein expression have also been observed for NR1, and NR2A-C in amoeboid microglia / macrophages 1-3 days after hypoxic exposure of one day old rats (NR3 was upregulated after 7-14 days) (Murugan et al., 2011). While only NR1 (not NR2A,B) was expressed 3-7 days after ischemia in adult rats (Gottlieb and Matute, 1997). None of these studies reported a constitutive expression of NMDAR subunits on microglia. However, one study has provided evidence that microglia might express NMDAR in the healthy brain. NR1 immunolabeling colocalizes with both $lectin^{+}$ and $Iba1^{+}$ microglia in tissue from P5 and P56 mice and $CD68^{+}$ microglia in fetal and adult human tissue. Microglial NR2B,D expression was also reported in infant mouse tissue. Functionally, depletion of CNS expression of NR1 selectively in microglia (conditional NR1 $LoxP^{+/+}$ LysM $Cre^{+/-}$ mice) resulted in reduction in lesion size compared to wild type mice in a model for excitotoxic brain damage (introduced by

intracerebral injection of a glutamate analogue, ibotenate in P10 and P56 mice) and mechanical head trauma (in P7 mice) (Kaindl et al., 2012). Local application of glutamate *in vivo* triggered a Ca^{2+} response in a subset of cortical microglia (2 out of 14 cells, similar to what was reported in cultured microglia following NMDA application). Application of a metabotropic glutamate receptor agonist (trans-ACPD) did not trigger a Ca^{2+} response under these conditions indicating that the glutamate potentially could act on microglial NMDA or AMPA receptors (Eichhoff et al., 2011). However, it could not be ruled out that glutamate is acting on ionotropic receptors on another cell type that then in turn triggered a secondary Ca^{2+} response in microglia e.g. as a result of glutamate-evoked ATP release. Hence, it would be interesting to repeat these experiments in the presence of a purinergic receptor antagonist or apyrase. Notably, in several other studies local application of glutamate evoked a current in voltage clamped neurons but not in voltage clamped microglia. ATP on the other hand evoked a current in microglia (Wu et al., 2007; Wu and Zhuo, 2008; Fontainhas et al., 2011) questioning whether glutamate and NMDA application has a direct effect on microglia.

1.3.4 NMDA-evoked opening of neuronal Panx1

Multiple brief applications of NMDA (100 µM, 10 sec duration at 1 min intervals) and a prolonged application of NMDA (100 µM, for 10-15 min) triggered a CBX-sensitive current in acutely isolated hippocampal neurons. Activation of NMDAR on neurons loaded with the Panx1 permeable dye, calcein (623 Da) together with a Panx1 non-permeable version of the calcium indicator Fluo-4, elegantly revealed an elevation in intracellular Ca^{2+} accompanied by efflux of calcein upon NMDAR activation. Calcein efflux was blocked by the presence of high extracellular Mg^{2+} (which blocks NMDAR), the Panx1 blocking peptide (^{10}panx), and siRNA

against Panx1. Application of NMDA also triggered a dramatic uptake of the Panx1 permeable dye, SR101 (607 Da) in CA1 neurons in acute brain slices. No NMDA-evoked SR101 uptake was observed in the presence of ^{10}panx, and the NMDAR blocker APV. Finally, removing Mg^{2+} (and adding 5 mM K^{+}) triggered seizure-like bursting in hippocampal neurons which were reduced by application of ^{10}panx (Thompson et al., 2008). In agreement with NMDA-evoked opening of Panx1, ischemic conditions, which are known to implicate activation of NMDAR (Lee et al., 1999; Rossi et al., 2000), also triggered opening of Panx1 in hippocampal neurons. Oxygen and glucose deprivation of acutely isolated hippocampal neurons evoked a CBX-sensitive current which recovered when oxygen and glucose were re-introduced. Removal of oxygen and glucose also evoked uptake of SR101 by cortical neurons which was blocked by CBX (Thompson et al., 2006). In agreement with this, anoxia depolarization evoked a large inward current in patch clamped CA1 pyramidal neurons in acute brain slices. This depolarization was significantly reduced by ^{10}panx, antibodies against Panx1 (included in the patch electrode), probenecid, and mice with reduced neuronal expression of Panx1 (flxPanx1-cre, reduced Panx1 expression was validated by IHC). Importantly, NMDAR and ischemic-induced opening of Panx1 was not caspase dependent (as observed during apoptosis) as it still occurred in the presence of zVAD-fmk. Instead, activation of Src family kinases was found to mediate NMDAR-evoked opening of Panx1. Anoxia is known to activate kinases of the Src family (Takagi et al., 1997; Takagi et al., 1999) and Src-mediated opening of Panx1 has previously been proposed (Iglesias et al., 2008). Inhibition of Src during anoxia prevented Panx1 opening and targeting Src's phosphorylation site on Panx1 (with an interfering peptide) attenuated the anoxia-induced ^{10}panx-sensitive current. Importantly, ischemia-induced opening of Panx1 was entirely NMDAR dependent as the NMDAR antagonist (2 R)-amino-5-

phosphonovaleric acid; (2 R)-amino-5-phosphonopentanoate (APV) resulted in a similar attenuation of the depolarization as APV together with ^{10}panx (Weilinger et al., 2012). Taken together, these data convincingly demonstrate that activation of NMDAR on CA1 pyramidal neurons either by application of exogenous NMDA or by an ischemic insult triggers opening of Panx1 hemichannels in these neurons.

Interestingly, activation of neuronal NMDAR is known to promote production of NO by stimulation of neuronal nitric oxide synthase (nNOS) (Christopherson et al., 1999; Sattler et al., 1999; d'Anglemont de Tassigny et al., 2007), and ischemia-induced NO production has been shown to potentially enhance Panx1 opening via NO-mediated S-nitrosylation of Panx1. Panx1 has two cysteine residues in its cytoplasmic C-terminal (which is also conserved in Cx) which potentially can be S-nitrosylated (Yen and Saier, 2007). Ischemia-induced dye efflux from cultured hippocampal neurons was shown to be NO-dependent and could be blocked by inhibition of S-nitrosylations (Zhang et al., 2008). In support of these observations, NMDAR-induced NO production by nNOS during cerebral ischemia in the CA1 promoted S-nitrosylation and activation of Src while inhibition of nNOS blocked it. Src kinases also phosphorylate NMDAR and thereby potentiate their responses (Yu et al., 1997; Salter and Pitcher, 2012; Tang et al., 2012).

A few studies have reported Panx1-mediated effects on microglial process dynamics. In retinal explants application of AMPA triggered microglial process outgrowth that was blocked by suramin (a non-selective purinergic receptor blocker) and probenecid. Suggesting that activation of AMPAR evoked ATP release through opening of Panx1 (Fontainhas et al., 2011). However, AMPAR activation was not performed in the presence of NMDAR blockers thus it could not be ruled out that the proposed opening of Panx1 hemichannels was evoked by

NMDAR stimulation secondary to AMPA-induced depolarization. Several studies have also reported that suramin inhibits glutamatergic synaptic transmission (Motin and Bennett, 1995; Gu et al., 1998), AMPAR and NMDAR mediated currents (Nakazawa et al., 1995; Ong et al., 1997; Peoples and Li, 1998), and binding of radioligands to both AMPAR and NMDAR (Balcar et al., 1995; Suzuki et al., 2004) but not kainate receptors (Ong et al., 1997). Kainate was reported to also trigger microglial process outgrowth (Fontainhas et al., 2011) thus it would have been interesting to see if suramin also blocked kainate-evoked microglial process outgrowth under these experimental conditions. Additional experiments with other purinergic blockers would also have been informative. Probenecid is a potent blocker of Panx1 but it also has a lot of other targets, hence additional experiments (e.g. blocking Panx1 with CBX or ideally performing the experiments in retina explants from Panx1 deficient mice) would be required to conclude that the AMPA-evoked changes observed in microglia morphology are due to ATP release via opening of Panx1 hemichannels.

In zebrafish larvae repetitive glutamate uncaging triggered a probenecid and CBX-sensitive current in tectal neurons (Li et al., 2012). This is in perfect agreement with the observation that multiple brief applications of NMDA triggered a CBX-sensitive current in hippocampal neurons in the rodent (Thompson et al., 2008). Importantly, the repetitive glutamate uncaging also triggered microglial process extension and the formation of bulbous tips which was significantly reduced by suramin, apyrase, probenecid, CBX, and knock down of Panx1 with two different morpholino constructs (Li et al., 2012). Taken together, this indicates that opening of neuronal Panx1, by repetitive stimulation of neuronal NMDAR, is a powerful mechanism for releasing ATP and a potential functional means for neurons to communicate with microglia and evoke

directed extension of microglial processes towards NMDAR and Panx1 containing neuronal dendrites.

1.3.5 ATP release through opening of Cx43 hemichannels

Cx 43 is the most prominent and most studied Cx protein in relation to gap junctions and potential for hemichannel opening and will be the focus of this section. Astrocyte expression of Cx43, Cx30, Cx26, Cx40, and Cx45 has been reported (Dermietzel et al., 1989; Nagy et al., 1999; Dermietzel et al., 2000). However, double knockdown of Cx30 and Cx43 abolished functional gap junction-mediated communication (Wallraff et al., 2006; Rouach et al., 2008) demonstrating that Cx30 and Cx43 are the main functional Cx in astrocytes. Astrocytic end-feet ensheathe blood vessels in the brain and are believed to provide structural integrity to the cerebral vasculature. A striking characteristic of astrocyte endfeet is their enrichment of Cx43 and Cx30 (co-immunolabeled with astrocytic markers, glial fibrillary acidic protein (GFAP), aquaporin4, and S-100β and the vascular marker laminin) (Yamamoto et al., 1990; El-Khoury et al., 2006; Ezan et al., 2012). Mice with selective depletion of astrocytic Cx30 and Cx43 display astrocytic endfeet edema and a weakened blood-brain barrier (BBB) indicating that astrocytic Cx are necessary for maintaining BBB integrity (Ezan et al., 2012). Traditionally, the stimuli required for opening of Cx43 hemichannels were non-physiological as it required depolarization of membrane potentials to around 60 mV which would make opening in non-excitable cells like astrocytes virtually impossible. However, hemichannel opening at resting membrane potentials are now broadly accepted (Contreras et al., 2003; Retamal et al., 2007; Orellana et al., 2011a; Orellana et al., 2011b).

Removal of extracellular Ca^{2+} is known as a reliable method to trigger opening of Cx43 hemichannels and it has been extensively investigated both in expression systems (i.e. HEK cells, HeLa cells, osteoblasts, and gliomacells), in cultured astrocytes and in astrocytes *in vivo*. At a holding potential of -80 mV, an inward current was triggered after removal of extracellular Ca^{2+} in HEK293 cells expressing Cx43. Re-introduction of Ca^{2+} reversed the current. Consistent with the known size selectivity of Cx hemichannels (< 1 kDa), removal of extracellular Ca^{2+} also triggered size-selective dye uptake. The Cx permeable dyes, calcein (660 Da) or propidium iodide (PI) (668 Da) were gradually taken up over time after removal of extracellular Ca^{2+} while the Cx non-permeable dye, dextran-fluorescein (1.5-3 kDa) was not (John et al., 1999; Kondo et al., 2000). Replacing Ca^{2+} with the Ca^{2+} chelater, ethylene glycol tetraacetic acid (EGTA) (2 mM) and elevating intracellular Ca^{2+} levels further enhanced the probability of opening of Cx43 hemichannels when expressed in HeLa cells (Contreras et al., 2003; Schalper et al., 2008; Wang et al., 2012). These data were supported by the finding that influx of lucifer yellow and Mn^{2+} into human osteoblasts transfected with Cx43 (measured as manganese-induced quenching of fura-2) occurred in 30-40% of transfected cells even when extracellular Ca^{2+} was removed. In contrast only 2-5% of cells took up Mn^{2+} and lucifer yellow in the presence of extracellular Ca^{2+} (2 mM) or the hemichannel blocker 18 β-glycyrrhetinic acid (Romanello and D'Andrea, 2001). Expression of Cx43 in C6 gliomacells demonstrated uptake of lucifer yellow and efflux of calcein (as previously observed) as well as efflux of ATP (Stout et al., 2002; Wang et al., 2013).

Removal of divalent cations triggered dye loading of Lucifer yellow (452 Da) in cultured hippocampal rat astrocytes. Restoring divalent cations or adding CBX blocked dye uptake in a dose-dependent manner. Uptake was also blocked by the Cx blocker FFA (Ye et al., 2003). Reducing extracellular Ca^{2+} has also been shown to trigger Cx43-mediated ATP release in acute

hippocampal brain slices from juvenile mice. The photolabile Ca^{2+} buffer, Diazo-2 was used to reduce $[Ca^{2+}]_{ex}$ (by local application of light pulses) in acute mouse hippocampal brain slices. The reduction of $[Ca^{2+}]_{ex}$ was pulse-dependent (detected by Ca^{2+} sensing electrodes) and multiple pulses reduced $[Ca^{2+}]_{ex}$ by 0.5-0.7 mM which were sufficient to trigger ATP release (Torres et al., 2012). One concern regarding quantifying $[Ca^{2+}]_{ex}$ is that changes in extracellular space might sway the measurements. ATP was detected via *in situ* bioluminescence imaging and no bioluminescence was observed in the absence of Diazo-2 (excluding chelation of Ca^{2+}) or luciferase (excluding ATP-mediated bioluminescene). In addition, reducing $[Ca^{2+}]_{ex}$ also evoked an increase in intracellular Ca^{2+} in astrocytes loaded with a Ca^{2+} indicator (Rhod2-AM) supposedly due to ATP-induced activation of astrocytic purinergic receptors as it was blocked by the suramin, PPADS, and RB2. Importantly, ATP release was abolished by CBX (50 µM) and in brain slices from transgenic mice deficient for Cx30 and astrocytic Cx43. ATP release was not inhibited in slices from Cx30 deficient mice (Torres et al., 2012). Cx43 deficiency is lethal at birth and was therefore conditionally deleted in deleted in astrocytes by induction of GFAP driven Cre recombinase (Theis et al., 2003). Additionally, Cx43 deletion is compensated for by up-regulation of Cx30 (Lin et al., 2008) thus floxed astrocytic Cx43 was introduced in Cx30 knock out (KO) mice. Cx43-mediated ATP release from astrocytes was further proven by demonstrating that the duration of astrocytic Ca^{2+} signals was increased in brain slices from transgenic mice with increased number of open Cx43 hemichannels (introduced by an astrocyte-targeted point mutation in Cx43, Cx43G138R (Dobrowolski et al., 2008)). Intracellular Ca^{2+} was measured in astrocytes at 50, 100, and 150 µm away from the site of photolysis of Diazo, where $[Ca^{2+}]_{ex}$ was not altered, thus it can be assumed that the increase in astrocytic Ca^{2+} is due to activation of purinergic receptors (either P2Y-mediated release of Ca^{2+} from intracellular stores

or P2X-mediated Ca^{2+} influx) rather than Ca^{2+} influx through opening of Cx43. Enhanced neuronal activation is known to trigger a reduction in $[Ca^{2+}]_{ex}$ (due to influx of Ca^{2+} through NMDAR) and both glutamate uncaging (using MNI-Glu) and high frequency stimulation caused a similar reduction in $[Ca^{2+}]_{ex}$ and consequently ATP release, as photolysis of Diazo-2, which were inhibited by blockage of AMPAR and NMDAR (by CNQX and APV respectively) (Torres et al., 2012).

Opening of astrocytic Cx43 hemichannels should also allow for the efflux of glutamate which is more than 3 times smaller than ATP and is abundant inside astrocytes. The intracellular concentration of astrocytic glutamate has been estimated to be 3-10 mM (Schousboe and Divac, 1979; Sonnewald et al., 2002). Intriguingly, lowering $[Ca^{2+}]_{ex}$ was also found to evoke CBX sensitive release of glutamate from cultured astrocytes independently of ATP as it was unaffected by blockage of purinergic receptors (with suramin and PPADS) (Ye et al., 2003). This indicates that both ATP and glutamate release occurs through opening of Cx43 hemichannels. Glutamate release was independent of intracellular Ca^{2+} as chelating intracellular Ca^{2+} (with BAPTA-AM) or depleting intracellular Ca^{2+} stores (with thapsigargin) did not affect glutamate release. Glutamate was also released from acutely isolated mouse optic nerves when exposed to divalent cation free solution containing EGTA and this release was blocked by CBX (Ye et al., 2003).

Similar to Panx1, Cx43 also contains two cysteine residues in its cytoplasmic C-terminal (Yen and Saier, 2007) and nitrosylation of Cx43 was also found to increase opening probability of Cx43 hemichannels in astrocytes. Application of S-Nitrosoglutathione evoked S-nitrosylation of Cx43 and increased ethidium bromide uptake, which was blocked by different reducing agents i.e. glutathione, trolox and dithiothreitol (Retamal et al., 2006). dithiothreitol did not affect the

rate of ethidium bromide uptake in HeLa cells that expressed a mutated form of Cx43 which lacks cytoplasmic cysteines (Saez et al., 2005).

On the other hand, phosphorylation of specific Cx43 serine or tyrosine residues decreased its opening probability (Lampe and Lau, 2000; Harris, 2001). Phosphorylation of Cx43 by protein kinase C abolished dye flux in oocytes (Bao et al., 2004b) and Cx43 hemichannel opening by low $[Ca^{2+}]_{ex}$ was blocked by activation of protein kinase C (Li et al., 1996; Liu et al., 1997). Expression of Cx43 with a mutated protein kinase C phosphorylation site increases opening probability (Bao et al., 2004b). The effect of dithiothreitol was not associated with phosphorylation (Saez et al., 2005).

Interestingly, only 10% of Cx43 in cultured astrocytes was expressed on the surface (could be biotinylated) under normal conditions while induction of free radicals doubled the surface expression of Cx43 and led to dephosphorylation of half of the Cx43 proteins thereby leading to enhanced opening probability (Retamal et al., 2006).

1.3.6 Lesion-induced ATP release

Damage to the cell membrane would evoke ATP efflux and laser-evoked lesions of cell membranes have become an established approach to trigger ATP-induced microglial process extention. However, it might seem unlikely that ATP efflux from damaged cells can sustain a gradient of ATP for minutes. This next section therefore discusses the sparse indications that lesion-induced microglial process outgrowth is more complex than ATP efflux from damage cell.

Lesion-induced microglial process extension in the zebrafish larvae was found to be dependent on neuronal NMDAR-mediated Ca^{2+} waves leading to release of ATP. The lesion-

induced Ca^{2+} waves were independent of ATP while process extension was blocked when the wave was abolished by either chelating extracellular Ca^{2+} (with EGTA) and by inhibition of NMDAR. These data indicate that glutamate efflux from the damaged area triggers the propagation of a Ca^{2+} wave by activation of NMDAR that in turn triggers ATP release. Depleting intracellular Ca^{2+} by thapsigargin did not affect the Ca^{2+} wave supporting the prediction that the Ca^{2+} wave is mediated by influx of extracellular Ca^{2+} through NMDAR. Uncaging of NMDA mimicked the effects of a lesion and triggered both a Ca^{2+} wave and microglial process extension. Process extension, but not the Ca^{2+} wave, was blocked by CBX and FFA indicating that ATP is released through opening of a hemichannel (Sieger et al., 2012).

Lesion-induced microglial process extension in the fundus of the eye has also been reported to cause a Ca^{2+} wave in astrocytes around the lesion site that lasted up to 30 min. However, this Ca^{2+} wave, in contrast to the wave in zebrafish larvae, was reported to be blocked by chelation of intracellular Ca^{2+} (with BAPTA) which supposedly also blocked microglial process extension.

It has also been shown both in vivo and in acute brain slices that microglial process extension to 'non-hydrolysable' ATP analogues (ATPγS, 2-MeSADP, and AMPPNP) is blocked by application of apyrase indicating that ATP-induced ATP release might be required for process extension (Davalos et al., 2005; Wu et al., 2007). Additionally, data from cultured microglia indicated that ATP induced ATP release is important for long-range extracellular signaling and that extracellular ATP might trigger ATP from microglia themselves through Ca^{2+}-dependent lysosomal exocytosis. Microglia migration triggered by a non-hydrolysable ATP analogue (ATPγS) was also blocked by apyrase (Dou et al., 2012). However, it is questionable whether apyrase and potentially endogenous ectonucleotidases are capable of hydrolyzing these ATP analogues (Picher et al., 1996; Burton et al., 2003). Adenosine has an inhibitory effect on field

EPSPs and application of ATPγS had the same inhibitory effect on EPSPs as ATP indicating that ATPγS gets hydrolyzed to adenosine as efficiently as ATP. Furthermore, the inhibitory effect of ATPγS was decreased by blocking the effect of CD39, by application of denosine deaminase (which converts adenosine into inosine), and by blocking A1 receptors while the inhibitory effect of ATPγS was increased in the presence of a adenosine uptake inhibitor (Cunha et al., 1998). As discussed previously the formation of a purinergic gradient is crucial for process outgrowth and no controls were included to validate that these ATP analogues did not get hydrolyzed by apyrase. Several studies have also suggested that ATP-induced microglial process extension require ATP-induced ATP release via hemichannel opening because process extension to laser-induced lesions and local ATP applications is blocked by the hemichannel blocker FFA (Davalos et al., 2005; Kim and Dustin, 2006; Wu et al., 2007). However, FFA is also known as a potent Cl^- channel blocker (White and Aylwin, 1990; Weber et al., 1995) and it has been determined that process outgrowth requires functional Cl^- channels (Hines et al., 2009) which might likely be an alternative explanation of why FFA blocked process outgrowth. We have performed pilot experiments using the potent hemichannel blocker CBX and we observed that neither lesion-induced microglial process extension nor ATP-induced process outgrowth was blocked in acute brain slices (data not shown).

1.3.7 Vesicular release of ATP

Neuronal Ca^{2+} dependent vesicular release of ATP has been demonstrated from whole-brain synaptosomes (White 1978) and several types of brain slice preparation, including hippocampal slices (Wieraszko et al. 1989; Cunha et al. 1996). Furthermore, ATP is taken up by isolated synaptic vesicles (Gualix et al. 1999). The vesicular nucleotide transporter (VNUT) also referred

to as *(solute carrier family 17 member 9)* SLC17A9 is the key transporter of ATP into vesicles in the brain (Sawada et al., 2008). It's highly expressed in the brain in particular in hippocampus, cortex and olfactory bulb. IHC and postembedding immunogold labeling revealed that VNUT co-localized with synaptic vesicles in both excitatory and inhibitory synapses in the hippocampus (Larsson et al., 2012). ATP release from hippocampal neurons evoked by depolarization was blocked by siRNA knockdown of VNUT (Sawada et al., 2008; Larsson et al., 2012) and did not occur in hippocampal neurons from VNUT deficient mice (Sakamoto et al., 2014). Blockage of ATP release from pancreatic cells, intestinal L cells, and airway epithelia was also significantly inhibited by siRNA knockdown of VNUT (Geisler et al., 2013; Sesma et al., 2013; Haanes et al., 2014; Harada and Hiasa, 2014) and ATP release from pancreatic islets was absent in VNUT deficient mice (Sakamoto et al., 2014). ATP uptake into VNUT expressing liposomes was blocked by DIDS (*4,4'-Diisothiocyano-2,2'-stilbenedisulfonic acid*, IC_{50} = 2.5 μM) and Evans blue (IC_{50} = 40 nM) (Sawada et al., 2008). Notably, expression of VNUT has also been reported in glial cells and VNUT-mediated ATP-release has been reported in cultured astrocytes (Oya et al., 2013), microglia (Imura et al., 2013; Shinozaki et al., 2014) and macrophages (Sakaki et al., 2013).

Interestingly, the synaptic vesicular protein SLC10A4, (Splinter et al., 2006; Geyer et al., 2008; Burger et al., 2011) also referred to as vesicular aminergic-associated transporter (VAAT) (Zelano et al., 2013; Larhammar et al., 2014; Patra et al., 2014), might potentially play a role in vesicular uptake of ATP. There is no direct evidence that VAAT-mediated ATP released occurs but VAAT has been demonstrated to be a transporter of negatively charged molecules (Larhammar et al., 2014) and depletion of VAAT was found to alter transmission in the

neuromuscular junction (Patra et al., 2014) where vesicular co-release of ATP together with acetylcholine is well known (De Lorenzo et al., 2006).

1.3.8 Non hemichannel pore-forming proteins

Certain P2X receptors have been reported to have the unique capacity of enlarging their pore to allow the permeability of molecules of up to 800 Da (Surprenant et al., 1996; Rassendren et al., 1997; Virginio et al., 1997). This property of pore dilation has been shown for P2X2,4,7 (Fujiwara and Kubo, 2004; Chaumont and Khakh, 2008; Bernier et al., 2012) primarily by investigations of dye up take but whether ATP efflux occurs through these pores remain questionable. However, P2X7 activation have been shown to be associated with the recruitment of pore-forming molecules such as Panx1 (Pelegrin and Surprenant, 2006; Locovei et al., 2007; Iglesias et al., 2008) and this ATP-mediated opening of large P2X pores is potentiated by removal of divalent cations (Trezise et al., 1994; Bernier et al., 2012).

Another interesting pore forming protein is the calcium homeostasis modulator (CALHM). In taste buds CALHM1 mediates taste stimuli-evoked ATP release which is required for taste perception (ATP acts as a neurotransmitter to activate afferent gustatory pathways) (Taruno et al., 2013). Opening of CALHM1 is dependent on $[Ca^{2+}]_{ex}$ and voltage. In HeLa cells expressing CALHM1 a dose-dependent release of ATP was observed with different concentrations of $[Ca^{2+}]_{ex}$. ATP release occurred when $[Ca^{2+}]_{ex}$ was reduced to 1 mM and it was increased 4 fold when $[Ca^{2+}]_{ex} < 0.1$ mM. CALHM1-mediated ATP release in HeLa cells was blocked by ruthenium red (20 µM), but not CBX (30 µM) and taste-evoked ATP release from gustatory tissue was abolished in CALHM KO mice (Taruno et al., 2013). Removal of divalent cations also evoked a CALHM1-evoked current in N2A cells which was blocked by ruthenium red, but

not CBX and did not occur in CALHM1 KO mice (Ma et al., 2012). Human CALHM1 mRNA was highly expressed throughout the brain and spinal cord (Dreses-Werringloer et al., 2008) while there are conflicting reports about the expression and function of murine CALHMs. CALHM1 mRNA was below detection level in mouse brain from E12 and up to one year of age while CALHM2 was highly expressed (Wu et al., 2012). At P7 CALHM2 was only expressed by microglia (Zhang et al., 2014b). However, reducing $[Ca^{2+}]_{ex}$ to 0.2 mM evoked a CALHM1 mediated current in cultured mouse cortical neurons which was absent in neurons from CALHM1 KO mice (Ma et al., 2012).

1.4 Rational and hypothesis

The last decade of research in the field of neuroimmunology has provided intriguing evidence that microglia constantly survey the neuropil, especially surrounding synapses, and several striking examples of microglia-neuron interaction have been provided. Microglia mediated synaptic pruning during development has been elegantly demonstrated to be crucial for brain wiring, as aberrant connectivity is associated with multiple neurological disorders. Absence of microglia functions enhanced NMDA-evoked neuronal excitotoxicity while neuronal activity was attenuated following contact with microglial processes. In the juvenile and adult CNS microglial processes have also been reported to interact with synapses in an activity dependent manner. Microglial processes would briefly pause upon contact with synaptic elements and lowering of neuronal activity would reduce the frequency and duration of the interactions between microglial process and synapses. However, the modes of communication between neuronal activity and microglial process dynamics have not been determined. Therefore, demonstrating that neuronal activity can trigger an alteration in microglial process dynamics

would be an important contribution to the overall understanding of the interplay between neurons and microglia, and thus represents the main objective of this dissertation **(chapter 2 and 3)**.

The dynamic nature of microglia and their rapid morphological changes following different external stimuli have made live imaging of microglial morphology a powerful tool for investigating and quantifying their responses under various circumstances. Two-photon laser scanning microscopy and the development of transgenic mouse lines, with fluorescent indicators genetically expressed in microglia, provide the unique opportunity to visualize and track changes in microglia morphology in real-time. Imaging of acute brain slices offers endless possibilities for manipulating the tissue via application of pharmacological agents or by insertion of electrodes, and it has previously been demonstrated that microglia maintain their ramified morphology in this preparation. However, visualization of rapid microglial process dynamics was limited to the use of transgenic mouse lines with genetically encoded indicators because there were no available methods to preserve the fine structures in acute slices. Hence, a second objective of this dissertation has been to develop a novel fixation and immunolabeling procedure that would preserve the fine dynamic structures in acute brain slices **(chapter 4)**.

Local application of ATP and damage-evoked release of ATP triggered microglial process extension towards the source of ATP. ATP is also known as a signaling molecule for attracting immune cells in the periphery. Thus we speculated that ATP might be released upon enhanced neuronal activity to attract microglial processes to synapses. ATP can be released by hemichannel opening, which has been shown to occur during high neuronal activity. Application of NMDA and ischemia-evoked activation of neuronal NMDAR induce opening of neuronal Panx1 hemichannels. High neuronal activity is also accompanied by a drop in extracellular Ca^{2+}

which induces opening of astrocytic Cx43 hemichannels. The following two hypotheses were therefore investigated (see schematic illustration below).

1.4.1 Hypothesis 1

Activation of neuronal NMDAR triggers ATP release via opening of neuronal Panx1 hemichannels and consequently a change in microglial process dynamics (chapter 2).

1.4.2 Hypothesis 2

Opening of astrocytic Cx43 hemichannels by removal of extracellular Ca^{2+} triggers ATP release and consequently an alteration in microglial process dynamics (chapter 3).

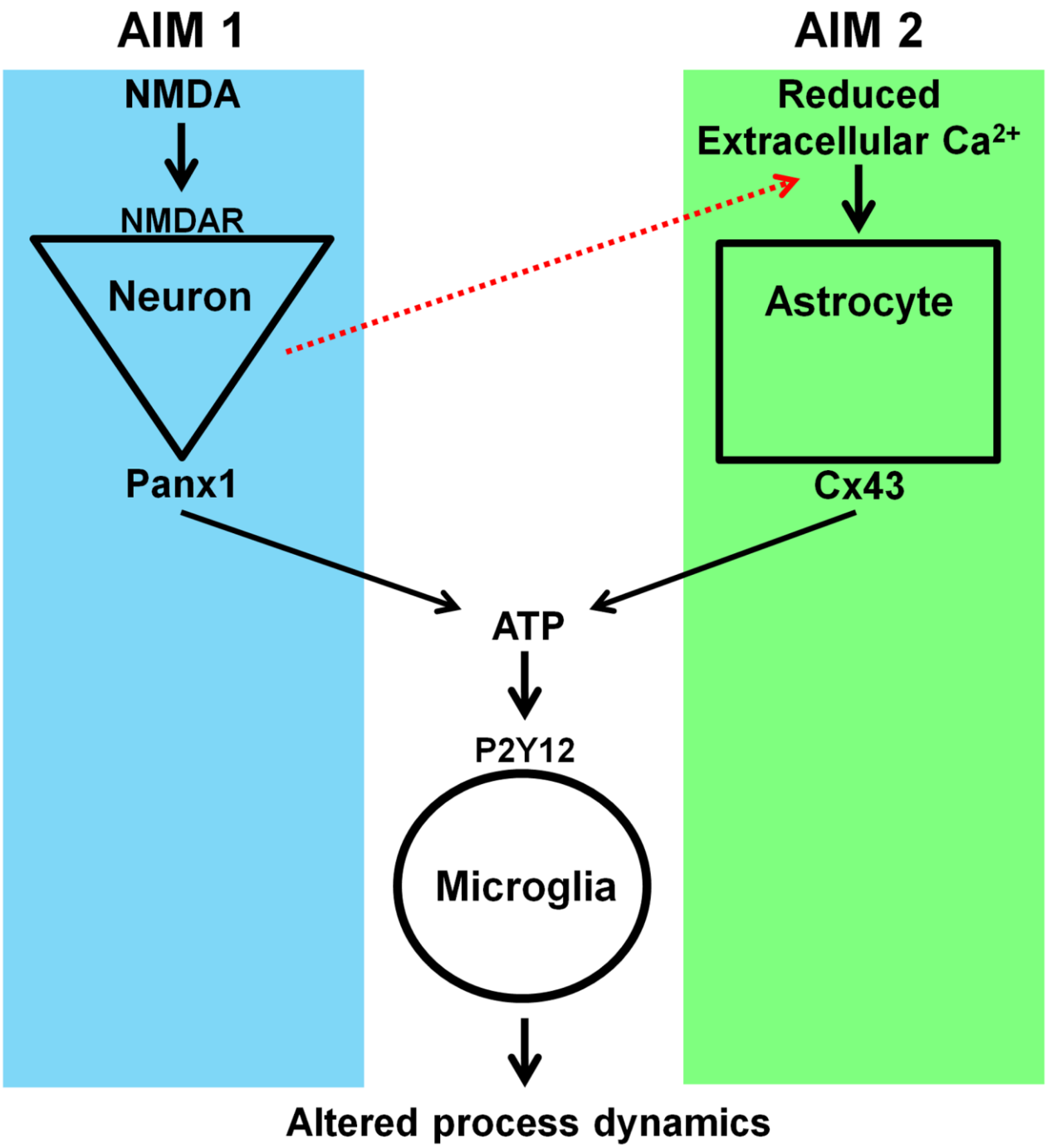

Figure 1-1. Schematic diagram illustrating the hypotheses.

Chapter 2: Activation of neuronal NMDA receptors triggers transient ATP-mediated microglial process outgrowth

2.1 Introduction

Microglia, the primary immune effectors in the brain, exhibit a ramified morphology with motile processes that survey their surroundings (Nimmerjahn et al., 2005). Ramified microglia are responsible for synaptic pruning (Paolicelli et al., 2011) and sculpting of synaptic connections during development (Schafer et al., 2012; Bialas and Stevens, 2013). In the adult CNS the motility of microglial processes decreases upon contact with synapses (Wake et al., 2009) and dendritic spines are significantly more likely to be eliminated following contact with microglial processes (Tremblay et al., 2010). However, previous studies examining the link between neuronal activity and microglia process dynamics in rodents have yielded contradictory findings. Blocking synaptic transmission did not alter microglial process motility (Nimmerjahn et al., 2005) whereas increasing neuronal activity by blocking inhibition (Nimmerjahn et al., 2005; Fontainhas et al., 2011) but not by electrophysiological stimulation (Wu and Zhuo, 2008) increased motility and extension of the microglial processes. Thus, identifying the molecular cue(s) mediating microglia responses and determining how the release of these signals are being triggered would be an important contribution to the overall understanding of neuron-microglia communication in the adult brain.

ATP is an important molecular chemoattractant mediating ‘find-me’ signals for immune cells (Elliott et al., 2009; Chekeni et al., 2010) and several studies have demonstrated that microglial processes rapid extend towards local tissue damage or locally applied ATP (Davalos et al., 2005; Haynes et al., 2006). P2Y12 receptors are selectively expressed by microglia in the

brain (Sasaki et al., 2003; Hickman et al., 2013) and are the critical purinergic receptors for microglial process extension *in vivo* and *in vitro* (Haynes et al., 2006; Orr et al., 2009; Ohsawa et al., 2010). In addition ATP metabolites such as adenosine may help establish the gradient for directed microglia extension (Ohsawa et al., 2012). These studies highlight ATP and its derivatives are signaling molecules that, when released, can mediate microglial process extension. ATP release via open pannexin 1 (Panx1) channels (Huang et al., 2007; Chekeni et al., 2010; Li et al., 2011b) has been observed in many cells. Repetitive stimulation of NMDA receptors (NMDAR) triggered neuronal Panx1 channel opening in rodents (Thompson et al., 2008). In zebra fish larvae, NMDA uncaging triggered microglial process extension (Sieger et al., 2012) while repetitive glutamate uncaging mediated Panx1 opening and promoted an ATP-induced neuron-microglia contact (Li et al., 2012). Thus, we investigated whether NMDAR activation in the adult rodent brain could evoke signaling to microglia and whether this form of communication relied on Panx1. To address these questions, an NMDAR stimulation paradigm in acute brain slices from mice was developed that allowed for pharmacological interventions during time lapse imaging of changes in microglia morphology. Furthermore, a novel protocol for fixation and immunolabeling of dynamic processes in whole brain slices was developed to visualize microglial morphology in brain slices from Panx1-deficient mice subjected to our NMDAR stimulation paradigm. Finally, to demonstrate that microglia responded to selective stimulation of neuronal NMDAR we activated NMDAR on single voltage clamped neurons and found this triggered microglia process outgrowth.

2.2 Materials and methods

Animals

CX3CR1$^{EGFP/EGFP}$ mice on a BALB/c background and CX3CR1$^{EGFP/+}$ on C57BL/6 background (Jung et al., 2000) were bred and housed under controlled conditions (12 h light/dark cycle) with water and food ad libitum. Panx1 KO mice on C57BL/6 background (Qu et al., 2011) and age matched C57BL/6 wild type mice were a gift from Dr Christian Naus. Emx-GCaMP3 mice (produced by crossing B6.129S2-Emx1$^{tm1(cre)Krj}$/J strain with B6;129S-Gt(ROSA)26Sor$^{tm38(CAG-GCaMP3)Hze}$/J strain) (Gorski et al., 2002) were a gift from Dr Timothy Murphy. Note that EGFP is introduced as a "knock-in" thus the CX3CR1 gene encoding the fractalkine receptor is replaced with the gene encoding for EGFP (i.e. mice heterozygous for EGFP are CX3CR1$^{-/+}$ while mice homozygous for EGFP are CX3CR1$^{-/-}$).

Slice preparation and maintenance

Mice (40-120 days, both males and females) were anaesthetized with halothane and decapitated according to protocols approved by the University of British Columbia committee on animal care. The brains were removed and sliced in an ice-cold solution containing (in mM): N-Methyl-D-glucamine (120), KCl (2.5), $NaHCO_3$ (25), $CaCl_2$ (1), $MgCl_2$ (7), NaH_2PO_4 (1.2), D-glucose (2), sodium pyruvate (2.4), and sodium L-ascorbate (1.3) that was constantly oxygenated with 95% O_2 and 5% CO_2. The brains were sliced horizontally (300 µm thick) using a vibratome (Leica VT1200S) with disposable razor blades (Canemco-Marivac) and incubated for 1 hour at room temperature (RT) in oxygenated artificial cerebrospinal fluid (ACSF) containing (in mM): NaCl (126), KCl (2.5), $NaHCO_3$ (26), $CaCl_2$ (2.0), $MgCl_2$ (2), NaH_2PO_4 (1.25), and D-glucose (10), pH at 7.3-7.4, osmolarity ~300 mOsm. Experiments were performed at RT with continuous

perfusion (3 ml/min) of oxygenated ACSF. For the experiments involving NMDA application the concentration of $MgCl_2$ was either reduced to 0.6 mM or increased to 6 mM (the NaCl concentration was adjusted to balance osmolarity and NaH_2PO_4 was omitted from the high Mg^{2+} solution) and 10 µM glycine was added.

Fixation and immunolabeling of brain slices using modified methods

Brain slices were fixed by immersion in 4% paraformaldehyde (PFA) at 80°C for 2 min and rinsed in 0.1 M phosphate buffered saline (PBS). The 300 µm thick slices were immunolabeled free-floating and each step was performed in 0.1M PBS with 20% dimethyl sulfoxide (DMSO), and 2% Triton X-100. In short; slices were blocked for 24 h in 10 % goat serum, incubated for 8 days with a polyclonal rabbit antibody against mouse ionized calcium binding adaptor molecule 1 (Iba1, 0.5 µg/ml) or a polyclonal rabbit antibody against mouse P2Y12 (Haynes et al., 2006) and 2.5% goat serum, washed for 24 h, incubated for 6 days with a polyclonal goat-anti-rabbit IgG antibody conjugated with Alexa 594 (1 µg/ml) and 2.5% goat serum, and rinsed in 0.1 M PBS. Prior to imaging the slices were mounted in FluorSave reagent on specially made microscope slides (Fisher Scientific) with the cover glass elevated 300 µm above the slide. This protocol gave us six unique capabilities. First, we could fix the tissue at any given time point during real time imaging (i.e. following a lesion or during ATP or NMDA applications) thereby obtaining a snapshot of the morphology at the exact time of fixation. Second, we could run simultaneous experiments under the same conditions with several slices prepared from the same brain (i.e. one slice subjected to ATP or NMDA applications and one slice serving as a non-treated control that was fixed simultaneously). Third, we could image microglia morphology at specific time points without live cell illumination with the ultrafast infrared laser for two photon

imaging thereby ruling out potential contributions of laser-induced photo-toxicity in our paradigm. Fourth, the fixation was fast enough to allow us to immunolabel target proteins and link their cellular location to the exact cellular morphology. Fifth, we could investigate the cellular responses in a large brain region at precisely the same time point (i.e. microglial responses to 5 NMDA applications across the stratum radiatum). Sixth, we could image cells after fixation and immunolabelling at comparable and defined depths within brain slices. The decision to fix the slices 8 min post the 5^{th} NMDA application was based on an early estimate of the peak outgrowth following 5^{th} NMDA applications. We named this modified method, SNAPSHOT (StaiNing of dynAmic ProcesseS in HOt-fixed Tissue).

Surgery for *in vivo* imaging

A round cranial window (2 mm diameter) was installed under general anesthesia (fentanyl, 0.05 mg/kg; midazolam, 5 mg/kg; medetomidine, 0.50 mg/kg). The anesthetized mice were secured on a modified stereotactic frame while placed on a heating pad. The skin and the periosteum were removed to expose the skull. Lines forming a circle (0.5 mm lateral of -0.5 mm of bregma) were gently drilled onto the skull surface. The respective portion of the skull was removed and the brain was kept moist at all times using surgical gel sponges in PBS (GelitaSpon). A custom-made titanium ring (14 mm diameter) was then sealed onto the skull above the cranial window with light-curing dental cement (Heraeus) to secure the mouse to a custom-made head fixation plate during imaging (Hefendehl et al., 2012). Finally, the dura mater was carefully removed.

Local application of ATP

Two electrodes (tip resistance 4-6 MΩ) were placed 100 µm apart at 150 µm below the surface of the slice using bright field illumination as guidance. Positive pressure (0.05 psi) was applied prior to entering the tissue and continuously throughout the experiments. One electrode (#1) contained ACSF and served as a reference while the other electrode (#2) contained ACSF with 4 mM ATP. 50 µM or 200 µM of the selective ectonucleotidase inhibitor ARL 67156 trisodium salt (ARL) was added to the ACSF in the bath. Alexa 594 hydrazide-sodium salt (100 µM) was added to the internal solution of each electrode for visualization of the tip. Image acquisition was initiated within 5 min of placement of the electrodes (defined as time 0 for quantification). Microglial process outgrowth towards the tip of the electrode was quantified as F/F_0 at 500-550 nm emission within circles (radius of 50 µm) centered at the tip of each electrode (F = fluorescence intensity at time x, F_0 = fluorescence intensity at time 0).

Astrocytic dye-coupling

Astrocytes were voltage clamped at −80 mV with an intracellular solution contained (in mM) potassium gluconate (124), $MgCl_2$ (4), 4-(2-hydroxyethyl)-1-piperazineethanesulfonic acid (HEPES, 10), EGTA (1), potassium ATP (4), sodium GTP (0.4), Na_2creatinePO_4, (10), Alexa 488 hydrazide-sodium salt (0.1) with pH adjusted to 7.2 with KOH and osmolarity adjusted to 290-300 mOsm. CBX, 100 µM was perfused onto slices 25 min prior to whole cell configuration and throughout the experiments. To ensure proper dialysis of the internal solution, image acquisition was not initiated before 20 min after whole cell configuration. Astrocytes were visualized prior to patching by staining brain slices with sulforhodamine 101, a specific marker for astrocytes (Nimmerjahn et al., 2004; Kafitz et al., 2008).

Neuronal patch clamping experiment

CA1 pyramidal neurons were voltage clamped at −70 mV using the blind patch clamp method (Castaneda-Castellanos et al., 2006). Patch electrodes (tip resistance 4-6 MΩ) were pulled from 1.5 mm outer diameter thin-walled glass capillaries (World Precision Instruments) using a Flaming-Brown micropipette puller (Sutter Instruments). The electrodes were lowered in the stratum oriens and aimed to approach the stratum pyramidale at 140-160 µm below the surface of the slice. Positive pressure (0.5 psi) was applied prior to entering the bath and kept until contact with a pyramidal cell. The intracellular solution contained (in mM) potassium ATP (4), potassium gluconate (108), $MgCl_2$ (2), HEPES (10), EGTA (1), sodium GTP (0.3), Sodium gluconate (8), KCl (8) Alexa 594 hydrazide-sodium salt (0.1) with pH adjusted to 7.2 with KOH and osmolarity adjusted to 285-290 mOsm. MK801 (1 mM) was added to the intracellular solution. The blind patch clamp method was chosen as it allowed for unbiased selection of CA1 pyramidal neurons and for targeting cells deep in the tissue.

Slice imaging

A two-photon scanning microscope (Coherent Chameleon Ultra II laser coupled to a Zeiss LSM510-Axioskop-2 microscope with a Zeiss 40X-W/1.0 numerical aperture objective) was used to image live and fixed hippocampal brain slices. Microglial cells were imaged in the stratum radiatum of the CA1 region at 150 +/- 25 µm below the surface of the slice. Images for time lapse analysis were collected at 512×512 pixels using 4-line averaging and acquired as time series of stacks (z = 15, 2 µm steps with the soma of the microglial cell(s) of interest in the middle of the stack) with a total scan time of ~1 min/stack. Images for 3D reconstruction were acquired as stacks of 75-90 images using 8-line averaging and stepping 0.5 µm in the z-axis

between frames. EGFP and GCaMP3 were excited at 920 nm and the emission was detected with a photo multiplier tube after passing through a 500-550 nm emission filter. The same filter and detector was also used for image acquisition during the patch-clamp experiments with Alexa 488 that was excited at 800 nm. For horizontal cross-sections of the stratum radiatum images of fixed slices were acquired as stacks (z = 25, 2 µm steps) with ~20% overlap with its neighboring images to allow alignment for tiling images. Alexa 594 and sulphorhodamine 101 were imaged using 800 nm excitation and a 600-660 nm emission filter. Lesions were induced by exposure of high laser power illumination to a restricted area. Non-saturated images (all pixels < 255) and images through the whole brain slice (z = 151, 2 µm steps with auto z brightness correction, ZEN 2012 software) were acquired using a Zeiss LSM7MP-AX10 microscope with a Zeiss 20X-W/1.0 numerical aperture objective.

In vivo imaging

In vivo imaging was performed on anesthetized mice (fentanyl, 0.05 mg/kg; midazolam, 5 mg/kg; medetomidine, 0.50 mg/kg) using a custom built two-photon microscope equipped with a Coherent Chameleon Ultra II laser and a Zeiss 40X-W/1 numerical aperture objective. Texas Red dextran (Invitrogen, 70 kDa; 12.5 mg/ml in sterile PBS) was injected intravenously, to visualize the blood vessels. The mice were secured under the microscope by fitting the titanium ring in a custom-built head fixation apparatus (Hefendehl et al, 2012) connected to a motorized xy stage (Sutter Instruments). EGFP and Texas Red were imaged simultaneously using 920 nm excitation and were detected via non-descanned detectors and ET525/50m-2P and ET605/70m-2P emission filters respectively (Chroma Technology). Images were collected at 512 × 512 pixels without averaging and acquired as stacks (z = 40, 1 µm steps) at a depth of 100-140 µm below

the cortical surface. ACSF was continuously perfused across the cortical surface (3 ml / min) using a custom made perfusion system that was designed to fit within the titanium ring and which allowed delivery and washout of ATP similar to the application used for slices. Laser power was kept constant for each experiment and did not exceed 45mW.

Image processing and analysis

All images were processed using ImageJ (Rasband, W.S., ImageJ, U. S. National Institutes of Health, http://imagej.nih.gov/ij/, 1997-2013). The following steps were used to prepare the time lapse images for analysis unless otherwise indicated: i) concatenation of the time series, ii) application of a median filter, iii) z-projection by maximum intensity of each stack (every time point), and iv) alignment of all images in xy-plane, thereby generating a 2D time series for further analysis. To quantify the morphological changes occurring over time we generated an unbiased and fully automated program using Matlab R2012b inspired by Kozlowski and Weimer (Kozlowski and Weimer, 2012). In short, only cells with their soma within the middle 5 images of each stack were included in the analysis. Each cell was subjected to 5 frame rolling average and made binary (threshold calculated by Otsu's method, Matlab graythresh function). The thresholded cell was identified as the largest connected region and its cross sectional area and perimeter was quantified. Additional quantifications were performed by determining the number of branch points using a 'skeletonized' model of the cell (i.e modeled by straight lines based on the shape of the largest connected region) as previously used by others for quantifying changes of microglial processes (Fontainhas et al., 2011). We found that applying a rolling averaging step prior to thresholding, improved the preservation of the connectivity of thin processes to the soma. The images acquired for 3D reconstruction were subjected to subtraction of the mean

value of a region defined as background, aligned and subjected to auto-adjustment of brightness and contrast. The center of mass was determined by the BoneJ plugin; 'Moments of Inertia' and 3D reconstructions were generated using ImageJ's 3D viewer. Non-saturated images were pseudocolored by intensity using ImageJ's lookup tables (fire) and cross-sections of the stratum radiatum were reconstructed of up to 6 images using the MosaicJ plugin.

Statistics

Statistical analyses were performed using GraphPad Prism version 6.0 for Mac. Gaussian distributions were assumed for all experiments and n-values represents the number of animals. For multiple comparisons, multiplicity adjusted p-values are indicated on the respective figures when appropriate otherwise the p-values were indicated by *, $P < 0.05$; **, $P < 0.01$; ***, $P < 0.001$.

Western blotting

Additional brain slices from mice, from which slices were used for imaging and fixation, were homogenized using lysis buffer containing (in mM): Tris (100, pH 7.0), EGTA (2), (*Ethylenediaminetetraacetic acid)* EDTA (5), NaF (30), sodium pyrophosphate (20) and 0.5% NP40 with phosphatase and protease inhibitors (Roche) and centrifuged at 13,000g for 20 min at 4°C. Protein concentration of the lysates were determined by Bradford assay using a DC protein assay dye (Bio-Rad) and 20 µg of protein (diluted in 2x Laemmli buffer with 5% β-mercaptoethanol and boiled for 5 min) was used for sodium dodecyl sulphate/polyacrylamide gel electrophoresis (10% precast gel, Lonza). The proteins were transferred to polyvinylidene fluoride membranes (Bio-Rad) and blocked in 5% nonfat milk prior to probing. Each step was

performed in Tris-buffered saline with 0.1% Tween 20. In short, the membranes were incubated with an affinity purified rabbit anti-mouse panx1 antibody (CT-395, 0.2 µg/ml) (Penuela et al., 2009, Bargiotas et al., 2011) for 12 h at 4°C, washed, incubated with goat-anti-rabbit IgG antibody conjugated with horseradish peroxidase (~0.2 µg/ml) for 1 h, washed and visualized on a molecular Imager (VersaDoc MP 5000, Bio-Rad) using enhanced chemiluminescence. Next, the membranes were re-probed with a goat-anti-mouse glyceraldehyde 3-phosphate dehydrogenase (GAPDH) antibody (0.5 µg/ml) and a donkey-anti-goat IgG antibody conjugated with horseradish peroxidise (0.2 µg/ml) and re-imaged.

Chemicals

For drugs that were dissolved as stock solutions (1000x) the solvents are indicated in parentheses with the exception of probenecid that was dissolved in 1M NaOH and added directly to ACSF (pH corrected to 7.35). *Abcam* supplied: 6-cyano-7-nitroquinoxaline-2,3-dione (CNQX disodium salt (DMSO)), (2R)-amino-5-phosphonovaleric acid (APV, D isomer (H_2O)), and tetrodotoxin citrate (TTX(H_2O)); *Amersham Bioscience* supplied: enhanced chemiluminescence; *Bio-Rad* supplied: β-mercaptoethanol; *Calbiochem* supplied: FluorSave reagent; *EMD* supplied: D-glucose and $NaHCO_3$; *FD NeuroTechnologies* supplied: paraformaldehylde; *Fisher Scientific* supplied: $CaCl_2$, DMSO, Glycine, NaH_2PO_4, KCl, and MgCl2; *GE HealthCare* supplied: chemiluminescence and goat-anti-rabbit IgG antibody conjugated with horseradish peroxidase; *Life Technologies* supplied the Alexa 594 conjugated antibody against rabbit IgG, Alexa 488 hydrazide-sodium salt and Texas red; *Oxoid* suppied; PBS (tablets); *Pfizer* supplied: medetomidine; *Research Biochemicals International* supplied: reactive blue 2 (RB2, dH_2O); *Sandos* supplied: Fentanyl and midazolam; *Santa Cruz* supplied:

antibody against GAPDH and donkey-anti-goat IgG antibody conjugated with horseradish peroxidase; *Sigma* supplied: 2x Laemmli buffer, ATP disodium salt hydrate (H_2O), PTIO, CBX disodium salt (H_2O), halothane, HEPES, NaCl, Na_2creatinePO_4, NMDA (H_2O), N-Methyl-D-glucamine, potassium ATP, potassium gluconate, potassium EGTA, Probenecid (1M NaOH), sodium GTP, sodium L-ascorbate, sodium pyruvate, Triton X-100, Tween 20; *Tocris bioscience* supplied: ARL, KN-62, L-NAME hydrochloride, MK 801 and PPADS tetrasodium salt;*Wako* supplied the antibody against Iba1. The antibody against mouse Panx1 was a kind gift from Dr Dale W. Laird. The antibody against mouse P2Y12 was a kind gift from Dr David Julius.

2.3 Results

Characteristics of ATP-induced microglial process outgrowth in slices and *in vivo*

We first established the validity of ATP-induced microglia responses in acutely prepared mouse brain slices. Bath application of ATP (500 µM) consistently induced dynamic morphological changes of microglial cells, which we refer to as microglial process outgrowth (Fig. 2.1A-C). This outgrowth was characterized by extension of existing processes, sprouting of new branches extending away from the soma and formation of bulbous tips (growth cone like structures at the leading edge of extending processes and branches). Importantly, every microglial cell (in control conditions) immediately responded to ATP and process outgrowth persisted as long as ATP was applied. The process outgrowth was completely reversible as microglia would return to their initial morphology within a few minutes upon removal of ATP. Furthermore, the process outgrowth could be repeated with additional ATP applications. To confirm that the characteristics of this ATP-induced microglial process outgrowth also occurred *in vivo*, ATP (10 mM) was topically applied to the intact cortex and a similar pattern of microglial process outgrowth was observed in microglia *in vivo* (Fig. 2.1D).

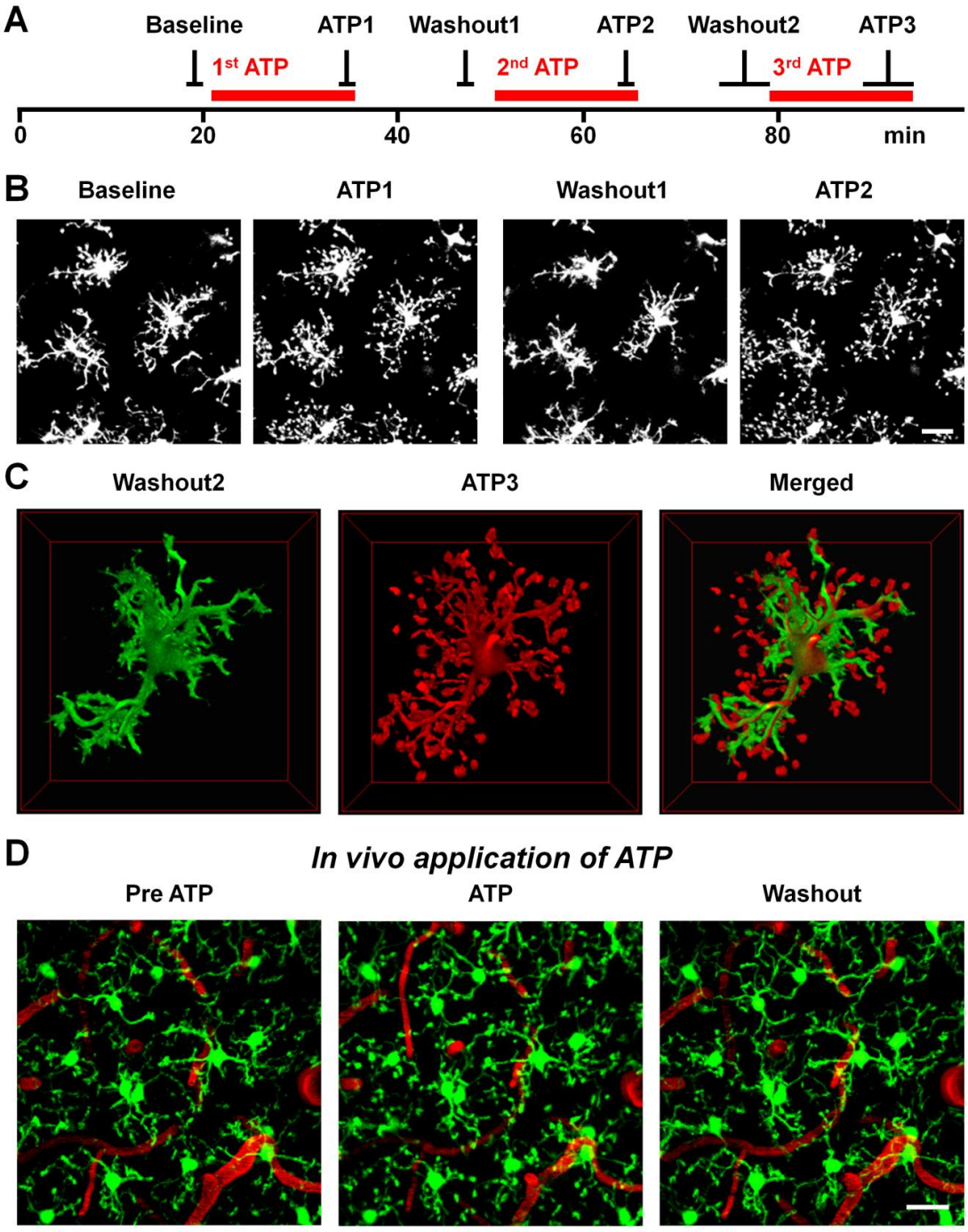

Figure 2-1 Patterns of microglial process outgrowth induced by ATP in slices and *in vivo*.

A, Timeline for image acquisition and ATP applications in slices. ***B,*** Bath application of ATP (500 µM, 15 min) induced microglial process outgrowth in slices, which is illustrated by the morphological changes of the cells shown in '*Baseline'* versus *'ATP1'*. This process outgrowth was reversed when ATP application was terminated *'Washout1'* and similar morphological changes were observed again with an additional application of ATP *'ATP2'*.

Scale bar; 20 µm. ***C,*** Colour-coded three dimensional reconstructions of one microglial cell, highlighting the morphological changes induced by ATP (*'Washout2'* in green versus *'ATP3'* in red). Note the ATP-induced extension of existing processes, sprouting of new branches, and formation of bulbous tips that are apparent in red at the *'Merged'* image. The images are shown as a bottom view of the xy-plane. Scale bar; 20 µm. ***D,*** Microglial process outgrowth *in vivo* following topical application of ATP (10 mM) to the intact cortex. Note that ATP induced similar morphological changes in vivo as compared to in slices that reversed during washout. Blood vessels are seen in red. Scale bar; 20 µm.

Characteristics of microglial process outgrowth triggered by NMDA

We observed that bath application of NMDA triggered a transient microglial process outgrowth that was similar to that induced by ATP. Transient exposure to NMDA triggered a reversible extension of existing processes, sprouting of new branches away from the soma and formation of bulbous tips (Fig. 2.2B) and was quantified (area, perimeter and number of branch points) as shown in Fig. 2.2C-D. We observed that the microglial response to NMDA was variable during the first three applications whereas subsequent applications were consistently stable (Fig. 2.2D), hence we established a paradigm with three initial NMDA applications separated by 20 min intervals followed by 40 min intervals before NMDA applications 4 and 5. Fig. 2.2D shows that the process outgrowth following the 4^{th} application of NMDA compared to the 1^{st} was significantly different with respect to the local baseline values obtained 5 min prior to the respective NMDA application. Importantly, comparisons of process outgrowth following the 4^{th} and the 5^{th} NMDA applications were not significantly different. This allowed us to test the effect of various blockers on the 5^{th} application. We thus could compare the outgrowth triggered by the 4^{th} NMDA application to the outgrowth triggered by the 5^{th} NMDA application in the presence of various blockers. The longer intervals were introduced to allow for the outgrowth to recover and to allow time for application of pharmacological agents (25 min) prior to the 5^{th} NMDA application.

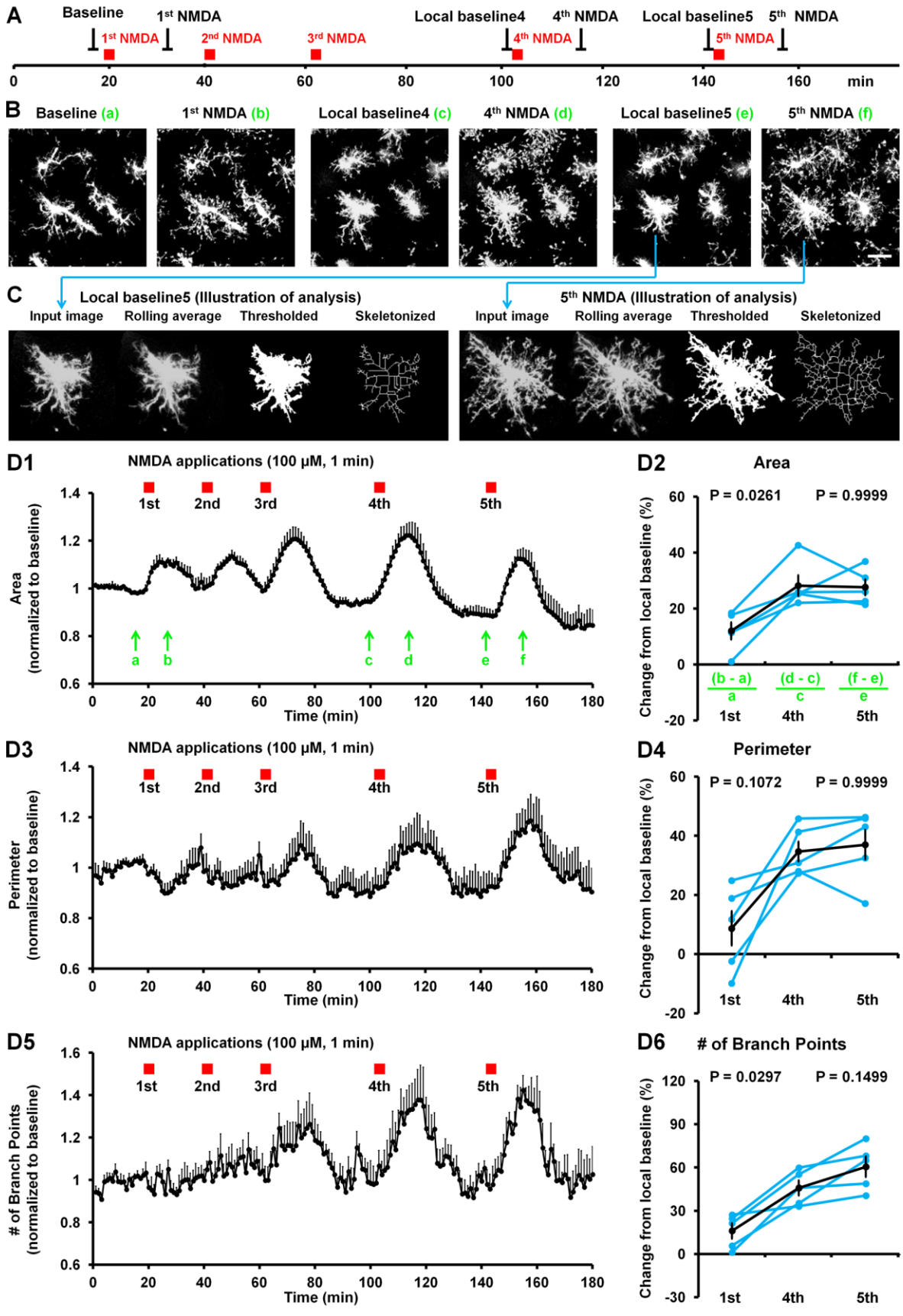
A
Baseline
1st NMDA
1st NMDA
2nd NMDA
3rd NMDA
Local baseline4
4th NMDA
4th NMDA
Local baseline5
5th NMDA
5th NMDA
0
20
40
60
80
100
120
140
160
min
B
Baseline (a)
1st NMDA (b)
Local baseline4 (c)
4th NMDA (d)
Local baseline5 (e)
5th NMDA (f)
C
Local baseline5 (Illustration of analysis)
Input image
Rolling average
Thresholded
Skeletonized
5th NMDA (Illustration of analysis)
Input image
Rolling average
Thresholded
Skeletonized
D1
NMDA applications (100 µM, 1 min)
1st
2nd
3rd
4th
5th
Area
(normalized to baseline)
a
b
c
d
e
f
Time (min)
D2
Area
P = 0.0261
P = 0.9999
Change from local baseline (%)
(b - a)
(d - c)
(f - e)
a
c
e
1st
4th
5th
D3
NMDA applications (100 µM, 1 min)
Perimeter
(normalized to baseline)
Time (min)
D4
Perimeter
P = 0.1072
P = 0.9999
Change from local baseline (%)
D5
NMDA applications (100 µM, 1 min)
# of Branch Points
(normalized to baseline)
Time (min)
D6
# of Branch Points
P = 0.0297
P = 0.1499
Change from local baseline (%)

Figure 2-2 Microglial process outgrowth triggered by NMDA was repeatable and reversible.

A, Timeline for image acquisition during NMDA applications***. B,*** Multiple bath applications of NMDA (100 µM, 1 min/application) consistently triggered microglial process outgrowth illustrated with this series of images obtained at the different time points prior to and following multiple NMDA applications as indicated in *A*. The sample images from this time series shows that the process outgrowth was reversible after each application and was induced again when NMDA was reintroduced each of these 5 times. Scale bar; 20 µm. ***C,*** Illustration of step-by-step analysis of the microglial cell indicated with the arrows from *B*. **D,** Graphic depiction of quantified microglial morphology for different parameters over time with NMDA applications indicated by red markers. D1, D3 and D5 show quantification of the surface area of the thresholded images, the perimeter of the thresholded images and the number of branch points of the skeletonized images, respectively with the values normalized to the baseline (average of the first 15 min) and graphed as the mean + standard error of the mean (SEM). D2, D4 and D6 show the quantification of the morphological changes following the 1^{st}, 4^{th} and 5^{th} NMDA applications from the respective local baseline (defined as the 5 min prior to the respective NMDA application and indicated by; a, c and e in *D1*) to the max value within 15 min following NMDA application (indicated by; b, d and f in *D1*). Each data point is represented with a blue dot and data points from the same experiments are connected with blue lines. The mean ± SEM is illustrated in black. The experiments were performed in low Mg^{2+} (0.6 mM) and in the presents of glycine (10 µM). Repeated measures ANOVA with Bonferroni's multiple comparison post test was used for statistical comparison of the change from local baseline between the groups (n = 5).

Comparison of microglia outgrowth triggered by NMDA versus ATP

We examined the difference between the patterns of process outgrowth triggered by NMDA versus ATP application on the same cells. This was investigated by acquiring z-stacks of images before and after NMDA and ATP application in order to create 3D reconstructions of microglia when process outgrowth was triggered by either stimulus. The microglial process outgrowth induced by NMDA was non-polarized resulting in a spatially uniform distribution of bulbous tips and a quantified polarization of approximately 50% (Fig. 2.3C1, D). In contrast process outgrowth induced by bath application of ATP was strikingly polarized with a greater extension of processes directed toward the surface of the brain slice where the ATP was diffusing into the tissue (Fig. 2.3C2, D). This is consistent with the hypothesis that ATP generates polarized outgrowth because a gradient is generated as the ATP diffuses into the brain slice. In contrast the

non-polarized process outgrowth in NMDA is consistent with the release of chemoattractant agents from neurons throughout the brain slice as a result of NMDAR activation. Additionally, we acquired images immediately after terminating the ATP application. We observed that the bulbous tips withdraw prior to the retraction of the extended processes when the ATP application is terminated.

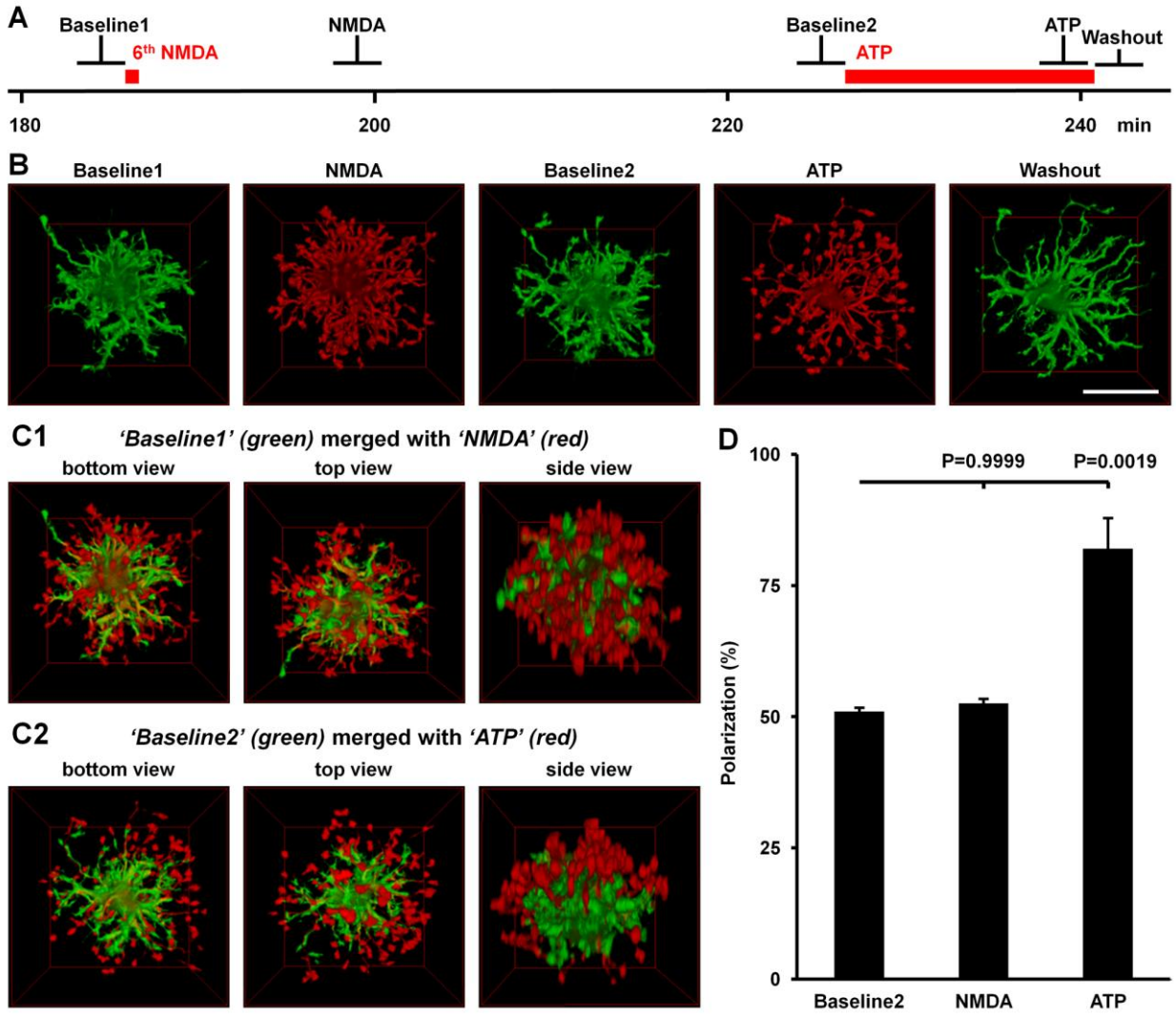

Figure 2-3 NMDA triggered a non-polarized outgrowth of microglia processes in contrast to ATP application.

A, Timeline for image acquisition to examine NMDA versus ATP induced outgrowth (note, that this is the 6th NMDA application). ***B,*** Three dimensional reconstructions (shown as bottom view, xy-plane) of a microglial cell at five different time points as indicated in *A*. Note, in '*Washout'* (immediately after termination of ATP application) that the microglial processes were still extended while the bulbous tips were collapsed. Scale bar; 20 µm. ***C,*** Merging of the images prior to (green) and following (additional portions of the cell are in red) either from NMDA ***C1*** or ATP application ***C2***. The merged three dimensional reconstructions are shown as bottom views (xy-plane), top view (xy-plane) and side views (zy-plane). Note, that outgrowth induced by NMDA-triggered ATP release is non-polarized (uniform distribution of red bulbous tips) while the red bulbous tips are polarized towards the top (surface of the slice) during ATP application. ***D,*** Bar graph depicting the microglial cell polarization in different conditions. The cell's center of mass at 'B*aseline1'* was used to determine changes in polarization (total fluorescence above the center of mass / total fluorescence below the center of mass) of the cell at the indicated time points. The groups were compared using repeated measures ANOVA with Bonferroni's multiple comparison post test (n = 3).

Outgrowth occurred independently of CX3CR1 stimulation

The fractalkine receptor on microglia is known to respond to neuronal fractalkine and is potentially a candidate in directing or triggering microglia process outgrowth (Liang et al., 2009). The expression of EGFP in microglia in our transgenic mice is driven by CX3CR1. To investigate whether the outgrowth would be altered by the presence or absence of the CX3CR1 fractalkine receptor, slices from both CX3CR1$^{-/-}$ and CX3CR1$^{-/+}$ mice were subjected to the multiple NMDA applications paradigm (Fig. 2.4). Similar outgrowth occurred in slices from both transgenic mice and no significant differences were observed for any of our 3 parameters. Thus, microglia process outgrowth did not require the fracktalkine receptor. CX3CR1$^{EGFP/EGFP}$ mice, which have optimal expression of EGFP and provide the best signal to noise ratio while imaging dynamic processes, were used for subsequent experiments.

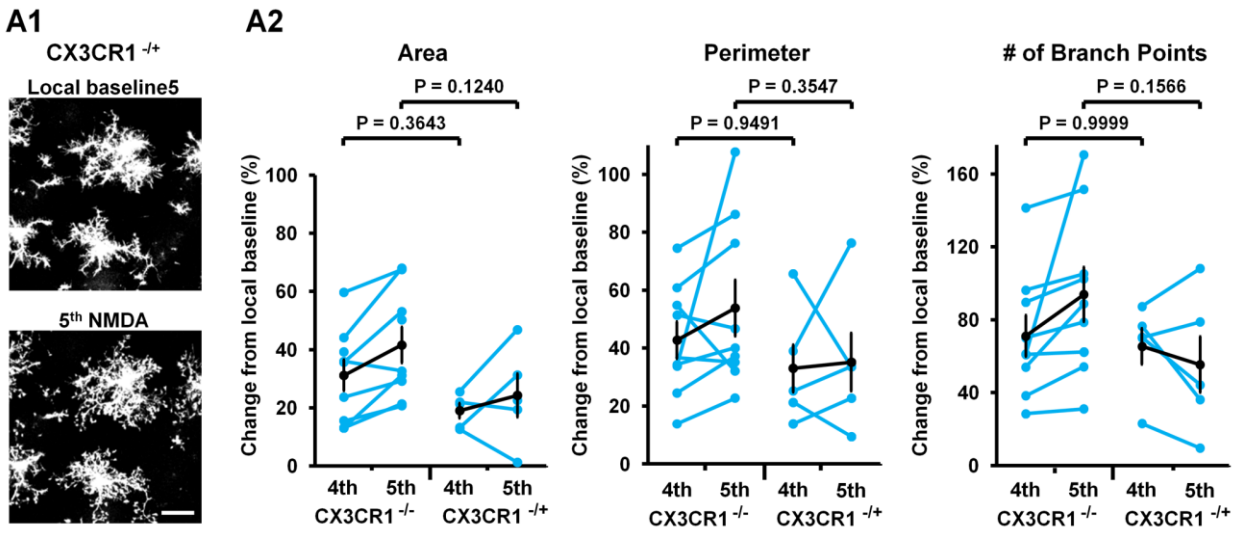

Figure 2-4 Outgrowth occurred independently of CX3CR1 expression.

Multiple bath applications of NMDA, using the paradigm presented in Fig. 2.2, led to a similar outgrowth in slices from CX3CR1 knock out ($CX3CR1^{-/-}$) and CX3CR1 heterozygous ($CX3CR1^{-/+}$) mice. ***A1,*** examples of outgrowth following the 5th NMDA application in comparison to the local baseline5 in a slice from a $CX3CR1^{-/+}$ mouse. Scale bar; 20 µM. ***A2,*** Graphic depiction of changes from the local baseline following the 4th and 5th NMDA application, determined as illustrated in Fig. 2.2, for both $CX3CR1^{-/-}$ and $CX3CR1^{-/+}$ mice. Each data point is represented with a blue dot and data points from the same experiments are connected with blue lines. The mean ± SEM is illustrated in black. One-way ANOVA with Bonferroni's multiple comparison post test was used for statistical comparison of the change from baseline following the 4th NMDA application in $CX3CR1^{-/-}$ and the 4th NMDA application in $CX3CR1^{-/+}$ mice as well as the 5th NMDA application in $CX3CR1^{-/-}$ and the 5th NMDA application in $CX3CR1^{-/+}$ mice; n = 9 for $CX3CR1^{-/-}$ (these are separate experiments than those depicted in Fig. 2.2D) and n = 5 for $CX3CR1^{-/+}$.

NMDA-triggered ATP release is selective to NMDAR stimulation

We next investigated whether ATP was released as a result of NMDA receptor activation or if NMDA directly activated microglial cells. As described above when NMDA was briefly applied at 5 different times there was no significant difference between the outgrowth following the 4th and the 5th NMDA applications. Therefore, we applied pharmacological agents 25 min prior to the 5th NMDA application and measured microglia process outgrowth to compare with the extent of outgrowth from the 4th NMDA application which is referred to as control (Fig. 2.5).

We determined, as expected, that the NMDA triggered outgrowth was due to NMDAR activation because process outgrowth was abolished by the NMDAR antagonist APV (Fig. 2.5A). Outgrowth still occurred in TTX to block action potentials and CNQX, at a concentration to block both AMPA and kainate receptors (Fig. 2.5B). Several studies have shown that ATP is a key trigger for microglial process outgrowth (Davalos et al., 2005; Haynes et al., 2006). We tested whether ATP release underlies the microglial response to NMDA by applying a broad spectrum ATP receptor antagonist, RB2 (Fig. 2.5C). RB2 is a potent competitive antagonist for P2Y12 (Hoffmann et al., 2008) and has previously been successfully used to block microglial process extension towards laser-induced lesions (Davalos et al., 2005). We found that RB2 completely blocked NMDA-triggered outgrowth indicating that microglial process outgrowth is mediated by a secondary release of purinergic agonists downstream of the action of NMDA.

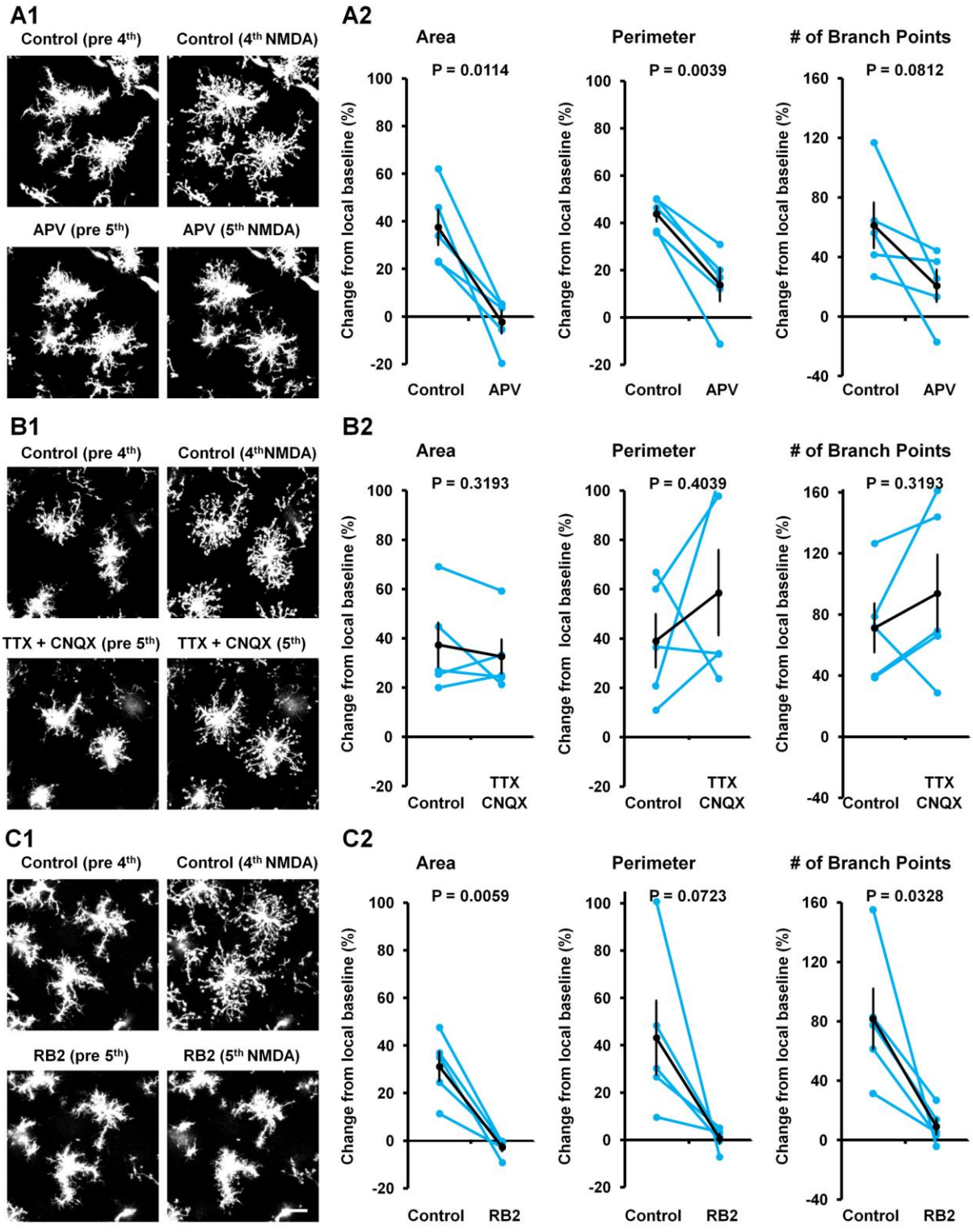
A1
Control (pre 4th)
Control (4th NMDA)
APV (pre 5th)
APV (5th NMDA)
A2
Area
P = 0.0114
Perimeter
P = 0.0039
# of Branch Points
P = 0.0812
Change from local baseline (%)
Control
APV
B1
Control (pre 4th)
Control (4thNMDA)
TTX + CNQX (pre 5th)
TTX + CNQX (5th)
B2
Area
P = 0.3193
Perimeter
P = 0.4039
# of Branch Points
P = 0.3193
Change from local baseline (%)
Control
TTX
CNQX
C1
Control (pre 4th)
Control (4th NMDA)
RB2 (pre 5th)
RB2 (5th NMDA)
C2
Area
P = 0.0059
Perimeter
P = 0.0723
# of Branch Points
P = 0.0328
Change from local baseline (%)
Control
RB2

Figure 2-5 NMDA triggered release of ATP is mediated by NMDA receptors and does not require action potentials or AMPA and kainate receptor stimulation.

A-C, Multiple bath applications of NMDA using the paradigm presented in Fig. 2.2 was performed with different pharmacological interventions initiated 25 min prior to the 5th NMDA application and continued throughout the experiment. ***A1-C1,*** Demonstration of microglial morphology shown at different time points (similar to Fig. 2.2, c, d, e and f). Local baselines are referred to as *'Pre NMDA'*. Scale bar; 20 µm. ***A1,*** Application of the NMDA receptor antagonist APV (100 µM) abolished the outgrowth '*APV (5th NMDA)'* compared to *'APV (pre 5th)'* versus *'Control (4th NMDA)'* compared to *'Control (pre 4th)'*. ***B1,*** Microglial process outgrowth still occurred independently of action potentials, blocked by TTX (1 µM), and AMPA and kainate receptors stimulation, blocked by CNQX (50 µM). ***C1,*** Application of the purinergic antagonist reactive blue 2 (RB2, 200 µM) completely abolished microglial process outgrowth. ***A2-C2,*** Graphic depiction of changes from the local baseline following the 4th NMDA application *'Control'* and the 5th NMDA application in the presence of the indicated pharmacological agents, determined as illustrated in Fig 2.2. Each data point is represented with a blue dot and data points from the same experiments are connected with blue lines. The mean ± standard error of the mean is illustrated in black. A paired t test was used to compare the two groups (n = 5).

NMDA-triggered microglial process outgrowth does not depend on NO or ATP-mediated ATP release

Since neuronal NMDAR activation is well known to result in nitric oxide (NO) production (Christopherson et al., 1999; Sattler et al., 1999; d'Anglemont de Tassigny et al., 2007), and NO has previously been reported to be a modulator of acute microglial reactions in the spinal white matter (Dibaj et al., 2010), we examined whether NMDA-induced NO formation contributed to microglia process outgrowth in our assay. Application of the potent blocker of NO-synthase L-NAME together with the NO-scavenger, PTIO did not block microglial process outgrowth (Fig. 2.6A), suggesting that the NMDA induced microglia process outgrowth was independent of NO production. In addition, the possibility that NMDA-triggered outgrowth required amplification of ATP itself via P2Y1 or P2X7 receptors was tested. Astrocytic P2Y1 receptors which are sensitive to broad spectrum purinergic inhibitors such as RB2 and PPADS and P2X7 receptors

that are inhibited by KN-62 have been reported to mediate ATP-induced ATP release (Pascual et al., 2012; Baroja-Mazo et al., 2013). Since RB2 blocked the microglia outgrowth, presumably by blocking P2Y12 receptors, we applied PPADS (which does not block P2Y12) together with the selective P2X7 blocker KN-62 (Baraldi et al., 2003), both of which failed to block NMDA induced microglia process outgrowth (Fig. 2.6B).

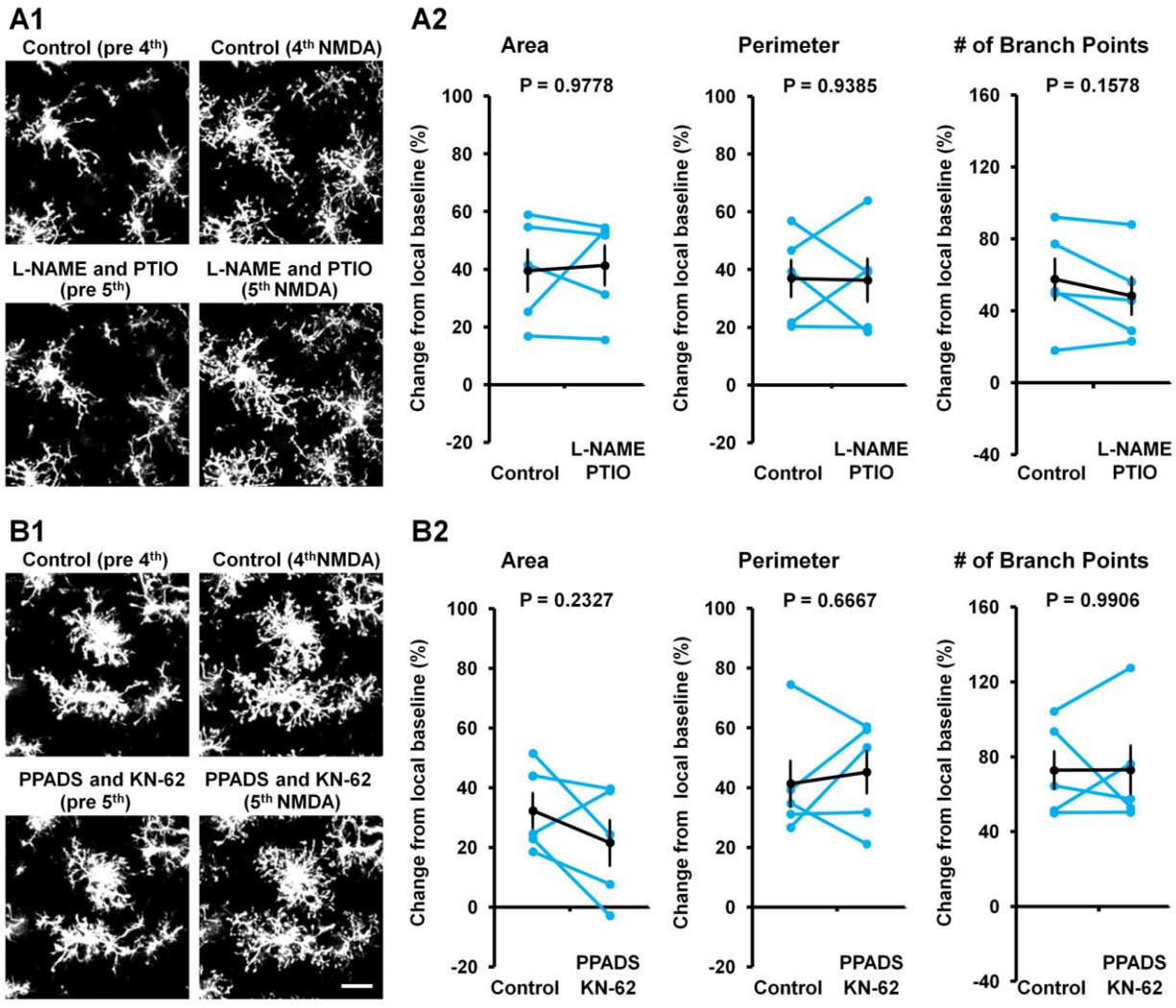

Figure 2-6 NMDA-triggered microglial process outgrowth does not depend on NO or ATP-mediated ATP release.

A-B, Multiple bath applications of NMDA using the paradigm presented in Fig. 2.2 was performed with different pharmacological interventions prior to the 5th NMDA application as described in Fig. 2.5. ***A1-B1,*** Demonstration of microglial morphology shown at different time points. Local baselines are referred to as *'Pre NMDA'*. Scale bar; 20 µm. ***A1,*** Application of the NO-synthase blocker L-NAME (1 mM) together with the NO-scavenger, PTIO (200 µM) had no effect on NMDA-triggered process outgrowth '*PTIO and L-NAME (5th NMDA)'* compared to '*PTIO and L-NAME (pre 5th)'* versus *'Control (4th NMDA)'* compared to *'Control (pre 4th)'*. ***B1,*** Application of the P2Y1 blocker PPADS (200 µM) together with the P2X7 blocker, KN-62 (15 µM) had no effect on NMDA-triggered process outgrowth 'KN-62 *and PPADS (5th NMDA)'* compared to 'KN-62 *and PPADS (pre 5th)'* versus *'Control (4th NMDA)'* compared to *'Control (pre 4th).* Each data point is represented with a blue dot and data points from the same experiments are connected with blue lines. The mean ± standard error of the mean is illustrated in black. A paired t test was used to compare the two groups (n = 5).

NMDA-triggered microglial process outgrowth requires ATP hydrolysis

Adenosine A3 receptor activation has also been reported to act synergistically with P2Y12 receptor stimulation to enhance microglia process outgrowth (Ohsawa et al., 2012). Thus we examined whether blocking the hydrolysis of ATP using the selective ectonucleotidase inhibitor ARL would alter the NMDA-triggered outgrowth (Fig. 2.7). ARL (50 µM) abolished the NMDA-triggered microglial process outgrowth (Fig. 2.7A) thereby indicating that local gradients of ATP and its derivates (ATP -> ADP -> AMP -> adenosine) by hydrolysis of ATP are crucial for microglial process outgrowth. We validated this observation by blocking the directed outgrowth to local application of ATP with ARL. 50 µM of ARL significantly reduced the outgrowth to 4 mM ATP and 200 µM of ALR completely blocked the directed outgrowth (Fig. 2.7B).

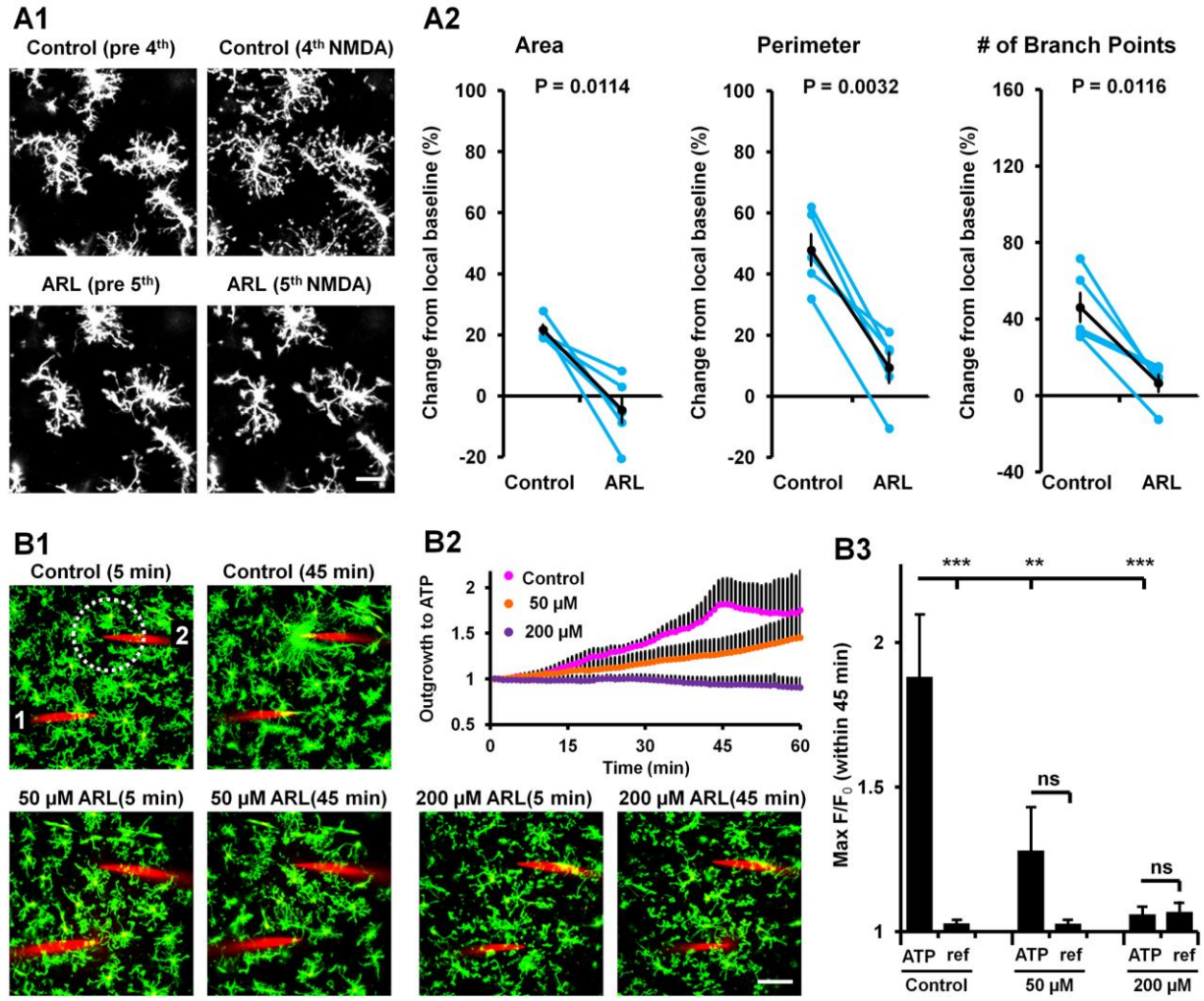

Figure 2-7 NMDA-triggered microglial process outgrowth was blocked by inhibiting hydrolysis of ATP.

A1-A2, Multiple bath applications of NMDA using the paradigm presented in Fig. 2.2 was performed with application of the ectonucleotidase inhibitor, ARL (50 µM) prior to the 5th NMDA application. ***A1,*** Demonstration of microglial morphology shown at different time points. Local baselines are referred to as *'Pre NMDA'*. Scale bar; 20 µm. ***A2,*** Application of ARL abolished NMDA-triggered process outgrowth 'ARL (*5th NMDA)'* compared to 'ARL *(pre 5th)'* versus *'Control (4th NMDA)'* compared to *'Control (pre 4th)'*. The mean ± standard error of the mean is illustrated in black. A paired t test was used to compare the two groups (n = 5). ***B1,*** Local application of ATP was used to validate the effect of ARL. Two electrodes was placed 100 µm apart. One electrode (#1) contained ACSF and served as a reference while the other electrode (#2) contained ACSF with 4 mM ATP. Note the processes surrounding the tip at 'Control (45 min)'. ***B2,*** Graphic depiction of outgrowth towards the ATP containing electrodes (measured as F/F_0). Note the peak after 45 in control when all the processes have reached the tip of the electrode. ***B3,*** Graphic depiction of max F/F_0 within the first 45 min. demonstrating a significant outgrowth towards the ATP containing electrode compared to the reference electrode (ref). 50 µM of ARL significantly reduced the

outgrowth to ATP compared to the outgrowth observed in control 200 μM of ALR completely blocked the directed outgrowth. One-way ANOVA with Bonferroni's multiple comparison post test was used for statistical comparison six groups (n = 3). **, P < 0.01; ***, P < 0.001; ns, non significant.

NMDA-triggered release of ATP occurred independently of Panx1 but was sensitive to probenecid

We next examined whether Panx1 channel opening was responsible for the release of ATP that induced process outgrowth when NMDAR were stimulated. We examined the activation of process outgrowth in microglia using the repetitive NMDA perfusion protocol described above with pharmacological interventions 25 min prior to the 5th NMDA application (Fig. 2.8). The non-selective Panx1 channel blocker, probenecid (Silverman et al., 2008) completely blocked process outgrowth (Fig. 2.8A). In contrast when we applied the potent blocker of Panx1 channels, CBX, (Thompson et al., 2006; Thompson et al., 2008) there was no significant decrease in any of the measures of process outgrowth (Fig. 2.8B). We performed additional control experiments to show that ATP-induced outgrowth still occurred in the presence of probenecid but was indeed blocked by RB2 (applied at the same concentration and at the same duration as for the NMDA experiments) (Fig. 2.8D). In addition, we ensured that CBX at this concentration effectively blocked dye-flux through astrocytic gap junctions (Fig. 2.8E), which are less sensitive than Panx1 to CBX (Spray et al., 2006). Thus the concentration of CBX would also block ATP release that might occur via connexin hemichannels(Pearson et al., 2005; Torres et al., 2012). The control experiments clearly demonstrated that ATP-induced outgrowth still occurred in the presence of probenecid and that CBX completely blocked dye-flux between astrocytes. Therefore based on the pharmacology the release mechanism does not appear to require Panx1 (or other connexin hemichannels) but is sensitive to probenecid.

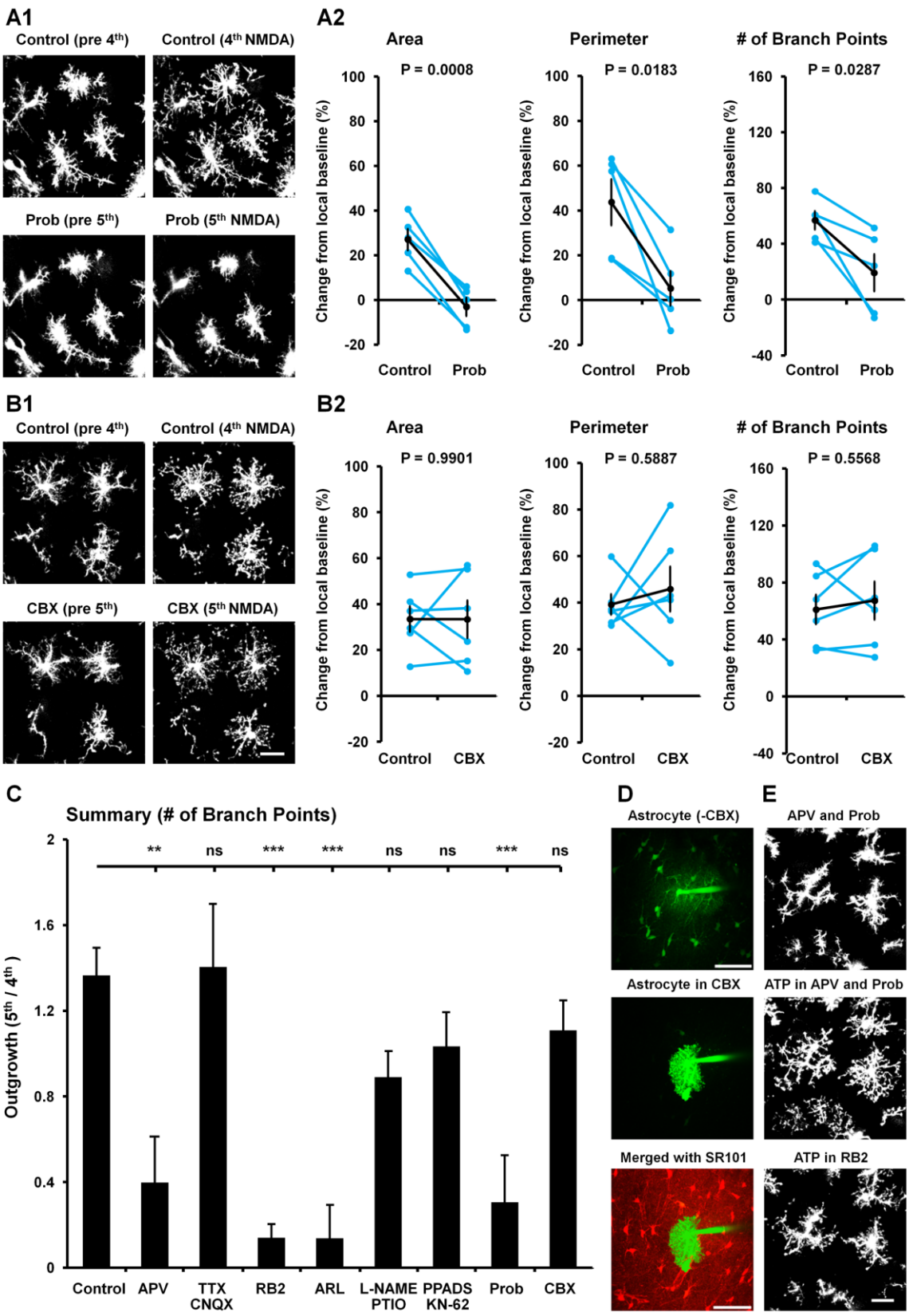
A1
Control (pre 4th)
Control (4th NMDA)
Prob (pre 5th)
Prob (5th NMDA)
A2
Area
P = 0.0008
Perimeter
P = 0.0183
# of Branch Points
P = 0.0287
Change from local baseline (%)
Control
Prob
B1
Control (pre 4th)
Control (4th NMDA)
CBX (pre 5th)
CBX (5th NMDA)
B2
Area
P = 0.9901
Perimeter
P = 0.5887
# of Branch Points
P = 0.5568
Control
CBX
C
Summary (# of Branch Points)
Outgrowth (5th / 4th)
** ns *** *** ns ns *** ns
Control
APV
TTX CNQX
RB2
ARL
L-NAME PTIO
PPADS KN-62
Prob
CBX
D
Astrocyte (-CBX)
Astrocyte in CBX
Merged with SR101
E
APV and Prob
ATP in APV and Prob
ATP in RB2

Figure 2-8 NMDA triggered ATP release is sensitive to probenecid but is not blocked by the Panx1 inhibitor carbenoxelone.

A-B, Multiple bath applications of NMDA using the paradigm presented in Fig. 2.2 was performed with different pharmacological interventions prior to the 5th NMDA application as described in Fig. 2.5. ***A1-B1,*** Demonstration of microglial morphology shown at different time points. Local baselines are referred to as *'Pre NMDA'*. Scale bar; 20 µm. **A1,** Application of probenecid (Prob, 2 mM) abolished the outgrowth. '*Prob (5th NMDA)'* compared to *'Prob (pre 5th)'* versus *'Control (4th NMDA)'* compared to *'Control (pre 4th)'*. **B1,** Microglial process outgrowth was not blocked by the potent Panx1 inhibitor, Carbenoxolone (CBX, 100 µM). ***A2-B2,*** Graphic depiction of changes from the local baseline following the 4th NMDA application *'Control'* and the 5th NMDA application in the presence of either Prob or CBX, determined as illustrated in Fig 2.2. Each data point is represented with a blue dot and data points from the same experiments are connected with blue lines. The mean ± SEM is illustrated in black. A paired t test was used to compare the two groups. n = 5 for A2 and n = 6 for B2. ***C,*** Graphic summary of the increase of number of branch points following NMDA triggered ATP release in the presence of the different pharmacological agents shown in Fig. 2.5A-C, Fig. 2.6A-B, Fig. 2.7A, and Fig. 2.8A-B. The increase in number of branch points is presented as the change from local baseline following the 5th NMDA application / the change from local baseline following the 4th NMDA application. The control group consists of the experiments depicted in Fig. 2.2 and Fig. 2.4A (n = 14). One-way ANOVA with Bonferroni's multiple comparison post test was used for statistical comparison of the nine groups. **, P < 0.01; ***, P < 0.001; ns, non significant. ***D-E,*** Demonstration of control experiments performed for CBX, APV, Prob, and RB2 respectively. ***D,*** In control, (absence of CBX) whole cell patch clamping of a single astrocyte with a fluorescent dye (Alexa 488, observed in green) inside the patch pipette allowed for dye diffusion through the gap junctions to surrounding astrocytes. However, in the presence of CBX the dye was restricted within the patched astrocyte and thus not observed in the surrounding astrocytes (loaded with Sulforhodamine 101, SR101 and observed in red) Scale bar; 50 µm. E, ATP-induced outgrowth still occurred in the presence of both APV and Prob but was blocked by RB2 (same concentration as used with NMDA applications). Scale bar; 20 µm.

SNAPSHOT preserved microglia morphology to demonstrate NMDA-triggered outgrowth and that P2Y12 and Iba1 were localized to growing bulbous tips

To gain novel insight into the location of the P2Y12 receptors during the morphological changes, we established a modified protocol for rapid and reliable fixation and immunolabeling of morphological changes in whole brain slices (Fig. 2.9). Our fixation protocol (SNAPSHOT) provided excellent preservation of microglia morphology when examining EGFP^{+}ve microglia

highlighted by the preservation of the processes growing towards a lesion (Fig. 2.9B-C1). Using our immunolabeling protocol we observed labeling of P2Y12 throughout the 300 µm thick slice. By acquiring non-saturated images of the expression of the membrane proteins P2Y12 and Iba1, we demonstrated a preferential accumulation of these proteins at the bulbous tips during outgrowth (Fig. 2.9C2-E. Importantly, we also demonstrated that this fixation protocol can preserve NMDA triggered process outgrowth (Fig. 2.9F) and thereby makes it an ideal tool for investigating the NMDA triggered outgrowth in CX3CR1$^{+/+}$ microglia that don't express EGFP.

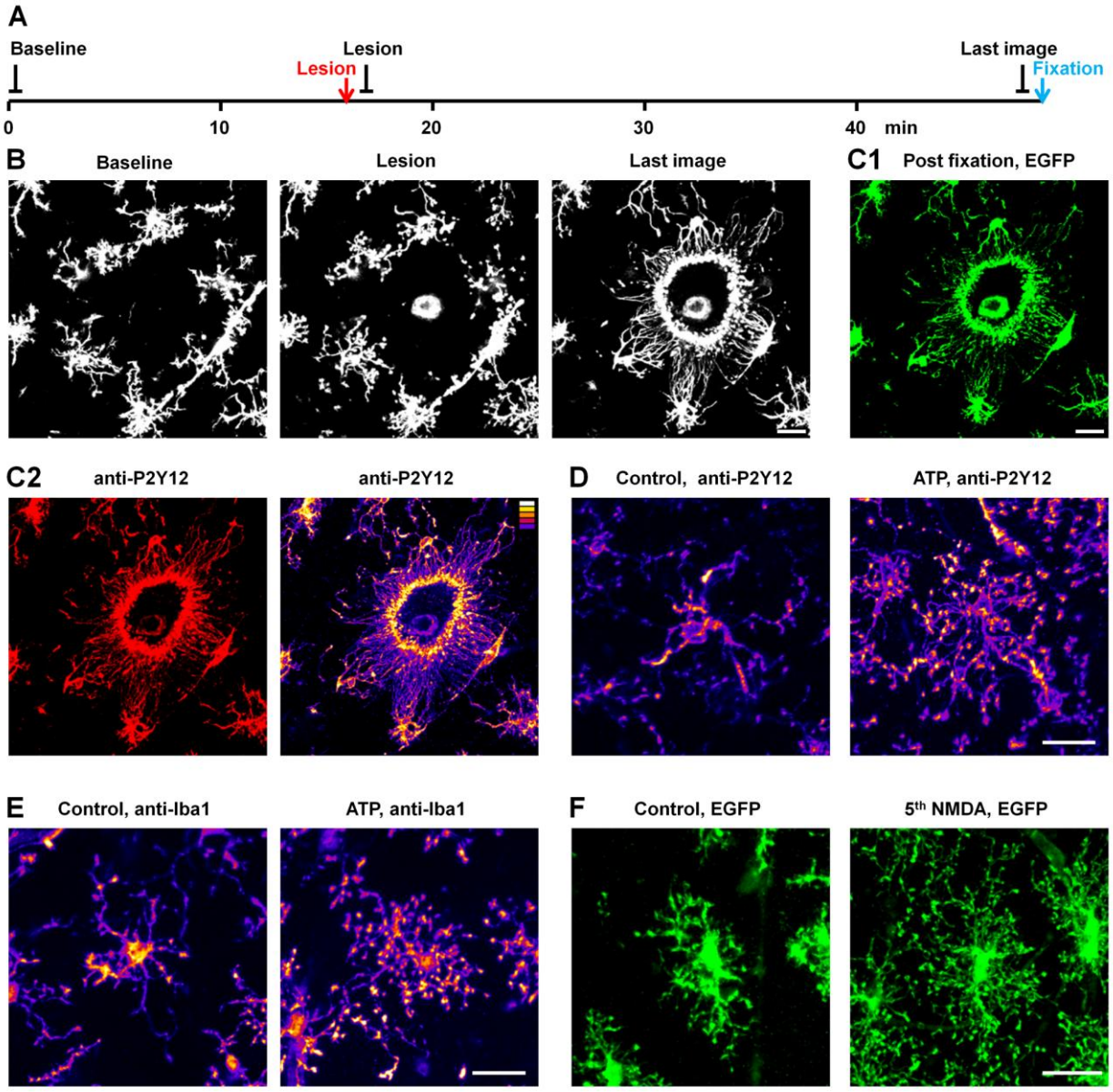

Figure 2-9 SNAPSHOT (StaiNing of dynAmic ProcesseS in HOt-fixed Tissue) allowed for morphological and immunohistochemical analysis of dynamic processes preserved at specific time points.

A, Timeline for image acquisition, formation of a lesion (indicated with a red arrow) and the time of fixation (indicated with a blue arrow). ***B,*** Example frames from real-time imaging of $EGFP^{+}$ve microglia over 48 min. The bright circular region in the *'lesion'* image is the lesion area that was induced by exposure of high laser power illumination restricted to this area. Note that the 'last image' was acquired < 1 min prior to fixation. Scale bar; 50 µm. ***C1-C2,*** Morphology of the brain slice that was fixed 30 min after lesioning and immunolabeled using the SNAPSHOT method. C1, microglial process outgrowth towards the lesion was preserved and could be visualized by imaging of EGFP. C2, illustration of P2Y12 immunolabeling and pseudocoloring of the non-saturated labeling

intensity (intensity scale for 8-bit image (top right corner); 0 (black), 50, 100, 150, 200, 255 (white)). The SNAPSHOT protocol allowed us to detect that high levels of P2Y12 receptors were located at the bulbous tips. ***D,*** A similar pattern of preferential distribution of P2Y12 immunolabeling to the growing tips was reproduced when SNAPSHOT was applied to preserve the microglial process outgrowth triggered by ATP application (15 min). Note the increased intensity of labeling at the bulbous tips compared to the processes in control conditions. Scale bar; 20 µm. ***E,*** A similar pattern of preferential localization at the bulbous tips was also observed with Iba-1 immunolabeling of ATP induced process outgrowth. Scale bar; 20 µm. ***F,*** Fixation of brain slices subjected to 5 NMDA applications demonstrated that NMDA triggered microglial process outgrowth (fixed eight min after the 5^{th} NMDA application) can be preserved using the SNAPSHOT method. Scale bar; 20 µm.

Microglial outgrowth still occurred in Panx1-deficient mice

In light of the discrepancies in the results obtained using pharmacological inhibitors of Panx1, we aimed to determine if NMDA still induced microglia process outgrowth in brain slices from $Panx1^{-/-}$ mice (Fig. 2.10). Western blots confirmed complete absence of Panx1 protein in the $Panx1^{-/-}$ mice at 6 weeks of age while the Panx1 protein was observed in strain specific WT (C57BL/6) and at similar levels in the transgenic strain used for microglial time lapse imaging ($CX_3CR1^{EGFP/EGFP}$, BALB/C) (Fig. 2.10C). We therefore tested whether NMDA could cause process outgrowth in brain slices from $Panx1^{-/-}$ mice that were subjected to multiple NMDA applications. The slices were fixed 8 min after the 5^{th} NMDA application using the protocol that we found to reliably preserve microglia morphology. Comparisons were made between brain slices treated with NMDA (10 slices from 5 animals) versus untreated brain slices that were perfused in tissue chambers for identical periods of time (5 slices from the same 5 animals). We used immunolabeling of Iba1, a specific microglia cell marker (Imai et al., 1996) to visualize microglia morphology. Extensive process outgrowth with bulbous tips was observed in microglia from $Panx1^{-/-}$ mice following 5 NMDA applications. Microglia in untreated slices showed a characteristic ramified morphology (Fig. 2.10D-E). This result also confirms that outgrowth occurs in $CX3CR1^{+/+}$ mice and laser-induced phototoxicity does not play any role in the

outgrowth observed in our paradigm. In addition the observation of outgrowth in microglia from NMDA application in Panx1$^{-/-}$ confirms the pharmacological data that the process does not require ATP release from Panx1 channels.

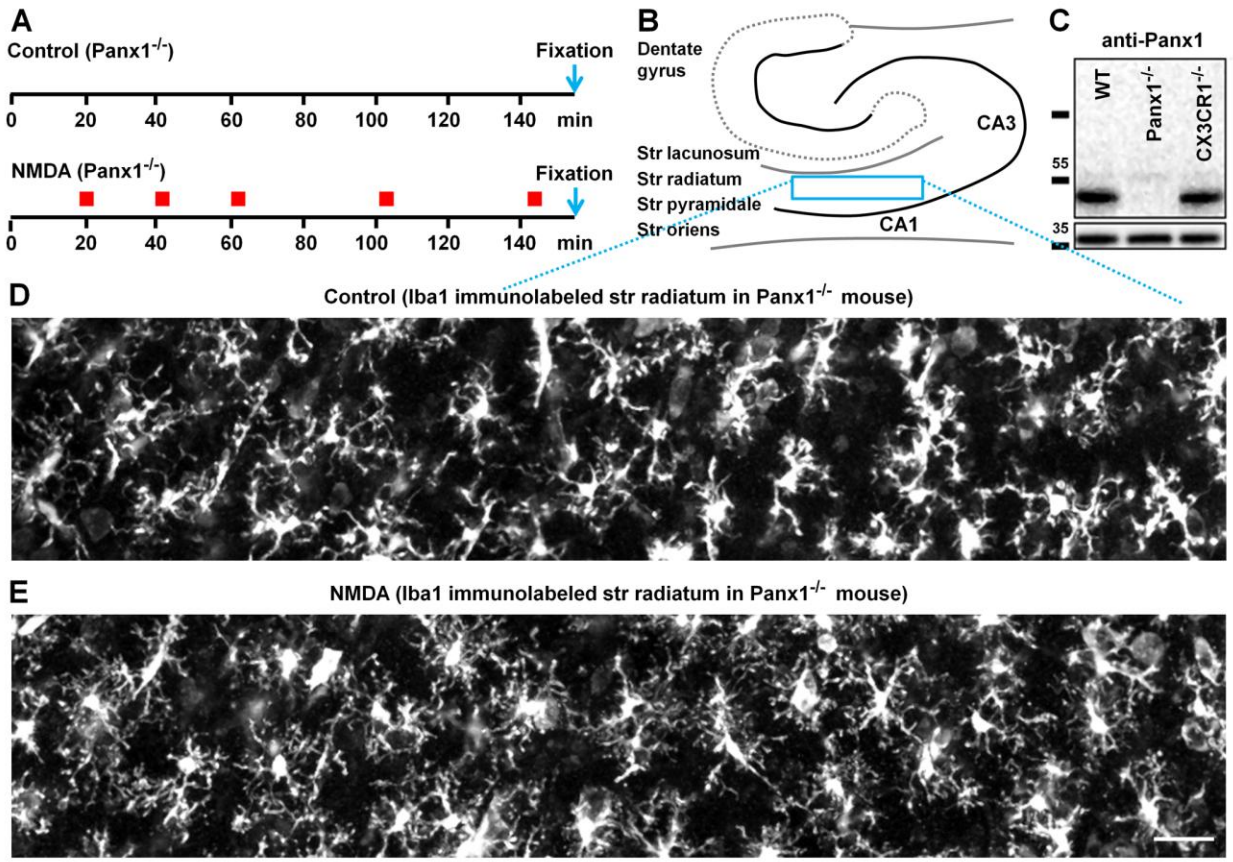

Figure 2-10 NMDA triggered ATP release is independent of Panx1 expression.

A, Timeline for NMDA applications (indicated with red markers) and time of fixation (indicated by blue arrows) compared to matched controls with no NMDA applications. ***B,*** Schematic showing the portion of the hippocampal CA1 region that was analyzed for morphological changes of microglia. **C**, Western blots of hippocampal brain slice homogenates obtained from Panx1-deficient mice (on C57BL/6 background) '*Panx1*$^{-/-}$', C57BL6 wild type mice '*WT*', and CX3CR1$^{EGFP/EGFP}$ mice (on BALB/c background) *'CX3CR1*$^{-/-}$*'* were stained with Panx1 antibodies (Panx1 expected size; 48 kDa) and re-probed with antibodies against GAPDH (expected size; 37 kDa). ***D-E,*** Using our protocol (SNAPSHOT) the microglial morphology at the time of fixation was preserved and visualized by Iba1 immunolabeling. ***D,*** Illustration of the microglia morphology in a horizontal cross-section of the stratum (Str) radiatum in the CA1 in a control slice from a *Panx1*$^{-/-}$ mice that was not subjected to NMDA

applications. ***E,*** Illustration of the change in microglia morphology in a slice (from the same *Panx1*$^{-/-}$ mouse shown in *D*) that was subjected to 5 NMDA applications, using the paradigm presented in *A*, and fixed eight min after the 5th NMDA application. Scale bars; 50 µm.

Microglial process outgrowth triggered by selective NMDAR activation on a single neuron

To determine whether the initial trigger of microglial process outgrowth can be ascribed to activation of dendritic neuronal NMDAR (versus potential NMDAR expression on glial cells) we patch clamped CA1 pyramidal neurons using a strategy to selectively activate NMDAR on a single neuron. Experiments were performed in the presence of high extracellular Mg^{2+} (6 mM) to block neuronal NMDAR at resting membrane potential. Additionally, TTX and CNQX (to block voltage gated sodium channels and AMPA/kainate receptors, respectively) were applied to prevent spontaneous depolarization of other neurons (Fig. 2.11). Single patch clamped neurons were depolarized to 0 mV, thereby removing the magnesium block and permitting activation of NMDAR on the clamped neuron while NMDAR on surrounding neurons were stilled blocked. In control experiments, neurons were kept hyperpolarized at -70 mV to maintain the Mg^{2+} block and prevent NMDAR activation or cells were patched and depolarized with MK-801 in the patch electrode to block open NMDA channels. Significant microglia outgrowth was observed only when the neuron was depolarized to allow NMDAR activation but not when the neuron was kept hyperpolarized or when the NMDAR open channel blocker, MK-801 was added to the internal solution (Fig. 2.11B-E). To confirm that 6 mM Mg^{2+} (plus TTX and CNQX) was sufficient to block the action of NMDA on non depolarized cells, NMDA was applied to brain slices from EMX–GCaMP3 mice to allow us to visualize intracellular calcium concentration ($[Ca^{2+}]_i$) changes that occur when NMDAR are activated on neurons. We found that the high Mg^{2+} conditions effectively blocked NMDA-triggered calcium signals in contrast to large $[Ca^{2+}]_i$

signals observed in 0 Mg^{2+} or 0.6 mM Mg^{2+}. The amplitude of the $[Ca^{2+}]_i$ signals evoked by NMDA in 0.6 mM Mg^{2+} was not reduced by TTX and CNQX demonstrating that block is entirely Mg^{2+} dependent. Additionally, since we found that probenecid (2 mM) blocked microglial process outgrowth we tested whether probenecid would affect NMDA-induced $[Ca^{2+}]_i$ signals. Probenecid had no effect on the amplitude of the $[Ca^{2+}]_i$ signals.

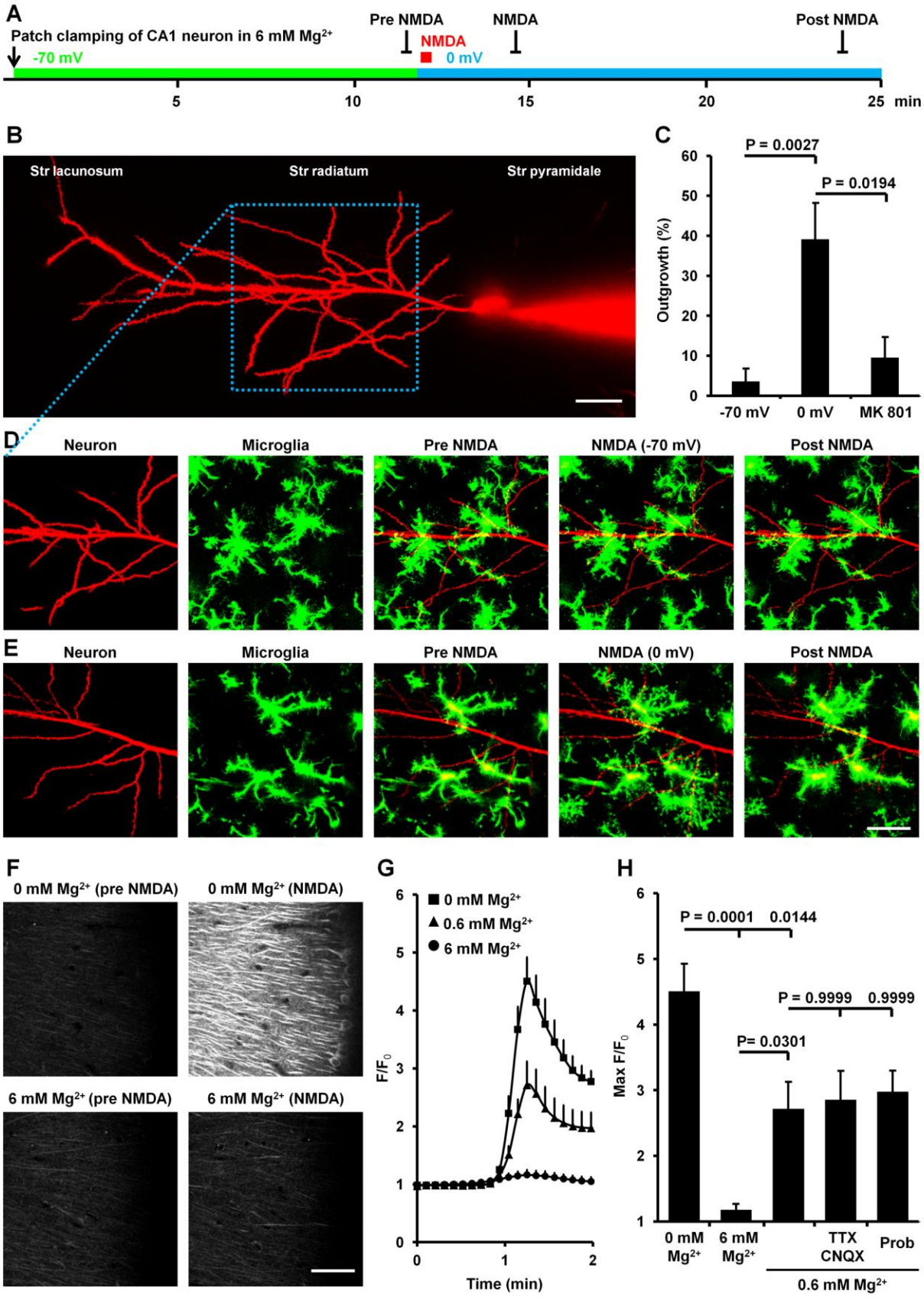
A
Patch clamping of CA1 neuron in 6 mM Mg2+
-70 mV
Pre NMDA
NMDA
0 mV
NMDA
Post NMDA
5
10
15
20
25 min
B
Str lacunosum
Str radiatum
Str pyramidale
C
P = 0.0027
P = 0.0194
Outgrowth (%)
60
50
40
30
20
10
0
-70 mV
0 mV
MK 801
D
Neuron
Microglia
Pre NMDA
NMDA (-70 mV)
Post NMDA
E
Neuron
Microglia
Pre NMDA
NMDA (0 mV)
Post NMDA
F
0 mM Mg2+ (pre NMDA)
0 mM Mg2+ (NMDA)
6 mM Mg2+ (pre NMDA)
6 mM Mg2+ (NMDA)
G
0 mM Mg2+
0.6 mM Mg2+
6 mM Mg2+
F/F0
Time (min)
H
P = 0.0001
0.0144
P = 0.9999
0.9999
P= 0.0301
Max F/F0
0 mM Mg2+
6 mM Mg2+
TTX
CNQX
Prob
0.6 mM Mg2+

Figure 2-11 Microglial process outgrowth is triggered by selective NMDAR activation on a single neuron.

A, Timeline for patch clamping, image acquisition, and depolarization during NMDA application**. *B,*** Illustration of the morphology of a patch clamped CA1 neuron dialyzed with internal solution containing Alexa 594. z-projection of 60 images (120 µm). Note the soma and the patching electrode in the stratum (Str) pyramidale. This blurry part of the image is due to light scattering because of the high cell density in Str pyramidale. Scale bar; 30 µm. ***C,*** Quantification of microglial processes outgrowth in the presence of high extracellular Mg^{2+} (6 mM) to block NMDAR in neurons at resting membrane potential. Significant microglia outgrowth was observed only when the neuron was depolarized to allow NMDAR activation but not when the neuron was kept hyperpolarized or when the neuron was depolarized with MK 801 added to the internal solution. One-way ANOVA with Bonferroni's multiple comparison post test was used for statistical comparison of the three groups. n-values; 6 (-70 mV), 5 (0 mV) and 4 (MK801). ***D,*** Demonstration of the microglial morphology shown at different time points together with part of the dendritic arbor (shown in B). z-projection of 20 images (40 µm). Note that NMDA (100 µM) does not trigger outgrowth when the neuron is kept hyperpolarized *'NMDA (-70 mV)'* compared to *'pre NMDA'* and *'post NMDA'*. ***E,*** Similar demonstration as shown in D but in this experiment the neuron was depolarized to remove its Mg^{2+} block prior to application of NMDA. Note the NMDA-triggered outgrowth '*NMDA (0 mV)'* compared to *'pre NMDA'* and *'post NMDA'*. Scale bar; 30 µm. ***F-H,*** NMDA application to brain slices from EMX–GCaMP3 mice that express the calcium indicator, GCaMP3 in neurons. **F,** Demonstration of NMDA-triggered Ca^{2+}_i signals in the presence of 0 or 6 mM Mg^{2+}. Note the elevation in Ca^{2+}_i in 0 mM Mg^{2+} *'NMDA'* versus *'pre NMDA'* compared to in 6 mM Mg^{2+} *'NMDA'* versus *'pre NMDA'.* Scale bar; 50 µm. ***G,*** Graphic depiction of NMDA-triggered Ca^{2+}_i signals in the presence of 0 mM, 0.6 mM, and 6 mM Mg^{2+} measured as F/F_0 in a 100 x 100 µm 'region of interest' placed in the Str radiatum. F = fluorescence intensity at time x and F_0 = fluorescence intensity at time 0. The traces were aligned for peak values. ***H,*** Graphic depiction of max F/F_0 demonstrating that 6 mM Mg^{2+} significantly blocked NMDA-triggered Ca^{2+}_i signals compared to the large Ca^{2+}_i signals that were observed in 0 mM Mg^{2+} and 0.6 mM Mg^{2+} conditions.. The amplitude of the neuronal Ca^{2+}_i signals evoked by NMDA in 0.6 mM Mg^{2+} was not reduced by TTX and CNQX. Probenecid had no effect on the NMDA induced Ca^{2+}_i signal at the concentration (2 mM) that prevented microglia process outgrowth from NMDAR activation. One-way ANOVA with Bonferroni's multiple comparison post test was used for statistical comparison of the five groups(n =3).

2.4 Discussion

Our results demonstrate that stimulation of neuronal NMDAR triggers microglial process outgrowth as a result of ATP efflux. The outgrowth following dendritic NMDAR stimulation was abolished in the presence of APV and MK-801 indicating that it was dependent on neuronal

NMDAR. The wide-spectrum purinergic inhibitor RB2 and the ectonucleotidase inhibitor ARL, also blocked NMDA-triggered microglial process outgrowth demonstrating that the outgrowth was caused by ATP and not by direct actions of NMDA itself. The mechanism underlying ATP efflux that in turn induces microglia process outgrowth was independent of Panx1 channel opening, ATP release from astrocytes via connexins and NO generation but it was sensitive to probenecid. Finally, we show that selective activation of dendritic NMDAR on a single neuron is sufficient to trigger microglial process outgrowth.

The patterns of process outgrowth induced by NMDA were similar to the outgrowth induced by direct ATP application although there were three interesting differences. First, under our experimental conditions we found that multiple applications of NMDA were required to trigger reliable and robust outgrowth whereas direct purinergic stimulation by a single ATP application immediately caused a pronounced outgrowth. Second, outgrowth triggered by a 1 min NMDA application could persist for up to 15 min. In contrast ATP-induced outgrowth reversed immediately after the ATP application was terminated. Third, outgrowth triggered by bath application of NMDA was non-polarized in that the number and extension of processes were isotropic. In contrast, the outgrowth induced by bath application of ATP was polarized towards the surface of the slice.

Considering that the application of ATP immediately triggers microglial process outgrowth, we hypothesize that the requirement of multiple NMDA applications for triggering a robust microglia process outgrowth is due to progressively enhanced ATP release following multiple NMDA applications. In addition, ATP is rapidly hydrolyzed to adenosine by ectonucleotidases within the tissue (Farber et al., 2008) resulting in an immediate decline in extracellular ATP concentrations following termination of ATP application. This rapid hydrolysis of ATP also

explains why the bulbous tips withdrew and the processes retracted rapidly upon removal of ATP. The protracted time course of process outgrowth (up to 15 min) triggered by NMDA application likely reflects a prolonged release of ATP which may be explained by slow NMDA washout in addition to the kinetics of the mechanisms of ATP release. We further demonstrate that the purinergic gradient generated by the extonucleotidases is crucial for directed microglia processes outgrowth.

The non-polarized outgrowth of microglial processes in response to NMDA application suggests that the extensive stimulation of NMDAR in the hippocampal dendritic region causes the release of ATP throughout the tissue. In contrast the polarization of process outgrowth towards the surface of the slice during ATP application suggests that bath application of ATP leads to the formation of a downward ATP gradient from the surface of the slice due to *in situ* hydrolysis of ATP. The NMDA-triggered microglial response was not the result of excitotoxic damage because the outgrowth triggered by NMDAR stimulation was reversible. Several studies have shown that outgrowth triggered by tissue damage causes microglial processes to extend towards and adhere to the site of damage (Kim and Dustin, 2006; Eter et al., 2008; Hines et al., 2009).

Importantly, we demonstrated that stimulation of neuronal NMDAR is the initial trigger of microglial process outgrowth as outgrowth in the presence of high extracellular Mg^{2+} only occurs when neurons are selectively depolarized. The outgrowth triggered by NMDA application was also abolished by blocking purinergic receptors and by inhibiting hydrolysis of ATP. Thus, we conclude that microglia process outgrowth triggered by NMDA application was due to release of ATP downstream of neuronal NMDAR stimulation and not by NMDA itself even

though NMDAR expression has been reported on a subset of microglia (Gottlieb and Matute, 1997; Liang et al., 2010; Murugan et al., 2011; Kaindl et al., 2012).

To investigate the expression of P2Y12 on microglia we developed a novel fixation and immunolabeling protocol (SNAPSHOT). Using SNAPSHOT we discovered that the P2Y12 receptor proteins accumulated at the bulbous tips during ATP-induced process outgrowth thereby spatially associating it with the leading edge of the extending processes.

Another key chemotactic microglial receptor is the CX3CR1 fractalkine receptor. Binding of fractalkine to CX3CR1 provides a tonic inhibitory signal that keeps the microglia in a quiescent surveillance mode (Wolf et al., 2013) and modifies the velocity of microglia processes (Liang et al., 2009). Therefore we examined whether microglial process outgrowth triggered by NMDAR stimulation was reduced or blocked in $CX3CR1^{-/+}$ or $CX3CR1^{+/+}$ mice compared to $CX3CR1^{-/-}$. No significant differences in outgrowth were seen in time-lapse imaging of slices from $CX3CR1^{-/+}$ mice or in fixed slices from $CX3CR1^{+/+}$ mice using SNAPSHOT. We conclude that NMDA-triggered process outgrowth in the adult mouse was independent of CX3CR1. However, our study does not exclude the possibility that CX3CR1 might play a role during development where CX3CR1-deficiency has been demonstrated to result in reduced microglial numbers, impaired switching of GluN2B-to-GluN2A and delays synaptic maturation (Paolicelli et al., 2011; Hoshiko et al., 2012).

Our finding that CBX does not block process outgrowth demonstrates that the release of ATP occurs independently of Panx1 as CBX has been demonstrated in numerous studies to abolish ATP release via Panx1 (Chekeni et al., 2010; Li et al., 2011b; Lohman et al., 2012). The absence of a block by CBX also excludes alternative ATP release pathways. The block of astrocytic dye-coupling confirmed that CBX at these concentrations completely blocks astrocytic

gap junctions that are primarily formed by connexin 43 (Dermietzel et al., 2000). Panx1 is blocked by CBX at a 10 times lower concentration than required for blockade of gap junctions (Spray et al., 2006). Therefore, the effective block of astrocyte dye-coupling via gap junctions indicates that Panx1 channels were blocked under these conditions. Astrocytes have been demonstrated to release ATP through opening of connexin 43 channels due to decreased extracellular Ca^{2+} following high neuronal activity (Cotrina et al., 1998; Torres et al., 2012). However, the block of connexin 43-mediated ATP release by CBX (Pearson et al., 2005; Torres et al., 2012) eliminates the possible role of astrocytic hemichannels in ATP efflux following induction of high neuronal activity induced by NMDAR stimulation. We further demonstrated that outgrowth occurred independent of ATP-induced ATP release from astrocytes.

Using SNAPSHOT on brain slices from Panx1-deficient mice subjected to 5 NMDA applications, we further demonstrate that NMDA-triggered microglial process outgrowth occurs independently of Panx1 expression. Whether Panx1 can play a role in neuron-microglia communication under other conditions such as necrosis or apoptosis is still to be investigated. Our results describe a pathway by which neuronal NMDAR activation mediates ATP-induced outgrowth independent of Panx1. Recent reports have indicated a functional role of Panx2 homomers in the brain, raising questions about involvement of Panx2 in our paradigm. Initial observations point towards CBX as being an effective inhibitor of Panx2 (Ambrosi et al., 2010; Bargiotas et al., 2011); however, more selective pharmacological agents are needed to resolve this question.

Notably, we found that the non-selective Panx1 blocker probenecid, which also inhibits several transporters of the ATP-binding cassette superfamily (e.g. organic anion transporters and multidrug resistance-associated proteins) (Di Virgilio et al., 1988; Lipman et al., 1990; Potschka

et al., 2004), blocked the NMDA-triggered microglial process outgrowth. It is unlikely that the effect of probenecid is due to attenuation of NMDA-induced currents as this inhibition requires concentrations 10 times higher than the concentration used in this study (Urenjak et al., 1997) and we demonstrate that 2 mM probenecid has no effect on NMDA-triggered calcium signals. Probenecid has previously been reported to block ATP-mediated microglial process outgrowth in the retina where outgrowth was triggered by a single bath application of AMPA or kainate (Fontainhas et al., 2011). While the discrepancy in the initial stimuli leading to ATP release might be ascribed to tissue specific differences (retina versus hippocampus), the fact that probenecid blocked the ATP-mediated outgrowth triggered by activation of any of the three main neuronal ionotropic glutamate receptors suggests a common, yet undetermined mechanism for neuron-microglia communication.

Microglia derived neurotrophins have been reported to promote synapse formation (Parkhurst et al., 2013) and ramified microglia limit neuronal degeneration following excessive NMDAR stimulation (Vinet et al., 2012). Our results demonstrate that activation of neuronal NMDAR triggers the release of ATP via a mechanism that is independent of cell death or Panx1 opening but is sensitive to probenecid. We suggest that ATP is an important molecular cue that enhances the surveillance exerted by microglial processes within the regions of the dendritic arbors following NMDAR activation on neuronal dendrites. The functional roles of this neuronal evoked enhanced surveillance are undetermined but could potentially lead to reciprocal communication via local release of neurotrophins. In conclusion, these findings demonstrate a form of neuron-microglia communication that is initiated by dendritic NMDAR activation in the adult brain.

Chapter 3: Opening of connexin hemichannels triggers ATP-mediated focalization of microglial processes

3.1 Introduction

A decade has passed since the initial discovery that resting microglial cells are highly dynamic surveillants of the healthy adult brain parenchyma. However, the functional role of microglia in the healthy adult CNS is unknown and whether microglial process dynamics are modified by synaptic transmission remains controversial (Nimmerjahn et al., 2005; Wu and Zhuo, 2008; Wake et al., 2009). Thus, identifying circumstances where neuronal and/or glial activity evokes changes in microglial process dynamics would be important for the overall understanding of the role of microglia in the healthy and the diseased nervous system. In chapter 2 we described a novel pathway by which ATP efflux, secondary to activation of neuronal NMDAR, triggers transient microglial process outgrowth (Dissing-Olesen et al., 2014). In this study it is clear that not only is ATP a potent signaling molecule mediating neuron-microglial communication but also that changes in microglial morphology can be taken as a reliable readout for ATP release.

Stimulation of P2Y12 receptors by ATP and ADP triggers a strong polarization of microglial processes towards the source of ATP accompanied by the formation of bulbous tips on the leading edges of extending processes (Davalos et al., 2005; Haynes et al., 2006; Dissing-Olesen et al., 2014). In addition the extension of microglial processes also requires a purinergic gradient generated by hydrolysis of ATP and its derivatives by ectonucleotidases (Farber et al., 2008; Ohsawa et al., 2012; Dissing-Olesen et al., 2014).

ATP release has been reported in many studies to be caused by the opening of Cx hemichannels which are large ATP-permeable pores. Cx43 and Cx30 are the main gap-junction

forming Cx in astrocytes (Dermietzel et al., 1989; Nagy et al., 1999) and Cx43 hemichannels have been reported to open under physiological and pathological conditions (Contreras et al., 2003; Retamal et al., 2006; Huang et al., 2012). Multiple reports have shown that Cx43 hemichannel opening is evoked by a decrease in extracellular Ca^{2+} (Ye et al., 2003) whereas normal levels of extracellular Ca^{2+} (1-2 mM) limit the probability of opening (Stout and Charles, 2003). Low extracellular Ca^{2+} has been shown to evoke the release of ATP and glutamate as well as efflux or uptake of small molecular dyes in astrocytes (Stout et al., 2002; Stout and Charles, 2003; Ye et al., 2003) and in Cx43-expressing HeLa cells (Contreras et al., 2003), C6 glioma cells (Stout et al., 2002), osteoblasts (Romanello and D'Andrea, 2001), and HEK cells (John et al., 1999; Kondo et al., 2000). Importantly, Cx43-mediated ATP efflux has also been demonstrated in acute brain slices by chelating extracellular Ca^{2+} or by indirectly lowering extracellular Ca^{2+} by increasing neuronal activity. ATP release was not observed in mice deficient for astrocytic Cx43 while transgenic mice carrying an astrocyte specific mutation causing increased opening of Cx43 resulted in enhanced and prolonged release of ATP (Torres et al., 2012).

We hypothesized that a drop in extracellular Ca^{2+} would trigger ATP efflux through opening of astrocytic Cx43 hemichannels and consequently a change in microglial process dynamics. To address this question, acute hippocampal brain slices from mice that express EGFP in microglia were imaged using two photon laser scanning microscropy. The acute slices were either imaged live or following fixation using our novel method for fixation of fine dynamic structures called SNAPSHOT. Pharmacological interventions against the P2Y12 receptor activation and hemichannel opening were applied to demonstrate that changes in microglial process dynamics were ATP dependent and that the source of ATP potentially was Cx43 hemichannel opening.

Additionally, intracellular Ca^{2+} in microglia and extracellular glutamate levels were imaged in real-time in slices from mice that expressed either expressed GCaMP3 or iGluSFnR.

3.2 Materials and methods

Animals

$CX3CR1^{EGFP/EGFP}$ mice on a BALB/c background (Jung et al., 2000) and CX3CR1-cre^{ER}-floxTNFalpha x ROSA26-GCaMP3 mice on a C57BL/6 background were bred and housed under controlled conditions (12 h light/dark cycle) with food and water ad libitum. CX3CR1-cre^{ER} males (homozygous) where crossed with ROSA26-GCaMP3 females (homozygous) and double heterozygous offspring were used for experiments. GCaMP3 was inserted into the ROSA26 locus where it is preceded by a promoter (CAG) and a loxp-flanked stop cassette. Tamoxifen induced expression of cre recombinase which excises the loxp codon then allows the transcription of GCaMP3. CX3CR1 is selective to microglia in the CNS, hence tamoxifen administration triggers selective microglial expression of GCaMP3 in our slice preparation.

Slice preparation

$CX3CR1^{EGFP/EGFP}$ and CX3CR1-cre^{ER}-floxTNFalpha x ROSA26-GCaMP3 mice (90-300 days, both males and females) were decapitated according to protocols approved by the University of British Columbia committee on animal care. The brains were removed and 300 µm thick horizontal slices were generated using the procedure described in chapter 2. Additionally, 400 µm thick coronal brain slices from male FVB/N mice that express iGluSnFr in the dorsal striatum were obtained in collaboration with Matthew P. Parsons, Pumin Wang, Timothy H. Murphy, and Lynn A. Raymond, University of British Columbia. Ideally, we would have

performed our investigation in hippocampal brain slices but half of the slices from these mice were used in another study that was investigating glutamate release in the dorsal striatum. At approximately 1 month of age these mice had AAV1.hSyn.iGluSnFr.WPRE.SV40 (Penn Vector; provided by Dr. Loren Looger, Janelia Farm Research Campus of the Howard Hughes Medical Institute) injected into the dorsal striatum. iGluSnFR expression was driven by the synapsin promoter which provides a uniform distribution on the surface of neuronal membranes (Marvin et al., 2013). Approximately one month after the injections the mice were decapitated and slices were prepared using a previously described procedure (Parsons et al., 2014).

0 mM Ca^{2+} experiments

All experiments were performed at room temperature (RT) in oxygenated ACSF (126 mM NaCl, 2.5 M KCl, 26 mM $NaHCO_3$, 2 mM $MgCl_2$, 1.25 mM NaH_2PO_4, and 10 mM D-glucose, 2.0 mM $CaCl_2$) at pH 7.3-7.4. For experiments involving 0 mM extracellular Ca^{2+}, $CaCl_2$ was replaced with 2 mM EGTA and pH was adjusted to 7.35 with 1 M NaOH. 2 mM EGTA was also included in the ACSF for the experiments investigating concentration-dependent microglial responses to different concentrations of free extracellular Ca^{2+}. The online Ca-EGTA Calculator v1.2 (maxchelator.stanford.edu/CaEGTA-NIST) was used to calculate the concentration of $CaCl_2$ required. Pharmacological interventions including application of mimetic peptides were performed in 0 mM Ca^{2+} with 2 mM EGTA for 1 hour without pretreatment.

Tail vein injections and perfusions

To provide a fluorescent angiogram the fluorescent dye Texas Red was injected intravenously (100 µl of 100 mg / ml in sterile PBS) 10 min prior to decapitation. To ensure that

the dye would stay within the vessels throughout the experiments Texas Red was conjugated with 70.000 MW dextran. Additionally, for the dye to be applicable to the SNAPSHOT method we chose a dextran containing fixable lysine residues (Invitrogen). To avoid auto-fluorescence from the vessel lumens in slices that would be fixed and immunolabeled using SNAPSHOT the mice were transcardially perfused with 30 mL ice cold 0.1 M PBS prior to decapitation.

Tamoxifen injection protocol

CX3CR1-cre^{ER} x ROSA26-GCaMP3 mice received three intraperitoneal injections of 4 mg tamoxifen with 48 hours in between (200 µl of 20 mg / ml in sterile peanut oil). Approximately one week after the last injection the mice were decapitated and slices were prepared as described above.

Mimetic Peptide

TAT-Gap19 (YGRKKRRQRRR-KQIEIKKFK) and Scrambled TAT-GAP19 (YGRKKRRQRRR-IEKFKIKQK) were dissolved directly in ACSF at 250 µM while ^{10}panx (WRQAAFVDSY) and scrambled ^{10}panx (FSVYWAQADR) were dissolved in DMSO 100 mM stocks and diluted in ACSF to a final concentration of 100 µM. All peptides were purchased at biomatik.

Fixation and immunolabeling of brain slices using modified methods

The slices where treated in specially made treatment chambers, containing 30 mL of ACSF and fixed after 60 min of treatment using SNAPSHOT. The 300 µm thick slices were either imaged directly or immunolabeled free-floating. In brief; the tissue was permeabilized with 20%

dimethyl sulfoxide (DMSO) and 2% Triton X-100, blocked for 24 h in 10 % goat serum and incubated for 8 days with a polyclonal rabbit antibody against mouse GFAP (0.5 µg/ml) and 2.5% goat serum. The tissue was then washed for 24 h, incubated for 8 days with a polyclonal goat-anti-rabbit IgG antibody conjugated with Alexa 594 (1 µg/ml) and 2.5% goat serum, and rinsed in 0.1 M PBS. Specially made microscope slides were used to keep the brain slices in place during imaging.

Imaging and quantification

A two-photon scanning microscope (Coherent Chameleon Ultra II laser coupled to a Zeiss LSM7MP-AX10 microscope with a Zeiss 20X-W/1.0 numerical aperture objective was used to image live and fixed hippocampal brain slices. For quantification of focalizing points the stratum radiatum of the CA1 region in fixed slices was identified using bright field imaging and stacks of 76 images were acquired between 75 and 225 µm below the surface of the slice (stepping 2 µm). EGFP was excited at 920 nm and its emission was filtered by a 520/60 nm filter and detected by a photomultiplier tube. To achieve a uniform illumination throughout the 150 µm of the stacks the auto z brightness correction was applied (Zen 2012 software). Images were collected at 512 × 512 pixels using 4-line averaging.

Time lapses of $EGFP^+$ microglial process dynamics were acquired as time series of stacks (z = 30, 2 µm steps with the microglial cells of interest in the middle of the stack with a total scan time of ~1 min/stack. GCaMP3 and iGluSnFR were also imaged using 920 nm but for optimal temporal resolution in order to detect rapid changes in intracellular Ca^{2+}, GCaMP3 was imaged in one focal plane. iGluSnFR was imaged either in one focal plane for optimal temporal resolution or as a stack of 15 stepping xx to enhance the probability of detecting focal points.

Stacks of images for 3D reconstruction were acquired as stacks of 75-90 images using 16-line averaging and stepping 1 µm in the z-axis between frames. Texas Red or Alexa 594 was imaged at 800 nm excitation using a 630/75 nm emission filter.

Statistics

Gaussian distributions were assumed for all experiments and statistical analyses were performed using GraphPad Prism version 6.0 for Mac. n-values represent unique treatments, hence 12 slices from one brain were grouped in e.g. six different treatment groups with two slices in each equals an n of one for each treatment group. The total number of animals used for each treatment was five or higher. For multiple comparisons p-values were indicated by *, $P < 0.05$; **, $P < 0.01$; ***, $P < 0.001$.

3.3 Results

Removal of extracellular Ca^{2+} leads to dramatic changes in microglia process dynamics

Time-lapse studies of microglial process dynamics were conducted during baseline (2 mM Ca^{2+}), in 0 mM Ca^{2+}, and following re-introduction of 2 mM Ca^{2+}. During baseline the microglia show their characteristic morphological ramification with long thin processes that survey the surrounding neuropil (Fig. 3.1A). Removal of extracellular Ca^{2+} (replacing $CaCl_2$ with EGTA) triggered extension of microglial processes towards focal points within the tissue (Fig. 3.1B). We refer to this phenomenon as microglial process focalization. We defined each focalizing point as a focal point with processes from three or more microglial cells extending towards it. Only processes with bulbous tips were included. Several focalizing points occurred at the same time and both the spatial and temporal distribution of these focalizing points appeared to be random.

The bulbous tips at the leading edge of the processes usually converged for 3-5 min at the targeted focal point before the convergance was lost with the processes dispersing and retracting. Most microglia had their processes polarized towards one focalizing point at a time but some microglia had their processes engaged against multiple focalizing points at once. This dramatic shift in microglial process dynamics in 0 mM Ca^{2+} compared to baseline was completely reversible as the microglial process polarization and focalization disappeared when Ca^{2+} was re-introduced.

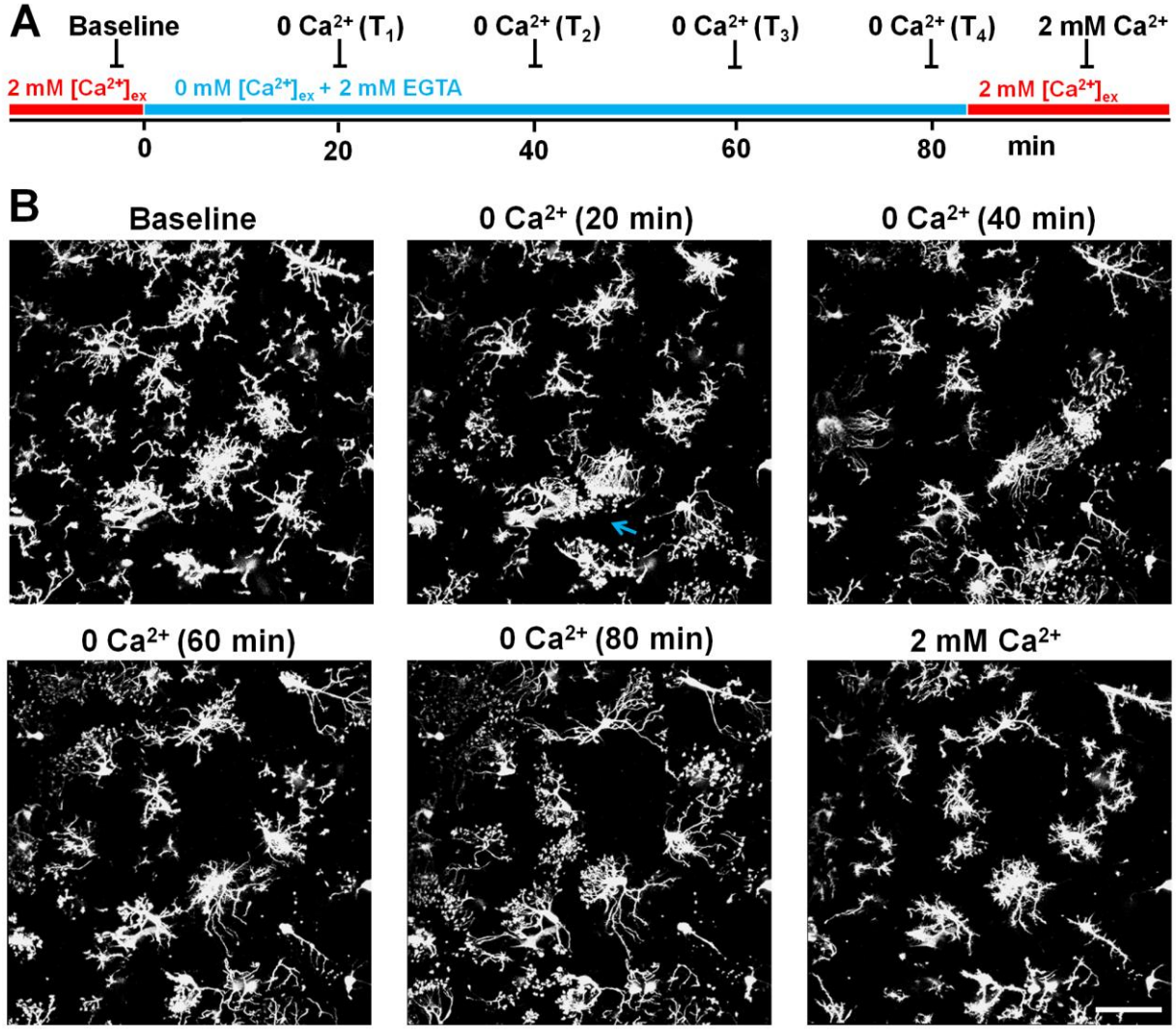

Figure 3-1 Removal of extracellular Ca^{2+} evoked a microglial process focalization

A, Timeline for image acquisition during removal and reintroduction of extracellular Ca^{2+}. ***B,*** Removal of extracellular Ca^{2+} by bath application of Ca^{2+} free ACSF containing 2 mM EGTA triggered a dramatic change in microglial process motility which is illustrated by the morphological changes of the cells shown in '*Baseline'* versus *'0 Ca^{2+} (20 min)'*. The morphological change was characterized by the appearance of bulbous tips at the end of extending processes and a polarization of microglial processes towards focal points within the tissue (as illustrated with the blue arrow). We refer to this as microglial process focalization when the processes from three or more cells are extending towards the same focal point. Over time the microglia process polarization would change and new focalizing points would appear i.e. *'0 Ca^{2+} (20 min)' versus '0 Ca^{2+} (40 min)'*. The alterations in microglial process dynamics were completely reversed when extracellular Ca^{2+} was reintroduction*'0 Ca^{2+} (80 min)' versus '2 mM Ca^{2+}'*. Images were acquired as stacks of 15 images (stepping 2 µm) and presented as max intensity projections for each time point. Acute hippocampal brain slices from CX3CR1-EGFP mice were used in these experiments. Scale bar; 40 µm.

Time course of microglial process dynamics in 0 Ca^{2+}

Multiple acute hippocampal brain slices from each brain were transferred to either a control chamber containing oxygenated ACSF with 2 mM Ca^{2+} or a treatment chamber containing Ca^{2+} free ACSF where $CaCl_2$ had been replaced by 2 mM EGTA. After 20, 40, 60, and 80 min a slice from each chamber was fixed using SNAPSHOT. As an additional control, slices that have been treated in 0 Ca^{2+} for 60 min were transferred to ACSF containing 2 mM Ca^{2+} for 20 min and then fixed using SNAPSHOT. The slices where imaged as previously described and the number of focalizing points within each stack was scored by the investigator who was blind to the treatment conditions (Fig. 3.2). We observed a significant increase in the number of focalizing points in 0 Ca^{2+} at 20, 40, 60, and 80 min compared to control treated (2 mM Ca^{2+}). No focalizing points were observed in control conditions. There was no significant difference between the number of focalizing points at 20, 40, 60 and 80 min. Re-introducing Ca^{2+} by transferring the slice to ACSF with 2 mM Ca^{2+} after 60 min in 0 mM Ca^{2+} abolished the presence of focalizing points.

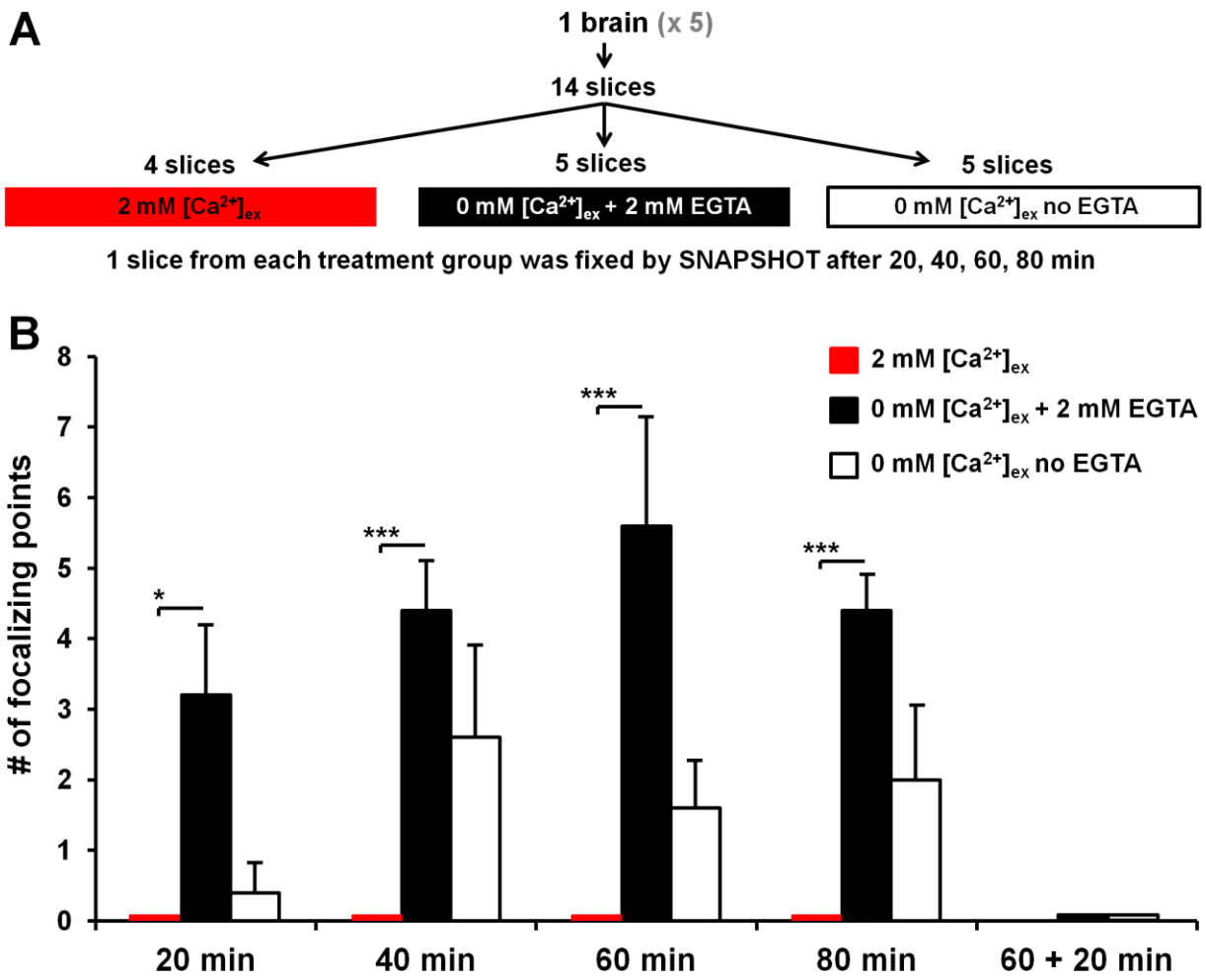

Figure 3-2 Time course of microglial process focalization.

A, Schematic diagram of the experimental design. 14 hippocampal slices were obtain from each brain and distributed in three different treatment groups. One slice from each treatment was fixed using SNAPSHOT after 20, 40, 60, and 80 min. Additionally, after 60 min one slice from each of the '0 mM $[Ca^{2+}]_{ex}$' treatments (with and without EGTA) was transferred for 20 min to '2 mM $[Ca^{2+}]_{ex}$' prior to fixation. This experiment was repeated for 5 different brains. ***B,*** Graphic depiction of quantified focalizing points. Stacks of 76 images (stepping 2 µm) were acquired in the stratum radiatum of the CA1 from each fixed slice, with each stack consisting of a volume of 0.03 mm^3 (x = 425 µm, y = 425 µm, and z = 150 µm). A focalizing point was defined as a focal point with processes from three or more microglial cells extending towards it, and the number of focalizing points was counted in each volume. All quantifications were performed blinded. Replacing extracellular Ca^{2+} with 2 mM EGTA triggered multiple focalizing points at each time point which was significantly different compared to the '2 mM $[Ca^{2+}]_{ex}$' treatment which did not trigger microglial process focalization at any of the investigated time points. Removal of extracellular Ca^{2+} but without addition of EGTA also triggered microglia process focalization. However, only very few focalizing points were observed after 20 min and even though more focalizing points were present at later time

points they were not significantly different from the '2 mM $[Ca^{2+}]_{ex}$' treatment. Transferring the slices from '0 mM $[Ca^{2+}]_{ex}$' treatments to '2 mM $[Ca^{2+}]_{ex}$' completely abolished microglial process focalization. Acute hippocampal brain slices from CX3CR1-EGFP mice were used in these experiments. Two-way ANOVA with Bonferroni's correction was used for statistical comparison of treatments at the different time points (n = 5).

Dose response to extracellular Ca^{2+}

To investigate and quantify the relationship between the concentration of extracellular Ca^{2+} and microglial process focalization a concentration-response study with different concentrations of Ca^{2+} was performed. Multiple acute hippocampal brain slices from each brain (a total 8 brains were examined) were transferred to either a control chamber containing oxygenated ACSF with 2 mM Ca^{2+} or to treatment chambers containing Ca^{2+} free ACSF or 0.1, 0.25, 0.5, 0.75 or 1 mM Ca^{2+}. The slices were fixed after 60 min using SNAPSHOT. The slices were imaged as previously described and the number of focalizing points within each stack was scored using a blind protocol (Fig. 3.3A). We observed a significant increase in the number of focalizing points at 0, 0.1, and 0.25 mM Ca^{2+} compared to control. Focalizing points was also observed at 0.5 and 0.75 mM Ca^{2+} while no focalizing points were observed in control conditions and at 1 mM Ca^{2+}.

Microglial process focalization is dependent on ATP release and stimulation of P2Y12 receptors

To investigate whether the observed microglial process focalization is dependent on ATP release, a dose-response study was performed using the P2Y12 selective antagonist PSB 0739. Multiple acute hippocampal brain slices from each brain were transferred to either a control chamber containing oxygenated ACSF with 2 mM Ca^{2+} or to a treatment chamber containing Ca^{2+} free ACSF with PSB at concentrations of 0.2, 1, 5, or 25 nM. The slices were fixed after 60 min using SNAPSHOT. The slices were then imaged as previously described and the number of

focalizing points within each stack was scored using a blind protocol (Fig. 3.3B). We observed a dose dependent and significant reduction in the number of focalizing points when PSB was added to Ca^{2+} free ACSF compared to when the drug was omitted. Focalizing points were still observed at 0.2, 1, and 5 nM PSB while completely absent at 25 nM PSB and in control conditions (2 mM Ca^{2+}).

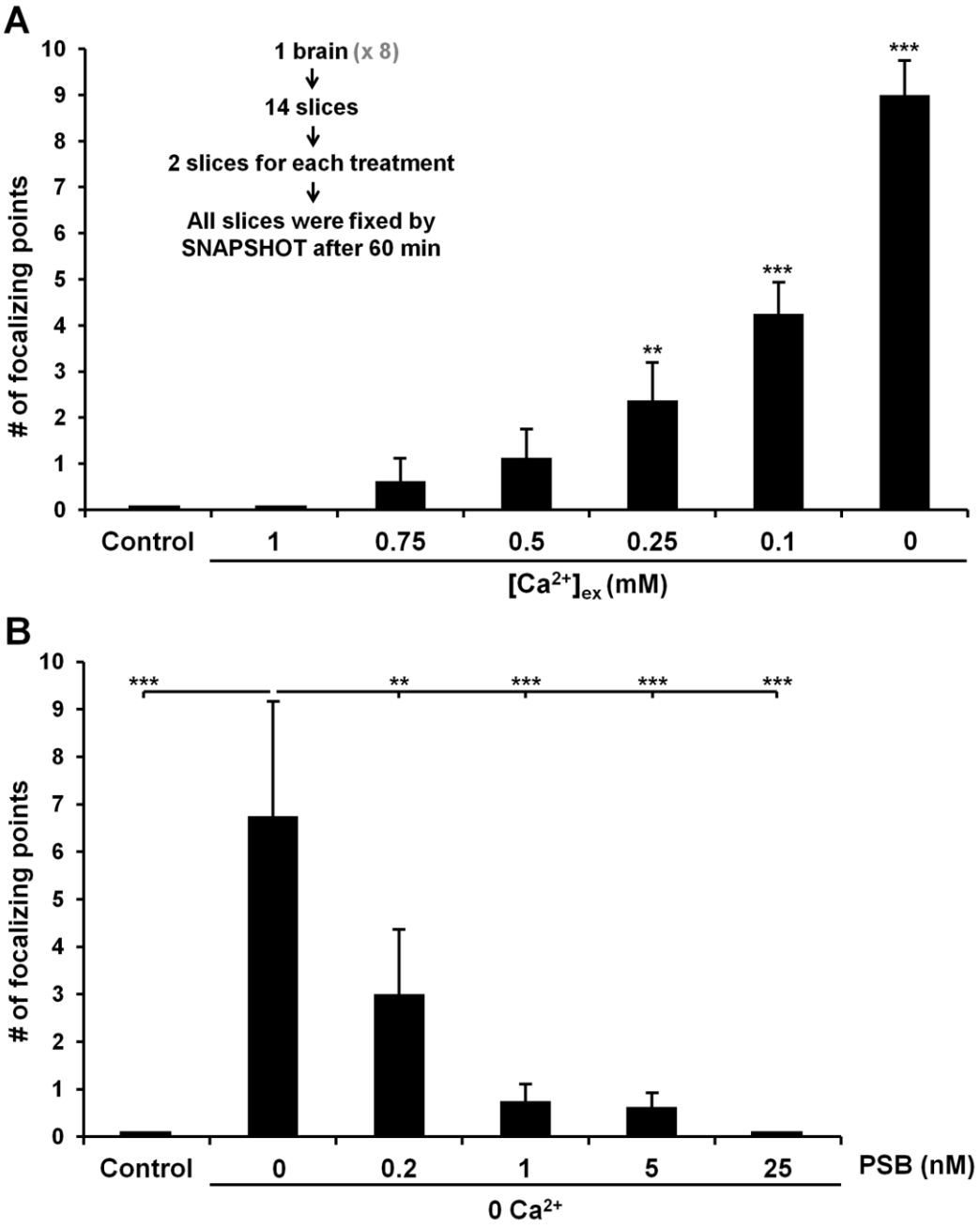

Figure 3-3 Microglial process focalization is inversely correlated with the $[Ca^{2+}]_{ex}$ and is dependent on ATP.

A, To determine the dose-response relation between microglial process focalization and $[Ca^{2+}]_{ex}$, the number of focalization points was compared between control (2 mM $[Ca^{2+}]_{ex}$) and various $[Ca^{2+}]_{ex}$ (ranging from 1 mM to 0.1 mM) . 2 mM EGTA was present throughout the different treatments. As indicated, 14 slices from each brain were evenly distributed over the seven different treatments (two slices in each) and fixed using SNAPSHOT after 60 min. This experiment was repeated eight times and the slices were imaged and quantified as described for Fig 3.2. Acute hippocampal brain slices from CX3CR1-EGFP mice were used in these experiments. Graphic depiction of the mean ± SEM for the number of focalizing points demonstrated that focalization occurs when $[Ca^{2+}]_{ex}$ was reduced to 0.75 mM and that it reached significance at 0.25 mM compared to control. No focalizing points were observed in control and at $[Ca^{2+}]_{ex}$ = 1 mM. Statistical comparisons were performed across the different treatments using repeated measures ANOVA with Bonferroni's multiple comparison post test (n = 8). *B,* To determine whether microglial process focalization was dependent on activation of the P2Y12 receptor, different concentrations of the selective P2Y12 receptor antagonist PSB 0739 (PSB) were applied (ranging from 0.2 to 25 nM) to treatments with 0 mM $[Ca^{2+}]_{ex}$ + 2 mM EGTA (0 Ca^{2+}). Experimental design, quantification and analysis were performed as described in A (n = 8). PSB blocked microglial process focalization in a dose-dependent manner and all the tested concentrations of PSB significantly reduced the microglial process focalization compared to '0 Ca^{2+}'

Microglial process focalization is dependent on opening of hemichannels

Having established that the microglial process focalization observed when Ca^{2+} is removed is mediated by ATP release we next investigated whether ATP is released through opening of Cx hemichannels. Thus a dose-response study was performed using a potent hemichannel blocker, CBX. Multiple acute hippocampal brain slices from each brain were transferred to either a control chamber containing oxygenated ACSF with 2 mM Ca^{2+} or to treatment chambers containing Ca^{2+} free ACSF with either: 10, 50, 100, or 200 µM of CBX or without CBX. The slices were fixed after 60 min using SNAPSHOT (Fig. 3.4A). We observed a significant dose dependent reduction in the number of focalizing points by CBX in the Ca^{2+} free ACSF compared to when the drug was omitted. Focalizing points were still observed at 10, 50, and 100 nM CBX while completely absent at 200 nM CBX and in control conditions (2 mM Ca^{2+}).

Microglial process focalization is independent of Panx1 opening

Mimetic peptides designed to block opening of Panx1 (^{10}panx) and Cx43 hemichannel opening (TAT-Gap19) were applied at concentrations previously reported to efficiently block opening of these channels. Scrambled peptides were applied at the same concentration as their respective counterparts to control for selectively. Multiple acute hippocampal brain slices from each brain were transferred to either a control chamber containing oxygenated ACSF with 2 mM Ca^{2+} or to treatment chambers containing Ca^{2+} free ACSF with either 100 µM of ^{10}panx, 100 µM of scrambled ^{10}panx, 250 µM of TAT-Gap19, 250 µM of scrambled TAT-Gap19 or without any peptide. The slices were fixed after 60 min using SNAPSHOT (Fig. 3.4B). Application of ^{10}panx and scrambled ^{10}panx peptide did not affect the microglial responses compared to the response in Ca^{2+} free ACSF. On the other hand both TAT-Gap19 and scrambled TAT-Gap19 completely blocked microglia process focalization similar to control conditions (2 mM Ca^{2+}).

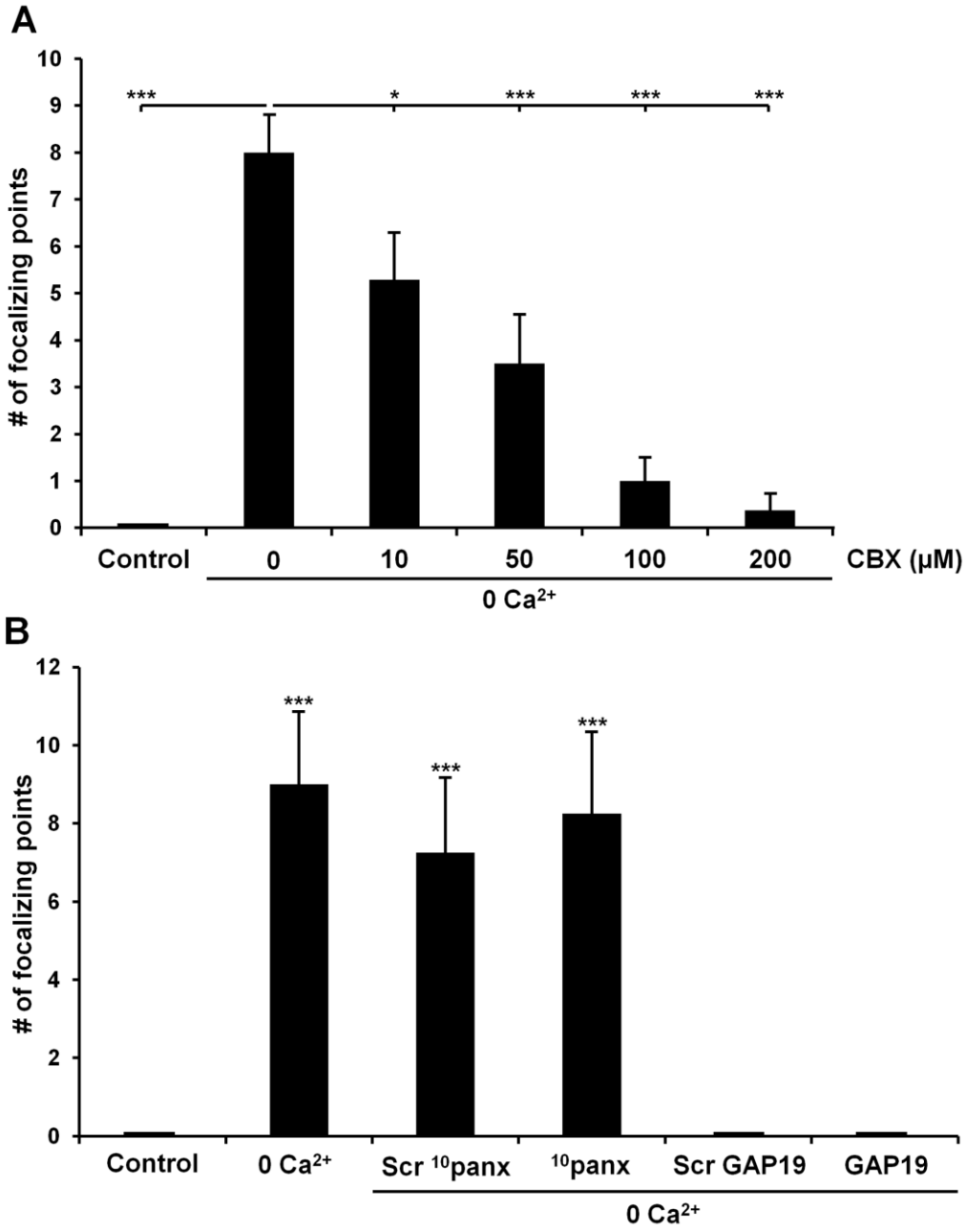

Figure 3-4 Microglial process focalization is sensitive to CBX

A, To determine whether microglial process focalization was dependent on hemichannel opening, the potent hemichannel blocker CBX was applied at different concentrations (ranging from 10 to 200 µM) to treatments with 0 mM $[Ca^{2+}]_{ex}$ + 2 mM EGTA (0 Ca^{2+}). The experiment design, quantification and analysis were performed as described for in Fig. 3.3A (n = 8). CBX blocked microglial process focalization in a dose-dependent manner and all the tested concentrations of CBX significantly reduced the microglial process focalization compared to '0 Ca^{2+}'. ***B,*** To investigate whether opening of Panx1 or Cx43 hemichannels are involved in triggering microglial process focalization, these hemichannels were targeted with mimetic peptides, ^{10}panx (100 µM) and GAP19 (250 µM)

respectively. As specificity controls, scrambled peptides were applied for each of the two peptides, 'Scr ^{10}panx' and 'Scr GAP19' respectively. The experimental design, quantification and analysis were performed as described in Fig. 3.3A (n = 8). There was no significant effect of application of either ^{10}panx or its scrambled peptide. On the other hand, both GAP19 and its scrambled peptide completely abolished microglial process focalization.

No co-localization between focalizing points and perivascular astrocytic endfeet

To investigate whether opening of Cx43 on perivascular astrocytic endfeet would lead to microglial process focalization, blood vessels were visualized by tail vein injections of Texas Red prior to decapitation. Acute hippocampal brain slices were incubated in a control chamber containing oxygenated ACSF with 2 mM Ca^{2+} or in a treatment chamber containing Ca^{2+} free ACSF. The slices were fixed after 60 min using SNAPSHOT and the $EGFP^{+}$ microglia and the Texas Red filled vessels were imaged using two-photon microscopy (Fig. 3.5B). Although some of the focalizing points were in close proximity to vessels, there was no qualitative indication that the focalizing points co-localize with perivascular astrocytic endfeet.

No co-localization between focalizing points and major $GFAP^{+}$ processes

To investigate whether the focalizing points co-localize to $GFAP^{+}$ astrocytic processes, acute hippocampal brain slices where fixed using SNAPSHOT. To avoid auto-fluorescence from the vessels, mice were transcardially perfused (with PBS 4°C) prior to decapitation. The brain slices were either incubated in a control chamber containing oxygenated ACSF with 2 mM Ca^{2+} or in a treatment chamber containing Ca^{2+} free ACSF. The slices were fixed after 60 min and processed for immunolabeling. GFAP was immunolabeled with Alexa594 and visualized together with $EGFP^{+}$ microglia (Fig. 3.5A). Although some of the focalizing points were in close proximity to $GFAP^{+}$ processes there was no qualitative indication that the focalizing points co-localize with major $GFAP^{+}$ astrocytic processes.

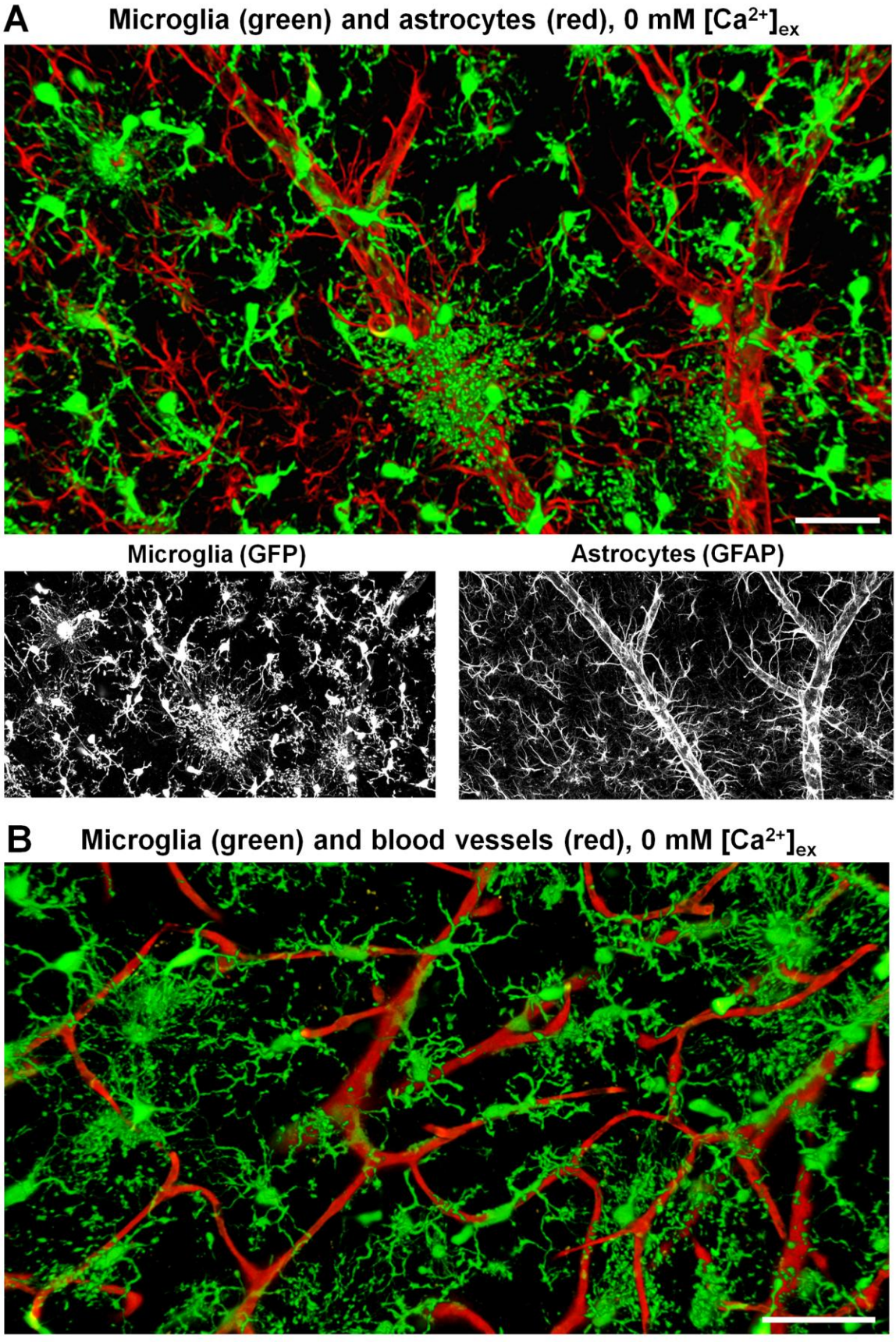
A
Microglia (green) and astrocytes (red), 0 mM [Ca2+]ex
Microglia (GFP)
Astrocytes (GFAP)
B
Microglia (green) and blood vessels (red), 0 mM [Ca2+]ex

Figure 3-5 Microglial process focalization did not co-localize with major astrocytic processes and endfeet or blood vessels.

A, To visualize both microglial process focalization and astrocytes, acute hippocampal brain slices from CX3CR1-EGFP mice were treated for 60 min in 0 mM $[Ca^{2+}]_{ex}$ + 2 mM EGTA prior to fixation and immunolabeling with antibodies against astrocytic GFAP. The top image shows a 3D reconstruction of microglia (green) and astrocytes (red) in a 90 µm thick stack. Scale bar; 40 µm. The two images below show max intensity projections of GFP^+ microglia and $GFAP^+$ immunolabeled astrocytes respectively. Focalizing points did not consistently co-localize with major astrocytic processes or endfeet. ***B,*** To visualize both microglial process focalization and the blood vessels, tail vein injections of Texas Red (conjugated to a 70.000 MW fixable dextran) were performed prior to decapitation to provide a fluorescent angiogram. Acute hippocampal brain slices were treated for 60 min in 0 mM $[Ca^{2+}]_{ex}$ + 2 mM EGTA and fixed using SNAPSHOT. The image shows a 3D reconstruction of microglia (green) and blood vessels (red) in a 56 µm thick stack. Focalizing points did not consistently co-localize with blood vessels. Scale bar; 40 µm.

Intracellular Ca^{2+} signals in microglia

To gain further insight into the mechanisms of microglial process dynamics beyond the morphological changes, we investigated changes in intracellular Ca^{2+} using CX3CR1-cre x ROSA26-GCaMP3 mice. The expression of functional GCaMP3 was extremely variable from mouse to mouse and the fluorescence was overall very dim. However, with the slices that showed the best expression we were able to obtain an interesting indication of the intracellular Ca^{2+} dynamics in microglia (Fig. 3.6). We first validated that ATP triggers an intracellular Ca^{2+} response in the microglia by application of exogenous ATP and by evoking endogenous ATP efflux by laser-induced lesions in ACSF with 2 mM extracellular Ca^{2+}. Bath application of ATP (500 µM) triggered an initial spike in intracellular Ca^{2+} that lasted a few sec even though ATP was continuously applied. A similar rapid but transient elevation in intracellular Ca^{2+} was observed in microglial cells in close proximity to the focal point of laser-induced lesions presumably due to lesion-evoked ATP efflux (Fig 3.6C). On the example traces of seven cells shown in Fig 3.6A we observed very sparse spontaneous activity during baseline (2 mM

extracellular Ca^{2+}). Removal of Ca^{2+} triggered transient responses in multiple cells but importantly, these spikes did not occur in synchrony and were dispersed over minutes. Bath application of ATP did not evoke additional spikes in intracellular Ca^{2+} (except for in one cell in which removal of Ca^{2+} failed to trigger a Ca^{2+} spike). Re-introducing extracellular Ca^{2+} evoked a strong transient elevation of intracellular Ca^{2+} in six out of seven cells and these responses all occurred in synchrony. Bath application of ATP (in the presence of 2 mM extracellular Ca^{2+}) now evoked an intracellular Ca^{2+} spike in all cells.

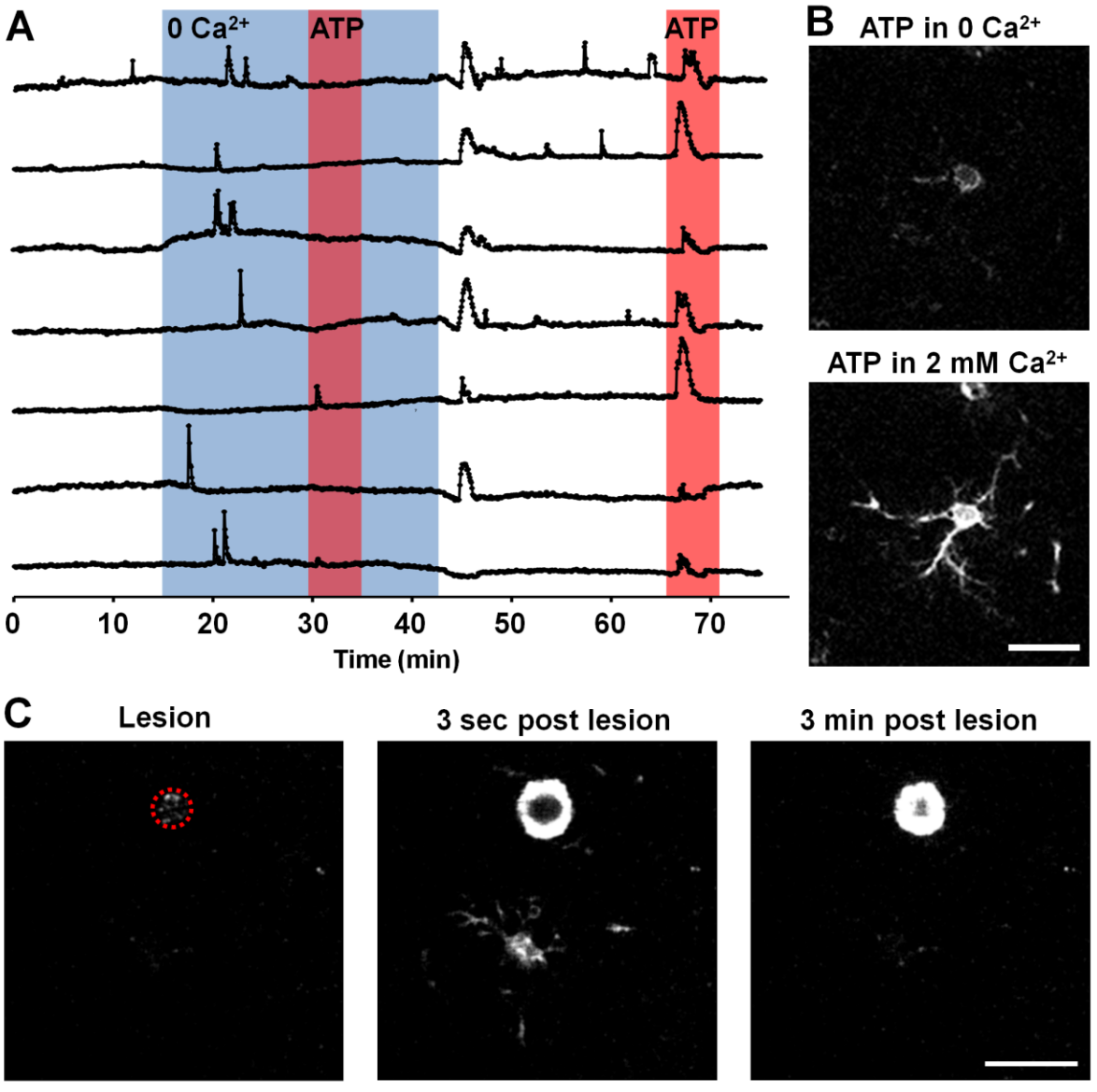

Figure 3-6 Example of how removal of extracellular Ca^{2+} was observed to trigger transient increases in microglial intracellular Ca^{2+}.

A, Microglial Ca^{2+} responses were investigated in acute hippocampal slices from CX3CR1-GCaMP3 mice. Ca^{2+}-free ACSF containing 2 mM EGTA (0 Ca^{2+}) was applied (indicated in blue) after a 15 min baseline in 2 mM extracellular Ca^{2+}. ATP (500 µM) was bath applied (indicated in red) both during 0 Ca^{2+} and after extracellular Ca^{2+} was reintroduced. Regions of interest for seven cells in the field of view (265 µm x 265 µm, imaged at 1/3 Hz in one focal plane) were determined based on a projection of standard deviations over time and the fluorescence intensity in each region was quantified over time and normalized to baseline. No intracellular Ca^{2+} response was observed during baseline but removal of extracellular Ca^{2+} triggered a non-synchronous response in microglia. Addition of ATP during 0 Ca^{2+} did not evoke a second response except for a minor response in one out of the seven cells that had not responded to the removal of extracellular Ca^{2+}. Reintroduction of extracellular Ca^{2+} evoked a synchronous response in microglia and application of ATP in the presence of extracellular Ca^{2+} triggered another synchronous response. ***B,*** Example of the ATP-evoked intracellular Ca^{2+} response in microglia in 0 Ca^{2+} (top image) and in the presence of extracellular Ca^{2+}. Scale bar; 20 µm. *C,* A transient microglial response was also observed within sec. after the induction of a laser-induced lesion (in the presence of 2 mM extracellular Ca^{2+}). Scale bar; 20 µm.

Glutamate release at focal hotspots

Opening of Cx hemichannels have been reported to lead to the efflux of glutamate (Ye et al., 2003). Thus, to investigate whether removal of extracellular Ca^{2+} also triggered the release of glutamate and to gain further insight into the spatial and temporal distribution of focal areas of glutamate and presumably ATP release, we performed time-lapse imaging of coronal slices with expression of the glutamate indicator, iGluSFnR in the dorsal striatum (Fig. 3.7)

We validated that microglial process focalization also occurred in the dorsal striatum (Fig. 3.7B). Time lapse imaging of microglia in coronal slices from CX3CR1-$EGFP^{+/+}$ mice demonstrated that removal of extracellular Ca^{2+} triggers a similar focalization of microglial processes as observed in the stratum radiatum of the CA1. Next we imaged iGluSFnR and observed that multiple hotspots of glutamate release occurred when extracellular Ca^{2+} was removed. We did not observe any of these focal hotspots during baseline (2 mM extracellular Ca^{2+}) and when Ca^{2+} was re-introduced. Time lapse imaging in one focal plane revealed that the

release of glutamate could last up to 4 min and stacks of images acquired over time demonstrated that multiple hotspots occurred at the same time (Fig. 3.7A). Laser-induced damage also triggered a pronounced release of glutamate that decayed dramatically within the first 10 min (Fig. 3.7B).

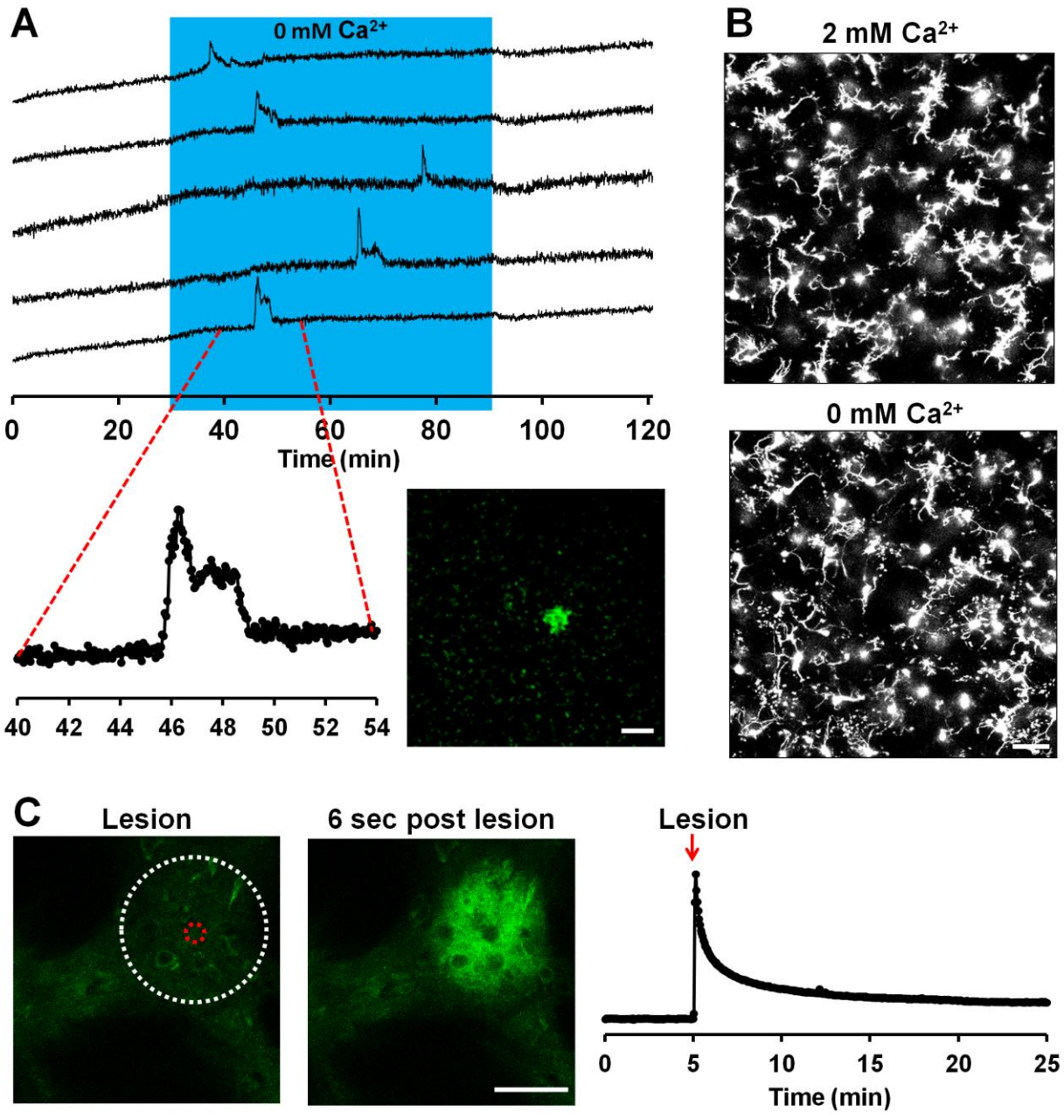

Figure 3-7 Example of how removal of extracellular Ca^{2+} was observed to trigger local hot spots of glutamate release.

A, Visualization of extracellular glutamate was performed in coronal slices from mice that expressed iGluSnFR in the dorsal striatum. Removal of extracellular Ca^{2+} for one hour (indicated in blue) gave rise to the occurrence of 5 glutamate hot spots in the field of view (512 µm x 512 µm, imaged at 1/3 Hz in one focal plane). The regions of interest were determined based on a projection of standard deviation over time and the fluorescent intensity in each region was quantified over time and normalized to baseline. The hot spots were transient and lasted up to 3-4 min and had a diameter of 15-20 µm as illustrated in the inserted image (bottom right, scale bar; 20 µm). ***B,*** Removal of extracellular Ca^{2+} from the dorsal striatum also triggered a focalization of microglial processes as observed for the CA1. This experiment was performed in coronal slices from CX3CR1-EGFP mice. Scale bar; 40 µm *C,* A transient glutamate signal was also observed within sec after the induction of a laser-induced lesion (in the presence of 2 mM extracellular Ca^{2+}). The red ring indicates the area of the lesion and the white ring indicates the region of interest for quantifying the glutamate response over time. Scale bar; 40 µm. The graphic depiction of the glutamate response (shown in the bottom right) was quantified as the change of fluorescence intensity within the white ring over time.

3.4 Discussion

Here we demonstrate that removal of extracellular Ca^{2+} triggered a transient focalization of microglial processes. We observed a strong inverse relationship between the concentration of extracellular Ca^{2+} and the number of focalizing points and demonstrated that the focalization was mediated by CBX sensitive release of ATP. Removal of extracellular Ca^{2+} also evoked an intracellular Ca^{2+} response in microglia, consistent with the presumed release of ATP. Interestingly, ATP release through astrocytic hemichannels has also been reported to be accompanied by the efflux of glutamate. By visualization of extracellular glutamate in real-time, using the iGluSFnR indicator, we observed that removal of extracellular Ca^{2+} gave rise to hot spots of high levels of extracellular glutamate, further supporting the notion that microglial process focalization is due to localized release of ATP through open hemichannels.

These discoveries adds and extends our previous work in which we demonstrated that stimulation of neuronal NMDAR also evoked a change in microglial process dynamics albeit via

a different ATP release mechanism. CBX did not block NMDA-evoked process outgrowth and the microglial response to NMDA was markedly different that observed following removal of extracellular Ca^{2+}. Bath application of NMDA led to non-polarized outgrowth of microglial processes most probably due to NMDA-mediated release of ATP throughout the tissue. In contrast, low extracellular Ca^{2+} triggered extension of processes to different focal points within the tissue, indicating that ATP is released from specific local areas apparently for discrete periods of time. Processes from multiple microglial cells focalized around each focal point in a similar fashion to what is observed after a laser-induced lesion or to the tip of an ATP-filled electrode. However, unlike the focalization at a lesioned area, where the bulbous tips remain for hours to days (Kim and Dustin, 2006; Eter et al., 2008), the bulbous tips on the focalized microglial processes in low extracellular Ca^{2+} reached the focal point and then dispersed within a few minutes followed by retraction. We have previously mimicked this reversibility by removing the source of ATP either by retraction of an ATP-filled electrode or terminating the bath application of ATP as shown in chapter 2. Importantly, bulbous tips persisted at the tip of the microglial processes as long as ATP is present (Haynes et al., 2006; Wu et al., 2007; Dissing-Olesen et al., 2014). Taken together, this demonstrates that microglial process focalization in low extracellular Ca^{2+} is due to reversible release of ATP and not due to tissue damage because the bulbous tips disperse. We can also rule out potential contributions of laser-induced phototoxicity in our paradigm because we observed a similar change in microglial process dynamics when the tissue was treated and fixed using SNAPSHOT which does not require live cell illumination using the ultrafast infrared laser for two-photon imaging. Interestingly, the data suggest a functional impact of microglia on ATP release as we interpret the dispersion of bulbous tips and

retraction of processes after they reached the focal point as evidence for a termination of ATP release.

Reducing extracellular Ca^{2+} has been shown to evoke ATP release selectively through opening of astrocytic Cx43 hemichannels as ATP release was completely abolished in slices from transgenic mice that lack astrocytic Cx43 (Torres et al., 2012). We therefore assume that the ATP-dependent microglial process focalization that we observe is due to opening of astrocytic Cx43 hemichannels. Interestingly, Cx43 are expressed on astrocytes throughout the tissue and extracellular Ca^{2+} is removed from the entire bath, thus we do not know why only ATP release occurs transiently from very specific areas. One plausible explanation is that even though removal of extracellular Ca^{2+} can trigger opening of Cx43 hemichannels the actual probability of opening is still low. Dye uptake in Cx43 expressing HEK cells occurred very gradually after extracellular Ca^{2+} was removed. After 30 min 20% of cells had taken up dye, 40% of cells after 60 min, and 60% of cells after 90 min (John et al., 1999; Kondo et al., 2000). A relatively low opening probability was also observed in Cx43 expressing HeLa cells where only a low number of cells would take up dye even though all cells expressed Cx43. Addition of EGTA and elevating intracellular Ca^{2+} levels enhanced the probability of opening (Contreras et al., 2003; Wang et al., 2012).

Decreasing the concentration of extracellular Ca^{2+} ($[Ca^{2+}]_{ex}$) to 0.75 mM was approximately the threshold to trigger microglial process focalization. In addition there was an inverse relationship between the $[Ca^{2+}]_{ex}$ and the number of focalizing points exists. This is in perfect agreement with previous investigations of hemichannel-mediated glutamate release in cultured astrocytes that also demonstrated an inverse relationship with $[Ca^{2+}]_{ex}$. Glutamate release at 1 mM $[Ca^{2+}]_{ex}$ was reported to be < 10% of the glutamate released in 0 mM $[Ca^{2+}]_{ex}$, while 0.5

mM $[Ca^{2+}]_{ex}$ dropped it to 20% and 0.1 mM $[Ca^{2+}]_{ex}$ reduced the release of glutamate by 40% (Ye et al., 2003). Together, these observations indicate that hemichannel opening can occur during specific biological circumstances where there is a decrease in $[Ca^{2+}]_{ex}$ to 0.75 mM and lower. Synchronous firing activity of large populations of neurons is known to cause a reduction in $[Ca^{2+}]_{ex}$ and several studies have investigated $[Ca^{2+}]_{ex}$ in the CNS of different species and under different conditions using Ca^{2+}-sensitive micropipettes. Locomotor activity reduced $[Ca^{2+}]_{ex}$ to a steady state of 0.8 mM in rodent spinal cords (Brocard et al., 2013) while repetitive stimulation of the cerebellum in rats and cats caused a drop in $[Ca^{2+}]_{ex}$ to 0.6 mM and 0.8 mM, respectively (Nicholson et al., 1977; Nicholson et al., 1978). Seizure activity in the cortex of cats decreased $[Ca^{2+}]_{ex}$ to 0.5-0.6 mM which remained for the whole duration of the seizure and for up to 5 min after (Heinemann et al., 1977; Amzica et al., 2002). Spreading depression in rat cerebellum and in cortex of cats dropped $[Ca^{2+}]_{ex}$ most dramatically to 0.12 mM (Nicholson et al., 1977; Nicholson et al., 1978). Taken together, this indicates that opening of Cx43 and consequently ATP-mediated microglial process focalization likely can occur under physiological conditions with high neuronal activity and may be very pronounced during seizure activity and spreading depression.

To determine if ATP release is truly mediated by opening of hemichannels, Ca^{2+} was removed in the presence of CBX. We observed a dose-dependent block of microglial process focalization by CBX which is in agreement with previous studies (Ye et al., 2003; Hansen et al., 2014). Hence, CBX (1 µM) only reduced dye uptake by 10% in cultured astrocytes (compared to dye uptake without CBX), 10 µM CBX reduced dye uptake by 70% and 100 µM CBX reduced dye uptake by approximately 80% (Ye et al., 2003). This was also observed for glutamate release

where 10 µM CBX also reduced glutamate release by 70% (compared to glutamate release in the absence of CBX) and 100 µM reduced it by 90%) (Ye et al., 2003).

To further investigate whether ATP release is mediated by opening of the hemichannels Cx43, Ca^{2+} was removed in the presence of mimetic peptide GAP19, which have been shown to be a potent inhibitor of Cx43 hemichannel opening. Additionally experiments were also performed in presence of the blocking peptide ^{10}panx, which blocks opening of Panx1 hemichannels and with scrambled peptide sequences for both GAP19 and ^{10}panx. Surprisingly, the scrambled peptide for the GAP19 peptide exerted a similarly efficient block as observed by application of the GAP19 peptide. It is therefore not possible to conclude that ATP release is mediated by opening of Cx43 hemichannels. There was no effect of ^{10}panx or its scrambled version on microglial process focalization. Scrambled peptides have previously been reported to exert similar effects as their target-peptide counterparts e.g the ZIP peptide (originally designed to block protein kinase Mζ) and its control scrambled peptide both blocked long term potentiation (Volk et al., 2013). Disruption of fear memories with myristoylated ZIP was not significantly different than the effect of myristoylated scrambled ZIP either (Kwapis et al., 2009). Thus, in order to determine whether Cx43 hemichannel opening play a significant role in our experimental paradigm more extensive investigations will be required. Future experiments performed with slices from Cx43 deficient mice might be needed to determine whether ATP is released through opening of Cx43 hemichannels as hypothesized.

An alternative strategy for testing the involvement of astrocytes was to detemine if microglia focalized to specific regions of astrocytes. The most straightforward strategy was to use our SNAPSHOT method to determine whether microglial processes focalize to astrocytic perivascular endfeet where Cx43 is highly enriched (Simard et al., 2003; Rouach et al., 2008;

Mathiisen et al., 2010; Ezan et al., 2012). The blood vessels were visualized by a tail vein injection of a fixable fluorescent dye allowed us to visualize the blood vessels and demonstrate that microglial processes did not focalize onto perivascular endfeet. We next investigated whether microglial processes would focalize onto $GFAP^+$ astrocytic processes or somas. However, microglial processes did not focalize onto $GFAP^+$ astrocytic processes or somas either. A plausible explanation might be that GFAP immunolabeling delineates only 15% of the total volume of astrocytes (Bushong et al., 2002; Pekny and Pekna, 2014) and Cx43 has previously been demonstrated to be predominantly expressed in astrocytic endfeet and at the overlapping interdigitation of fine $GFAP^-$ astrocytic processes (Huang et al., 2012; Pekny and Pekna, 2014).

An individual focal point (determined by the converged bulbous tips of the microglia processes) are approximately 10 μm in diameter and it would therefore be very challenging to interpret whether the microglial processes truly are focalizing onto the fine astrocytic processes which would cover most of the parenchyma with a mesh like structure if all astrocytes are labeled.

Preliminary experiments were undertaken to examine intracellular Ca^{2+} dynamics in microglia to determine whether release of endogenous ATP would trigger a response in microglia. A recent study using *in vivo* imaging of intracellular Ca^{2+} in microglia (OGB-1 was introduced into GFP^+ microglia via single cell electroporation) showed very low spontaneous Ca^{2+} fluctuations under normal conditions and a transient Ca^{2+} signal to local ATP applications and to neuronal damage (Eichhoff et al., 2011). In accordance with these findings we also observed a very low spontaneous Ca^{2+} activity in microglia and a brief initial Ca^{2+} spike to prolonged bath application of ATP or a laser-induced lesion. We know that ATP-induced microglial processes extension persists for 20-30 min with continues application of ATP or when

evoked by a laser-induced lesion. Thus, these results indicate that ATP trigger an initial Ca^{2+} spike, but that Ca^{2+} signals are not required for maintaining and guiding microglial processes. Ca^{2+} signals induced by P2Y receptor stimulation depend on Ca^{2+} release from intracellular stores and were therefore abolished by depletion of Ca^{2+} from intracellular stores by thapsigargin (Eichhoff et al., 2011). Interestingly, thapsigargin treatment also blocked damage-induced Ca^{2+} signals and induction of a neuronal damage in the presence of a P2Y receptor agonist completely failed to trigger an additional Ca^{2+} signal (Eichhoff et al., 2011). Therefore damage-induced Ca^{2+} signals are mediated by P2Y receptor activation and that additional stimulation of P2Y receptors by damage-evoked released ATP did not trigger any additional Ca^{2+} signals. This is in agreement with our data and supports the idea that ATP release, evoked by removal of extracellular Ca^{2+}, leads to stimulation of microglial P2Y receptors which then triggers an initial Ca^{2+} spike due to release of Ca^{2+} from intracellular stores. Additional application of endogenous ATP in Ca^{2+} free ACSF did not trigger additional Ca^{2+} spikes potentially because high levels of endougenous ATP were already present and potentially because activation of P2Y receptors in Ca^{2+} free ACSF may have depleted internal Ca^{2+} stores in microglia. Hence the intracellular Ca^{2+} signal that occurred when Ca^{2+} was re-introduced might be driven by Ca^{2+} entry via store-operated Ca^{2+} channels. Taken together, these data further signify that ATP is released and activate microglial P2Y receptors when extracellular Ca^{2+} is removed. Importantly, the data also indicate that intracellular Ca^{2+} signaling might play a role for initiating microglial process outgrowth but that it is not required for maintaining process extension and coordinating the direct outgrowth. Further investigations of the relationship between microglial process dynamics and intracellular Ca^{2+} signaling would require a more reliable genetically encoded Ca^{2+} indicator combined with a fluorescence marker of morphology. A Cre-dependent GCaMP5G-IRES-tdTomato reporter

mouse has recently been generated which uses Polr2a instead of Rosa26 and Hoxb8 instead of CX3CR1 to achieve selective expression of GCaMP5 and tdTomato in microglia (Gee et al., 2014).

Our data and the literature discussed above suggest that under circumstances with high neuronal activity, in particular during seizures or spreading depression, opening of astrocytic Cx43 hemichannels is triggered by a decrease in extracellular Ca^{2+}. Opening of Cx43 hemichannels resulted in release of ATP which stimulate P2Y12-mediated microglial process extension towards open Cx43 hemichannels via a purinergic gradient. In addition the preliminary data suggests that glutamate is also released. Our data indicate that ATP release is terminated shortly after the arrival of microglial processes and we speculate that microglia potentially play a functional role in closing Cx43 hemichannels. Interestingly, neurotrophins which are locally released by microglia (Parkhurst et al., 2013) have been shown to induce a rapid phosphorylation of Cx43 hemichannels (within 5 min), and phosphorylation of Cx43 hemichannels is known to close these channels (Li et al., 1996; Liu et al., 1997; Lampe and Lau, 2000; Harris, 2001; Bao et al., 2004b). Thus, we predict that impairments in microglial process dynamics as observed during inflammation and old age might lead to inadequate handling of hemichannel opening and consequently exacerbation of seizure activity due to prolonged release of ATP and glutamate which might shift non-pathological neuronal activity to an excitotoxic state and consequently neuronal death.

.

Chapter 4: Fixation and immunolabeling of brain slices: SNAPSHOT method

4.1 Introduction

The ability to visualize cellular structures has, together with electrophysiological recordings, largely contributed to our current understanding of the cellular mechanisms of the brain. Acute brain slices are widely used during electrophysiological experiments and live imaging using two-photon laser scanning microscopy, which allows for visualization of cells deep within the tissue. Acute brain slices provide the convenience of cultured cells in terms of timely pharmacological interventions and easy manipulations (e.g. accessibility of electrodes) while preserving the cytoarchitecture and natural cell-cell interactions of the brain region of interest. However, although immunolabeling is routinely used to visualize target proteins in cultured cells and in thin cryostat sections of brains fixed by transcardial perfusion it is not commonly used for acute brain slices. One of the reasons for this is because the optimal thickness for acute brain slices is between 300-400 µm, which compromises the penetration of both fixatives and antibodies. Consequently, it becomes problematic to fix fine dynamic structures within the tissue and subsequent immunolabeling of target proteins requires cryostat re-sectioning. Thus, a method to rapidly fix and immunolabel target proteins within thick brain slices would allow us to apply the extensive repertoire of antibodies that are currently used for immunolabling of target molecules in cultures and thin cryostat section and would provide a unique model for visualizing target proteins that might be altered during pharmacological treatment.

Here, we describe a novel and simple protocol called “SNAPSHOT” (StaiNing of dynAmic ProcesseS in HOt-fixed Tissue). The purpose of SNAPSHOT is to rapidly fix fine dynamic structures in acute brain slices and visualize target molecules by IHC, thereby achieving a snapshot of the cellular morphology and/or localization of target proteins at the exact time of

fixation. The protocol consists of one or two steps, which can be performed independently or in combination with any acute brain slice experiment whether it is real-time imaging, patch-clamp recordings of a dye-filled cell, or treatment of slices with various pharmacological agents. We have previously demonstrated, using electron microscopy, that our rapid fixation procedure preserves the ultra structure of the tissue (Mills et al., 2014) and thereby a snapshot of the cellular morphology at the exact time of fixation. Importantly, using our optimized fixation procedure we can achieve a uniform immunolabeling throughout 300-400 µm thick brain slices as shown in chapter 2. SNAPSHOT has proven to be advantageous for addressing several interesting biological questions and will be of great value to the broad community of neuroscientists.

4.2 Materials and methods

Reagents and solutions

ACSF; NaCl (126 mM), KCl (2.5 mM), $NaHCO_3$ (26 mM), $CaCl_2$ (2.0 mM), $MgCl_2$ (2 mM), NaH_2PO_4 (1.25 mM), and D-glucose (10 mM), oxygenated with 95 % O_2 and 5 % CO_2, pH at 7.35, osmolarity ~300 mOsm), Phosphate buffered saline with 4 % PFA, (FD Neurotechnologies, cat# PF101), 0.1 M PBS, (tablets, Oxoid, cat# BR0014G), DMSO (Fisher Chemicals, D128-1), 2 % Trition X-100 (J.T. Baker, X198-05), Permeabilizing / washing solution (0.1 M PBS (tablet, Oxoid, BR0014G), 2 % Trition X-100, and 20 % DMSO), Blocking solution (Similar to the washing solution added 10 % serum -from the species in which the secondary (or tertiary if required) antibody is raised), Staining solution (Similar to the washing solution added 2.5 % serum from the same species as used for blocking), Krazy Glue (Elmer's), Corn oil (Sigma, cat# C8267).

Equipment

General Purpose Transfer Pipettes (Electron Microscope Sciences, cat# 70960-1), Fume hood (e.g. Bedcolab), Waterbath (e.g. VWR, cat # 89501-460), 6- and 12-well Tissue Culture Plates (Falcon, cat# 08-772-1B or cat# 08-772-29), Metal Spatula (VWR, Cat# 82027-528), Platform Rotator (e.g. Fisher Scientific, cat# 13-687-705PM), Plastic bags (6x8 Reloc Zippit 4Mil re-closable bags, US Plastic Corp, Cat # 48367), Manual Impulse Sealer (e.g. Tecknopack, Model E-MMS-200), Microcentrifuge tube, 1.7 ml (VWR, Cat# 20172-778, 'Eppendorf tube'), Microscope slides (Fisher Scientific, cat# 12-544-2), Cover glasses (Fisher Scientific, cat# 12-548-5G), Two-photon scanning microscope (e.g. Coherent Chameleon Ultra II laser coupled to a Zeiss LSM7MP-AX10 microscope with a Zeiss 20x W/1.0 NA objective)

Protocol Steps

1. Attach a tissue culture plate in a water bath (6- or 12-well plate) and ensure that the water is covering the top half of the frame on the plate. Turn on the water bath to 80 °C 1-2 hrs prior to fixation to ensure that the water in the bath reaches the correct temperature. Importantly, refill the bath as often as required to keep the surface of the water at the level of the plate.

2. Fill the wells in the tissue culture plate in the water bath with 4 % PFA (15 ml in each well if using a 6-well plate or 6 ml if using a 12-well plate). This step should be done 15-20 min prior to fixation to ensure that the temperature of the PFA reaches 80 °C. However, make sure not to perform this step earlier than 20 min prior to fixation to reduce evaporation from occuring. Depending on the amount of ACSF that is transferred together with each slice, the heated PFA can be used for several rounds of fixation.

3. Transfer the acute brain slices from ACSF to the heated PFA using a transfer pipette (general purpose transfer pipette with the tip cut off) (Fig. 4.1A). Be careful not to transfer a bigger volume of ACSF than necessary to keep the slice in solution during the transfer to avoid diluting the PFA. We recommend being consistent with the orientation of the brain slices prior to fixation (which side is up during treatment) so that the slice can be imaged at the same orientation. Importantly, ensure that the brain slice gets completely immersed in the heated PFA. Occasionally the brain slice may float to the surface of the heated PFA because an air bubble has attached to the slice. If this occurs, make sure to completely immerse the slice below the liquid surface to dislodge the bubble. It may require a little practice to use the transfer pipettes efficiently.

4. After exactly 2 min in heated PFA transfer the slices to 0.1 M PBS at room temperature (RT) (use 12- or 24-well plate). The thick slices are too firm to transfer with a paintbrush (as normally used for transferring thin tissue sections) so we recommend using a metal spatula with the tip bended 90 degrees (Fig. 4.1B). The 'L'-shape can be used to easily scoop up the brain slice and it also reduces the amount of solution transferred and it is easy to clean by rinsing with water. A gentle tap at the bottom of the well next to the brain slice or swirling the tip of the spatula in the solution around the slice allows the slice to float and makes it easier to place the 'L'-shape spatula below it. The slices can be stored for months in 0.1 M PBS at 4 °C. The slices can be labeled by writing on the lid of the plate. If the target of interest is already fluorescent (e.g. genetically encoded fluorophores or live tissue dye uptake during the manipulation step) it is recommended that the slices are protected from light exposure by covering the plate with tinfoil.

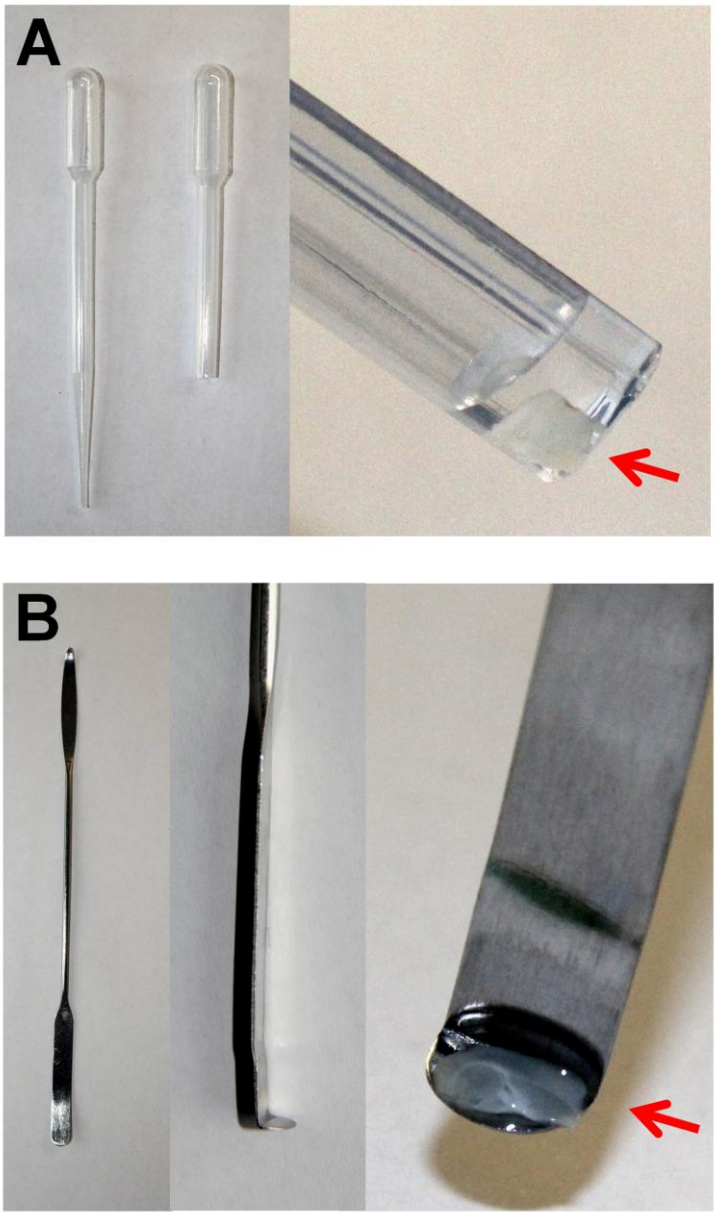

Figure 4-1 Transfer of acute brain slices.

We recommend two different ways of transferring brain slices. ***A,*** For live tissue we recommend a transfer pipette with the tip cut off. This allows for the slice to be immersed in ACSF and remain undisturbed during the transfer. Importantly, to ensure reliable fixation we recommend transferring a small volume of ACSF. ***B,*** For fixed tissue we recommend using an L-shaped metal spatula. Brain slices are indicated with red arrows.

5. At this step of the protocol the endogenous fluorescence can be imaged (see step 14). Dispose PFA in the appropriate waste disposal bin.

6. To initiate the immunolabeling steps, rinse the slices in a 6- or 12-well plate containing 0.1 M PBS and place it on a platform rotator to remove any residual PFA. We recommend using the 'L'-shaped spatula for transferring the slices.

The slices will be immunolabeled free floating and step 7, 8, 10, and 12 are all performed in 12-well plates on a platform rotator at room temperature (unless otherwise stated). The times indicated below are suggestions and can be adjusted.

7. Permeabilize the tissue using permeabilizing solution for a minimum of 2 hrs. This is the first step of the immunolabeling portion of the protocol that differentiates it from standard immunolabeling protocols because after a couple of hours the tissue will become slightly translucent. Please note that this step can't be applied to thin cryostat sections because they will disintegrate during this step.

8. Block non-target epitopes using the blocking solution. This step can be done over night at RT.

9. Incubate with primary antibodies diluted to the required concentrations in staining solution. We recommend that each slice is incubated in a small plastic bag made by using a Manual Impulse Sealer (for details see Fig. 4.2). This method of incubation is recommended for several reasons: i) it allows for perfusion from both sides of the slice, ii) it eliminates the risk of evaporation, iii) it lowers the required volume of staining solution and thereby reduces the cost of antibodies (20-800 µl). To ensure a uniform immunolabeling of target epitopes throughout the tissue we recommend incubating the tissue for 6-10 days at 4 °C on a platform rotator or a 360

degrees rotisserie wheel (preferred method). The same considerations in regard to spices specificity and immunoglobulin isoform apply as for immunolabeling of thin sections using standard immunolabeling protocols. We also recommend starting out using the similar concentration of antibodies. It is not necessary to prevent bubbles from forming in the small plastic bags as it might be beneficial for the immunolabeling process as bubbles help keep the slice moving.

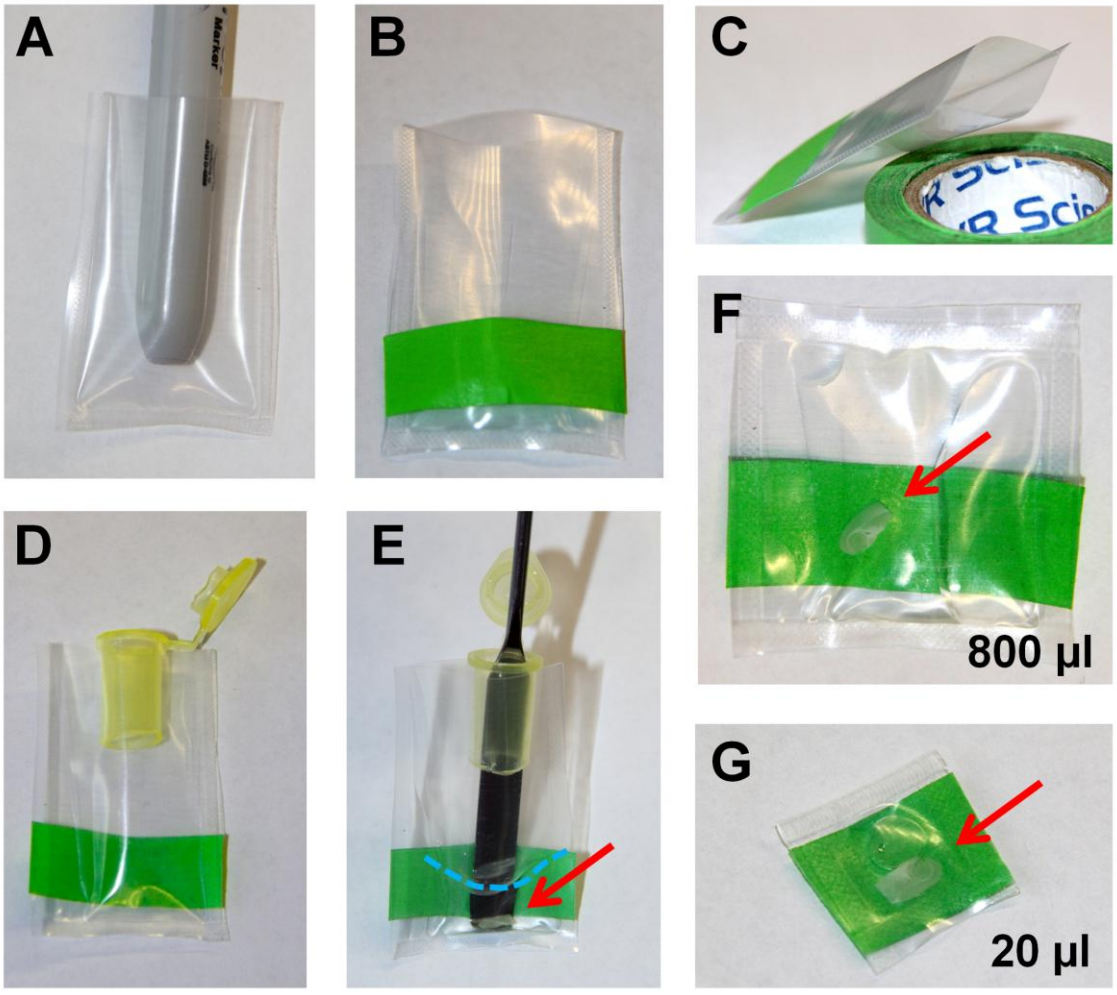

Figure 4-2 Incubate the slices in small plastic bags.

Small bags are made using a Manual Impulse Sealer and the plastic from a Reloc Zippit 4Mil bag. ***A,*** The end of an object is placed inside the bag to keep it open. ***B,*** A piece of tape is placed across the lower part of the bag. ***C,*** The tape allows for labeling of the slice and prevents the bag from closing. ***D,*** Cut an eppendorf tube in half and

place the top part in the opening of the bag. ***E,*** The Eppendorf tube ensures that the plastic bag will not collapse and makes it easier to add staining solution and to guide the metal spatula when transferring the slice. The stripped blue line indicates the surface of the staining solution. ***F-G,*** Example of sealed plastic bags containing 800 µl of staining solution **(*F*)** and 20 µl of staining solution **(*G*)**. Note that the sealed bag forms a pocket around the brain slice because the tape prevented it from collapsing (this allows for optimal penetration). Brain slices are indicated with red arrows.

10. Wash the tissue using washing solution 3-5 times over the course of a day.

11. Incubate with secondary antibodies diluted to the required concentrations in staining solution. Use the same procedure as for incubation with primary antibody and incubate the tissue for 4-6 days at 4 °C. Light exposure of the fluorophores should be reduced.

12. Wash the tissue using washing solution 3-5 times over the course of a day.

13. Rinse the tissue 3-5 times in PBS. The slices can be stored in PBS at 4 °C for many weeks but we recommend imaging the slices as soon as possible.

14. To image the slices, place each slice on a specially made microscope slide using a transfer pipette with the tip cut off. This microscope slide consists of one microscope slide with two stacks of two cover glasses glued onto it. The two stacks of cover glasses can be glued together and then glued onto the microscope slide using Krazy Glue. Two cover glasses in each stack is optimal for brain slices that are sliced 300-400 µm. There should be enough space in between the two stacks of cover glasses to fit the brain slice but they should also be close enough together to support the cover glass used to cover the brain slice (Fig. 4.3A). It is designed for

keeping the slice immersed in PBS while imaging and to ensure an even surface of the slice without any flattening (For details see Fig. 4.3). To avoid misplacement of the brain slice below the cover glass we recommend to only add a small drop of PBS on top of the brain slice prior to placing the cover glass over the brain slice (Fig. 4.3B). Even though the cover glass will be elevated by the two supportive stacks glued on to the microscope slide it should still connect with the entire surface of the brain slice and thereby create an even surface for imaging (if bubbles are observed, repeat the procedure until cover slide is correctly positioned) (Fig. 4.3C). PBS evaporates quickly so for best imaging results add corn oil to each side of the microscope slide (Fig. 4.3D).

15. The immunolabeled brain slice can be imaged.

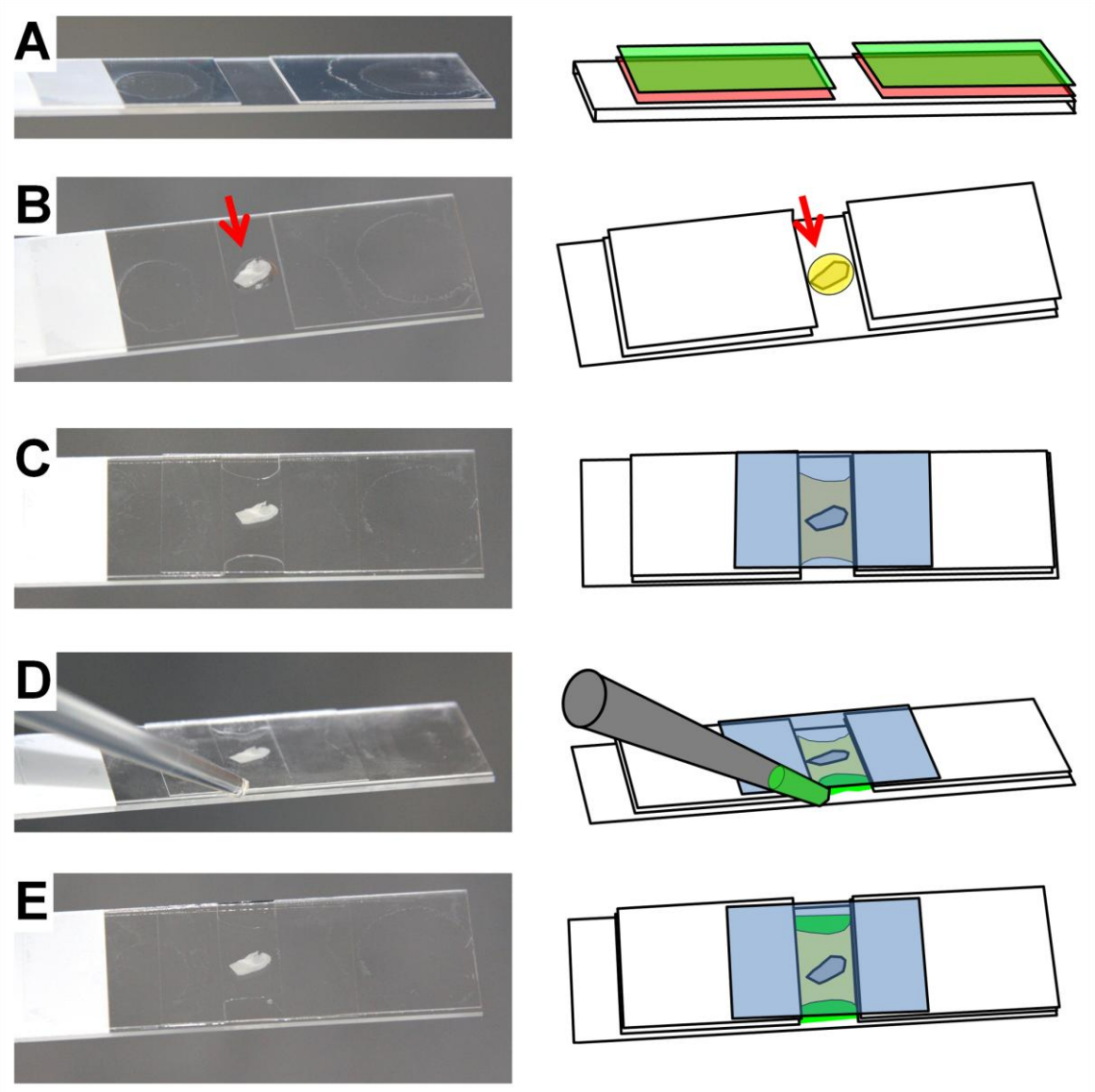

Figure 4-3 Hydration of the brain slice on the microscope slide.

For successful imaging of the slice it is important that the slice remains hydrated in PBS on the microscope slide. ***A,*** Two stacks of two cover glasses are glued on to the microscope slide (first layer illustrated in red and second layer illustrated in green). ***B,*** The brain slice (indicated by red arrows) is placed in between the two stacks in a drop of PBS (illustrated in yellow). ***C,*** A fifth cover glass (illustrated in blue) is placed on top of the brain and the two stacks of cover glasses. The cover glass will connect with the entire surface of the brain slice and push the PBS to the sides but it should not push it all the way to the edges. ***D,*** Add corn oil (illustrated in green) using an intact transfer pipette into the space between the microscope slide and the cover glass from both sides to fill up the compartment below the cover glass. This prevents the PBS from evaporating. ***E,*** The brain slice is now secured in PBS and is ready to image.

Critical Parameters and Troubleshooting

Quenching of endogenous fluorophores present in the tissue at the time of fixation (e.g. GFP) will occur in a time dependent manner when using PFA at 80 °C (Fig. 4.4C2) and can therefore be reduced by lowering the fixation time. Qualitative analysis of microglial fine processes demonstrated that immersion of 300 µm slices in 4 % PFA at 80 °C for >30 sec is sufficient to preserve the fine processes throughout the slice. However, we routinely use 2 min, which we find extremely reliable, and the quenched fluorescence can be compensated for by increasing exposure time and/or laser power.

In general we have not found autofluorescence to be a big concern, with the exception of blood vessels (Fig. 4.4C1) and the fluorescent pigment lipofuscin when slices are prepared from old animals as lipofuscin accumulates in the cytoplasm of cell with increased age (Schnell et al., 1999). Autofluorescence specifically becomes an issue if the endogenous fluorophores become quenched during the fixation, the immunolabeling is targeting proteins associated with vessels, or the immunolabeling results in a dim fluorescent signal. Autofluorescence in the vessels can be eliminated by perfusing the animal with PBS (on ice, 30 ml) prior to removing the brain and autofluorescence due to lipofuscin can be quenched using different marsking or reducing agents (in weight / volume; 0.001 % Sudan black (Schnell et al., 1999), 1 % Sodium azide (Karadottir and Attwell, 2006), 0.05 % sodium borohydrate (Copray et al., 1991)), although we have not found the need for using any of these for our studies.

DMSO will facilitate the removal of unfixed autofluorescent molecules, however it will also remove unfixed dyes (e.g. lipophilic dyes like DiI) though we recommend using fixable dyes for cell loading (e.g. Dextran conjugated with Alexa Fluor 594, Cat# D-22913 that contains free amines).

4.3 Discussion

Here we described a stepwise protocol called “SNAPSHOT” that will allow the ultrastucture of the tissue to be preserved reliably in every brain slice. Furthermore, the morphology of fine dynamic structures will be preserved at the exact time of fixation. Finally, a uniform immunolabeling throughout the tissue will be achieved with a comparable or better quality as observed with immunolabeling the same epitopes in thin re-sectioned slices.

Two-photon scanning microscopy of live brain tissue has revealed the dynamic nature of fine structures within the tissue in particular the processes of microglia, the brain’s immune cells. Microglia are morphologically dynamic cells with long thin processes that rapidly move around within the tissue surveying the environment (Nimmerjahn et al., 2005). Several intriguing questions emerged throughout this investigations presented in chapter 2 and 3 that couldn’t be addressed with the methods available at the present time. This encouraged us to establish the SNAPSHOT method. Microglia rapidly alter their morphology to changes in the environment e.g. tissue damage and efflux of ATP trigger process extension (Davalos et al., 2005) thereby making microglia unique *in situ* sensors for rapid changes in the environment. We predicted that preservation of the microglial morphology would be an ideal readout for establishing a rapid fixation method for preserving fine dynamic structures in thick brain slices.

Rational for heating PFA for fixation

Most antibodies for IHC are validated on thin cryostat sections from brains that are fixed by transcardial perfusion with PFA. Thus, we decided to base our fixation method on PFA, in order to preserve an antigenicity similar to that of a thin cryostat section. Existing protocols for fixation of acute brain slices with PFA rely on long fixation procedures (hours) in 4 % PFA

either at 4ºC or at room temperature (Karadottir and Attwell, 2006; Takano et al., 2014) and the preservation of dynamic structures is questionable (Fig. 4.4A-B). Keeping in mind how rapidly fine dynamics structures change within the tissue we found it crucial that the fixation occurred as quickly as possible. We hypothesized that heating the PFA solution to more than 60 °C would be advantageous because temperatures above 60 °C ensure monomeric formaldehyde (methylene hydrate) as the solute. Monomeric formaldehyde is a more potent fixative than polymeric formaldehyde and penetrates more easily through the tissue. Higher temperatures also increase the diffusion of the fixative through the tissue and accelerate its chemical reactions. Irradiation temperatures of up to 90 °C have successfully been applied when using microwave fixation (Login et al., 1998). However, it appeared controversial whether high temperatures are beneficial or detrimental for preserving fine biological structures (Jensen and Harris, 1989). We found that immersing brain slices for 2 min in 4 % PFA heated to 80 °C preserved the fine dynamic processes of $EGFP^+$ microglia (Fig. 4.4C).

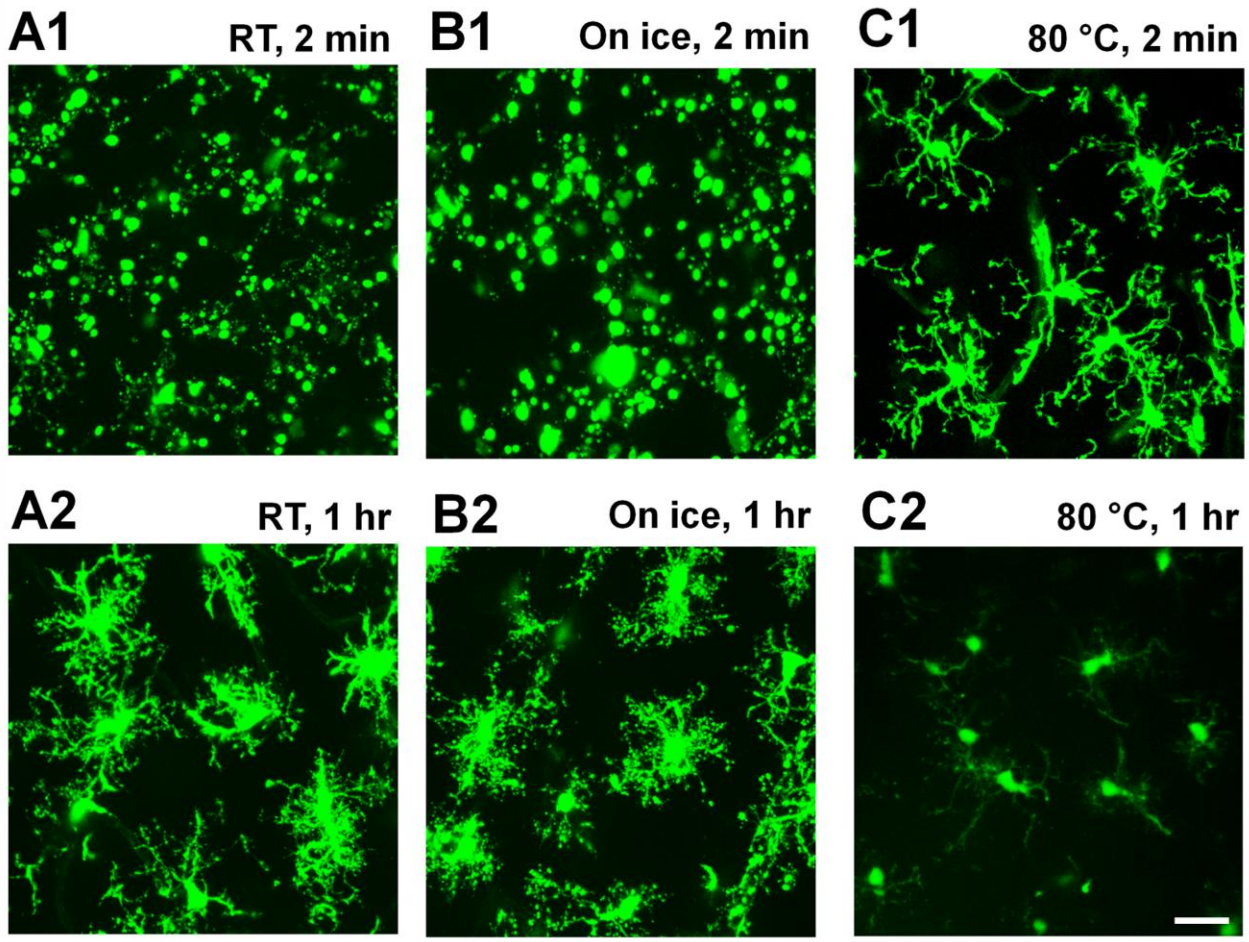

Figure 4-4 Rapid fixation of fine dynamic structures.

300 µm thick brain slices from mice that express EGFP in the microglia were immersion fixed using 4 % PFA at three different temperatures. *A1-C1*, Fixation for 2 min in PFA at RT, on ice, and, at 80 °C. Note, that the intact ramified morphology of microglia with long fine processes is preserved only when PFA is heated to 80 °C. *A2-C2*, Fixation for 1 hr in PFA at RT, on ice, and, at 80 °C (*C1*). Note, that the extended time has improved the fixation procedure for PFA at RT (*A2*) and on ice (*B2*). However, the fine microglia processes looks retracted and beaded in both cases. Prolonged fixation at 80 °C resulted in quenching of the fluorophore in this case EGFP (*C2*). All six images are projects of stacks of images (stepping 1 µm) acquired in the CA1 region of the hippocampus, between 125 and 175 µm below the surface of the slice using the exact same setting (laser power, gain, and off-set). Scale bar: 20 µm

Rational for using DMSO to improve immunolabeling

Standard IHC protocols typically allow labeling at a depth of ~50 µm below the surface of the slice (Karadottir and Attwell, 2006; Snippert et al., 2011) and therefore often require cryostat resectioning of the fixed slice. We aimed to optimize the current standard IHC protocols and immunolabel the intact free floating slices to completely avoid the risk of embedding, freezing, and slicing artifacts associated with re-sectioning. DMSO is a cheap and safe pharmaceutical penetration enhancer and it is capable of enhancing the permeation of both hydrophobic and hydrophilic molecules across cell membranes (Marren, 2011). We hypothesized that DMSO would facilitate the penetration of antibodies through the fixed brain slices and that it would help clear the tissue from unfixed molecules without disturbing the cytostructures. By addition of 20 % DMSO at each step of the immunolabeling protocol we achieved a uniform labeling of our target proteins throughout 300 µm thick slices as shown in chapter 2. To further permeabilize the tissue and improve antibody penetration through the slices we also applied the standard detergent for IHC, Triton X-100, at different concentrations (0.5, 1, 2 and 5 %). We found that we could increase the concentration of Triton X-100 to 2 % without affecting the morphology of fine structures. Importantly, Zukor and colleagues had previously reach the same conclusion after testing various detergents at different concentration (i.e. Triton X-100, Tween-20, NP-40, CHAPS, and sodium dodecyl sulfate) for fluorescent probe penetration of adult newt spinal cords (Zukor et al., 2010).

Utilizing SNAPSHOT to address unique biological questions

Utilizing SNAPSHOT we were able to demonstrate that the ATP receptor P2Y12, which is crucial for microglial process extension, is located at the leading edge of the extending

microglial processes as shown in chapter 2. SNAPSHOT also allowed us to validate microglia dynamics without live cell illumination thereby ruling out potential contributions of laser-induced photo-toxicity. Importantly, we could also visualize the microglia morphology by immunolabeling ionized calcium-binding adapter molecule 1 following activation of NMDA receptors in acute brain slices from wild type and knock-out mice which did not express EGFP in their microglia. The possible applications of SNAPSHOT are endless and it provides an opportunity to expand on the knowledge that can be gained from experiments using brain slices. We additionally utilized the rapid fixation step combined with immunogold labeling and electron microscopy to investigate NMDA-induced internalization of synaptic proteins (Mills et al., 2014).

The greatest contribution of SNAPSHOT to the scientific communities is that it allows for scientists to rethink their experimental designs of studies that involve acute brain slices. SNAPSHOT provides the opportunity for increasing the throughput of acute brain slice experiments to become comparable to the experimental designs currently applied to cultured cells. For example, it is now possible to run simultaneous experiments under the same conditions with multiple slices prepared from the same brain (i.e. control conditions and several different treatment groups). This eliminates the issues of time after slicing between slices, and it maximizes the amount of data that can be acquired from each brain (potentially reducing the number of animals required). Compared to live imaging of acute brain slices, SNAPSHOT offers the possibility to investigate cellular responses that occurred at precisely the same time point in a large brain region or across multiple different brain regions (i.e. cortex, striatum and hippocampus if the brain is sliced in the coronal plane). Furthermore, the resolution of the z plane is always compromised in live slice imaging but the fixed slices can be cut and rotated 90

degrees to also image that plane at high resolution (e.g. to investigate structures that are polarized towards or away from the surface of the slice). Imaging the intact brain slice also gives great advantages compared to thin cryostat sections because cell-cell interactions and networks of interest (e.g. clusters of microglia and astrocytic networks) can be investigated without the need for reconstructions. Importantly, morphological structures like vessels that normally won't be maintained within the focal plane of a thin slice can easily be tracked over greater distances (Fig. 4.5).

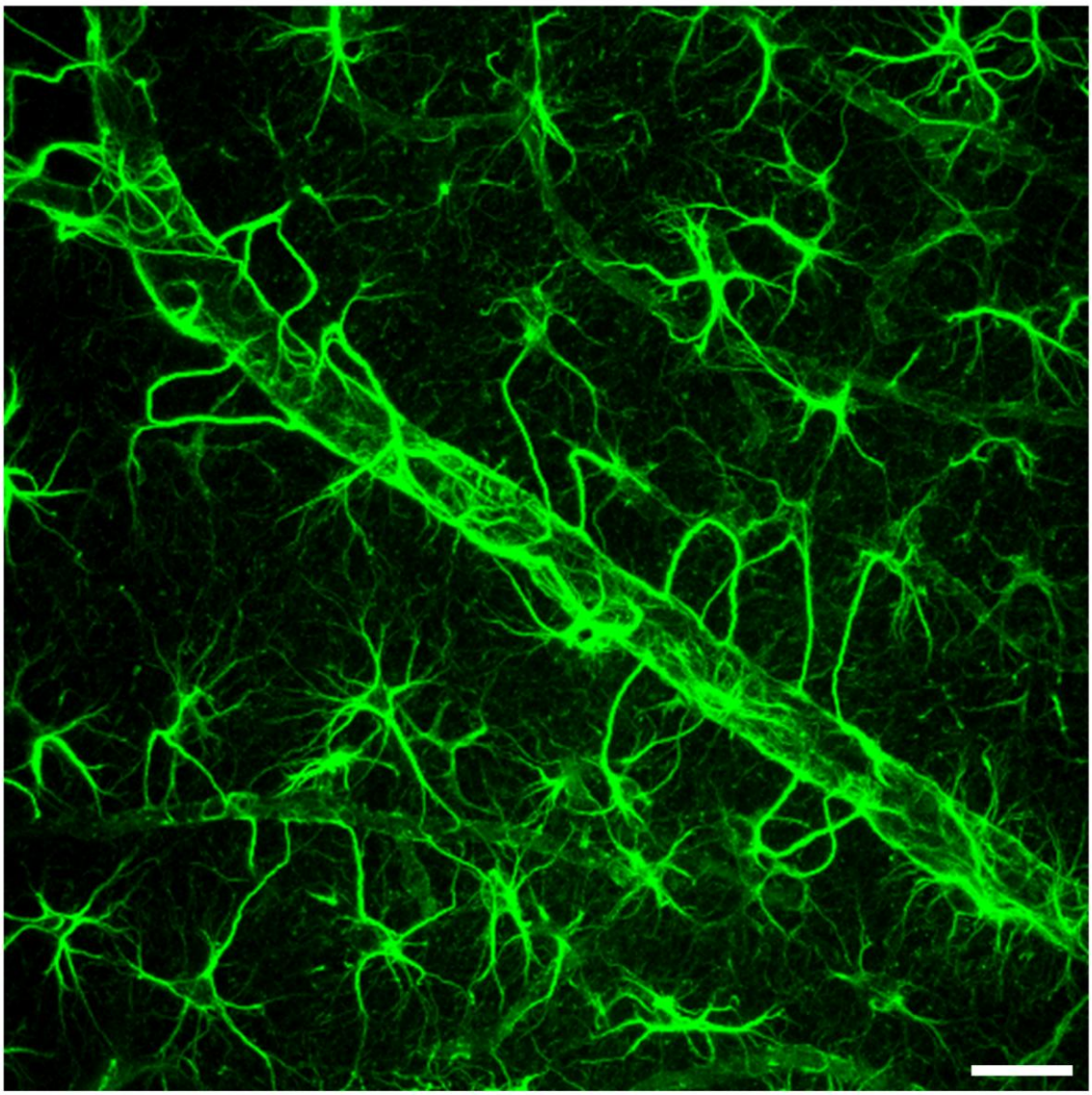

Figure 4-5 Tracking astrocytic processes along a vessel.

SNAPSHOT was utilized to fix and immunolabel glial fibrillary acidic protein (GFAP) in a 400 µm thick horizontal slice from a P30 rat brain (primary antibody; polyclonal anti-GFAP antibody, from Abcam, cat # ab7260, 8 days incubation and secondary antibody; goat-anti-rabbit IgG from Life Technologies, cat # A-11034, 6 days incubation). The image is a projection of a stack of images (stepping 1.5 µm) acquired in the CA1 region of the hippocampus, between 110 and 170 µm below the surface of the slice. The main $GFAP^+$ enwrapped vessel in the image was identified and the stack of images was acquired with the fist image below the vessel and the top image above the vessel. The entire vessel within the stack could therefore be visualized by projection of the stack of images (max intensity projection) without the need for reconstruction and the risk of re-sectioning artifacts which would have been required if thin cryostat sections had been used. Scale bar: 20 µm

Entering a new era of optical tissue clearing

Over the last years several different optical clearing agents and techniques have successfully been developed which has made it possible to make entire rodents brains optically transparent and permeable to macromolecules e.g. benzylalcohol-benzylbenzoate (Dodt et al., 2007), Phenylmethoxymethylbenzene (Becker et al., 2012), Tetrahydrofuran (Erturk et al., 2012), Sca*l*e (urea based) (Hama et al., 2011), SeeDB (fructose and α-thioglycerol based), and CLARITY (sodium dodecyl sulfate based and with the introduction of electrophoresis for lipid removal). SNAPSHOT can potentially also be successfully combined with an optical clearing procedure like SeeDB (which doesn't require dehydration of the tissue). Presumably additional clearing of the brain slice would assist antibody penetration and therefore decrease the time required for incubations and it would allow the immunolabeled brain slices to be imaged using a confocal microscope. The advantage of SNAPSHOT in relation to these optical clearing agents is the rapid and simple fixation procedure that we have optimized for brain slices. SNAPSHOT is an ideal approach for fixation of morphological changes of fine dynamic structures that have been

triggered by direct manipulation of live brain slices (e.g. by application of a pharmacological agent, uncaging of a caged compound, or electrical stimulation). Advanced tools using high-pressure freezing have recently been developed for capturing of cellular responses with a temporal resolution of milliseconds (e.g. Leica EM HPM100 and EM PACT2, HPM 010 from Boeckler Instruments, Wohlwend HPF Compact 02). The major limitations with these cryo-immobilization techniques are that ACSF needs to be substituted with a low-hydro filler (e.g. 1-hexadecene yeast paste) and that adequate freezing of 300-400 µm thick brain slices requires anti-freezing agents which are normally not incorporated by living cells (Kaech and Ziegler, 2014). However, ultrafast endocytosis in cultured neurons has been elegantly demonstrated by combining high-pressure freezing and optogenetics (Watanabe et al., 2013). Taken together, SNAPSHOT provides a novel, convenient, and economical approach for fixation and immunolabeling of brain slices directly in line with the current direction of state-of-the-art techniques.

Chapter 5: Conclusion

Summary

The work presented in this dissertation demonstrates two novel communication pathways between neuronal activity and ATP-mediated microglial process dynamics. Additionally, a novel tissue fixation method for the preservation and visualization of fine dynamic structures in acute brain slices were developed. The new fixation method, named SNAPSHOT provided a technique that was required to rapidly preserve dynamic processes in order to quantify the two separate communication pathways involving ATP release from neurons and astrocytes.

5.1 Hypothesis 1

Addressing the hypothesis that; *activation of neuronal NMDAR triggers ATP release via opening of neuronal Panx1 hemichannels and consequently a change in microglial process dynamics* resulted in several interesting discoveries. We demonstrated for the first time, using a novel NMDAR stimulation paradigm, that activation of NMDAR triggered ATP-mediated microglial process outgrowth and these findings were published in The Journal of Neuroscience (Dissing-Olesen et al., 2014). In support of our discoveries, the same issue of The Journal of Neuroscience also included a manuscript from Dr. Wu's lab (Eyo et al., 2014) that reported very similar observations but also some intriguing differences. While our paradigm included multiple brief applications of NMDA (1 min, 100 μM) resulting in a reversible and re-inducible microglial process outgrowth, Eyo and colleagues bath applied NMDA for 15 min (30 μM) to evoke a similar morphological change in microglia (Eyo et al., 2014). Although it was not reported or discussed whether microglial processes retracted after the prolonged NMDA application. We demonstrated that the NMDA evoked outgrowth was depending on release of

ATP by demonstrating that outgrowth did not occur in the presence of the commonly used purinergic blocker RB2. However, RB2 has been reported to potentially inhibit NMDAR (Nakazawa et al., 1995; Peoples and Li, 1998). At the time of the study RB2 was the only purinergic receptor antagonist available to us that would block microglial process outgrowth to application of ATP. In order to strengthen the link to ATP release we also investigated the impact of preventing the formation of purinergic gradients by applying an ectonucleotidase inhibitor to block the breakdown of ATP. Inhibiting the formation of purinergic gradients abolished both ATP-evoked and NMDA-evoked process outgrowth. As expected, microglia did not respond to bath application of NMDA in acute slices from P2Y12 deficient mice either (Eyo et al., 2014) thereby confirming that NMDA-evoked microglial process outgrowth are dependent ATP release.

We discovered, in agreement with the current literature, that bath application of ATP triggered extension of microglial processes both *in vivo* and in acute hippocampal slices. The reversible nature of the microglial response, when ATP was removed, has only previously been reported in retinal microglial (Fontainhas et al., 2011) and we further demonstrate that microglial process outgrowth can be reliably re-introduced with an additional application of ATP. We therefore designed our NMDAR stimulation paradigm to determine whether microglial processes retracted after NMDA application. Hence, we allowed 40 min intervals between the NMDA applications. The advantage of this paradigm is that it allowed us to investigate the involvement of different candidate proteins (e.i. NMDAR and purinergic receptors) by applying pharmacological antagonists (e.g. with APV and RB2) and then quantifying and comparing the microglia responses to NMDA (5^{th} application) in the presence of the drug to how these same cells responded to application of NMDA without the drug (4^{th} NMDA application).

ATP release is selective to NMDAR activation but independent of Panx1 hemichannel opening

Application of glutamate, but not kainate, also triggered microglial process outgrowth, similar to application of NMDA, in both acute hippocampal slices and *in vivo*. Glutamate-evoked outgrowth was also blocked by APV (Eyo et al., 2014) which confirmed our finding that NMDA-induced outgrowth occurred when synaptic transmission and AMPA receptors were blocked. This is in sharp contrast to studies in the retina where stimulation of AMPA and kainate receptors but not NMDAR were reported to trigger microglial process outgrowth (Fontainhas et al., 2011). Intriguingly, we observed that multiple brief activations of NMDAR were required for triggering microglial process outgrowth. This is in line with our hypothesis, since both multiple brief applications of NMDA and prolonged application of NMDA has been reported to evoke opening of Panx1 hemichannels in CA1 pyramidal neurons (Thompson et al., 2008). However, both NMDAR stimulation paradigms (i.e. multiple brief applications and prolonged application) triggered microglial process outgrowth in the presence of the potent hemichannel blocker CBX (50-100 μM) indicating that ATP release in these paradigms does not depend on hemichannel opening. We further validated that outgrowth occurred independently of Panx1 by visualizing NMDA-evoked process outgrowth by immunolabeling microglia in fixed acute brain slices using the novel SNAPSHOT method. We therefore rejected the hypothesized involvement of Panx1 hemichannel opening for NMDA-evoked microglial process outgrowth under these experimental conditions.

NMDA-evoked ATP release is independent of excitotoxic damage

Interestingly, the microglial response in both NMDAR stimulation paradigms was blocked by probenecid (2-5 mM). Notably, probenecid also blocked AMPA- and kainate-evoked

microglial process outgrowth in the retina (Fontainhas et al., 2011). We validated that probenecid did not block ATP-induced outgrowth and it did not affect NMDA-evoked Ca^{2+} signals in pyramidal neurons. These findings indicate that the ATP release observed in these experimental paradigms is mediated by a probenecid-sensitive mechanism and not a loss of membrane integrity due to neuronal excitotoxicity. This is also supported by the reversibility of the processes outgrowth in the different paradigms including both brief application of NMDA as well as AMPA, and kainate (Fontainhas et al., 2011). Following a laser-induced damage the microglial processes will adhere to the damaged area for hours to days and damaged cells will take up dyes through their compromised membranes. Bath application of glutamate (1 mM) and NMDA (30 μM) for 10 min did not trigger either PI or SYTOX uptake (Eyo et al., 2014). This lack of dye uptake further supports our conclusion that ATP release is not due to excitotoxic damage or opening of hemichannels which would also have allowed for influx of PI and SYTOX.

The initial trigger of ATP release is activation of dendritic NMDAR

We hypothesize that the initial trigger of NMDA-evoked ATP release is activation of neuronal NMDAR and not NMDAR on glial cells and we also assumed that Ca^{2+} influx through the NMDAR would be required for this function and that preventing Ca^{2+} influx through NMDAR would therefore block release of ATP. Our data demonstrate that this assumption was valid and it is further supported by the finding that removal of extracellular Ca^{2+} completely blocked NMDA-evoked neuronal Ca^{2+} signals and microglial process outgrowth while microglia process extension towards a laser-induced lesion still occurred when extracellular Ca^{2+} was depleted (Eyo et al., 2014).. GluN2A,B are the predominant NMDAR subunits in the CA1 and

they exert high sensitivity for Mg^{2+}. Hence the presence of high extracellular levels of Mg^{2+} results in a voltage dependent block of Ca^{2+} influx through NMDAR. GluN2C,D on the other hand has relatively low sensitivity for Mg^{2+} (Monyer et al., 1992; Ishii et al., 1993; Kuner and Schoepfer, 1996; Schwartz et al., 2012) but their expression (if any) in the adult CA1 has been reported to be very sparse. *In situ* hybridization revealed that GluN2C mRNA is only expressed for a restricted period between P7 and P14 in the CA1 (Pollard et al., 1993; Monyer et al., 1994) and protein levels has not been detected (Thompson et al., 2002). GluN2D mRNA was found to be highly expresses prenatally and until around P12 but not in the adult hippocampus (Monyer et al., 1994; Paoletti, 2011). GluN2D immunoreactivity was also reported to be totally excluded from pyramidal cells (Thompson et al., 2002). In addition recordings from astrocytes in the cortex have shown that high Mg^{2+} does not block astrocyte responses to NMDA that are possibly due to GluN3 subtypes expression (Lalo et al., 2006). We therefore designed an experiment to investigate whether selective activation of NMDAR on a single neuron would be sufficient to trigger a microglial response and thereby demonstrate that the initial trigger of NMDA-evoked ATP release is activation of neuronal NMDAR. Bath application of NMDA in the of presence of high extracellular Mg^{2+} did not trigger neuronal Ca^{2+} signals or microglial process outgrowth, indicating that all neuronal NMDAR were blocked by Mg^{2+} and that ATP release did not occur. Astonishing, when the Mg^{2+} block was selectively relieved when the patched clamped neuron was depolarized, then bath application of NMDA triggered microglial process outgrowth. Repeating the same experiment but with an NMDAR channel blocker (MK801) inside the patch electrode abolished NMDAR-evoked microglial process outgrowth demonstrating that the initial trigger of NMDA-evoked ATP release is activation of neuronal NMDAR and not NMDAR on glial cells. Blockage of astrocytic functions by application of the astrocyte toxin fluoroacetate did

not affect the NMDA-evoked microglial response (Eyo et al., 2014), supporting our conclusion that ATP release is mediated by activation of neuronal NMDAR and not astrocytic NMDAR. However, no control experiments were done to validate that fluoroacetate truly blocked astrocytic release of ATP. Increased numbers of contacts between neurons and microglial processes was also reported during bath application of glutamate using a double transgenic mouse ($EGFP^+$ microglia and YFP^+ neurons) (Eyo et al., 2014). However, we did not observe directed outgrowth toward the patched neuron and it is not surprising that the number of contacts increases when outgrowth occurs due to the overall increase in number of process with bulbous tips. It would have been reassuring if the same experiments had been performed by Eyo et al with application of ATP (instead of glutamate) and with labeled astrocytes (instead of neurons) to show that application of NMDA (and not ATP) triggered an increased number of contacts between microglial processes and neurons (but not astrocytes). To rule out a direct effect of NMDA on microglial NMDAR, brief application of (1-2 sec) of NMDA was applied which triggered an inward current in patch clamped neurons but not in patch clamped microglia. Importantly, longer application of NMDA (3-4 min) triggered an outward current in patch clamped microglia similar to the current induced by application of ATP (Eyo et al., 2014). Thereby demonstrating that microglia responded to ATP and not NMDA. It would have been interesting to see if prolonged application of NMDA would evoke an outward current in P2Y12 deficient microglia or in the presence of a purinergic receptor antagonist.

ATP could potentially be released from astrocytes. Activation of neuronal NMDAR causes an influx of Ca^{2+} and Na^+ as previously discussed but it also allows for efflux of K^+. Increases in extracellular K^+ (10 mM) have previously been shown to affect astrocytes e.g. enhance astrocytic glycolysis and trigger astrocytic release of lactate in acute brain slices (Choi et al., 2012). High

(10 mM) K^+ triggered ATP release from cultured murine astrocytes (Xu et al., 2014) supposedly via vesicular exocytosis (Maienschein et al., 1999; Bal-Price et al., 2002; Pryazhnikov and Khiroug, 2008; Heinrich et al., 2012; Yan et al., 2013). However, increases in extracellular K^+ due to endogenous release might be considered modest in acute brain slice preparations because of continuous exchange with bath ACSF which contains low K^+ (2.5 mM).

Priming effect of NMDA applications

Interestingly, multiple brief applications of NMDA were required to trigger a robust microglial response thus an intriguing question is obviously how and why these responses differ when the stimuli is the same (application of 100 µM NMDA for 1 min). Time after slicing did not change the response as we have done several controls where we omitted the first NMDA applications and applied NMDA after two hours without observing a microglial response (data not shown). It is tempting to propose that multiple stimulations are pushing the microglia towards a more hypersensitive 'primed' phenotype as described with aging and following inflammatory stimuli where 'primed' microglia present exaggerated responsiveness (Norden and Godbout, 2013; Norden et al., 2014; Perry and Holmes, 2014). However, ATP-evoked microglial process outgrowth does not require 'priming' and the response to ATP following multiple NMDA applications was unaltered. Thus, we predict that under these experimental conditions the 'priming' effect can be neglected for microglia and plausibly ascribed to an exaggeration of the mechanism of ATP release. It would be very interesting to quantify the release of ATP over time to investigate if it correlates with microglial process outgrowth as would be expected.

The P2Y12 receptor accumulates at the bulbous tips of extending microglial processes

Based on previous studies we hypothesized that P2Y12 and Iba1 would localize at the bulbous tips of microglial processes. G-protein coupled receptors has been shown to localize at the leading edge of chemotaxing cells (Meili et al., 1999; Parent and Devreotes, 1999) (Meili et al., 1999) and activated Rac, which co-localize with Iba1 during membrane ruffling, has been shown to localize to the bulbous tips of microglial processes (Li et al., 2012). Indeed, using our SNAPSHOT method we demonstrated a very high level of both P2Y12 and Iba1 immunoreactivity in the bulbous tip of extending processes following laser-induced lesion and ATP application. It would be interesting to further investigate the ultrastructure of bulbous tips using EM. We have already validated that SNAPSHOT preserves the ultrastructure of the tissue (Mills et al., 2014) and immunolabeling of P2Y12 and Iba1 could be used to identify bulbous tips.

Possible mechanisms of NMDA-evoked ATP release

In conclusion, we have demonstrated a novel form of neuron-microglia communication that is initiated by activation of dendritic NMDAR. However, the mechanism of ATP release remains to be resolved. The fact that NMDA-evoked microglial process outgrowth, but not neuronal Ca^{2+} signals and ATP-induced process outgrowth, is blocked by probenecid strongly indicate that the mechanism of ATP release is sensitive to probenecid. This might provide a very useful hint about the possible mechanism of NMDA-evoked ATP release. Besides blocking Panx1 hemichannel opening, probenecid also inhibits transporters of the ATP binding cassette superfamily such as multidrug resistance-associated proteins (Gerk and Vore, 2002; Potschka et

al., 2004) and organic anion transporters (Di Virgilio et al., 1988; Lipman et al., 1990). Thus, with the right pharmacological approaches these targets should be investigated.

5.2 Hypothesis 2

Addressing the hypothesis that "*Opening of astrocytic Cx43 hemichannels, by removal of extracellular Ca^{2+}, triggers ATP release and consequently an alteration in microglial process dynamics*" resulted in several interesting discoveries and strongly indicated that hemichannel opening triggers ATP-mediated microglial responses. As hypothesized, removing or even reducing extracellular Ca^{2+} resulted in release of ATP and extension of microglial processes that, to our surprise, were directed towards focal points randomly distributed throughout the tissue. A similar type of directed extension of microglial processes towards specific focal points is also observed following laser-induced lesions or local application of ATP. Thus we have discovered a biological condition in which a similar focalization of microglial processes is triggered. Interestingly, this focalization stands in sharp contrast to the global process outgrowth observed following activation of dendritic NMDAR. Due to the rapid reversibility of this focalization it also differs from lesion-induced focalization of microglial processes. The focalization was characterized using real-time two-photon imaging of acute brain slices but it also occurred without illumination of the live slices as determined using the SNAPSHOT method. Our pharmacological interventions demonstrate that focalization of microglial processes was mediated by activation of microglial P2Y12 receptors secondary to ATP/ADP release through hemichannel opening.

Recent developments in the field

After submitting this dissertation to the supervisory committee, a brief communication by Dr. Wu's lab was published in The Journal of Neuroscience (Eyo et al., 2015), in which they also describe that reducing extracellular Ca^{2+} evoked transient focalizations of microglial processes both in acute brain slices and *in vivo*. In agreement with our data they reported that focalization required P2Y12 receptors as it did not occur in slices from P2Y12 deficient mice and that the focalization could be disrupted by bath application of ATP (Eyo et al., 2015). Interestingly, in contrast to our findings they did not observe an effect of CBX (50-100 µM) on focalization and they concluded that microglial processes converge onto neuronal dendrites independently of astrocytic hemichannel opening. However, their arguments are questionable and not strongly supported by their reported observations. To demonstrate that microglial processes converge onto neurons and not astrocytes they removed extracellular Ca^{2+} from slices from either double transgenic mice with $EGFP^{+}$ microglia and YFP^{+} neurons or from slices loaded with SR101 to visualize astrocytes. First of all, only a sparse population of neurons were YFP^{+} and it is therefore not viable to conclude that microglial processes converge onto neuronal dendrites based on the few incidents where a focalization point happen to co-localize with YFP^{+} dendrites. Secondly, they could not resolve spines versus astrocyte processes that enwrapped spines. Considering that the diameter of converged microglial bulbous tips at a focal point is 5-10 µm, it is impossible to evaluate whether the microglial bulbous tips converged onto 0.5-1 µm (YFP^{+}) presynaptic spines or to the fine surrounding astrocytic processes. SR101 staining is only observed in astrocyte soma and the initial part of the major processes and is not observed in most of the astrocyte fine processes. Cx43 expression is predominantly in astrocytic endfeet and at the interdigitation of fine astrocytic processes where they form gap junction connections with

surrounding astrocytes (Huang et al., 2012; Pekny and Pekna, 2014). To further support that astrocytes do not play an important function they apply the astrocyte toxin fluoroacetate (which they have also previously used (Eyo et al., 2014)) and reported that microglial process focalization was unaltered. They reported a control experiment showing that fluoroacetate abolishes the spontaneous intracellular Ca^{2+} transients in astrocytes. However, it can be argued that hemichannel opening evoked by reducing extracellular Ca^{2+} might occur independently of intracellular Ca^{2+}. Hemichannel mediated release of glutamate from astrocyte cultures has been reported to occur when intracellular Ca^{2+} is depleted with thapsigargin or chelated with BAPTA (Ye et al., 2003). Hence, we believe that further investigations are required to elucidate the mechanisms of ATP release and the cellular origin in this paradigm. Based on our findings and the literature discussed in chapter 1 we consider opening of astrocytic Cx43 hemichannels the most likely candidate for ATP release in reduced extracellular Ca^{2+}.

Mimetic peptides against Cx43 hemichannel opening

The synthetic blocking peptide TAT-Gap19 was selected over the other Cx43 mimetic peptides (i.e. Gap26 and Gap27) because it is the only peptide that blocks Cx43 hemichannels but not gap junctions (Wang et al., 2013). Therefore TAT-Gap19 should selectively target our hypothesized source of ATP release without interfering with astrocyte-astrocyte communication. We decided to use the peptide sequence that includes TAT in order to facilitate and increase the membrane permeability of the peptide in the 300 μm thick slices. We applied 250 μM of TAT-GAP19 which has been reported to blocked Cx43-mediated ATP release by ~97% (Wang et al., 2013). TAT-Gap19 completely blocked microglial process focalization while the Panx1 blocking peptide ^{10}panx did not. Unfortunately, this observation is inconclusive as the scramble TAT-

peptide for Gap19 also abolished microglial process focalization. Previously, mutated Gap19 has been used as a negative control but we decided to use a traditional scrambled peptide with a unique sequence containing the same nine amino acids as Gap19 and with the TAT sequence unaltered. It was previously reported that mutated Gap19 did not affect Cx43 hemichannel opening when Cx43 were expressed in HeLa cells or C6 cells lines. However mutated Gap19 has been reported to have off-target effects. It significant reduced ischemia-evoked swelling compared to no treatment controls and also reduced the infarct area following ischemia/reperfusion (Wang et al., 2013). Therefore mutated GAP19 mutated peptide might also have off-target effects that should be taken into consideration. Concerns have also previously been raised regarding the specificity of other mimetic peptides because similar effects have been observed with application of their scrambled counterparts. For example the PKM-ζ mimetic peptide ZIP, which is myristoylated to enhance permeability, reversed long term potentiation in acute hippocampal slices but the scrambled version of ZIP was found to be similarly effective (Volk et al., 2013). Both ZIP and the scrambled version of ZIP also reduced the time of freezing in mice that were reported to have PKM-ζ–dependent fear memories (Kwapis et al., 2009).

Cx43 deficient mice

Ideally, to determine whether ATP is released through opening of astrocytic Cx43 hemichannels, extracellular Ca^{2+} could be removed from brain slices generated from transgenic mice deficient for Cx43 selectively in astrocytes. We predict that ATP mediated microglial process focalization following removal of extracellular Ca^{2+} would be abolished in these mice while ATP and lesion-induced outgrowth would occur as observed in WT controls. The SNAPSHOT method offers an ideal tool for visualizing microglial processes in slices from these

mice, which does not express a genetically encoded fluorescent indicator in the microglia. Expression of GluSFnR could also been introduced into this strain of mice (using viral delivery) and we predict that the spontaneous hot spots of glutamate release that occurred following removal of extracellular Ca^{2+} would be abolished when astrocytic Cx43 is absence. Lesion-evoked glutamate release would still occur.

Opening of gap junction plaques

Our data indicate that the mechanism of release is localized to selective areas and that the probability of ATP release is low. It seems unlikely that opening of individual hemichannels is sufficient to trigger a focalization of microglial processes that qualitatively appear similar to the focalization evoked laser-induced lesion (20-30 µm in diameter) considering how efficiently ATP is hydrolyzed. Our preliminary observations also show that glutamate was detected in an area as wide as 20 µm in diameter. In comparison, lesion-evoked glutamate release could be detected 30 µm away from the lesion. However, glutamate uptake, which is normally very efficient, has been shown to be impaired in divalent cation free solution (Ye et al., 2003) and glutamate might therefore diffuse further in absence of Ca^{2+}. We therefore speculate that multiple Cx43 hemichannels in clusters would have to open in synchrony at the selective focal points to trigger microglial processes to focalize and for glutamate to be detected. Freeze-fracture electron micrographs have revealed that Cx gap junctions can cluster together in closely packed arrangements that are referred to as gap junction plaques (Tani et al., 1973; Shivers and McVicar, 1995). We speculate that removal of extracellular Ca^{2+} reduces the strength of adhesion between Cx43 gap junctions within a plaque and thereby promoting the disconnection of gap junctions and hence the opening of clusters of Cx43 hemichannels on each of the adjacent

astrocytes. Gap junction plaques have been reported to be 1 µm in diameter (Fujimoto, 1995; Nagy and Rash, 2000) and can potentially be visualized by immunolabeling of Cx43 using SNAPSHOT. The extracellular loops of the Cx43 protein are masked in gap junctions but exposed in hemichannels and antibodies against the extracellular loop have successfully been used to block hemichannels and not gap junctions (Riquelme et al., 2013). Thus, antibodies against the extracellular loops of Cx43 could potentially be used to visualize the presence of hemichannels versus gap junctions. Although, it would not give any information of whether these hemichannels are open or closed it would be very convincing if microglial process would focalize around specific areas with high immunoreactivity for antibodies against the extracellular loops of Cx43. Transgenic mice with GFP tagged Cx43 do exist, however, GFP-tagged Cx43 exhibit an altered conductance compared to the conductance of WT Cx43 when reconstituted in planar lipid bilayers (Carnarius et al., 2012) and it does not allow for the visualization of Cx43 hemichannels selectively.

Co-localizing the center of microglial process focalization with hemichannel opening

To further investigate the role of hemichannel opening for microglial process focalization the opening of hemichannels could be visualized. A commonly used approached for visualizing hemichannel opening is dye uptake. However most of the small dyes including PI and SYTOX, work by binding or chelating to DNA and thereby introducing a spatial distortion between the label nuclei and the potential site of uptake. It is therefore challenging to co-localize the site of hemichannel opening (site of dye uptake) with the center of focalization. Alternatively, dye efflux could be investigated in acute slices by preloading the tissue with a small (< 1 kDa) AM-dye such as calcein-AM, which could be co-loaded with SR101 to validate that astrocytes are

getting loaded. Hydrolysis of acetoxymethyl esters by intracellular esterases will keep the dye trapped inside the cells unless hemichannel opening is triggered. We predict that removal of extracellular Ca^{2+} would trigger dye efflux. However, one caveat of studying dye flux through astrocytic hemichannels is that astrocytes are coupled via gap junctions, which allows the dye to diffuse throughout the astrocytic network leading to a loss of cell specificity. Hemichannel-mediated loss of dye from one astrocyte might also be hard to detect because dye from surrounding astrocytes most likely will restore the loss via dye flux through gap junction and to our knowledge there are no pharmacological interventions that block gap junctions but not hemichannels. Taken together, it might be challenging to co-localize the site of dye uptake with the center of microglial process focalization. However, dye uptake might potentially be very useful to verify that removal of extracellular Ca^{2+} triggers opening of astrocytic hemichannels. Ideally, removal of extracellular Ca^{2+} would result in an enhanced uptake of SYTOX green in SR101 loaded astrocytes compared to control conditions with 2 mM extracellular Ca^{2+}. Our data could be further validated by application of CBX which we expect will block the dye uptake. Dye uptake should also be abolished in slices from Cx43 deficient mice while the P2Y12 blocker PSB (used to inhibit microglial process focalization) should not affect dye uptake. If dye uptake occurs in other cells than astrocytes, the SNAPSHOT method could be utilized to determine the specific cell type(s) (e.g. $NG2^{+}$ oligodendrocyte precursors, which express Cx26 or $NeuN^{+}$ interneurons that express Cx36).

Microglial bulbous tips promote closing of hemichannels

Our data indicate that convergence of the bulbous tips at the site of release might have a functional impact on the release mechanism and that the bulbous tips potentially inhibit the

release of ATP and glutamate plausibly by promoting the closing of hemichannels. We know from previous experiments that the bulbous tips will remain at the tip of an ATP-filled electrode for as long as ATP is released. However, upon removal of the electrode the bulbous tips disperse and the processes retract which is exactly what occurs a few minutes after the bulbous tips have converged at a focal point during low extracellular Ca^{2+}. This observation was also reported by Eyo et al who quantified that microglial processes converged for an average of approximately 4 min. It is therefore attractive to propose that release of ATP and glutamate would be prolonged if microglial processes were prevented from focalizing. One way to address this question would be to image the release of glutamate in the presence of PSB, which prevents the microglial process from focalizing. However, a careful look at our preliminary GluSFnR imaging revealed that the hot spots persists for 4-5 min which is shorter than the time it takes the microglial processes to reach the release site in most cases. This could potentially be due to a run-down of intracellular glutamate prior to the convergence of microglial bulbous tips. Alternatively, detection of ATP with a fluorescent indicator or an *in situ* ATP sensor might be necessary for addressing whether microglial play a functional role in terminating the release of ATP. Rat P2X2 receptors have been genetically engineered to carry a (*fluorescence resonance energy transfer)* FRET-based calcium sensor and used to image activation of ATP-gated P2X receptors in hippocampal neurons (Richler et al., 2008). We predict that visualization of ATP release will demonstrate the presence of local hot spots similar to the glutamate release. Hypothetically, it would be very interesting to visualize and quantify the release of ATP in the presence of PSB or in slices from P2Y12 deficient mice. We predict that without microglial process extension each hot spot of ATP release will no longer be transient but remain as long as extracellular Ca^{2+} is omitted resulting in an accumulation of hot spots over time. Combining ATP imaging and visualization

of microglial morphology could be extremely beneficial for addressing several interesting questions and for validating our findings. We predict that multiple NMDA applications will trigger a global almost uniform release of ATP throughout the tissue that will persist for up to 15 min and decline in synchrony with the retraction of microglial processes. On the other hand lesion-induced ATP release will trigger an initial dramatic spread of ATP away from the lesion site similar to what we observed for glutamate. Within the following 20-30 min (the time it takes for the microglial processes to reach the lesion site) the sphere of ATP release will shrink as the microglial processes focalize due to hydrolyze of ATP by CD39 on the bulbous tips.

5.3 Overall significance

The discoveries presented in this dissertation demonstrate that high neuronal activity can trigger a dramatic ATP-mediated alteration in microglial process dynamics. Both NMDA-evoked neuronal activation and removal of extracellular Ca^{2+}, to mimic high neuronal activity, transiently converted the surveillance by ramified microglia from a presumably random sampling to a seemingly goal-directed ATP-dependent action. We hereby demonstrated two novel modes of communication between neuronal activity and microglial process dynamics in the adult rodent brain.

The function(s) of these acute alterations in microglial process dynamics remain speculative but the demonstration of neuron-microglial communication in the adult rodent CNS is a significant contribution to the overall understanding of microglial physiology and these results have laid the foundation for multiple investigations in the future.

Potential functions of microglial BDNF

It is attractive to speculate that microglia might play a function role in determining the fate of postsynaptic dendritic spines during high neuronal activity by either promoting their survival through release of neurotrophins or actively removing spines by phagocytosis. Neurotrophins such as BDNF are critical mediators of neuronal survival and plasticity and are produced by both neurons and glial cells in response to high neuronal activity in the adult brain (Balkowiec and Katz, 2000; Dougherty et al., 2000; Chao, 2003; Coull et al., 2005; Rex et al., 2007; Rauskolb et al., 2010; Zheng et al., 2011). Importantly, ATP is the major trigger for neurotrophin release from microglia (Khakh and North, 2012). Thus ATP might be ascribed a dual function during high neuronal activity as the substrate for the generation of a purinergic gradient for recruiting and directing microglial processes and subsequently also for stimulating the local release of neurotrophins from microglial bulbous tips in close proximity to specific synapses, thereby, allowing microglia to locally manipulate synaptic transmission and plasticity in a synapse activity-dependent fashion. It has recently been demonstrated that specific depletion of microglia was associated with deficits in several different learning tasks (rotarod learning, fear learning and novel object recognition) and altered learning-induced synaptic remodeling. Similar deficits were recapitulated with genetic depletion of BDNF from microglia selectively in both young and adult mice (Parkhurst et al., 2013). Underscoring, that an important functional role of microglia in the adult CNS might be to promote dendritic spine formation and survival rather than spine elimination. We suggest that the reversibility of microglial process outgrowth in our NMDAR activation paradigm points towards neurotrophic release while we would expect that an alteration of the paradigm (i.e. prolonged NMDAR stimulation) could shift the response towards spine elimination.

Our data also indicate that contact between microglial bulbous tips and hemichannels, might promote hemichannels closing. Interestingly, neurotrophins (i.e. nerve growth factor) have been identified as potent triggers of phosphorylation of Cx43 proteins (Cushing et al., 2005) and phosphorylation is known to maintain Cx43 hemichannels in a closed state (Li et al., 1996; Liu et al., 1997; Lampe and Lau, 2000; Harris, 2001; Bao et al., 2004b). Hence, this suggests that microglial processes might also serve a functional role in limiting the efflux of ATP and glutamate to the extracellular space.

The importance of ATP hydrolysis by microglia

One would assume that cells would guard their intracellular ATP at all costs and that ATP release only occurs upon damage. However, besides being a efficient signal molecule, extracellular ATP also acts as an excitatory neurotransmitter (Pankratov et al., 1998; Mori et al., 2001; Fields and Burnstock, 2006) that enhances depolarization of CA1 pyramidal neurons by promoting P2X receptor-mediated Ca^{2+} influx (Edwards et al., 1992; Bardoni et al., 1997; Mori et al., 2001; Pankratov et al., 2002; Pankratov et al., 2006, 2007). Interestingly, on the hippocampal circuit level, ATP has been proposed to act as a physiological 'brake' against excitotoxicity by heightening overall GABAergic inhibition via enhancing stimulation of interneurons (Bowser and Khakh, 2004). ATP activates presynaptic P2X2 receptors on interneurons and at the same time augments postsynaptic depolarization by binding to P2Y1 (Khakh et al., 2003; Bowser and Khakh, 2004; Kawamura et al., 2004; Baxter et al., 2011). However, the local action of ATP itself in the stratum radiatum is excitatory (Wieraszko and Seyfried, 1989; Pankratov et al., 1998; Mori et al., 2001; Bowser and Khakh, 2004; Fields and Burnstock, 2006; Pankratov et al., 2006) and uncontrolled extracellular levels of ATP in the CA1

can trigger excitotoxicity (Braun et al., 1998; Juranyi et al., 1999; Melani et al., 2005; Arbeloa et al., 2012). Hence, it is appealing to think that ATP-mediated microglial process outgrowth also serves a crucial function in regulating extracellular ATP levels by hydrolyzing ATP and focalization of microglial processes can plausibly restrain excessive ATP release to a restricted area and eventually terminate it. By hydrolyzing ATP, microglia are also promoting the generation of adenosine that inhibits synaptic transmission (by binding to A1 receptors) or modulates it (by binding to A2A receptors) (Lee et al., 1981; Cunha et al., 1994; Cunha et al., 1998). Taken together this indicates that high neuronal activity triggers an ATP-mediated alteration in microglial processes dynamics that in turn indirectly affect synaptic transmission by regulating the local levels of adenosine.

Direct clinical impact of ATP-mediated microglial processes dynamics

Hippocampal seizure activity has been reported to trigger a change in microglial morphology (Beach et al., 1995; Eyo et al., 2014). Seizure activity requires NMDAR stimulation and causes a pronounced reduction in extracellular Ca^{2+} levels (Heinemann et al., 1977; During and Spencer, 1993; Amzica et al., 2002; Cavus et al., 2005; Meurs et al., 2008). Based on our observations the morphological changes in microglia observed during seizure is likely due to release of ATP. Remarkably, deficiency in the microglial P2Y12 receptor, which is required for microglial process outgrowth and focalization, exacerbates seizure activity by evoking earlier onset and prolonging the duration of the seizure, and consequently, 40% of P2Y12 deficient mice died while all wild type mice survived (Eyo et al., 2014). Thus, ATP-mediated communication between neurons and microglia serves an important function and further understanding of the

modes of communication presented in this dissertation will be of high therapeutic interest and direct future research.

References

Ajami B, Bennett JL, Krieger C, Tetzlaff W, Rossi FM (2007) Local self-renewal can sustain CNS microglia maintenance and function throughout adult life. Nat Neurosci 10:1538-1543.

Ajami B, Bennett JL, Krieger C, McNagny KM, Rossi FM (2011) Infiltrating monocytes trigger EAE progression, but do not contribute to the resident microglia pool. Nat Neurosci 14:1142-1149.

Ambrosi C, Gassmann O, Pranskevich JN, Boassa D, Smock A, Wang J, Dahl G, Steinem C, Sosinsky GE (2010) Pannexin1 and Pannexin2 channels show quaternary similarities to connexons and different oligomerization numbers from each other. J Biol Chem 285:24420-24431.

Amzica F, Massimini M, Manfridi A (2002) Spatial buffering during slow and paroxysmal sleep oscillations in cortical networks of glial cells in vivo. J Neurosci 22:1042-1053.

Andersson M, Blomstrand F, Hanse E (2007) Astrocytes play a critical role in transient heterosynaptic depression in the rat hippocampal CA1 region. J Physiol 585:843-852.

Arbeloa J, Perez-Samartin A, Gottlieb M, Matute C (2012) P2X7 receptor blockade prevents ATP excitotoxicity in neurons and reduces brain damage after ischemia. Neurobiol Dis 45:954-961.

Bal-Price A, Moneer Z, Brown GC (2002) Nitric oxide induces rapid, calcium-dependent release of vesicular glutamate and ATP from cultured rat astrocytes. Glia 40:312-323.

Balcar VJ, Dias LS, Li Y, Bennett MR (1995) Inhibition of [3H]CGP 39653 binding to NMDA receptors by a P2 antagonist, suramin. Neuroreport 7:69-72.

Balkowiec A, Katz DM (2000) Activity-dependent release of endogenous brain-derived neurotrophic factor from primary sensory neurons detected by ELISA in situ. J Neurosci 20:7417-7423.

Banati RB (2002) Brain plasticity and microglia: is transsynaptic glial activation in the thalamus after limb denervation linked to cortical plasticity and central sensitisation? J Physiol Paris 96:289-299.

Bao L, Locovei S, Dahl G (2004a) Pannexin membrane channels are mechanosensitive conduits for ATP. FEBS Lett 572:65-68.

Bao X, Altenberg GA, Reuss L (2004b) Mechanism of regulation of the gap junction protein connexin 43 by protein kinase C-mediated phosphorylation. Am J Physiol Cell Physiol 286:C647-654.

Baraldi PG, del Carmen Nunez M, Morelli A, Falzoni S, Di Virgilio F, Romagnoli R (2003) Synthesis and biological activity of N-arylpiperazine-modified analogues of KN-62, a potent antagonist of the purinergic P2X7 receptor. J Med Chem 46:1318-1329.

Baranova A, Ivanov D, Petrash N, Pestova A, Skoblov M, Kelmanson I, Shagin D, Nazarenko S, Geraymovych E, Litvin O, Tiunova A, Born TL, Usman N, Staroverov D, Lukyanov S, Panchin Y (2004) The mammalian pannexin family is homologous to the invertebrate innexin gap junction proteins. Genomics 83:706-716.

Bardehle S, Kruger M, Buggenthin F, Schwausch J, Ninkovic J, Clevers H, Snippert HJ, Theis FJ, Meyer-Luehmann M, Bechmann I, Dimou L, Gotz M (2013) Live imaging of astrocyte responses to acute injury reveals selective juxtavascular proliferation. Nat Neurosci 16:580-586.

Bardoni R, Goldstein PA, Lee CJ, Gu JG, MacDermott AB (1997) ATP P2X receptors mediate fast synaptic transmission in the dorsal horn of the rat spinal cord. J Neurosci 17:5297-5304.

Bargiotas P, Krenz A, Monyer H, Schwaninger M (2012) Functional outcome of pannexin-deficient mice after cerebral ischemia. Channels (Austin) 6:453-456.

Bargiotas P, Krenz A, Hormuzdi SG, Ridder DA, Herb A, Barakat W, Penuela S, von Engelhardt J, Monyer H, Schwaninger M (2011) Pannexins in ischemia-induced neurodegeneration. Proc Natl Acad Sci U S A 108:20772-20777.

Baroja-Mazo A, Barbera-Cremades M, Pelegrin P (2013) The participation of plasma membrane hemichannels to purinergic signaling. Biochim Biophys Acta 1828:79-93.

Barragan-Iglesias P, Pineda-Farias JB, Cervantes-Duran C, Bravo-Hernandez M, Rocha-Gonzalez HI, Murbartian J, Granados-Soto V (2014) Role of spinal P2Y6 and P2Y11 receptors in neuropathic pain in rats: possible involvement of glial cells. Mol Pain 10:29.

Baxter AW, Choi SJ, Sim JA, North RA (2011) Role of P2X4 receptors in synaptic strengthening in mouse CA1 hippocampal neurons. Eur J Neurosci 34:213-220.

Beach TG, Woodhurst WB, MacDonald DB, Jones MW (1995) Reactive microglia in hippocampal sclerosis associated with human temporal lobe epilepsy. Neurosci Lett 191:27-30.

Becker K, Jahrling N, Saghafi S, Weiler R, Dodt HU (2012) Chemical clearing and dehydration of GFP expressing mouse brains. PLoS One 7:e33916.

Bernier LP, Ase AR, Boue-Grabot E, Seguela P (2012) P2X4 receptor channels form large noncytolytic pores in resting and activated microglia. Glia 60:728-737.

Besseling RM, Overvliet GM, Jansen JF, van der Kruijs SJ, Vles JS, Ebus SC, Hofman PA, de Louw AJ, Aldenkamp AP, Backes WH (2013) Aberrant functional connectivity between motor and language networks in rolandic epilepsy. Epilepsy Res 107:253-262.

Beutner C, Linnartz-Gerlach B, Schmidt SV, Beyer M, Mallmann MR, Staratschek-Jox A, Schultze JL, Neumann H (2013) Unique transcriptome signature of mouse microglia. Glia 61:1429-1442.

Bialas AR, Stevens B (2013) TGF-beta signaling regulates neuronal C1q expression and developmental synaptic refinement. Nat Neurosci 16:1773-1782.

Bianco F, Fumagalli M, Pravettoni E, D'Ambrosi N, Volonte C, Matteoli M, Abbracchio MP, Verderio C (2005) Pathophysiological roles of extracellular nucleotides in glial cells: differential expression of purinergic receptors in resting and activated microglia. Brain Res Brain Res Rev 48:144-156.

Biber K, Neumann H, Inoue K, Boddeke HW (2007) Neuronal 'On' and 'Off' signals control microglia. Trends Neurosci 30:596-602.

Billaud M, Lohman AW, Straub AC, Looft-Wilson R, Johnstone SR, Araj CA, Best AK, Chekeni FB, Ravichandran KS, Penuela S, Laird DW, Isakson BE (2011) Pannexin1 regulates alpha1-adrenergic receptor- mediated vasoconstriction. Circ Res 109:80-85.

Blinzinger K, Kreutzberg G (1968) Displacement of synaptic terminals from regenerating motoneurons by microglial cells. Z Zellforsch Mikrosk Anat 85:145-157.

Boassa D, Ambrosi C, Qiu F, Dahl G, Gaietta G, Sosinsky G (2007) Pannexin1 channels contain a glycosylation site that targets the hexamer to the plasma membrane. J Biol Chem 282:31733-31743.

Boengler K, Ungefug E, Heusch G, Leybaert L, Schulz R (2013) Connexin 43 impacts on mitochondrial potassium uptake. Front Pharmacol 4:73.

Bowser DN, Khakh BS (2004) ATP excites interneurons and astrocytes to increase synaptic inhibition in neuronal networks. J Neurosci 24:8606-8620.
Braun N, Lenz C, Gillardon F, Zimmermann M, Zimmermann H (1997) Focal cerebral ischemia enhances glial expression of ecto-5'-nucleotidase. Brain Res 766:213-226.
Braun N, Zhu Y, Krieglstein J, Culmsee C, Zimmermann H (1998) Upregulation of the enzyme chain hydrolyzing extracellular ATP after transient forebrain ischemia in the rat. J Neurosci 18:4891-4900.
Braun N, Sevigny J, Robson SC, Enjyoji K, Guckelberger O, Hammer K, Di Virgilio F, Zimmermann H (2000) Assignment of ecto-nucleoside triphosphate diphosphohydrolase-1/cd39 expression to microglia and vasculature of the brain. Eur J Neurosci 12:4357-4366.
Brawek B, Schwendele B, Riester K, Kohsaka S, Lerdkrai C, Liang Y, Garaschuk O (2014) Impairment of in vivo calcium signaling in amyloid plaque-associated microglia. Acta Neuropathol.
Brimecombe JC, Gallagher MJ, Lynch DR, Aizenman E (1998) An NR2B point mutation affecting haloperidol and CP101,606 sensitivity of single recombinant N-methyl-D-aspartate receptors. J Pharmacol Exp Ther 286:627-634.
Brocard F, Shevtsova NA, Bouhadfane M, Tazerart S, Heinemann U, Rybak IA, Vinay L (2013) Activity-dependent changes in extracellular Ca2+ and K+ reveal pacemakers in the spinal locomotor-related network. Neuron 77:1047-1054.
Bruzzone R, Hormuzdi SG, Barbe MT, Herb A, Monyer H (2003) Pannexins, a family of gap junction proteins expressed in brain. Proc Natl Acad Sci U S A 100:13644-13649.
Burger S, Doring B, Hardt M, Beuerlein K, Gerstberger R, Geyer J (2011) Co-expression studies of the orphan carrier protein Slc10a4 and the vesicular carriers VAChT and VMAT2 in the rat central and peripheral nervous system. Neuroscience 193:109-121.
Burnstock G (2006) Purinergic signalling. Br J Pharmacol 147 Suppl 1:S172-181.
Burnstock G (2007) Purine and pyrimidine receptors. Cell Mol Life Sci 64:1471-1483.
Burnstock G, Knight GE (2004) Cellular distribution and functions of P2 receptor subtypes in different systems. Int Rev Cytol 240:31-304.
Burton RE, Baker TA, Sauer RT (2003) Energy-dependent degradation: Linkage between ClpX-catalyzed nucleotide hydrolysis and protein-substrate processing. Protein Sci 12:893-902.
Bushong EA, Martone ME, Jones YZ, Ellisman MH (2002) Protoplasmic astrocytes in CA1 stratum radiatum occupy separate anatomical domains. J Neurosci 22:183-192.
Butovsky O, Jedrychowski MP, Moore CS, Cialic R, Lanser AJ, Gabriely G, Koeglsperger T, Dake B, Wu PM, Doykan CE, Fanek Z, Liu L, Chen Z, Rothstein JD, Ransohoff RM, Gygi SP, Antel JP, Weiner HL (2014) Identification of a unique TGF-beta-dependent molecular and functional signature in microglia. Nat Neurosci 17:131-143.
Buvinic S, Almarza G, Bustamante M, Casas M, Lopez J, Riquelme M, Saez JC, Huidobro-Toro JP, Jaimovich E (2009) ATP released by electrical stimuli elicits calcium transients and gene expression in skeletal muscle. J Biol Chem 284:34490-34505.
Cao N, Yao ZX (2013) Oligodendrocyte N-Methyl-D-aspartate Receptor Signaling: Insights into Its Functions. Mol Neurobiol 47:845-856.
Carnarius C, Kreir M, Krick M, Methfessel C, Moehrle V, Valerius O, Bruggemann A, Steinem C, Fertig N (2012) Green fluorescent protein changes the conductance of connexin 43 (Cx43) hemichannels reconstituted in planar lipid bilayers. J Biol Chem 287:2877-2886.

Castaneda-Castellanos DR, Flint AC, Kriegstein AR (2006) Blind patch clamp recordings in embryonic and adult mammalian brain slices. Nat Protoc 1:532-542.
Cattaneo M, Gachet C (1999) ADP receptors and clinical bleeding disorders. Arterioscler Thromb Vasc Biol 19:2281-2285.
Cavus I, Kasoff WS, Cassaday MP, Jacob R, Gueorguieva R, Sherwin RS, Krystal JH, Spencer DD, Abi-Saab WM (2005) Extracellular metabolites in the cortex and hippocampus of epileptic patients. Ann Neurol 57:226-235.
Chao MV (2003) Neurotrophins and their receptors: a convergence point for many signalling pathways. Nat Rev Neurosci 4:299-309.
Chaumont S, Khakh BS (2008) Patch-clamp coordinated spectroscopy shows P2X2 receptor permeability dynamics require cytosolic domain rearrangements but not Panx-1 channels. Proc Natl Acad Sci U S A 105:12063-12068.
Chekeni FB, Elliott MR, Sandilos JK, Walk SF, Kinchen JM, Lazarowski ER, Armstrong AJ, Penuela S, Laird DW, Salvesen GS, Isakson BE, Bayliss DA, Ravichandran KS (2010) Pannexin 1 channels mediate 'find-me' signal release and membrane permeability during apoptosis. Nature 467:863-867.
Chen Y, Corriden R, Inoue Y, Yip L, Hashiguchi N, Zinkernagel A, Nizet V, Insel PA, Junger WG (2006) ATP release guides neutrophil chemotaxis via P2Y2 and A3 receptors. Science 314:1792-1795.
Choi HB, Gordon GR, Zhou N, Tai C, Rungta RL, Martinez J, Milner TA, Ryu JK, McLarnon JG, Tresguerres M, Levin LR, Buck J, MacVicar BA (2012) Metabolic communication between astrocytes and neurons via bicarbonate-responsive soluble adenylyl cyclase. Neuron 75:1094-1104.
Christopherson KS, Hillier BJ, Lim WA, Bredt DS (1999) PSD-95 assembles a ternary complex with the N-methyl-D-aspartic acid receptor and a bivalent neuronal NO synthase PDZ domain. J Biol Chem 274:27467-27473.
Collingridge GL, Olsen RW, Peters J, Spedding M (2009) A nomenclature for ligand-gated ion channels. Neuropharmacology 56:2-5.
Contreras JE, Saez JC, Bukauskas FF, Bennett MV (2003) Gating and regulation of connexin 43 (Cx43) hemichannels. Proc Natl Acad Sci U S A 100:11388-11393.
Copray JC, Liem RS, Ter Horst GJ, van Willigen JD (1991) Origin, distribution and morphology of serotonergic afferents to the mesencephalic trigeminal nucleus of the rat. Neurosci Lett 121:97-101.
Cordina SM, Hassan AE, Ezzeddine MA (2009) Prevalence and clinical characteristics of intracerebral hemorrhages associated with clopidogrel. J Vasc Interv Neurol 2:136-138.
Cotrina ML, Lin JH, Alves-Rodrigues A, Liu S, Li J, Azmi-Ghadimi H, Kang J, Naus CC, Nedergaard M (1998) Connexins regulate calcium signaling by controlling ATP release. Proc Natl Acad Sci U S A 95:15735-15740.
Coull JA, Beggs S, Boudreau D, Boivin D, Tsuda M, Inoue K, Gravel C, Salter MW, De Koninck Y (2005) BDNF from microglia causes the shift in neuronal anion gradient underlying neuropathic pain. Nature 438:1017-1021.
Cull-Candy S, Brickley S, Farrant M (2001) NMDA receptor subunits: diversity, development and disease. Curr Opin Neurobiol 11:327-335.
Cunha RA, Sebastiao AM, Ribeiro JA (1998) Inhibition by ATP of hippocampal synaptic transmission requires localized extracellular catabolism by ecto-nucleotidases into adenosine and channeling to adenosine A1 receptors. J Neurosci 18:1987-1995.

Cunha RA, Johansson B, van der Ploeg I, Sebastiao AM, Ribeiro JA, Fredholm BB (1994) Evidence for functionally important adenosine A2a receptors in the rat hippocampus. Brain Res 649:208-216.

Cushing P, Bhalla R, Johnson AM, Rushlow WJ, Meakin SO, Belliveau DJ (2005) Nerve growth factor increases connexin43 phosphorylation and gap junctional intercellular communication. J Neurosci Res 82:788-801.

d'Anglemont de Tassigny X, Campagne C, Dehouck B, Leroy D, Holstein GR, Beauvillain JC, Buee-Scherrer V, Prevot V (2007) Coupling of neuronal nitric oxide synthase to NMDA receptors via postsynaptic density-95 depends on estrogen and contributes to the central control of adult female reproduction. J Neurosci 27:6103-6114.

Dalmau I, Vela JM, Gonzalez B, Castellano B (1998) Expression of purine metabolism-related enzymes by microglial cells in the developing rat brain. J Comp Neurol 398:333-346.

Damani MR, Zhao L, Fontainhas AM, Amaral J, Fariss RN, Wong WT (2011) Age-related alterations in the dynamic behavior of microglia. Aging Cell 10:263-276.

Dantzer R, O'Connor JC, Freund GG, Johnson RW, Kelley KW (2008) From inflammation to sickness and depression: when the immune system subjugates the brain. Nat Rev Neurosci 9:46-56.

Das S, Sasaki YF, Rothe T, Premkumar LS, Takasu M, Crandall JE, Dikkes P, Conner DA, Rayudu PV, Cheung W, Chen HS, Lipton SA, Nakanishi N (1998) Increased NMDA current and spine density in mice lacking the NMDA receptor subunit NR3A. Nature 393:377-381.

Davalos D, Grutzendler J, Yang G, Kim JV, Zuo Y, Jung S, Littman DR, Dustin ML, Gan WB (2005) ATP mediates rapid microglial response to local brain injury in vivo. Nat Neurosci 8:752-758.

Davalos D, Ryu JK, Merlini M, Baeten KM, Le Moan N, Petersen MA, Deerinck TJ, Smirnoff DS, Bedard C, Hakozaki H, Gonias Murray S, Ling JB, Lassmann H, Degen JL, Ellisman MH, Akassoglou K (2012) Fibrinogen-induced perivascular microglial clustering is required for the development of axonal damage in neuroinflammation. Nat Commun 3:1227.

De Lorenzo S, Veggetti M, Muchnik S, Losavio A (2006) Presynaptic inhibition of spontaneous acetylcholine release mediated by P2Y receptors at the mouse neuromuscular junction. Neuroscience 142:71-85.

Dermietzel R, Traub O, Hwang TK, Beyer E, Bennett MV, Spray DC, Willecke K (1989) Differential expression of three gap junction proteins in developing and mature brain tissues. Proc Natl Acad Sci U S A 86:10148-10152.

Dermietzel R, Gao Y, Scemes E, Vieira D, Urban M, Kremer M, Bennett MV, Spray DC (2000) Connexin43 null mice reveal that astrocytes express multiple connexins. Brain Res Brain Res Rev 32:45-56.

Desplantez T, Verma V, Leybaert L, Evans WH, Weingart R (2012) Gap26, a connexin mimetic peptide, inhibits currents carried by connexin43 hemichannels and gap junction channels. Pharmacol Res 65:546-552.

Di Virgilio F, Fasolato C, Steinberg TH (1988) Inhibitors of membrane transport system for organic anions block fura-2 excretion from PC12 and N2A cells. Biochem J 256:959-963.

Di Virgilio F, Chiozzi P, Falzoni S, Ferrari D, Sanz JM, Venketaraman V, Baricordi OR (1998) Cytolytic P2X purinoceptors. Cell Death Differ 5:191-199.

Dibaj P, Nadrigny F, Steffens H, Scheller A, Hirrlinger J, Schomburg ED, Neusch C, Kirchhoff F (2010) NO mediates microglial response to acute spinal cord injury under ATP control in vivo. Glia 58:1133-1144.

Diener HC, Bogousslavsky J, Brass LM, Cimminiello C, Csiba L, Kaste M, Leys D, Matias-Guiu J, Rupprecht HJ (2004) Aspirin and clopidogrel compared with clopidogrel alone after recent ischaemic stroke or transient ischaemic attack in high-risk patients (MATCH): randomised, double-blind, placebo-controlled trial. Lancet 364:331-337.

Dingledine R, Borges K, Bowie D, Traynelis SF (1999) The glutamate receptor ion channels. Pharmacol Rev 51:7-61.

Dissing-Olesen L, LeDue JM, Rungta RL, Hefendehl JK, Choi HB, MacVicar BA (2014) Activation of Neuronal NMDA Receptors Triggers Transient ATP-Mediated Microglial Process Outgrowth. J Neurosci 34:10511-10527.

Dobrowolski R, Sasse P, Schrickel JW, Watkins M, Kim JS, Rackauskas M, Troatz C, Ghanem A, Tiemann K, Degen J, Bukauskas FF, Civitelli R, Lewalter T, Fleischmann BK, Willecke K (2008) The conditional connexin43G138R mouse mutant represents a new model of hereditary oculodentodigital dysplasia in humans. Hum Mol Genet 17:539-554.

Dodt HU, Leischner U, Schierloh A, Jahrling N, Mauch CP, Deininger K, Deussing JM, Eder M, Zieglgansberger W, Becker K (2007) Ultramicroscopy: three-dimensional visualization of neuronal networks in the whole mouse brain. Nat Methods 4:331-336.

Dou Y, Wu HJ, Li HQ, Qin S, Wang YE, Li J, Lou HF, Chen Z, Li XM, Luo QM, Duan S (2012) Microglial migration mediated by ATP-induced ATP release from lysosomes. Cell Res 22:1022-1033.

Dougherty KD, Dreyfus CF, Black IB (2000) Brain-derived neurotrophic factor in astrocytes, oligodendrocytes, and microglia/macrophages after spinal cord injury. Neurobiol Dis 7:574-585.

Dreses-Werringloer U et al. (2008) A polymorphism in CALHM1 influences Ca2+ homeostasis, Abeta levels, and Alzheimer's disease risk. Cell 133:1149-1161.

Duan Y, Sahley CL, Muller KJ (2009) ATP and NO dually control migration of microglia to nerve lesions. Dev Neurobiol 69:60-72.

Duan Y, Haugabook SJ, Sahley CL, Muller KJ (2003) Methylene blue blocks cGMP production and disrupts directed migration of microglia to nerve lesions in the leech CNS. J Neurobiol 57:183-192.

Dubyak GR, el-Moatassim C (1993) Signal transduction via P2-purinergic receptors for extracellular ATP and other nucleotides. Am J Physiol 265:C577-606.

Dunwiddie TV, Diao L, Proctor WR (1997) Adenine nucleotides undergo rapid, quantitative conversion to adenosine in the extracellular space in rat hippocampus. J Neurosci 17:7673-7682.

During MJ, Spencer DD (1993) Extracellular hippocampal glutamate and spontaneous seizure in the conscious human brain. Lancet 341:1607-1610.

Edwards FA, Gibb AJ, Colquhoun D (1992) ATP receptor-mediated synaptic currents in the central nervous system. Nature 359:144-147.

Eichhoff G, Brawek B, Garaschuk O (2011) Microglial calcium signal acts as a rapid sensor of single neuron damage in vivo. Biochim Biophys Acta 1813:1014-1024.

El-Khoury N, Braun A, Hu F, Pandey M, Nedergaard M, Lagamma EF, Ballabh P (2006) Astrocyte end-feet in germinal matrix, cerebral cortex, and white matter in developing infants. Pediatr Res 59:673-679.

Elliott MR, Chekeni FB, Trampont PC, Lazarowski ER, Kadl A, Walk SF, Park D, Woodson RI, Ostankovich M, Sharma P, Lysiak JJ, Harden TK, Leitinger N, Ravichandran KS (2009) Nucleotides released by apoptotic cells act as a find-me signal to promote phagocytic clearance. Nature 461:282-286.

Enomoto A, Murakami H, Asai N, Morone N, Watanabe T, Kawai K, Murakumo Y, Usukura J, Kaibuchi K, Takahashi M (2005) Akt/PKB regulates actin organization and cell motility via Girdin/APE. Dev Cell 9:389-402.

Erturk A, Mauch CP, Hellal F, Forstner F, Keck T, Becker K, Jahrling N, Steffens H, Richter M, Hubener M, Kramer E, Kirchhoff F, Dodt HU, Bradke F (2012) Three-dimensional imaging of the unsectioned adult spinal cord to assess axon regeneration and glial responses after injury. Nat Med 18:166-171.

Eter N, Engel DR, Meyer L, Helb HM, Roth F, Maurer J, Holz FG, Kurts C (2008) In vivo visualization of dendritic cells, macrophages, and microglial cells responding to laser-induced damage in the fundus of the eye. Invest Ophthalmol Vis Sci 49:3649-3658.

Evans WH, Boitano S (2001) Connexin mimetic peptides: specific inhibitors of gap-junctional intercellular communication. Biochem Soc Trans 29:606-612.

Eyo UB, Peng J, Swiatkowski P, Mukherjee A, Bispo A, Wu LJ (2014) Neuronal Hyperactivity Recruits Microglial Processes via Neuronal NMDA Receptors and Microglial P2Y12 Receptors after Status Epilepticus. J Neurosci 34:10528-10540.

Eyo UB, Gu N, De S, Dong H, Richardson JR, Wu LJ (2015) Modulation of microglial process convergence toward neuronal dendrites by extracellular calcium. J Neurosci 35:2417-2422.

Ezan P, Andre P, Cisternino S, Saubamea B, Boulay AC, Doutremer S, Thomas MA, Quenech'du N, Giaume C, Cohen-Salmon M (2012) Deletion of astroglial connexins weakens the blood-brain barrier. J Cereb Blood Flow Metab 32:1457-1467.

Farber K, Markworth S, Pannasch U, Nolte C, Prinz V, Kronenberg G, Gertz K, Endres M, Bechmann I, Enjyoji K, Robson SC, Kettenmann H (2008) The ectonucleotidase cd39/ENTPDase1 modulates purinergic-mediated microglial migration. Glia 56:331-341.

Fastbom J, Pazos A, Palacios JM (1987) The distribution of adenosine A1 receptors and 5'-nucleotidase in the brain of some commonly used experimental animals. Neuroscience 22:813-826.

Fields RD, Burnstock G (2006) Purinergic signalling in neuron-glia interactions. Nat Rev Neurosci 7:423-436.

Fintel DJ (2007) Antiplatelet therapy in cerebrovascular disease: implications of Management of Artherothrombosis with Clopidogrel in High-risk Patients and the Clopidogrel for High Artherothrombotic Risk and Ischemic Stabilization, Management, and Avoidance studies' results for cardiologists. Clin Cardiol 30:604-614.

Fischer G, Mutel V, Trube G, Malherbe P, Kew JN, Mohacsi E, Heitz MP, Kemp JA (1997) Ro 25-6981, a highly potent and selective blocker of N-methyl-D-aspartate receptors containing the NR2B subunit. Characterization in vitro. J Pharmacol Exp Ther 283:1285-1292.

Fleming IN, Gray A, Downes CP (2000) Regulation of the Rac1-specific exchange factor Tiam1 involves both phosphoinositide 3-kinase-dependent and -independent components. Biochem J 351:173-182.

Fonnum F, Johnsen A, Hassel B (1997) Use of fluorocitrate and fluoroacetate in the study of brain metabolism. Glia 21:106-113.

Fontainhas AM, Wang M, Liang KJ, Chen S, Mettu P, Damani M, Fariss RN, Li W, Wong WT (2011) Microglial morphology and dynamic behavior is regulated by ionotropic glutamatergic and GABAergic neurotransmission. PLoS One 6:e15973.

Foster CJ, Prosser DM, Agans JM, Zhai Y, Smith MD, Lachowicz JE, Zhang FL, Gustafson E, Monsma FJ, Jr., Wiekowski MT, Abbondanzo SJ, Cook DN, Bayne ML, Lira SA, Chintala MS (2001) Molecular identification and characterization of the platelet ADP receptor targeted by thienopyridine antithrombotic drugs. J Clin Invest 107:1591-1598.

Fredholm BB, Chern Y, Franco R, Sitkovsky M (2007) Aspects of the general biology of adenosine A2A signaling. Prog Neurobiol 83:263-276.

Fujimoto K (1995) Freeze-fracture replica electron microscopy combined with SDS digestion for cytochemical labeling of integral membrane proteins. Application to the immunogold labeling of intercellular junctional complexes. J Cell Sci 108 (Pt 11):3443-3449.

Fujiwara Y, Kubo Y (2004) Density-dependent changes of the pore properties of the P2X2 receptor channel. J Physiol 558:31-43.

Gee JM, Smith NA, Fernandez FR, Economo MN, Brunert D, Rothermel M, Morris SC, Talbot A, Palumbos S, Ichida JM, Shepherd JD, West PJ, Wachowiak M, Capecchi MR, Wilcox KS, White JA, Tvrdik P (2014) Imaging activity in neurons and glia with a Polr2a-based and cre-dependent GCaMP5G-IRES-tdTomato reporter mouse. Neuron 83:1058-1072.

Geisler JC, Corbin KL, Li Q, Feranchak AP, Nunemaker CS, Li C (2013) Vesicular nucleotide transporter-mediated ATP release regulates insulin secretion. Endocrinology 154:675-684.

Gerk PM, Vore M (2002) Regulation of expression of the multidrug resistance-associated protein 2 (MRP2) and its role in drug disposition. J Pharmacol Exp Ther 302:407-415.

Geyer J, Fernandes CF, Doring B, Burger S, Godoy JR, Rafalzik S, Hubschle T, Gerstberger R, Petzinger E (2008) Cloning and molecular characterization of the orphan carrier protein Slc10a4: expression in cholinergic neurons of the rat central nervous system. Neuroscience 152:990-1005.

Ginhoux F, Greter M, Leboeuf M, Nandi S, See P, Gokhan S, Mehler MF, Conway SJ, Ng LG, Stanley ER, Samokhvalov IM, Merad M (2010) Fate mapping analysis reveals that adult microglia derive from primitive macrophages. Science 330:841-845.

Godecke S, Roderigo C, Rose CR, Rauch BH, Godecke A, Schrader J (2012) Thrombin-induced ATP release from human umbilical vein endothelial cells. Am J Physiol Cell Physiol 302:C915-923.

Goepfert C, Sundberg C, Sevigny J, Enjyoji K, Hoshi T, Csizmadia E, Robson S (2001) Disordered cellular migration and angiogenesis in cd39-null mice. Circulation 104:3109-3115.

Gorski JA, Talley T, Qiu M, Puelles L, Rubenstein JL, Jones KR (2002) Cortical excitatory neurons and glia, but not GABAergic neurons, are produced in the Emx1-expressing lineage. J Neurosci 22:6309-6314.

Gottlieb M, Matute C (1997) Expression of ionotropic glutamate receptor subunits in glial cells of the hippocampal CA1 area following transient forebrain ischemia. J Cereb Blood Flow Metab 17:290-300.

Grathwohl SA, Kalin RE, Bolmont T, Prokop S, Winkelmann G, Kaeser SA, Odenthal J, Radde R, Eldh T, Gandy S, Aguzzi A, Staufenbiel M, Mathews PM, Wolburg H, Heppner FL, Jucker M (2009) Formation and maintenance of Alzheimer's disease beta-amyloid plaques in the absence of microglia. Nat Neurosci 12:1361-1363.

Gu JG, Bardoni R, Magherini PC, MacDermott AB (1998) Effects of the P2-purinoceptor antagonists suramin and pyridoxal-phosphate-6-azophenyl-2',4'-disulfonic acid on glutamatergic synaptic transmission in rat dorsal horn neurons of the spinal cord. Neurosci Lett 253:167-170.

Gyoneva S, Traynelis SF (2013) Norepinephrine modulates the motility of resting and activated microglia via different adrenergic receptors. J Biol Chem.

Haanes KA, Kowal JM, Arpino G, Lange SC, Moriyama Y, Pedersen PA, Novak I (2014) Role of vesicular nucleotide transporter VNUT (SLC17A9) in release of ATP from AR42J cells and mouse pancreatic acinar cells. Purinergic Signal 10:431-440.

Hama H, Kurokawa H, Kawano H, Ando R, Shimogori T, Noda H, Fukami K, Sakaue-Sawano A, Miyawaki A (2011) Scale: a chemical approach for fluorescence imaging and reconstruction of transparent mouse brain. Nat Neurosci 14:1481-1488.

Han J, Luby-Phelps K, Das B, Shu X, Xia Y, Mosteller RD, Krishna UM, Falck JR, White MA, Broek D (1998) Role of substrates and products of PI 3-kinase in regulating activation of Rac-related guanosine triphosphatases by Vav. Science 279:558-560.

Hanisch UK, Kettenmann H (2007) Microglia: active sensor and versatile effector cells in the normal and pathologic brain. Nat Neurosci 10:1387-1394.

Hansen DB, Ye ZC, Calloe K, Braunstein TH, Hofgaard JP, Ransom BR, Nielsen MS, MacAulay N (2014) Activation, permeability, and inhibition of astrocytic and neuronal large pore (hemi)channels. J Biol Chem 289:26058-26073.

Harada Y, Hiasa M (2014) Immunological identification of vesicular nucleotide transporter in intestinal L cells. Biol Pharm Bull 37:1090-1095.

Harris AL (2001) Emerging issues of connexin channels: biophysics fills the gap. Q Rev Biophys 34:325-472.

Hart RG, Tonarelli SB, Pearce LA (2005) Avoiding central nervous system bleeding during antithrombotic therapy: recent data and ideas. Stroke 36:1588-1593.

Hassan AE, Zacharatos H, Suri MF, Qureshi AI (2007) Drug evaluation of clopidogrel in patients with ischemic stroke. Expert Opin Pharmacother 8:2825-2838.

Haynes SE, Hollopeter G, Yang G, Kurpius D, Dailey ME, Gan WB, Julius D (2006) The P2Y12 receptor regulates microglial activation by extracellular nucleotides. Nat Neurosci 9:1512-1519.

Hefendehl JK, Neher JJ, Suhs RB, Kohsaka S, Skodras A, Jucker M (2014) Homeostatic and injury-induced microglia behavior in the aging brain. Aging Cell 13:60-69.

Hefendehl JK, Milford D, Eicke D, Wegenast-Braun BM, Calhoun ME, Grathwohl SA, Jucker M, Liebig C (2012) Repeatable target localization for long-term in vivo imaging of mice with 2-photon microscopy. J Neurosci Methods 205:357-363.

Heinemann U, Lux HD, Gutnick MJ (1977) Extracellular free calcium and potassium during paroxsmal activity in the cerebral cortex of the cat. Exp Brain Res 27:237-243.

Heinrich A, Ando RD, Turi G, Rozsa B, Sperlagh B (2012) K+ depolarization evokes ATP, adenosine and glutamate release from glia in rat hippocampus: a microelectrode biosensor study. Br J Pharmacol 167:1003-1020.

Henneberger C, Papouin T, Oliet SH, Rusakov DA (2010) Long-term potentiation depends on release of D-serine from astrocytes. Nature 463:232-236.

Heo WD, Meyer T (2003) Switch-of-function mutants based on morphology classification of Ras superfamily small GTPases. Cell 113:315-328.

Heppner FL, Greter M, Marino D, Falsig J, Raivich G, Hovelmeyer N, Waisman A, Rulicke T, Prinz M, Priller J, Becher B, Aguzzi A (2005) Experimental autoimmune encephalomyelitis repressed by microglial paralysis. Nat Med 11:146-152.

Hickman SE, Kingery ND, Ohsumi TK, Borowsky ML, Wang LC, Means TK, El Khoury J (2013) The microglial sensome revealed by direct RNA sequencing. Nat Neurosci 16:1896-1905.

Higuchi M, Masuyama N, Fukui Y, Suzuki A, Gotoh Y (2001) Akt mediates Rac/Cdc42-regulated cell motility in growth factor-stimulated cells and in invasive PTEN knockout cells. Curr Biol 11:1958-1962.

Hines DJ, Hines RM, Mulligan SJ, Macvicar BA (2009) Microglia processes block the spread of damage in the brain and require functional chloride channels. Glia 57:1610-1618.

Hoffmann K, Sixel U, Di Pasquale F, von Kugelgen I (2008) Involvement of basic amino acid residues in transmembrane regions 6 and 7 in agonist and antagonist recognition of the human platelet P2Y(12)-receptor. Biochem Pharmacol 76:1201-1213.

Hollopeter G, Jantzen HM, Vincent D, Li G, England L, Ramakrishnan V, Yang RB, Nurden P, Nurden A, Julius D, Conley PB (2001) Identification of the platelet ADP receptor targeted by antithrombotic drugs. Nature 409:202-207.

Honda S, Sasaki Y, Ohsawa K, Imai Y, Nakamura Y, Inoue K, Kohsaka S (2001) Extracellular ATP or ADP induce chemotaxis of cultured microglia through Gi/o-coupled P2Y receptors. J Neurosci 21:1975-1982.

Hoshiko M, Arnoux I, Avignone E, Yamamoto N, Audinat E (2012) Deficiency of the microglial receptor CX3CR1 impairs postnatal functional development of thalamocortical synapses in the barrel cortex. J Neurosci 32:15106-15111.

Huang C, Han X, Li X, Lam E, Peng W, Lou N, Torres A, Yang M, Garre JM, Tian GF, Bennett MV, Nedergaard M, Takano T (2012) Critical role of connexin 43 in secondary expansion of traumatic spinal cord injury. J Neurosci 32:3333-3338.

Huang YA, Dando R, Roper SD (2009) Autocrine and paracrine roles for ATP and serotonin in mouse taste buds. J Neurosci 29:13909-13918.

Huang YJ, Maruyama Y, Dvoryanchikov G, Pereira E, Chaudhari N, Roper SD (2007) The role of pannexin 1 hemichannels in ATP release and cell-cell communication in mouse taste buds. Proc Natl Acad Sci U S A 104:6436-6441.

Huston JP, Haas HL, Boix F, Pfister M, Decking U, Schrader J, Schwarting RK (1996) Extracellular adenosine levels in neostriatum and hippocampus during rest and activity periods of rats. Neuroscience 73:99-107.

Iglesias R, Spray DC, Scemes E (2009) Mefloquine blockade of Pannexin1 currents: resolution of a conflict. Cell Commun Adhes 16:131-137.

Iglesias R, Locovei S, Roque A, Alberto AP, Dahl G, Spray DC, Scemes E (2008) P2X7 receptor-Pannexin1 complex: pharmacology and signaling. Am J Physiol Cell Physiol 295:C752-760.

Imai T, Hieshima K, Haskell C, Baba M, Nagira M, Nishimura M, Kakizaki M, Takagi S, Nomiyama H, Schall TJ, Yoshie O (1997) Identification and molecular characterization of fractalkine receptor CX3CR1, which mediates both leukocyte migration and adhesion. Cell 91:521-530.

Imai Y, Kohsaka S (2002) Intracellular signaling in M-CSF-induced microglia activation: role of Iba1. Glia 40:164-174.

Imai Y, Ibata I, Ito D, Ohsawa K, Kohsaka S (1996) A novel gene iba1 in the major histocompatibility complex class III region encoding an EF hand protein expressed in a monocytic lineage. Biochem Biophys Res Commun 224:855-862.

Imura Y, Morizawa Y, Komatsu R, Shibata K, Shinozaki Y, Kasai H, Moriishi K, Moriyama Y, Koizumi S (2013) Microglia release ATP by exocytosis. Glia 61:1320-1330.

Inoue T, Meyer T (2008) Synthetic activation of endogenous PI3K and Rac identifies an AND-gate switch for cell polarization and migration. PLoS One 3:e3068.

Irino Y, Nakamura Y, Inoue K, Kohsaka S, Ohsawa K (2008) Akt activation is involved in P2Y12 receptor-mediated chemotaxis of microglia. J Neurosci Res 86:1511-1519.

Ishii T, Moriyoshi K, Sugihara H, Sakurada K, Kadotani H, Yokoi M, Akazawa C, Shigemoto R, Mizuno N, Masu M, et al. (1993) Molecular characterization of the family of the N-methyl-D-aspartate receptor subunits. J Biol Chem 268:2836-2843.

Jensen FE, Harris KM (1989) Preservation of neuronal ultrastructure in hippocampal slices using rapid microwave-enhanced fixation. J Neurosci Methods 29:217-230.

Ji K, Akgul G, Wollmuth LP, Tsirka SE (2013) Microglia actively regulate the number of functional synapses. PLoS One 8:e56293.

Jin J, Kunapuli SP (1998) Coactivation of two different G protein-coupled receptors is essential for ADP-induced platelet aggregation. Proc Natl Acad Sci U S A 95:8070-8074.

John SA, Kondo R, Wang SY, Goldhaber JI, Weiss JN (1999) Connexin-43 hemichannels opened by metabolic inhibition. J Biol Chem 274:236-240.

Jung S, Aliberti J, Graemmel P, Sunshine MJ, Kreutzberg GW, Sher A, Littman DR (2000) Analysis of fractalkine receptor CX(3)CR1 function by targeted deletion and green fluorescent protein reporter gene insertion. Mol Cell Biol 20:4106-4114.

Juranyi Z, Sperlagh B, Vizi ES (1999) Involvement of P2 purinoceptors and the nitric oxide pathway in [3H]purine outflow evoked by short-term hypoxia and hypoglycemia in rat hippocampal slices. Brain Res 823:183-190.

Kaech A, Ziegler U (2014) High-pressure freezing: current state and future prospects. Methods Mol Biol 1117:151-171.

Kafitz KW, Meier SD, Stephan J, Rose CR (2008) Developmental profile and properties of sulforhodamine 101--Labeled glial cells in acute brain slices of rat hippocampus. J Neurosci Methods 169:84-92.

Kaindl AM, Degos V, Peineau S, Gouadon E, Chhor V, Loron G, Le Charpentier T, Josserand J, Ali C, Vivien D, Collingridge GL, Lombet A, Issa L, Rene F, Loeffler JP, Kavelaars A, Verney C, Mantz J, Gressens P (2012) Activation of microglial N-methyl-D-aspartate receptors triggers inflammation and neuronal cell death in the developing and mature brain. Ann Neurol 72:536-549.

Karadottir R, Attwell D (2006) Combining patch-clamping of cells in brain slices with immunocytochemical labeling to define cell type and developmental stage. Nat Protoc 1:1977-1986.

Karadottir R, Cavelier P, Bergersen LH, Attwell D (2005) NMDA receptors are expressed in oligodendrocytes and activated in ischaemia. Nature 438:1162-1166.

Kardash E, Reichman-Fried M, Maitre JL, Boldajipour B, Papusheva E, Messerschmidt EM, Heisenberg CP, Raz E (2010) A role for Rho GTPases and cell-cell adhesion in single-cell motility in vivo. Nat Cell Biol 12:47-53; sup pp 41-11.

Kawamura M, Gachet C, Inoue K, Kato F (2004) Direct excitation of inhibitory interneurons by extracellular ATP mediated by P2Y1 receptors in the hippocampal slice. J Neurosci 24:10835-10845.
Kettenmann H, Hanisch UK, Noda M, Verkhratsky A (2011) Physiology of microglia. Physiol Rev 91:461-553.
Khakh BS (2001) Molecular physiology of P2X receptors and ATP signalling at synapses. Nat Rev Neurosci 2:165-174.
Khakh BS, North RA (2012) Neuromodulation by extracellular ATP and P2X receptors in the CNS. Neuron 76:51-69.
Khakh BS, Gittermann D, Cockayne DA, Jones A (2003) ATP modulation of excitatory synapses onto interneurons. J Neurosci 23:7426-7437.
Kierdorf K et al. (2013) Microglia emerge from erythromyeloid precursors via Pu.1- and Irf8-dependent pathways. Nat Neurosci 16:273-280.
Kim JV, Dustin ML (2006) Innate response to focal necrotic injury inside the blood-brain barrier. J Immunol 177:5269-5277.
Kobayashi K, Yamanaka H, Yanamoto F, Okubo M, Noguchi K (2012) Multiple P2Y subtypes in spinal microglia are involved in neuropathic pain after peripheral nerve injury. Glia 60:1529-1539.
Kobayashi K, Yamanaka H, Fukuoka T, Dai Y, Obata K, Noguchi K (2008) P2Y12 receptor upregulation in activated microglia is a gateway of p38 signaling and neuropathic pain. J Neurosci 28:2892-2902.
Koizumi S, Shigemoto-Mogami Y, Nasu-Tada K, Shinozaki Y, Ohsawa K, Tsuda M, Joshi BV, Jacobson KA, Kohsaka S, Inoue K (2007) UDP acting at P2Y6 receptors is a mediator of microglial phagocytosis. Nature 446:1091-1095.
Kondo RP, Wang SY, John SA, Weiss JN, Goldhaber JI (2000) Metabolic inhibition activates a non-selective current through connexin hemichannels in isolated ventricular myocytes. J Mol Cell Cardiol 32:1859-1872.
Kozlowski C, Weimer RM (2012) An automated method to quantify microglia morphology and application to monitor activation state longitudinally in vivo. PLoS One 7:e31814.
Krabbe G, Matyash V, Pannasch U, Mamer L, Boddeke HW, Kettenmann H (2012) Activation of serotonin receptors promotes microglial injury-induced motility but attenuates phagocytic activity. Brain Behav Immun 26:419-428.
Krebs C, Fernandes HB, Sheldon C, Raymond LA, Baimbridge KG (2003) Functional NMDA receptor subtype 2B is expressed in astrocytes after ischemia in vivo and anoxia in vitro. J Neurosci 23:3364-3372.
Kreutzberg GW (1996) Microglia: a sensor for pathological events in the CNS. Trends Neurosci 19:312-318.
Kreutzberg GW, Barron KD, Schubert P (1978) Cytochemical localization of 5'-nucleotidase in glial plasma membranes. Brain Res 158:247-257.
Kuner T, Schoepfer R (1996) Multiple structural elements determine subunit specificity of Mg2+ block in NMDA receptor channels. J Neurosci 16:3549-3558.
Kwapis JL, Jarome TJ, Lonergan ME, Helmstetter FJ (2009) Protein kinase Mzeta maintains fear memory in the amygdala but not in the hippocampus. Behav Neurosci 123:844-850.
Lai CP, Bechberger JF, Thompson RJ, MacVicar BA, Bruzzone R, Naus CC (2007) Tumor-suppressive effects of pannexin 1 in C6 glioma cells. Cancer Res 67:1545-1554.

Laki K (1972) Our ancient heritage in blood clotting and some of its consequences. Ann N Y Acad Sci 202:297-307.
Lalo U, Pankratov Y, Kirchhoff F, North RA, Verkhratsky A (2006) NMDA receptors mediate neuron-to-glia signaling in mouse cortical astrocytes. J Neurosci 26:2673-2683.
Lammermann T, Afonso PV, Angermann BR, Wang JM, Kastenmuller W, Parent CA, Germain RN (2013) Neutrophil swarms require LTB4 and integrins at sites of cell death in vivo. Nature 498:371-375.
Lampe PD, Lau AF (2000) Regulation of gap junctions by phosphorylation of connexins. Arch Biochem Biophys 384:205-215.
Larhammar M, Patra K, Blunder M, Emilsson L, Peuckert C, Arvidsson E, Ronnlund D, Preobraschenski J, Birgner C, Limbach C, Widengren J, Blom H, Jahn R, Wallen-Mackenzie A, Kullander K (2014) SLC10A4 Is a Vesicular Amine-Associated Transporter Modulating Dopamine Homeostasis. Biol Psychiatry.
Larsson M, Sawada K, Morland C, Hiasa M, Ormel L, Moriyama Y, Gundersen V (2012) Functional and anatomical identification of a vesicular transporter mediating neuronal ATP release. Cereb Cortex 22:1203-1214.
Lazarowski ER (2010) Quantification of extracellular UDP-galactose. Anal Biochem 396:23-29.
Lee JE, Liang KJ, Fariss RN, Wong WT (2008) Ex vivo dynamic imaging of retinal microglia using time-lapse confocal microscopy. Invest Ophthalmol Vis Sci 49:4169-4176.
Lee JM, Zipfel GJ, Choi DW (1999) The changing landscape of ischaemic brain injury mechanisms. Nature 399:A7-14.
Lee KS, Schubert P, Emmert H, Kreutzberg GW (1981) Effect of adenosine versus adenine nucleotides on evoked potentials in a rat hippocampal slice preparation. Neurosci Lett 23:309-314.
Lee MC, Ting KK, Adams S, Brew BJ, Chung R, Guillemin GJ (2010) Characterisation of the expression of NMDA receptors in human astrocytes. PLoS One 5:e14123.
Lehmenkuhler A, Sykova E, Svoboda J, Zilles K, Nicholson C (1993) Extracellular space parameters in the rat neocortex and subcortical white matter during postnatal development determined by diffusion analysis. Neuroscience 55:339-351.
Leon C, Freund M, Ravanat C, Baurand A, Cazenave JP, Gachet C (2001) Key role of the P2Y(1) receptor in tissue factor-induced thrombin-dependent acute thromboembolism: studies in P2Y(1)-knockout mice and mice treated with a P2Y(1) antagonist. Circulation 103:718-723.
Li H, Liu TF, Lazrak A, Peracchia C, Goldberg GS, Lampe PD, Johnson RG (1996) Properties and regulation of gap junctional hemichannels in the plasma membranes of cultured cells. J Cell Biol 134:1019-1030.
Li S, Tomic M, Stojilkovic SS (2011a) Characterization of novel Pannexin 1 isoforms from rat pituitary cells and their association with ATP-gated P2X channels. Gen Comp Endocrinol 174:202-210.
Li S, Bjelobaba I, Yan Z, Kucka M, Tomic M, Stojilkovic SS (2011b) Expression and roles of pannexins in ATP release in the pituitary gland. Endocrinology 152:2342-2352.
Li Y, Du XF, Liu CS, Wen ZL, Du JL (2012) Reciprocal Regulation between Resting Microglial Dynamics and Neuronal Activity In Vivo. Dev Cell 23:1189-1202.
Liang J, Takeuchi H, Jin S, Noda M, Li H, Doi Y, Kawanokuchi J, Sonobe Y, Mizuno T, Suzumura A (2010) Glutamate induces neurotrophic factor production from microglia via protein kinase C pathway. Brain Res 1322:8-23.

Liang KJ, Lee JE, Wang YD, Ma W, Fontainhas AM, Fariss RN, Wong WT (2009) Regulation of dynamic behavior of retinal microglia by CX3CR1 signaling. Invest Ophthalmol Vis Sci 50:4444-4451.

Light AR, Wu Y, Hughen RW, Guthrie PB (2006) Purinergic receptors activating rapid intracellular Ca increases in microglia. Neuron Glia Biol 2:125-138.

Lin B, Holmes WR, Wang CJ, Ueno T, Harwell A, Edelstein-Keshet L, Inoue T, Levchenko A (2012) Synthetic spatially graded Rac activation drives cell polarization and movement. Proc Natl Acad Sci U S A 109:E3668-3677.

Lin JH, Lou N, Kang N, Takano T, Hu F, Han X, Xu Q, Lovatt D, Torres A, Willecke K, Yang J, Kang J, Nedergaard M (2008) A central role of connexin 43 in hypoxic preconditioning. J Neurosci 28:681-695.

Lipman BJ, Silverstein SC, Steinberg TH (1990) Organic anion transport in macrophage membrane vesicles. J Biol Chem 265:2142-2147.

Liu TF, Paulson AF, Li HY, Atkinson MM, Johnson RG (1997) Inhibitory effects of 12-O-tetradecanoylphorbol-13-acetate on dye leakage from single Novikoff cells and on dye transfer between reaggregated cell pairs. Methods Find Exp Clin Pharmacol 19:573-577.

Lloyd HG, Lindstrom K, Fredholm BB (1993) Intracellular formation and release of adenosine from rat hippocampal slices evoked by electrical stimulation or energy depletion. Neurochem Int 23:173-185.

Locovei S, Scemes E, Qiu F, Spray DC, Dahl G (2007) Pannexin1 is part of the pore forming unit of the P2X(7) receptor death complex. FEBS Lett 581:483-488.

Login GR, Leonard JB, Dvorak AM (1998) Calibration and standardization of microwave ovens for fixation of brain and peripheral nerve tissue. Methods 15:107-117.

Lohman AW, Isakson BE (2014) Differentiating connexin hemichannels and pannexin channels in cellular ATP release. FEBS Lett 588:1379-1388.

Lohman AW, Weaver JL, Billaud M, Sandilos JK, Griffiths R, Straub AC, Penuela S, Leitinger N, Laird DW, Bayliss DA, Isakson BE (2012) S-nitrosylation inhibits pannexin 1 channel function. J Biol Chem 287:39602-39612.

Ma Z, Siebert AP, Cheung KH, Lee RJ, Johnson B, Cohen AS, Vingtdeux V, Marambaud P, Foskett JK (2012) Calcium homeostasis modulator 1 (CALHM1) is the pore-forming subunit of an ion channel that mediates extracellular Ca2+ regulation of neuronal excitability. Proc Natl Acad Sci U S A 109:E1963-1971.

Maienschein V, Marxen M, Volknandt W, Zimmermann H (1999) A plethora of presynaptic proteins associated with ATP-storing organelles in cultured astrocytes. Glia 26:233-244.

Marren K (2011) Dimethyl sulfoxide: an effective penetration enhancer for topical administration of NSAIDs. Phys Sportsmed 39:75-82.

Marvin JS, Borghuis BG, Tian L, Cichon J, Harnett MT, Akerboom J, Gordus A, Renninger SL, Chen TW, Bargmann CI, Orger MB, Schreiter ER, Demb JB, Gan WB, Hires SA, Looger LL (2013) An optimized fluorescent probe for visualizing glutamate neurotransmission. Nat Methods 10:162-170.

Mathiisen TM, Lehre KP, Danbolt NC, Ottersen OP (2010) The perivascular astroglial sheath provides a complete covering of the brain microvessels: an electron microscopic 3D reconstruction. Glia 58:1094-1103.

Matthews DA, Cotman C, Lynch G (1976) An electron microscopic study of lesion-induced synaptogenesis in the dentate gyrus of the adult rat. II. Reappearance of morphologically normal synaptic contacts. Brain Res 115:23-41.

Meili R, Ellsworth C, Lee S, Reddy TB, Ma H, Firtel RA (1999) Chemoattractant-mediated transient activation and membrane localization of Akt/PKB is required for efficient chemotaxis to cAMP in Dictyostelium. EMBO J 18:2092-2105.

Melani A, Turchi D, Vannucchi MG, Cipriani S, Gianfriddo M, Pedata F (2005) ATP extracellular concentrations are increased in the rat striatum during in vivo ischemia. Neurochem Int 47:442-448.

Meurs A, Clinckers R, Ebinger G, Michotte Y, Smolders I (2008) Seizure activity and changes in hippocampal extracellular glutamate, GABA, dopamine and serotonin. Epilepsy Res 78:50-59.

Micu I, Jiang Q, Coderre E, Ridsdale A, Zhang L, Woulfe J, Yin X, Trapp BD, McRory JE, Rehak R, Zamponi GW, Wang W, Stys PK (2006) NMDA receptors mediate calcium accumulation in myelin during chemical ischaemia. Nature 439:988-992.

Mildner A, Mack M, Schmidt H, Bruck W, Djukic M, Zabel MD, Hille A, Priller J, Prinz M (2009) CCR2+Ly-6Chi monocytes are crucial for the effector phase of autoimmunity in the central nervous system. Brain 132:2487-2500.

Milks LC, Kumar NM, Houghten R, Unwin N, Gilula NB (1988) Topology of the 32-kd liver gap junction protein determined by site-directed antibody localizations. EMBO J 7:2967-2975.

Mills F, Bartlett TE, Dissing-Olesen L, Wisniewska MB, Kuznicki J, Macvicar BA, Wang YT, Bamji SX (2014) Cognitive flexibility and long-term depression (LTD) are impaired following beta-catenin stabilization in vivo. Proc Natl Acad Sci U S A 111:8631-8636.

Monyer H, Burnashev N, Laurie DJ, Sakmann B, Seeburg PH (1994) Developmental and regional expression in the rat brain and functional properties of four NMDA receptors. Neuron 12:529-540.

Monyer H, Sprengel R, Schoepfer R, Herb A, Higuchi M, Lomeli H, Burnashev N, Sakmann B, Seeburg PH (1992) Heteromeric NMDA receptors: molecular and functional distinction of subtypes. Science 256:1217-1221.

Morales-Ruiz M, Fulton D, Sowa G, Languino LR, Fujio Y, Walsh K, Sessa WC (2000) Vascular endothelial growth factor-stimulated actin reorganization and migration of endothelial cells is regulated via the serine/threonine kinase Akt. Circ Res 86:892-896.

Mori M, Heuss C, Gahwiler BH, Gerber U (2001) Fast synaptic transmission mediated by P2X receptors in CA3 pyramidal cells of rat hippocampal slice cultures. J Physiol 535:115-123.

Motin L, Bennett MR (1995) Effect of P2-purinoceptor antagonists on glutamatergic transmission in the rat hippocampus. Br J Pharmacol 115:1276-1280.

Muller CE, Jacobson KA (2011) Recent developments in adenosine receptor ligands and their potential as novel drugs. Biochim Biophys Acta 1808:1290-1308.

Murugan M, Sivakumar V, Lu J, Ling EA, Kaur C (2011) Expression of N-methyl D-aspartate receptor subunits in amoeboid microglia mediates production of nitric oxide via NF-kappaB signaling pathway and oligodendrocyte cell death in hypoxic postnatal rats. Glia 59:521-539.

Nagy JI, Rash JE (2000) Connexins and gap junctions of astrocytes and oligodendrocytes in the CNS. Brain Res Brain Res Rev 32:29-44.

Nagy JI, Patel D, Ochalski PA, Stelmack GL (1999) Connexin30 in rodent, cat and human brain: selective expression in gray matter astrocytes, co-localization with connexin43 at gap junctions and late developmental appearance. Neuroscience 88:447-468.

Nakazawa K, Inoue K, Ito K, Koizumi S (1995) Inhibition by suramin and reactive blue 2 of GABA and glutamate receptor channels in rat hippocampal neurons. Naunyn Schmiedebergs Arch Pharmacol 351:202-208.

Nasu-Tada K, Koizumi S, Inoue K (2005) Involvement of beta1 integrin in microglial chemotaxis and proliferation on fibronectin: different regulations by ADP through PKA. Glia 52:98-107.

Newman EA (2003) Glial cell inhibition of neurons by release of ATP. J Neurosci 23:1659-1666.

Ngu EM, Sahley CL, Muller KJ (2007) Reduced axon sprouting after treatment that diminishes microglia accumulation at lesions in the leech CNS. J Comp Neurol 503:101-109.

Nicholson C, Bruggencate GT, Steinberg R, Stockle H (1977) Calcium modulation in brain extracellular microenvironment demonstrated with ion-selective micropipette. Proc Natl Acad Sci U S A 74:1287-1290.

Nicholson C, ten Bruggencate G, Stockle H, Steinberg R (1978) Calcium and potassium changes in extracellular microenvironment of cat cerebellar cortex. J Neurophysiol 41:1026-1039.

Niethammer P, Grabher C, Look AT, Mitchison TJ (2009) A tissue-scale gradient of hydrogen peroxide mediates rapid wound detection in zebrafish. Nature 459:996-999.

Nimmerjahn A, Kirchhoff F, Helmchen F (2005) Resting microglial cells are highly dynamic surveillants of brain parenchyma in vivo. Science 308:1314-1318.

Nimmerjahn A, Kirchhoff F, Kerr JN, Helmchen F (2004) Sulforhodamine 101 as a specific marker of astroglia in the neocortex in vivo. Nat Methods 1:31-37.

Norden DM, Godbout JP (2013) Review: microglia of the aged brain: primed to be activated and resistant to regulation. Neuropathol Appl Neurobiol 39:19-34.

Norden DM, Muccigrosso MM, Godbout JP (2014) Microglial Priming and Enhanced Reactivity to Secondary Insult in Aging, and Traumatic CNS injury, and Neurodegenerative Disease. Neuropharmacology.

Ohsawa K, Imai Y, Kanazawa H, Sasaki Y, Kohsaka S (2000) Involvement of Iba1 in membrane ruffling and phagocytosis of macrophages/microglia. J Cell Sci 113 (Pt 17):3073-3084.

Ohsawa K, Sanagi T, Nakamura Y, Suzuki E, Inoue K, Kohsaka S (2012) Adenosine A3 receptor is involved in ADP-induced microglial process extension and migration. J Neurochem 121:217-227.

Ohsawa K, Irino Y, Sanagi T, Nakamura Y, Suzuki E, Inoue K, Kohsaka S (2010) P2Y12 receptor-mediated integrin-beta1 activation regulates microglial process extension induced by ATP. Glia 58:790-801.

Ong WY, Motin LG, Hansen MA, Dias LS, Ayrout C, Bennett MR, Balcar VJ (1997) P2 purinoceptor blocker suramin antagonises NMDA receptors and protects against excitatory behaviour caused by NMDA receptor agonist (RS)-(tetrazol-5-yl)-glycine in rats. J Neurosci Res 49:627-638.

Orellana JA, Diaz E, Schalper KA, Vargas AA, Bennett MV, Saez JC (2011a) Cation permeation through connexin 43 hemichannels is cooperative, competitive and saturable with parameters depending on the permeant species. Biochem Biophys Res Commun 409:603-609.

Orellana JA, Froger N, Ezan P, Jiang JX, Bennett MV, Naus CC, Giaume C, Saez JC (2011b) ATP and glutamate released via astroglial connexin 43 hemichannels mediate neuronal death through activation of pannexin 1 hemichannels. J Neurochem 118:826-840.

Orr AG, Orr AL, Li XJ, Gross RE, Traynelis SF (2009) Adenosine A(2A) receptor mediates microglial process retraction. Nat Neurosci 12:872-878.
Oya M, Kitaguchi T, Yanagihara Y, Numano R, Kakeyama M, Ikematsu K, Tsuboi T (2013) Vesicular nucleotide transporter is involved in ATP storage of secretory lysosomes in astrocytes. Biochem Biophys Res Commun 438:145-151.
Pankratov Y, Castro E, Miras-Portugal MT, Krishtal O (1998) A purinergic component of the excitatory postsynaptic current mediated by P2X receptors in the CA1 neurons of the rat hippocampus. Eur J Neurosci 10:3898-3902.
Pankratov Y, Lalo U, Verkhratsky A, North RA (2006) Vesicular release of ATP at central synapses. Pflugers Arch 452:589-597.
Pankratov Y, Lalo U, Verkhratsky A, North RA (2007) Quantal release of ATP in mouse cortex. J Gen Physiol 129:257-265.
Pankratov YV, Lalo UV, Krishtal OA (2002) Role for P2X receptors in long-term potentiation. J Neurosci 22:8363-8369.
Paoletti P (2011) Molecular basis of NMDA receptor functional diversity. Eur J Neurosci 33:1351-1365.
Paolicelli RC, Bolasco G, Pagani F, Maggi L, Scianni M, Panzanelli P, Giustetto M, Ferreira TA, Guiducci E, Dumas L, Ragozzino D, Gross CT (2011) Synaptic pruning by microglia is necessary for normal brain development. Science 333:1456-1458.
Parent CA, Devreotes PN (1999) A cell's sense of direction. Science 284:765-770.
Parkhurst CN, Yang G, Ninan I, Savas JN, Yates JR, 3rd, Lafaille JJ, Hempstead BL, Littman DR, Gan WB (2013) Microglia Promote Learning-Dependent Synapse Formation through Brain-Derived Neurotrophic Factor. Cell 155:1596-1609.
Parsons MP, Kang R, Buren C, Dau A, Southwell AL, Doty CN, Sanders SS, Hayden MR, Raymond LA (2014) Bidirectional control of postsynaptic density-95 (PSD-95) clustering by Huntingtin. J Biol Chem 289:3518-3528.
Pascual O, Ben Achour S, Rostaing P, Triller A, Bessis A (2012) Microglia activation triggers astrocyte-mediated modulation of excitatory neurotransmission. Proc Natl Acad Sci U S A 109:E197-205.
Patra K, Lyons DJ, Bauer P, Hilscher MM, Sharma S, Leao RN, Kullander K (2014) A role for solute carrier family 10 member 4, or vesicular aminergic-associated transporter, in structural remodelling and transmitter release at the mouse neuromuscular junction. Eur J Neurosci.
Pearson RA, Dale N, Llaudet E, Mobbs P (2005) ATP released via gap junction hemichannels from the pigment epithelium regulates neural retinal progenitor proliferation. Neuron 46:731-744.
Pekny M, Pekna M (2014) Astrocyte Reactivity and Reactive Astrogliosis: Costs and Benefits. Physiol Rev 94:1077-1098.
Pelegrin P, Surprenant A (2006) Pannexin-1 mediates large pore formation and interleukin-1beta release by the ATP-gated P2X7 receptor. EMBO J 25:5071-5082.
Penuela S, Gehi R, Laird DW (2013) The biochemistry and function of pannexin channels. Biochim Biophys Acta 1828:15-22.
Penuela S, Bhalla R, Gong XQ, Cowan KN, Celetti SJ, Cowan BJ, Bai D, Shao Q, Laird DW (2007) Pannexin 1 and pannexin 3 are glycoproteins that exhibit many distinct characteristics from the connexin family of gap junction proteins. J Cell Sci 120:3772-3783.

Peoples RW, Li C (1998) Inhibition of NMDA-gated ion channels by the P2 purinoceptor antagonists suramin and reactive blue 2 in mouse hippocampal neurones. Br J Pharmacol 124:400-408.
Perez-Otano I, Schulteis CT, Contractor A, Lipton SA, Trimmer JS, Sucher NJ, Heinemann SF (2001) Assembly with the NR1 subunit is required for surface expression of NR3A-containing NMDA receptors. J Neurosci 21:1228-1237.
Perry VH, Holmes C (2014) Microglial priming in neurodegenerative disease. Nat Rev Neurol 10:217-224.
Peyrollier K, Hajduch E, Gray A, Litherland GJ, Prescott AR, Leslie NR, Hundal HS (2000) A role for the actin cytoskeleton in the hormonal and growth-factor-mediated activation of protein kinase B. Biochem J 352 Pt 3:617-622.
Picher M, Sevigny J, D'Orleans-Juste P, Beaudoin AR (1996) Hydrolysis of P2-purinoceptor agonists by a purified ectonucleotidase from the bovine aorta, the ATP-diphosphohydrolase. Biochem Pharmacol 51:1453-1460.
Pocock JM, Kettenmann H (2007) Neurotransmitter receptors on microglia. Trends Neurosci 30:527-535.
Pollard H, Khrestchatisky M, Moreau J, Ben Ari Y (1993) Transient expression of the NR2C subunit of the NMDA receptor in developing rat brain. Neuroreport 4:411-414.
Ponsaerts R, De Vuyst E, Retamal M, D'Hondt C, Vermeire D, Wang N, De Smedt H, Zimmermann P, Himpens B, Vereecke J, Leybaert L, Bultynck G (2010) Intramolecular loop/tail interactions are essential for connexin 43-hemichannel activity. FASEB J 24:4378-4395.
Poon IK, Chiu YH, Armstrong AJ, Kinchen JM, Juncadella IJ, Bayliss DA, Ravichandran KS (2014) Unexpected link between an antibiotic, pannexin channels and apoptosis. Nature 507:329-334.
Potschka H, Baltes S, Loscher W (2004) Inhibition of multidrug transporters by verapamil or probenecid does not alter blood-brain barrier penetration of levetiracetam in rats. Epilepsy Res 58:85-91.
Premkumar LS, Auerbach A (1996) Identification of a high affinity divalent cation binding site near the entrance of the NMDA receptor channel. Neuron 16:869-880.
Pryazhnikov E, Khiroug L (2008) Sub-micromolar increase in [Ca(2+)](i) triggers delayed exocytosis of ATP in cultured astrocytes. Glia 56:38-49.
Qu Y, Misaghi S, Newton K, Gilmour LL, Louie S, Cupp JE, Dubyak GR, Hackos D, Dixit VM (2011) Pannexin-1 is required for ATP release during apoptosis but not for inflammasome activation. J Immunol 186:6553-6561.
Quinn MJ, Fitzgerald DJ (1999) Ticlopidine and clopidogrel. Circulation 100:1667-1672.
Radulovacki M, Virus RM, Djuricic-Nedelson M, Green RD (1984) Adenosine analogs and sleep in rats. J Pharmacol Exp Ther 228:268-274.
Ransford GA, Fregien N, Qiu F, Dahl G, Conner GE, Salathe M (2009) Pannexin 1 contributes to ATP release in airway epithelia. Am J Respir Cell Mol Biol 41:525-534.
Rassendren F, Buell GN, Virginio C, Collo G, North RA, Surprenant A (1997) The permeabilizing ATP receptor, P2X7. Cloning and expression of a human cDNA. J Biol Chem 272:5482-5486.
Rauskolb S, Zagrebelsky M, Dreznjak A, Deogracias R, Matsumoto T, Wiese S, Erne B, Sendtner M, Schaeren-Wiemers N, Korte M, Barde YA (2010) Global deprivation of

brain-derived neurotrophic factor in the CNS reveals an area-specific requirement for dendritic growth. J Neurosci 30:1739-1749.
Resendiz JC, Feng S, Ji G, Francis KA, Berndt MC, Kroll MH (2003) Purinergic P2Y12 receptor blockade inhibits shear-induced platelet phosphatidylinositol 3-kinase activation. Mol Pharmacol 63:639-645.
Retamal MA, Cortes CJ, Reuss L, Bennett MV, Saez JC (2006) S-nitrosylation and permeation through connexin 43 hemichannels in astrocytes: induction by oxidant stress and reversal by reducing agents. Proc Natl Acad Sci U S A 103:4475-4480.
Retamal MA, Schalper KA, Shoji KF, Bennett MV, Saez JC (2007) Opening of connexin 43 hemichannels is increased by lowering intracellular redox potential. Proc Natl Acad Sci U S A 104:8322-8327.
Rex CS, Lin CY, Kramar EA, Chen LY, Gall CM, Lynch G (2007) Brain-derived neurotrophic factor promotes long-term potentiation-related cytoskeletal changes in adult hippocampus. J Neurosci 27:3017-3029.
Richler E, Chaumont S, Shigetomi E, Sagasti A, Khakh BS (2008) Tracking transmitter-gated P2X cation channel activation in vitro and in vivo. Nat Methods 5:87-93.
Riquelme MA, Kar R, Gu S, Jiang JX (2013) Antibodies targeting extracellular domain of connexins for studies of hemichannels. Neuropharmacology 75:525-532.
Roberts JA, Vial C, Digby HR, Agboh KC, Wen H, Atterbury-Thomas A, Evans RJ (2006) Molecular properties of P2X receptors. Pflugers Arch 452:486-500.
Robson SC, Sevigny J, Zimmermann H (2006) The E-NTPDase family of ectonucleotidases: Structure function relationships and pathophysiological significance. Purinergic Signal 2:409-430.
Romanello M, D'Andrea P (2001) Dual mechanism of intercellular communication in HOBIT osteoblastic cells: a role for gap-junctional hemichannels. J Bone Miner Res 16:1465-1476.
Rossi DJ, Oshima T, Attwell D (2000) Glutamate release in severe brain ischaemia is mainly by reversed uptake. Nature 403:316-321.
Rouach N, Koulakoff A, Abudara V, Willecke K, Giaume C (2008) Astroglial metabolic networks sustain hippocampal synaptic transmission. Science 322:1551-1555.
Ryan JW, Smith U (1971) Metabolism of adenosine 5'-monophosphate during circulation through the lungs. Trans Assoc Am Physicians 84:297-306.
Saez JC, Retamal MA, Basilio D, Bukauskas FF, Bennett MV (2005) Connexin-based gap junction hemichannels: gating mechanisms. Biochim Biophys Acta 1711:215-224.
Sakaki H, Tsukimoto M, Harada H, Moriyama Y, Kojima S (2013) Autocrine regulation of macrophage activation via exocytosis of ATP and activation of P2Y11 receptor. PLoS One 8:e59778.
Sakamoto S, Miyaji T, Hiasa M, Ichikawa R, Uematsu A, Iwatsuki K, Shibata A, Uneyama H, Takayanagi R, Yamamoto A, Omote H, Nomura M, Moriyama Y (2014) Impairment of vesicular ATP release affects glucose metabolism and increases insulin sensitivity. Sci Rep 4:6689.
Salter MG, Fern R (2005) NMDA receptors are expressed in developing oligodendrocyte processes and mediate injury. Nature 438:1167-1171.
Salter MW, Pitcher GM (2012) Dysregulated Src upregulation of NMDA receptor activity: a common link in chronic pain and schizophrenia. FEBS J 279:2-11.

Sandilos JK, Chiu YH, Chekeni FB, Armstrong AJ, Walk SF, Ravichandran KS, Bayliss DA (2012) Pannexin 1, an ATP release channel, is activated by caspase cleavage of its pore-associated C-terminal autoinhibitory region. J Biol Chem 287:11303-11311.

Sasaki Y, Hoshi M, Akazawa C, Nakamura Y, Tsuzuki H, Inoue K, Kohsaka S (2003) Selective expression of Gi/o-coupled ATP receptor P2Y12 in microglia in rat brain. Glia 44:242-250.

Sattler R, Xiong Z, Lu WY, Hafner M, MacDonald JF, Tymianski M (1999) Specific coupling of NMDA receptor activation to nitric oxide neurotoxicity by PSD-95 protein. Science 284:1845-1848.

Sawada K, Echigo N, Juge N, Miyaji T, Otsuka M, Omote H, Yamamoto A, Moriyama Y (2008) Identification of a vesicular nucleotide transporter. Proc Natl Acad Sci U S A 105:5683-5686.

Scemes E, Suadicani SO, Dahl G, Spray DC (2007) Connexin and pannexin mediated cell-cell communication. Neuron Glia Biol 3:199-208.

Schafer DP, Lehrman EK, Kautzman AG, Koyama R, Mardinly AR, Yamasaki R, Ransohoff RM, Greenberg ME, Barres BA, Stevens B (2012) Microglia sculpt postnatal neural circuits in an activity and complement-dependent manner. Neuron 74:691-705.

Schalper KA, Palacios-Prado N, Retamal MA, Shoji KF, Martinez AD, Saez JC (2008) Connexin hemichannel composition determines the FGF-1-induced membrane permeability and free [Ca2+]i responses. Mol Biol Cell 19:3501-3513.

Schenk U, Westendorf AM, Radaelli E, Casati A, Ferro M, Fumagalli M, Verderio C, Buer J, Scanziani E, Grassi F (2008) Purinergic control of T cell activation by ATP released through pannexin-1 hemichannels. Sci Signal 1:ra6.

Schipke CG, Ohlemeyer C, Matyash M, Nolte C, Kettenmann H, Kirchhoff F (2001) Astrocytes of the mouse neocortex express functional N-methyl-D-aspartate receptors. FASEB J 15:1270-1272.

Schnell SA, Staines WA, Wessendorf MW (1999) Reduction of lipofuscin-like autofluorescence in fluorescently labeled tissue. J Histochem Cytochem 47:719-730.

Schoen SW, Graeber MB, Kreutzberg GW (1992) 5'-Nucleotidase immunoreactivity of perineuronal microglia responding to rat facial nerve axotomy. Glia 6:314-317.

Schousboe A, Divac I (1979) Difference in glutamate uptake in astrocytes cultured from different brain regions. Brain Res 177:407-409.

Schwartz EJ, Rothman JS, Dugue GP, Diana M, Rousseau C, Silver RA, Dieudonne S (2012) NMDA receptors with incomplete Mg(2)(+) block enable low-frequency transmission through the cerebellar cortex. J Neurosci 32:6878-6893.

Seminario-Vidal L, Okada SF, Sesma JI, Kreda SM, van Heusden CA, Zhu Y, Jones LC, O'Neal WK, Penuela S, Laird DW, Boucher RC, Lazarowski ER (2011) Rho signaling regulates pannexin 1-mediated ATP release from airway epithelia. J Biol Chem 286:26277-26286.

Servant G, Weiner OD, Herzmark P, Balla T, Sedat JW, Bourne HR (2000) Polarization of chemoattractant receptor signaling during neutrophil chemotaxis. Science 287:1037-1040.

Sesma JI, Kreda SM, Okada SF, van Heusden C, Moussa L, Jones LC, O'Neal WK, Togawa N, Hiasa M, Moriyama Y, Lazarowski ER (2013) Vesicular nucleotide transporter regulates the nucleotide content in airway epithelial mucin granules. Am J Physiol Cell Physiol 304:C976-984.

Shinozaki Y, Nomura M, Iwatsuki K, Moriyama Y, Gachet C, Koizumi S (2014) Microglia trigger astrocyte-mediated neuroprotection via purinergic gliotransmission. Sci Rep 4:4329.

Shivers RR, McVicar LK (1995) Gap junctions revealed by freeze-fracture electron microscopy. Microsc Res Tech 31:437-445.

Sieger D, Moritz C, Ziegenhals T, Prykhozhij S, Peri F (2012) Long-range Ca2+ waves transmit brain-damage signals to microglia. Dev Cell 22:1138-1148.

Silverman W, Locovei S, Dahl G (2008) Probenecid, a gout remedy, inhibits pannexin 1 channels. Am J Physiol Cell Physiol 295:C761-767.

Simard M, Arcuino G, Takano T, Liu QS, Nedergaard M (2003) Signaling at the gliovascular interface. J Neurosci 23:9254-9262.

Snippert HJ, Schepers AG, Delconte G, Siersema PD, Clevers H (2011) Slide preparation for single-cell-resolution imaging of fluorescent proteins in their three-dimensional near-native environment. Nat Protoc 6:1221-1228.

Sogn CJ, Puchades M, Gundersen V (2013) Rare contacts between synapses and microglial processes containing high levels of Iba1 and actin - a postembedding immunogold study in the healthy rat brain. Eur J Neurosci.

Sonnewald U, Qu H, Aschner M (2002) Pharmacology and toxicology of astrocyte-neuron glutamate transport and cycling. J Pharmacol Exp Ther 301:1-6.

Sosinsky GE, Boassa D, Dermietzel R, Duffy HS, Laird DW, MacVicar B, Naus CC, Penuela S, Scemes E, Spray DC, Thompson RJ, Zhao HB, Dahl G (2011) Pannexin channels are not gap junction hemichannels. Channels (Austin) 5:193-197.

Splinter PL, Lazaridis KN, Dawson PA, LaRusso NF (2006) Cloning and expression of SLC10A4, a putative organic anion transport protein. World J Gastroenterol 12:6797-6805.

Spray DC, Ye ZC, Ransom BR (2006) Functional connexin "hemichannels": a critical appraisal. Glia 54:758-773.

Sridharan M, Adderley SP, Bowles EA, Egan TM, Stephenson AH, Ellsworth ML, Sprague RS (2010) Pannexin 1 is the conduit for low oxygen tension-induced ATP release from human erythrocytes. Am J Physiol Heart Circ Physiol 299:H1146-1152.

Srinivasan S, Wang F, Glavas S, Ott A, Hofmann F, Aktories K, Kalman D, Bourne HR (2003) Rac and Cdc42 play distinct roles in regulating PI(3,4,5)P3 and polarity during neutrophil chemotaxis. J Cell Biol 160:375-385.

Stephan KE, Friston KJ, Frith CD (2009) Dysconnection in schizophrenia: from abnormal synaptic plasticity to failures of self-monitoring. Schizophr Bull 35:509-527.

Stevens B, Allen NJ, Vazquez LE, Howell GR, Christopherson KS, Nouri N, Micheva KD, Mehalow AK, Huberman AD, Stafford B, Sher A, Litke AM, Lambris JD, Smith SJ, John SW, Barres BA (2007) The classical complement cascade mediates CNS synapse elimination. Cell 131:1164-1178.

Stout C, Charles A (2003) Modulation of intercellular calcium signaling in astrocytes by extracellular calcium and magnesium. Glia 43:265-273.

Stout CE, Costantin JL, Naus CC, Charles AC (2002) Intercellular calcium signaling in astrocytes via ATP release through connexin hemichannels. J Biol Chem 277:10482-10488.

Strecker RE, Morairty S, Thakkar MM, Porkka-Heiskanen T, Basheer R, Dauphin LJ, Rainnie DG, Portas CM, Greene RW, McCarley RW (2000) Adenosinergic modulation of basal

forebrain and preoptic/anterior hypothalamic neuronal activity in the control of behavioral state. Behav Brain Res 115:183-204.
Streit WJ (2002) Microglia as neuroprotective, immunocompetent cells of the CNS. Glia 40:133-139.
Surprenant A, Rassendren F, Kawashima E, North RA, Buell G (1996) The cytolytic P2Z receptor for extracellular ATP identified as a P2X receptor (P2X7). Science 272:735-738.
Suzuki E, Kessler M, Montgomery K, Arai AC (2004) Divergent effects of the purinoceptor antagonists suramin and pyridoxal-5'-phosphate-6-(2'-naphthylazo-6'-nitro-4',8'-disulfonate) (PPNDS) on alpha-amino-3-hydroxy-5-methyl-4-isoxazolepropionic acid (AMPA) receptors. Mol Pharmacol 66:1738-1747.
Swinnen N, Smolders S, Avila A, Notelaers K, Paesen R, Ameloot M, Brone B, Legendre P, Rigo JM (2013) Complex invasion pattern of the cerebral cortex bymicroglial cells during development of the mouse embryo. Glia 61:150-163.
Sykova E (2004) Diffusion properties of the brain in health and disease. Neurochem Int 45:453-466.
Takagi N, Shinno K, Teves L, Bissoon N, Wallace MC, Gurd JW (1997) Transient ischemia differentially increases tyrosine phosphorylation of NMDA receptor subunits 2A and 2B. J Neurochem 69:1060-1065.
Takagi N, Cheung HH, Bissoon N, Teves L, Wallace MC, Gurd JW (1999) The effect of transient global ischemia on the interaction of Src and Fyn with the N-methyl-D-aspartate receptor and postsynaptic densities: possible involvement of Src homology 2 domains. J Cereb Blood Flow Metab 19:880-888.
Takano T, He W, Han X, Wang F, Xu Q, Wang X, Oberheim Bush NA, Cruz N, Dienel GA, Nedergaard M (2014) Rapid manifestation of reactive astrogliosis in acute hippocampal brain slices. Glia 62:78-95.
Tang LJ, Li C, Hu SQ, Wu YP, Zong YY, Sun CC, Zhang F, Zhang GY (2012) S-nitrosylation of c-Src via NMDAR-nNOS module promotes c-Src activation and NR2A phosphorylation in cerebral ischemia/reperfusion. Mol Cell Biochem 365:363-377.
Tani E, Nishiura M, Higashi N (1973) Freeze-fracture studies of gap junctions of normal and neoplastic astrocytes. Acta Neuropathol 26:127-138.
Taruno A, Vingtdeux V, Ohmoto M, Ma Z, Dvoryanchikov G, Li A, Adrien L, Zhao H, Leung S, Abernethy M, Koppel J, Davies P, Civan MM, Chaudhari N, Matsumoto I, Hellekant G, Tordoff MG, Marambaud P, Foskett JK (2013) CALHM1 ion channel mediates purinergic neurotransmission of sweet, bitter and umami tastes. Nature.
Theis M, Jauch R, Zhuo L, Speidel D, Wallraff A, Doring B, Frisch C, Sohl G, Teubner B, Euwens C, Huston J, Steinhauser C, Messing A, Heinemann U, Willecke K (2003) Accelerated hippocampal spreading depression and enhanced locomotory activity in mice with astrocyte-directed inactivation of connexin43. J Neurosci 23:766-776.
Thompson CL, Drewery DL, Atkins HD, Stephenson FA, Chazot PL (2002) Immunohistochemical localization of N-methyl-D-aspartate receptor subunits in the adult murine hippocampal formation: evidence for a unique role of the NR2D subunit. Brain Res Mol Brain Res 102:55-61.
Thompson RJ, Zhou N, MacVicar BA (2006) Ischemia opens neuronal gap junction hemichannels. Science 312:924-927.

Thompson RJ, Jackson MF, Olah ME, Rungta RL, Hines DJ, Beazely MA, MacDonald JF, MacVicar BA (2008) Activation of pannexin-1 hemichannels augments aberrant bursting in the hippocampus. Science 322:1555-1559.

Torres A, Wang F, Xu Q, Fujita T, Dobrowolski R, Willecke K, Takano T, Nedergaard M (2012) Extracellular Ca(2)(+) acts as a mediator of communication from neurons to glia. Sci Signal 5:ra8.

Tovar KR, Westbrook GL (1999) The incorporation of NMDA receptors with a distinct subunit composition at nascent hippocampal synapses in vitro. J Neurosci 19:4180-4188.

Trapp BD, Wujek JR, Criste GA, Jalabi W, Yin X, Kidd GJ, Stohlman S, Ransohoff R (2007) Evidence for synaptic stripping by cortical microglia. Glia 55:360-368.

Traynelis SF, Wollmuth LP, McBain CJ, Menniti FS, Vance KM, Ogden KK, Hansen KB, Yuan H, Myers SJ, Dingledine R (2010) Glutamate receptor ion channels: structure, regulation, and function. Pharmacol Rev 62:405-496.

Tremblay ME, Lowery RL, Majewska AK (2010) Microglial interactions with synapses are modulated by visual experience. PLoS Biol 8:e1000527.

Trezise DJ, Bell NJ, Kennedy I, Humphrey PP (1994) Effects of divalent cations on the potency of ATP and related agonists in the rat isolated vagus nerve: implications for P2 purinoceptor classification. Br J Pharmacol 113:463-470.

Unger VM, Kumar NM, Gilula NB, Yeager M (1999) Three-dimensional structure of a recombinant gap junction membrane channel. Science 283:1176-1180.

Urenjak J, Obrenovitch TP, Zilkha E (1997) Effect of probenecid on depolarizations evoked by N-methyl-D-aspartate (NMDA) in the rat striatum. Naunyn Schmiedebergs Arch Pharmacol 355:36-42.

van den Heuvel MP, Kahn RS (2011) Abnormal brain wiring as a pathogenetic mechanism in schizophrenia. Biol Psychiatry 70:1107-1108.

Vanden Abeele F, Bidaux G, Gordienko D, Beck B, Panchin YV, Baranova AV, Ivanov DV, Skryma R, Prevarskaya N (2006) Functional implications of calcium permeability of the channel formed by pannexin 1. J Cell Biol 174:535-546.

Varvel NH, Grathwohl SA, Baumann F, Liebig C, Bosch A, Brawek B, Thal DR, Charo IF, Heppner FL, Aguzzi A, Garaschuk O, Ransohoff RM, Jucker M (2012) Microglial repopulation model reveals a robust homeostatic process for replacing CNS myeloid cells. Proc Natl Acad Sci U S A 109:18150-18155.

Verkhratsky A, Krishtal OA, Burnstock G (2009) Purinoceptors on neuroglia. Mol Neurobiol 39:190-208.

Villarroel A, Burnashev N, Sakmann B (1995) Dimensions of the narrow portion of a recombinant NMDA receptor channel. Biophys J 68:866-875.

Vinet J, Weering HR, Heinrich A, Kalin RE, Wegner A, Brouwer N, Heppner FL, Rooijen N, Boddeke HW, Biber K (2012) Neuroprotective function for ramified microglia in hippocampal excitotoxicity. J Neuroinflammation 9:27.

Virginio C, Church D, North RA, Surprenant A (1997) Effects of divalent cations, protons and calmidazolium at the rat P2X7 receptor. Neuropharmacology 36:1285-1294.

Visentin S, Nuccio CD, Bellenchi GC (2006) Different patterns of Ca(2)(+) signals are induced by low compared to high concentrations of P2Y agonists in microglia. Purinergic Signal 2:605-617.

Vogt A, Hormuzdi SG, Monyer H (2005) Pannexin1 and Pannexin2 expression in the developing and mature rat brain. Brain Res Mol Brain Res 141:113-120.

Volk LJ, Bachman JL, Johnson R, Yu Y, Huganir RL (2013) PKM-zeta is not required for hippocampal synaptic plasticity, learning and memory. Nature 493:420-423.
Wake H, Moorhouse AJ, Jinno S, Kohsaka S, Nabekura J (2009) Resting microglia directly monitor the functional state of synapses in vivo and determine the fate of ischemic terminals. J Neurosci 29:3974-3980.
Wall MJ, Dale N (2007) Auto-inhibition of rat parallel fibre-Purkinje cell synapses by activity-dependent adenosine release. J Physiol 581:553-565.
Wallraff A, Kohling R, Heinemann U, Theis M, Willecke K, Steinhauser C (2006) The impact of astrocytic gap junctional coupling on potassium buffering in the hippocampus. J Neurosci 26:5438-5447.
Wang F, Herzmark P, Weiner OD, Srinivasan S, Servant G, Bourne HR (2002) Lipid products of PI(3)Ks maintain persistent cell polarity and directed motility in neutrophils. Nat Cell Biol 4:513-518.
Wang J, Dahl G (2010) SCAM analysis of Panx1 suggests a peculiar pore structure. J Gen Physiol 136:515-527.
Wang N, De Bock M, Antoons G, Gadicherla AK, Bol M, Decrock E, Evans WH, Sipido KR, Bukauskas FF, Leybaert L (2012) Connexin mimetic peptides inhibit Cx43 hemichannel opening triggered by voltage and intracellular Ca2+ elevation. Basic Res Cardiol 107:304.
Wang N et al. (2013) Selective inhibition of Cx43 hemichannels by Gap19 and its impact on myocardial ischemia/reperfusion injury. Basic Res Cardiol 108:309.
Wang TF, Guidotti G (1996) CD39 is an ecto-(Ca2+,Mg2+)-apyrase. J Biol Chem 271:9898-9901.
Warner A, Clements DK, Parikh S, Evans WH, DeHaan RL (1995) Specific motifs in the external loops of connexin proteins can determine gap junction formation between chick heart myocytes. J Physiol 488 (Pt 3):721-728.
Watanabe S, Rost BR, Camacho-Perez M, Davis MW, Sohl-Kielczynski B, Rosenmund C, Jorgensen EM (2013) Ultrafast endocytosis at mouse hippocampal synapses. Nature 504:242-247.
Weber WM, Liebold KM, Reifarth FW, Uhr U, Clauss W (1995) Influence of extracellular Ca2+ on endogenous Cl- channels in Xenopus oocytes. Pflugers Arch 429:820-824.
Weilinger NL, Tang PL, Thompson RJ (2012) Anoxia-induced NMDA receptor activation opens pannexin channels via Src family kinases. J Neurosci 32:12579-12588.
Weiner OD, Neilsen PO, Prestwich GD, Kirschner MW, Cantley LC, Bourne HR (2002) A PtdInsP(3)- and Rho GTPase-mediated positive feedback loop regulates neutrophil polarity. Nat Cell Biol 4:509-513.
White MM, Aylwin M (1990) Niflumic and flufenamic acids are potent reversible blockers of Ca2(+)-activated Cl- channels in Xenopus oocytes. Mol Pharmacol 37:720-724.
Wieraszko A, Seyfried TN (1989) ATP-induced synaptic potentiation in hippocampal slices. Brain Res 491:356-359.
Williams K (1993) Ifenprodil discriminates subtypes of the N-methyl-D-aspartate receptor: selectivity and mechanisms at recombinant heteromeric receptors. Mol Pharmacol 44:851-859.
Williams KA, Mehta NS, Redei EE, Wang L, Procissi D (2014) Aberrant resting-state functional connectivity in a genetic rat model of depression. Psychiatry Res 222:111-113.

Wolf Y, Yona S, Kim KW, Jung S (2013) Microglia, seen from the CX3CR1 angle. Front Cell Neurosci 7:26.
Wollmuth LP, Kuner T, Sakmann B (1998) Adjacent asparagines in the NR2-subunit of the NMDA receptor channel control the voltage-dependent block by extracellular Mg2+. J Physiol 506 (Pt 1):13-32.
Wu J, Peng S, Wu R, Hao Y, Ji G, Yuan Z (2012) Generation of Calhm1 knockout mouse and characterization of calhm1 gene expression. Protein Cell 3:470-480.
Wu LJ, Zhuo M (2008) Resting microglial motility is independent of synaptic plasticity in mammalian brain. J Neurophysiol 99:2026-2032.
Wu LJ, Vadakkan KI, Zhuo M (2007) ATP-induced chemotaxis of microglial processes requires P2Y receptor-activated initiation of outward potassium currents. Glia 55:810-821.
Xie L, Kang H, Xu Q, Chen MJ, Liao Y, Thiyagarajan M, O'Donnell J, Christensen DJ, Nicholson C, Iliff JJ, Takano T, Deane R, Nedergaard M (2013) Sleep drives metabolite clearance from the adult brain. Science 342:373-377.
Xu HT, Pan F, Yang G, Gan WB (2007) Choice of cranial window type for in vivo imaging affects dendritic spine turnover in the cortex. Nat Neurosci 10:549-551.
Xu J, Song D, Bai Q, Zhou L, Cai L, Hertz L, Peng L (2014) Role of glycogenolysis in stimulation of ATP release from cultured mouse astrocytes by transmitters and high K+ concentrations. ASN Neuro 6:e00132.
Yamamoto T, Ochalski A, Hertzberg EL, Nagy JI (1990) LM and EM immunolocalization of the gap junctional protein connexin 43 in rat brain. Brain Res 508:313-319.
Yan E, Li B, Gu L, Hertz L, Peng L (2013) Mechanisms for L-channel-mediated increase in [Ca(2+)]i and its reduction by anti-bipolar drugs in cultured astrocytes combined with its mRNA expression in freshly isolated cells support the importance of astrocytic L-channels. Cell Calcium 54:335-342.
Yang HW, Shin MG, Lee S, Kim JR, Park WS, Cho KH, Meyer T, Heo WD (2012) Cooperative activation of PI3K by Ras and Rho family small GTPases. Mol Cell 47:281-290.
Ye ZC, Wyeth MS, Baltan-Tekkok S, Ransom BR (2003) Functional hemichannels in astrocytes: a novel mechanism of glutamate release. J Neurosci 23:3588-3596.
Yeager M, Gilula NB (1992) Membrane topology and quaternary structure of cardiac gap junction ion channels. J Mol Biol 223:929-948.
Yen MR, Saier MH, Jr. (2007) Gap junctional proteins of animals: the innexin/pannexin superfamily. Prog Biophys Mol Biol 94:5-14.
Yokomizo T, Izumi T, Chang K, Takuwa Y, Shimizu T (1997) A G-protein-coupled receptor for leukotriene B4 that mediates chemotaxis. Nature 387:620-624.
Yu XM, Askalan R, Keil GJ, 2nd, Salter MW (1997) NMDA channel regulation by channel-associated protein tyrosine kinase Src. Science 275:674-678.
Yusuf S, Zhao F, Mehta SR, Chrolavicius S, Tognoni G, Fox KK (2001) Effects of clopidogrel in addition to aspirin in patients with acute coronary syndromes without ST-segment elevation. N Engl J Med 345:494-502.
Zappala A, Cicero D, Serapide MF, Paz C, Catania MV, Falchi M, Parenti R, Panto MR, La Delia F, Cicirata F (2006) Expression of pannexin1 in the CNS of adult mouse: cellular localization and effect of 4-aminopyridine-induced seizures. Neuroscience 141:167-178.
Zelano J, Mikulovic S, Patra K, Kuhnemund M, Larhammar M, Emilsson L, Leao RN, Kullander K (2013) The synaptic protein encoded by the gene Slc10A4 suppresses

epileptiform activity and regulates sensitivity to cholinergic chemoconvulsants. Exp Neurol 239:73-81.
Zhan Y, Paolicelli RC, Sforazzini F, Weinhard L, Bolasco G, Pagani F, Vyssotski AL, Bifone A, Gozzi A, Ragozzino D, Gross CT (2014) Deficient neuron-microglia signaling results in impaired functional brain connectivity and social behavior. Nat Neurosci 17:400-406.
Zhang FL, Luo L, Gustafson E, Lachowicz J, Smith M, Qiao X, Liu YH, Chen G, Pramanik B, Laz TM, Palmer K, Bayne M, Monsma FJ, Jr. (2001) ADP is the cognate ligand for the orphan G protein-coupled receptor SP1999. J Biol Chem 276:8608-8615.
Zhang J, Malik A, Choi HB, Ko RW, Dissing-Olesen L, MacVicar BA (2014a) Microglial CR3 activation triggers long-term synaptic depression in the hippocampus via NADPH oxidase. Neuron 82:195-207.
Zhang L, Deng T, Sun Y, Liu K, Yang Y, Zheng X (2008) Role for nitric oxide in permeability of hippocampal neuronal hemichannels during oxygen glucose deprivation. J Neurosci Res 86:2281-2291.
Zhang Y, Chen K, Sloan SA, Bennett ML, Scholze AR, O'Keeffe S, Phatnani HP, Guarnieri P, Caneda C, Ruderisch N, Deng S, Liddelow SA, Zhang C, Daneman R, Maniatis T, Barres BA, Wu JQ (2014b) An RNA-sequencing transcriptome and splicing database of glia, neurons, and vascular cells of the cerebral cortex. J Neurosci 34:11929-11947.
Zheng K, An JJ, Yang F, Xu W, Xu ZQ, Wu J, Hokfelt TG, Fisahn A, Xu B, Lu B (2011) TrkB signaling in parvalbumin-positive interneurons is critical for gamma-band network synchronization in hippocampus. Proc Natl Acad Sci U S A 108:17201-17206.
Zhu X, Birnbaumer L (1996) G protein subunits and the stimulation of phospholipase C by Gs- and Gi-coupled receptors: Lack of receptor selectivity of Galpha(16) and evidence for a synergic interaction between Gbeta gamma and the alpha subunit of a receptor activated G protein. Proc Natl Acad Sci U S A 93:2827-2831.
Zigmond SH (1977) Ability of polymorphonuclear leukocytes to orient in gradients of chemotactic factors. J Cell Biol 75:606-616.
Zimmermann H (1992) 5'-Nucleotidase: molecular structure and functional aspects. Biochem J 285 (Pt 2):345-365.
Zimmermann H (2006) Nucleotide signaling in nervous system development. Pflugers Arch 452:573-588.
Zimmermann H, Vogel M, Laube U (1993) Hippocampal localization of 5'-nucleotidase as revealed by immunocytochemistry. Neuroscience 55:105-112.
Zoidl G, Petrasch-Parwez E, Ray A, Meier C, Bunse S, Habbes HW, Dahl G, Dermietzel R (2007) Localization of the pannexin1 protein at postsynaptic sites in the cerebral cortex and hippocampus. Neuroscience 146:9-16.
Zukor KA, Kent DT, Odelberg SJ (2010) Fluorescent whole-mount method for visualizing three-dimensional relationships in intact and regenerating adult newt spinal cords. Dev Dyn 239:3048-3057.